# BIOCHIP AND LAB-ON-CHIP FOR GENOMIC AND PROTEOMIC APPLICATIONS

**Lucia Rotiroti**

Dottorato in Scienze Biotecnologiche – XXI ciclo
Indirizzo Biotecnologie Industriali
Università di Napoli Federico II

Dottorato in Scienze Biotecnologiche – XXI ciclo
Indirizzo Biotecnologie Industriali
Università di Napoli Federico II

# BIOCHIP AND LAB-ON-CHIP FOR GENOMIC AND PROTEOMIC APPLICATIONS

**Lucia Rotiroti**

Dottoranda: *Rotiroti Lucia*

Relatore: Dr. De Stefano Luca

Coordinatore: Prof. Giovanni Sannia

*The most beautiful thing we can experience is the mysterious.*
*It is the source of all true art and science.*
*Albert Einstein*

*A TE*
*. . . che hai sempre confidato in me e nelle mie capacità. . .*
*. . . che mi hai dato forza, sempre. . .*
*. . . che hai sostenuto ogni mia scelta di vita. . .*
*. . . illuminandone la via con straordinaria discrezione. . .*
*. . . a te. . . grazie!*

## INDICE

## SUMMARY

There is no other inorganic material that brings together such much intriguing features like porous silicon (PSi) for people working in the optical sensing field. Porous silicon was unexpectedly discovered in the late fifties when chemists attempted to electropolish silicon wafers with an electrolyte containing hydrofluoric acid to get better electrical contacts in the first integrated electronic circuit fabrications. The acid dissolution left a sponge-like nanocrystalline silicon structure on the wafer. Today, the electrochemical etching is a standard method to fabricate nanostructured porous silicon: a proper choice of the applied current density, the electrolyte composition, and the silicon doping allow precise control over the morphology and, consequently, on the physical and chemical properties of the porous silicon structure. Computer controlled electrochemical etching processes are exploited for the realization of porous silicon films of controlled thickness and porosity (defined as the percentage of void in the silicon volume). Nanoporous, mesoporous and macroporous structures can be achieved, with pore size ranging from few nanometers up to microns. Moreover, since the etching process is self-stopping, it is possible to fabricate with a single run process multilayer stacks made of single layers of different porosity. The dielectric properties of each PSi layer, and in particular its refractive index *n*, can be namely modulated between those of crystalline silicon (*n = 3.54*, porosity = 0) and air (*n= 1*, porosity = 100 %); so that alternating high and low porosity layers, lot of photonic structures, such as Fabry-Perot interferometers, omni-directional Bragg reflectors, optical filters based on microcavities, and even complicated quasi-periodic sequences can be simply realized.

The other key feature for a transducer material is the large area and the chemistry of its surface: the porous silicon exhibits a very reactive hydrogenated specific area of the order of 200 – 500 $m^2$ $cm^{-3}$, which assures an effective interaction with several adsorbates. The porous silicon optical sensing features are based on the changes of its photonic properties, such as photoluminescence or reflectance, on exposure to the gaseous or liquid substances. Of course, these interactions are not specific. Therefore, the porous silicon hydrogenated surface has to be chemically or physically modified in order to achieve the sensing selectivity through specific biochemical interactions. The biosensor reliability strongly depends on the functionalization process: how simple, homogenous and repeatable it can be. The substitution of the superficial Si-H bonds with Si-C ones or Si-O-C guarantees a much more stable surface interface from the thermodynamic point of view. Several functionalization strategies were investigated. Testing and demonstrating the porous silicon capabilities as a useful functional material in the immobilization of biological probes and in the optical transduction of biochemical interactions is only the first action in the realisation of an optical biochip based on this nanostructured material. In this case, all the fabrication processes should be compatible with the utilisation of biological probes and the feasibility of such devices must be proven. This means that the standard integrated circuit micro-technologies should be modified and adapted to this new field of application. The porous silicon low cost technology could thus provide a link between the conventional CMOS technology and the photonic devices in the realization of the so-called smart sensors and biochips. A very strong interdisciplinary approach is required to match and resolve all the technological problems. The purpose of this thesis was to design and fabricate different resonant optical structures, integrate in simple lab-on-chip devices based on the porous silicon nanotechnology, and it was focused on optical biosensing applications of social interest, such as environmental monitoring and biomedical diagnostics.

**RIASSUNTO**

Una delle più importanti scoperte scientifiche di tutti i tempi è sicuramente la decodifica del genoma umano portata a termine nel 2000 dal progetto internazionale Human Genome Organization. Lo studio del genoma consiste nel descrivere la struttura, la posizione e la funzione dei circa 25.000 geni che caratterizzano la specie umana. A tal fine i genetisti hanno dovuto sequenziare i circa due metri di DNA contenuto in ogni cellula umana e quindi identificare la sequenza di approssimativamente tre miliardi di coppie di basi azotate che ne compongono la molecola. Come in ogni grande impresa scientifica, lo sviluppo tecnologico ha fortemente influenzato i tempi di esecuzione e termine di questo lavoro: basti pensare che il primo miliardo di basi è stato decodificato in quattro anni, mentre il secondo miliardo in solo quattro mesi. Oggigiorno il ritmo di sequenziamento delle basi è dell'ordine di diverse decine di migliaia di basi al minuto, a seconda della tecnologia utilizzata. Lo studio dei geni permette l'identificazione non solo del loro ruolo ma soprattutto dei loro malfunzionamenti che sono alla base delle malattie: le prospettive della medicina genomica sono talmente vaste da non esser ancora state tutte catalogate e pienamente comprese. Il successo del progetto genoma umano è dovuto principalmente ad un fattore chiave: la miniaturizzazione della strumentazione di laboratorio, in particolare di quella dedicata alla PCR (*Polymerase Chain Reaction*) e delle matrici a DNA, i cosiddetti "*microarray*" o "*biochip*", che permettono di esaminare il profilo d'espressione di un gene o di identificare la presenza di un gene specifico con elevatissima precisione e ripetibilità.

I biochip sono una particolare categoria di dispositivi più complessi comunemente indicati come BioMEMS (Sistemi Micro-Elettro-Meccanici Biologici) che, negli ultimi anni, hanno trovato un numero sempre crescente di applicazioni biologiche e biomediche. Lo sviluppo di questi dispositivi è parallelo a quello dei *Lab-on-chip* (LOC) che rappresentano l'evoluzione tecnologica più spinta del laboratorio analitico tradizionale: i LOC sono dei microsistemi complessi che coniugano tutte le funzioni generalmente svolte da strumentazione da banco in un unico dispositivo fabbricato su di un supporto monolitico, tipicamente di silicio cristallino, ed assemblato con altri materiali compatibili, come il silicio poroso ed il vetro o i polimeri, aventi ciascuno una propria specifica funzionalità. Entrambe le due categorie di dispositivi, i *biochip* ed i LOC, beneficano degli sviluppi di quello che è sicuramente il campo più avanzato della tecnologia umana e cioè la microelettronica integrata: la produzione di computer sempre più potenti è legata alla capacità di fabbricare dispositivi su scala micrometrica e nanometrica con una capacità di controllo della materia solida prossima al limite atomico. La possibilità di miniaturizzare la componentistica di laboratorio (separatori, concentratori, analizzatori, sensori, e così via) fa sì che il campo di applicazione dei LOC abbia una evoluzione esponenziale trovando impiego dalla diagnostica al monitoraggio ambientale alla rivelazione di agenti pericolosi nella sicurezza civile e militare, fino alle applicazioni industriali in chimica sintetica (per esempio in prove rapidi in microreattori per la farmaceutica).

A partire dai biochip a DNA, è stata sviluppata una serie di dispositivi che utilizzano altri organismi biologici quali anticorpi, enzimi, proteine, cellule. Data la capacità di queste biomolecole di agire come sonde altamente specifiche rispetto ai rispettivi ligandi, la principale applicazione dei dispositivi è come biosensori e cioè nel riconoscimento della presenza dei ligandi in miscele complesse quale può essere il sangue umano. Un biosensore, il cui schema è rappresentato in Figura 1, lavora con un elemento biologico, detto biorecettore, fissato su un substrato ove avviene una reazione biologica specifica tra il biorecettore e l'elemento ricercato. L'evento di riconoscimento biomolecolare è rilevato da un trasduttore che lo converte in un segnale elettrico, ottico o chimico, che può essere osservato e misurato. La sensibilità e la selettività dei biosensori è tale da poter applicare questi strumenti anche nello studio delle interazioni biomolecolari: un chiaro successo

commerciale di questi dispositivi è il Biacore®, dispositivo ottico comunemente utilizzato nella caratterizzazione della cinetica molecolare e nel calcolo delle costanti di dissociazione e di affinità tra biomolecole.

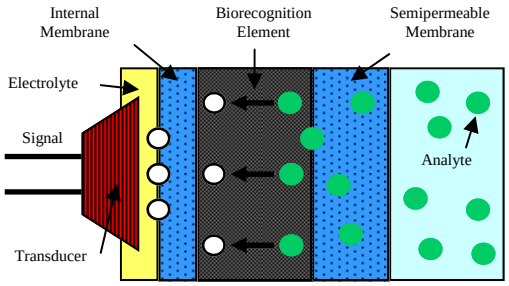


Figura 1 Schema generale di un biosensore.

Sulla base del metodo di trasduzione impiegato, i biosensori possono essere raggruppati, in quattro gruppi fondamentali:

1. Elettrochimici;
2. Termici;
3. Ottici;
4. Acustici;

Le prime due tecniche di trasduzione vengono spesso impiegate nella realizzazione di dispositivi il cui biorecettore è un enzima; mentre i trasduttori più comunemente utilizzati per la realizzazione di biosensori di affinità (anticorpo/antigene) sono di tipo ottico ed acustico. I biosensori ottici sono di gran lunga i più diffusi grazie ad alcuni vantaggi legati alla natura della luce: innanzitutto la possibilità di vedere a livello micrometrico e sub micrometrico la distribuzione delle sonde molecolari con meccanismi di contrasto che vanno dalla fluorescenza al contrasto di fase; la non invasività dovuta alla non interazione di alcune lunghezze d'onda con le biomolecole; l'elevata sensibilità e così via. Se le tecniche di visualizzazione ("*imaging*") e spettroscopia in fluorescenza rappresentano la storia dei saggi biologici e lo stato dell'arte nei *microarray* per applicazioni genomiche, vi è un crescente impulso scientifico e tecnologico, testimoniato da numerosi lavori scientifici negli ultimi cinque anni, per la realizzazione di dispositivi ottici che permettono di misurare direttamente le reazioni di riconoscimento biomolecolare senza dover ricorrere a dei marcatori fluorescenti. Queste tecniche "*label free*" offrono vantaggi non secondari derivanti proprio dall'evitare l'operazione di marcatura con fluorofori della molecola interessata: benché quest'operazione non sia particolarmente complicata, non sempre è possibile disporre di un saggio che prevede la marcatura del ligando, inoltre legare un fluoroforo ad una molecola significa perturbare in maniera non banale la struttura della stessa cambiandone così il comportamento biologico.

Il progetto di ricerca oggetto della presente tesi di dottorato si inserisce in questo filone di ricerca biotecnologica internazionale ed è stato finalizzato in particolare alla realizzazione di un microsistema ottico per lo studio delle interazioni biomelocolari tra singole eliche di DNA oppure tra proteine e ligandi, sia per applicazioni genomiche e proteomiche, ma anche capace di configurarsi come biosensore abile all'individuazione di analiti bersaglio in miscele eterogenee. La realizzazione di un dispositivo del genere è un progetto complesso che può essere schematizzato nelle sue varie fasi come indicato in Figura 2: si parte dall'individuazione di un materiale di supporto che abbia opportune caratteristiche ottiche di trasduzione, che possa essere opportunamente funzionalizzato con sonde molecolari e che possa essere integrato in un microsistema completo di microfluidica. La realizzazione di questo microsistema ha richiesto un approccio fortemente multi-disciplinare nonché l'interazione con figure professionali specializzate in ambiti scientifici complementari ma molto distanti tra loro come la fisica dei semiconduttori, la biologia

molecolare, la chimica delle superfici, l'ingegneria microelettronica. Il materiale scelto quale supporto ed elemento trasduttore è il silicio poroso: la sua caratteristica morfologica è quella di una struttura spugnosa interconnessa da nanocristalli di silicio che possono avere disposizione ordinata o quasi caotica a seconda delle procedure di produzione adottate. Questa morfologia tipica gli conferisce un'elevata superficie specifica che assicura un'efficace interazione con agenti esterni. Inoltre varia fortemente le sue caratteristiche chimico-fisiche quando esposto ad agenti biochimici.
Le problematiche tecnico-scientifiche affrontate nel corso dei tre anni del dottorato, sono state quindi in particolare:

1. la fabbricazione del silicio poroso, quale elemento di supporto del biosensore e sistema di trasduzione del segnale ottico;
2. lo studio di una procedura affidabile di funzionalizzazione della superficie di silicio poroso in grado di ancorare in modo covalente le molecole sonda al materiale supporto;
3. l'individuazione di sonde molecolari particolarmente stabili e compatibili con la realizzazione di biosensori riutilizzabili, quali ad esempio le proteine purificate da organismi estremofili;
4. la messa a punto di opportuni protocolli sperimentali per la definizione dell'attività delle sonde una volta agganciate al supporto trasduttore;
5. lo sviluppo di tecniche di microlavorazione del silicio, del vetro e di altri materiali eventualmente impiegati per la realizzazione di un prototipo di "lab-on-chip", compatibili con l'utilizzo di sonde molecolari biologiche.

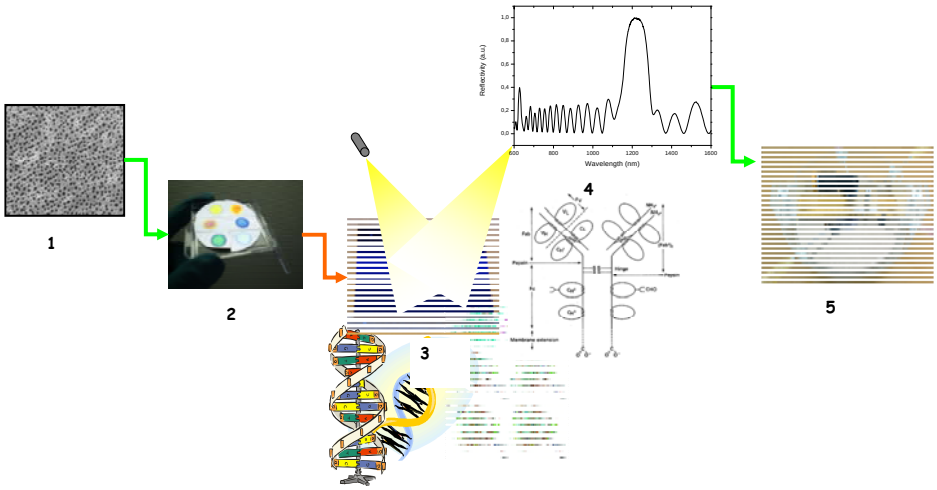

Figura 2: schematizzazione grafica del progetto di tesi

L'integrazione di un biosensore con le tecnologie tipiche della microelettronica e dei circuiti integrati infatti non è mai una evoluzione diretta del dispositivo sensibile in un microsistema, perché l'impiego di sonde biologiche introduce una difficoltà in più legata alla stabilità delle stesse in condizioni di temperatura diverse da quelle ambientali.
Il microsistema realizzato è stato utilizzato per rivelare l'ibridazione tra eliche di DNA complementari e per studiare gli eventi di riconoscimento molecolare tra proteina e ligando. In quanto segue si riportano le metodologie ed i principali risultati ottenuti durante il lavoro di tesi.

**Produzione e caratterizzazione del materiale Silicio Poroso (J3, J11)**
Il Silicio Poroso (PSi) è prodotto per dissoluzione elettrochimica di silicio cristallino drogato, ed ha una morfologia spugnosa che gli conferisce una superficie specifica molto elevata, dell'ordine di alcune centinaia di metri quadri per centimetro cubo. La dissoluzione

del silicio coinvolge due portatori liberi di carica (elettroni *e* e lacune *h*) come riportato nello schema di reazione riportato in Figura 3.

$$Si + 2\,F^{\ominus} + 2\,h^{+} \longrightarrow SiF_2$$

$$SiF_2 + 4\,HF \longrightarrow H_2SiF_6 + H_2 \begin{cases} SiF_2 + 4F^{\ominus} \longrightarrow SiF_6^{2-} + 2e^{\ominus} \\ 2H^{+} + 2e^{\ominus} \longrightarrow H_2 \end{cases}$$

Figura 3: semireazioni di dissoluzione elettrochimica del silicio cristallino

Le dimensioni dei pori della struttura sono variabili da qualche nanometro fino a più di un micron a seconda del tipo di substrato di silicio cristallino utilizzato, della composizione della soluzione chimica e della corrente erogata nella cella durante il processo di fabbricazione.
La porosità **P** è definita come la percentuale di aria presente in uno strato di materiale (ad esempio uno strato di silicio poroso, con porosità del 60 %, sarà composto da silicio nanocristallino solo per il 40 % in massa), e può essere misurata con una tecnica di tipo gravimetrico a partire dal rapporto tra la massa di silicio dissolto $M_{dis}$, durante il processo d'anodizzazione, e la massa totale di silicio sottoposto all'attacco $M_{Si}$. La determinazione dello spessore e della porosità di uno strato prodotto con un singolo processo può essere effettuata alternativamente con un metodo di caratterizzazione ottica quale l'ellissometria spettroscopica ad angolo variabile. Per ottenere una differenziazione tra le varie tipologie di PSi, può essere utilizzata una classificazione in base al diametro medio **d** dei pori (standard IUPAC):

1. Silicio *microporoso* (diametro medio del poro $d < 2nm$);
2. Silicio *mesoporoso* (diametro medio del poro *d* compreso nell'intervallo 2 – 50 nm);
3. Silicio *macroporoso* (diametro medio del poro $d > 50nm$).

Spesso la classificazione fatta utilizzando soltanto la dimensione del diametro ***d*** del poro è riduttiva ed insufficiente per descrivere interamente la struttura dello strato poroso ottenuto. La dimensione dei pori, infatti, non contiene informazioni riguardo la morfologia. Con questo termine s'intende la forma, l'orientazione e l'interazione tra pori. Le proprietà termiche, elettriche, ottiche, del silicio poroso dipendono fortemente sia dal valore della porosità **P** che dalla morfologia della matrice spugnosa. Il parametro che influenza maggiormente la morfologia del PSi è il drogaggio del silicio cristallino di partenza: campioni poco drogati danno pori piccoli e solitamente allineati lungo una direzione privilegiata, mentre campioni molto drogati una volta attaccati si ramificano in una matrice caotica di tipo spugnoso. Alcune morfologie di silicio poroso sono mostrate come esempio in Figura 4.

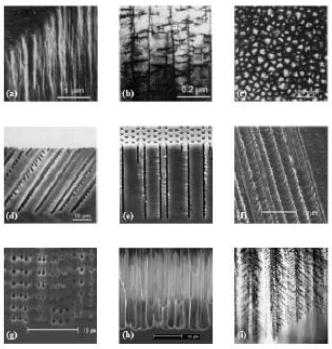

Figura 4: Possibili morfologie di film di silicio poroso su substrati di tipo p e n.

Per ottimizzare l'interazione del silicio poroso con le soluzioni biologiche si è scelto di lavorare con un materiale mesoporoso e cioè costituito da pori con dimensioni medie

dell'ordine dei 10-100 nm. Questo si ottiene dalla parziale dissoluzione di silicio di tipo $p^+$, con elevato numero di portatori liberi di carica dunque, in una soluzione di acido fluoridrico ed etanolo in rapporto 1:1. Per ottenere strati di silicio poroso con porosità e spessore definiti è stato necessario, una volta fissata la composizione della soluzione elettrolitica ed il tipo e livello di drogaggio del substrato di silicio cristallino, calibrare il sistema di produzione e cioè costruire delle curve sperimentali che determinano la velocità di attacco ("*etch rate*" [nm/s] ) e la porosità, ottenuta al variare della densità di corrente applicata alla cella.
Una delle caratteristiche peculiari del processo di produzione del silicio poroso è di essere "*self-stopping*": se si interrompe l'attacco elettrochimico fermando l'erogazione di corrente, lo strato di poroso formatosi è svuotato dai portatori liberi di carica che hanno partecipato alla dissoluzione del silicio cristallino, per cui riprendendo ad erogare corrente il processo riparte dall'interfaccia silicio poroso-silicio cristallino, ove sono presenti i portatori di carica. In questo modo è possibile creare, durante un unico processo di attacco, strati successivi e adiacenti di silicio poroso con spessori e porosità diverse l'uno dall'altro partendo dall'alto (prima superficie esposta) verso il basso (fondo del wafer di silicio cristallino). Il buon controllo del processo di attacco permette la progettazione e la realizzazione di strutture in PSi con specifiche caratteristiche ottiche. È possibile realizzare dispositivi a singolo strato, questi si comportano dal punto di vista ottico come degli interferometri (Fabry-Perot) il cui spettro in riflessione è riportato in Figura 5 *(a)* o progettare dispositivi multistrato a specifiche lunghezze d'onda di risonanza, quali microcavità ottiche *(b)*, specchi di Bragg *(c)* e sequenze Thue-Morse *(d)*.

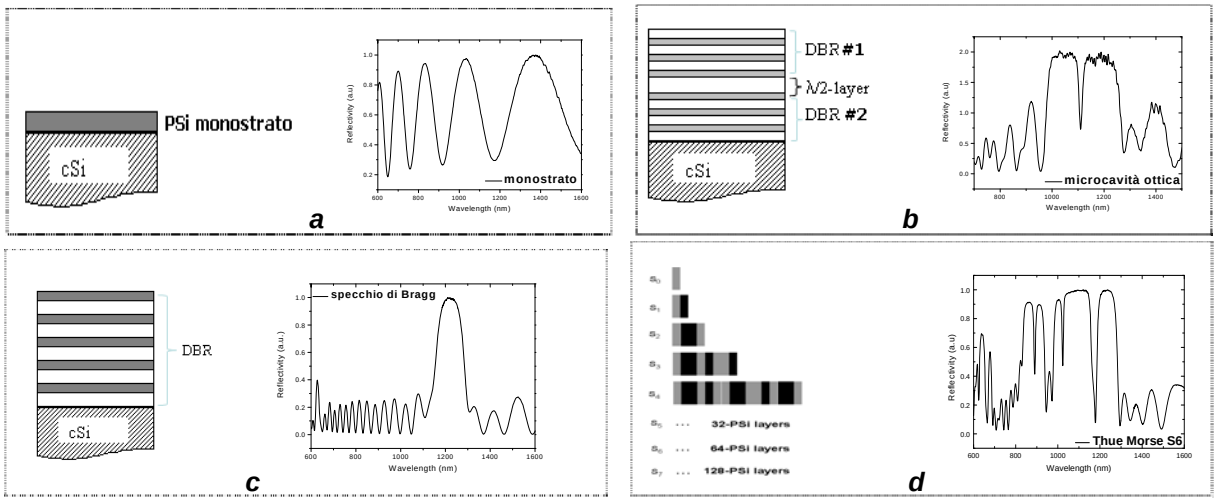

Figura 5: schematizzazioni e spettri in riflessione dei dispositivi in silicio poroso ottenuti illuminando con luce bianca.

Lo spettro in riflessione si ottiene facendo incidere sul dispositivo un fascio di luce collimato, proveniente da una sorgente ad ampio spettro (400-1600 nm), ed inviando la luce riflessa ad un analizzatore ottico di spettro secondo lo schema riportato in Figura 6.

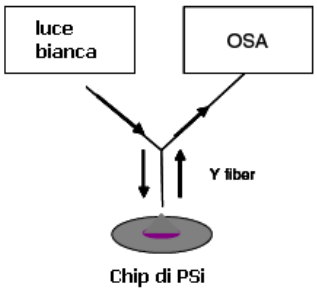

Figura 6: apparato sperimentale utilizzato per misurare gli spettri ottici di riflessione dei campioni in PSi

I sensori ottici basati sul silicio poroso sfruttano le variazioni delle proprietà dielettriche di questo materiale quando esso è esposto all'analita che penetra nei suoi pori. (Figura 7)

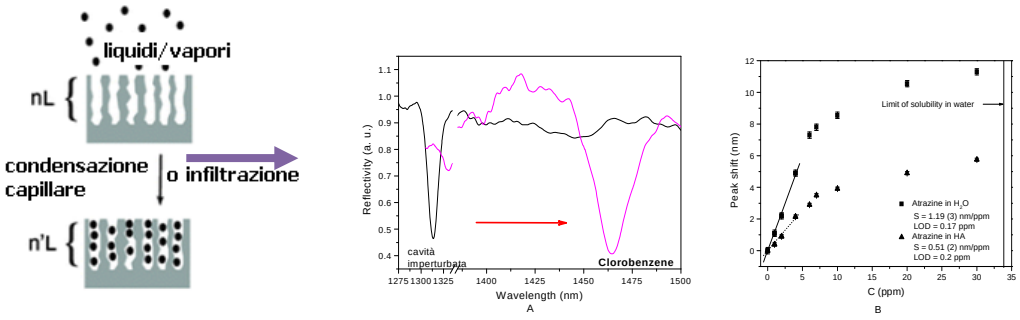


Figura 7: schematizzazioni del meccanismo di riconoscimento; A) spettri in riflessione di una micro cavità ottica sottoposta a vapori di sostanze organiche; B) curva dose-risposta del sensore sottoposto a concentrazioni diverse di pesticida in soluzione acquosa.

L'elevato rapporto superficie-volume del silicio poroso e la risposta ottica dei dispositivi, permettono di monitorare gli effetti dei cambiamenti in indice di rifrazione dello strato di poroso, dovuti alla presenza di sostanze liquide o gassose.La sostituzione dell'aria presente nei pori con le molecole delle sostanze organiche, provoca uno spostamento verso lunghezze d'onda maggiori come indicato nella Figura 7A.
Dal momento che il meccanismo di rivelazione non è selettivo e non riesce a distinguere analiti presenti in miscele complesse è necessario implementare la selettività del silicio poroso utilizzando sonde molecolari ad alta selettività che possono essere legate covalentemente alla sua superficie con opportune tecniche di funzionalizzazione chimica.

**Funzionalizzazione chimica della superficie del Silicio Poroso (J6, J12, J21)**
La superficie del silicio poroso appena prodotto è fortemente reattiva in quanto idrogenata, presenta cioè legami Si-H che sono termodinamicamente instabili: tendono infatti a reagire con l'ossigeno presente in atmosfera per creare legami tipo Si-O-Si molto più stabili. Inoltre una superficie idrogenata è altamente idrofobica, pertanto una passivazione chimica o fisica ha la funzione non solo di indurre specifici legami tra gli atomi di silicio ed altre specie chimiche in modo da essere capace di legare selettivamente composti chimici o molecole di origine biologica, ma anche di rendere la superficie idrofilica in modo da permettere una facile penetrazione del materiale biologico, spesso in soluzione acquosa. In Figura 8 sono riportate le misure di angolo di contatto della superficie del PSi appena prodotto (A), superficie altamente idrofobica ($\theta$=131°), e dopo funzionalizzazione chimica (B) da cui si ottiene una superficie idrofilica ($\theta$=42°).

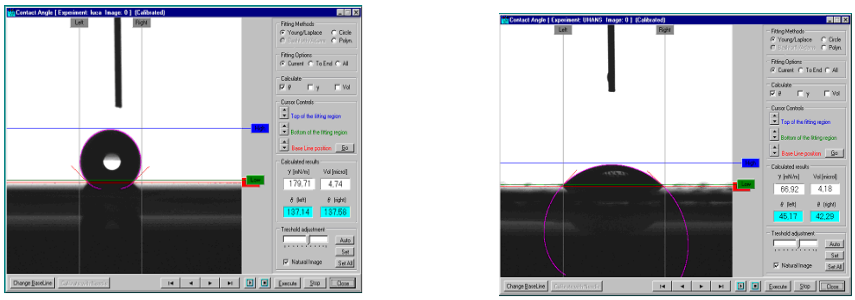

**A** **B**

Figura 8: caratterizzazione della superficie del PSi tramite misure di angolo di contatto. A) la superficie del PSi appena prodotto si presenta altamente idrofobica. B) dopo il processo di passivazione la superficie del PSi diventa idrofilica permettendo così la penetrazione delle soluzioni biologiche.

Un caso particolarmente interessante è quello in cui i legami con l'idrogeno sono sostituiti con legami Si-C  i quali sono molto stabili sia rispetto alle variazioni di temperatura sia rispetto alle interazioni con gruppi nucleofili che hanno grande potere ossidante.
Per individuare la procedura di modifica chimica della superficie di silicio poroso in grado di ancorare in modo covalente le molecole sonda, sono state sperimentate quattro tecniche di funzionalizzazione dei dispositivi ottici:

1. una funzionalizzazione chimica ad opera dei reattivi di Grignard;
2. una funzionalizzazione fotochimica, indotta da radiazione ultravioletta e condotta in atmosfera inerte immergendo il campione in una soluzione di estere succinimmidico  di acido undecenoico;
3. una funzionalizzazione *in situ*, ottenuta introducendo il linker organico, sotto forma di acido carbossilico, direttamente nella soluzione di attacco elettrochimico;
4. una funzionalizzazione della superficie del silicio poroso ossidata ad opera di alcossi silani.

Per analizzare la composizione superficiale del PSi si utilizza la tecnica della spettroscopia infrarossi a trasformata di Fourier (FTIR), che permette di acquisire informazioni sia quantitative sia qualitative riguardo alla chimica della superficie. In Figura 9 è mostrato un esempio di caratterizzazione prima e dopo il processo di funzionalizzazione, si monitora la scomparsa dei picchi caratteristici del PSi appena prodotto (SiH a 2100cm$^{-1}$) a favore della comparsa di quelli caratteristici del linker chimico utilizzato.

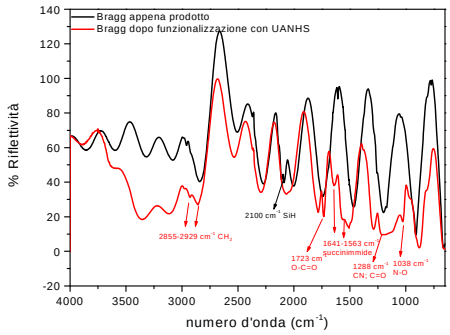


Figura 9: spettro FTIR di un dispositivo in PSi prima (nero) e dopo (rosso) la funzionalizzazione chimica.

Sulla base dei gruppi funzionali disponibili sulla sonda da immobilizzare (DNA singola eliche, proteine, enzimi), è possibile individuare una procedura di passivazione chimica adatta al processo di funzionalizzazione: per esempio, è possibile funzionalizzare la superficie del silicio poroso con un silossano -$NH_2$ terminale in modo da consentire l'ancoraggio di biomolecole o crosslinker carbossi terminali. In Figura 10 si riporta uno schema dei passaggi di funzionalizzazione a partire dal PSi appena prodotto fino all'immobilizzazione delle sonde molecolari.

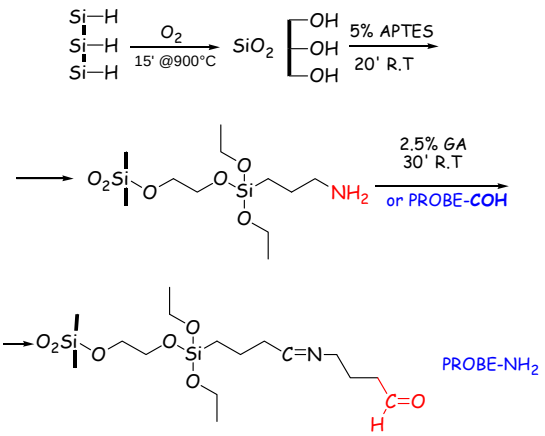


Figura 10: schema di funzionalizzazione chimica della superficie del PSi

Un'alternativa ai metodi classici di funzionalizzazione è rappresentata dalla possibilità di infiltrare un polimero biocompatibile contenente pendagli funzionali regolarmente spaziati lungo la catena. In questo modo i gruppi funzionali sono reattivi e disponibili per l'ancoraggio delle sonde biologiche.
Il polimero scelto per gli esperimenti in questo lavoro di tesi, è il Poli(ε-caprolattone) (PCL), polimero alifatico idrofobico il cui impiego è stato ampiamente studiato negli ultimi anni, in campi di applicazione che vanno dalla realizzazione di tessuti ingegnerizzati al rilascio controllato di farmaci.
Sono state messe a punto le condizioni di deposizione per rotazione veloce ("spin coating"). Questa tecnica è utilizzata per depositare un film sottile ed uniforme su un substrato solido piano. La quantità in eccesso di una soluzione molto diluita della specie che si vuole depositare viene depositata sul substrato, che è successivamente messo in rapida rotazione, al fine di distribuire il fluido sul substrato per effetto della forza centrifuga. È stata quindi determinata la concentrazione ottimale del polimero per avere un film con uno spessore confrontabile con la dimensione dei pori, dell'ordine dei 10 nanometri. In Figura 11 sono riportati lo schema di deposizione per *spin coating* (*a)* ed il grafico della variazione dello spessore del film al variare della concentrazione di polimero (*b*).

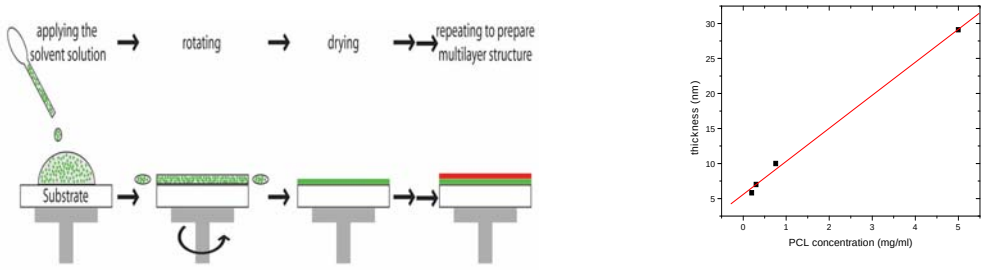


***a*** ***b***

Figura 11: a) Schema di deposizione di film sottili per *Spin coating;* b) variazione dello spessore in funzione della concentrazione di PCL.

La caratterizzazione in spettroscopia ellissometrica ad angolo variabile mostra che l'infiltrazione di PCL porta ad una riduzione di porosità da 79% fino ad un valore di 75.2 % con una disomogeneità verticale nella distribuzione del polimero. Il polimero infatti penetra nell'intera struttura ma si accumula sul fondo dove la presenza di idrogeno è maggiore, a causa dell'interazione idrofobica tra polimero e superficie idrogenata del PSi. Attraverso misure di angolo di contatto, variando la concentrazione del polimero infiltrato, si definisce come varia la bagnabilità della superficie di PSi appena prodotto: all'aumentare della

concentrazione aumenta la bagnabilità della superficie passando così da una superficie idrofobica ad una idrofilica.
Essendo l'idrossido di sodio in soluzione acquosa un agente altamente corrosivo per il silicio poroso, è stata condotta una prova di resistenza ad una soluzione di [NaOH]=0,1M; sono stati realizzati due campioni di PSi gemelli, in uno è stato infiltrato il PCL mentre nel controllo no. Il campione infiltrato ha resistito per 18 minuti alla corrosione dovuta all'NaOH, raggiungendo poi una stazionarietà. È stata infiltrata anche una struttura multistrato in PSi, ed in particolare un Bragg costituito da 15 coppie di monostrati a due porosità diverse. Il dispositivo ha resistito 15 minuti (Figura 12), mantenendo la classica risposta ottica della struttura risonante.

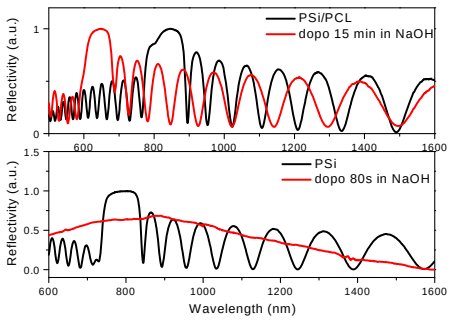


Figura 12: Confronto tra un dispositvo di silicio poroso infiltrato (A) ed uno no (B) prima (nero) e dopo l'immersione in una soluzione di NaOH 0.1 M (rosso).

Sul campione è stato infine condotto un esperimento di sensing di solventi organici, per verificare che il trattamento alcalino non avesse alterato la struttura porosa del dispositivo. Il Bragg funziona ancora come sensore di composti chimici volatili, poiché sottoponendo la struttura ad atmosfera satura di solventi organici questi hanno provocato uno spostamento dello spettro di riflessione verso lunghezze d'onda maggiori, chiaro segno di una sostituzione dell'aria all'interno dei pori con una sostanza ad indice di rifrazione maggiore. Lo spettro si sposta verso il rosso in maniera proporzionale all'aumentare dell'indice di rifrazione delle sostanze, con una sensibilità di 585 nm/RIU (RIU: Unità di Indice di Rifrazione) ed un LOD (Limite di rilevabilità) di $5*10^{-4}$RIU.

**Sonde biologiche utilizzate**
Sono state studiate, in collaborazione con il gruppo di ricerca del Prof. P. Arcari del Dipartimento di Biochimica e Biotecnologie Mediche dell'Università di Napoli "Federico II", le interazioni *ss*DNA-*c*DNA e DNA/PNA

- **DNA:** è stata utilizzata una sequenza singola di DNA (ssDNA: 5'GGACTTGCCCGAATCTACGTGTCCA3',Primm), questa per gli esperimenti di fluorescenza è stata marcata con Fluoresceina CY3.5 (con picco di assorbimento a 581 nm e di emissione a 596 nm).

ed in collaborazione col gruppo del dr. S. D'Auria dell'Istituto di Biochimica delle Proteine del Consiglio Nazionale delle Ricerche le interazioni proteina-proteina quali: GlnBP-Glutamina, GlnBP-Gliadina, e TMBP-Glucosio.

- **Glutamine-binding protein (GlnBP):** la GlnBP, purificata da *E. coli* è una proteina monomerica composta da 224 residui amminoacidici (26 kDa) responsabile del primo step nel trasporto attivo della L-glutamina (Gln) attraverso la membrana citoplasmatica. La Gln è la risorsa principale di azoto e carbonio nel mezzo di coltura cellulare: il suo monitoraggio è quindi fondamentale nel controllo dei bioprocessi. Tra tutti gli amminoacidi presenti in natura la GlnBP lega unicamente la Gln con una costante di dissociazione $K_d$ di $5 \times 10^{-9}$ M. È stata utilizzata anche per

verificare la sua capacità di legare con alta affinità gli amminoacidi presenti nella gliadina (proteina presente in quasi tutti i cereali derivata dal glutine e ritenuta responsabile del morbo celiaco) costituita da una sequenza polimerica di gln.

- **D-trehalose/D-maltose-binding protein (TMBP):** la TMBP è una componente del sistema rifornimento del trealosio (Tre) e del maltosio (Mal) nell'ipertermofilo *T. litoralis*. La TMBP estratta da T. litoralis è una macromolecola (48 kDa) costituita da due domini e contenente 12 residui di triptofano. La struttura tridimensionale della TMBP è comune ad un gran numero di altre proteine atti a legare gli zuccheri. È stato recentemente studiato che la TMBP è capace di legare anche le molecole di glucosio oltre a quelle dei due zuccheri, dimeri del glucosio. Poiché il sangue umano non contiene né Tre né Mal, si è pensato di realizzare un biochip non invasivo per il monitoraggio del glucosio utilizzando questa proteina estratta da estremofili e per questo più stabile rispetto ad altre.

**Studio delle interazioni biomolecolari con dispositivi ottici (J2, J4, J5, J8, J14, J16, J17, J19, J20, J23)**

Una volta messa a punto la procedura di modifica chimica della superficie del silicio poroso sono stati condotti esperimenti di immobilizzazione delle sonde biologiche (DNA singola eliche, proteine, enzimi). Inizialmente sono stati utilizzati campioni marcati con fluorofori, al fine di verificare, con l'ausilio di un macroscopio a fluorescenza, l'efficienza e la stabilità della funzionalizzazione della superficie di silicio poroso.

L'obiettivo finale del progetto è la realizzazione di un sistema ottico di analisi delle interazioni biologiche che non richieda l'uso di marcatori: le interazioni specifiche sonda-ligando vengono studiate mediante riflettometria in luce bianca in strutture fotoniche con precisa risposta ottica, funzionalizzate con sonde non marcate. L'incremento dell'indice di rifrazione medio del dispositivo, dovuto all'introduzione di materiale organico nei pori del dispositivo, che ivi permane anche dopo lavaggi in quanto agganciato alla rispettiva sonda, è rilevabile sperimentalmente da uno spostamento verso lunghezze d'onda maggiori dello spettro in riflessione ottenuto facendo incidere sul dispositivo un fascio di luce collimato, proveniente da una sorgente ad ampio spettro.

La prima parte della sperimentazione è consistita nel determinare la concentrazione ottimale delle sonde per ottenere un ricoprimento uniforme della superficie di silicio poroso. A tal fine sono state utilizzate sonde marcate con un opportuno gruppo cromoforo (Fluoresceina CY3.5, o Rhodamina), tramite la misura dell'intensità di fluorescenza in funzione della concentrazione di sonda, prima e dopo tre lavaggi nelle soluzioni buffer e due dialisi della durata di una notte. In questo modo, sono state stabilite le concentrazioni di saturazione. Passo successivo è, dopo aver legato covalentemente la sonda non marcata alla superficie del silicio poroso, la rivelazione dell'interazione molecolare con il rispettivo ligando misurando lo spostamento dello spettro di riflessione del dispositivo dopo il processo di interazione che avviene direttamente su chip a temperatura ambiente.

Gli esperimenti di riconoscimento molecolare sono stati ripetuti con diverse concentrazioni di ligando. È stato così possibile ottenere curve dose-riposta (Figura 13b) calcolando, per ogni concentrazione di ligando, la differenza di cammino ottico causata dalla variazione dell'indice di rifrazione medio del silicio poroso dovuta all'introduzione del materiale biologico (Figura 13a). Per verificare che la variazione dello spettro di riflessione non fosse dovuta ad interazioni aspecifiche dei ligandi nella struttura porosa, è stata ripetuta la procedura sperimentale utilizzando dei controlli negativi, nei quali non si registrava alcuna variazione dello spettro di riflessione.

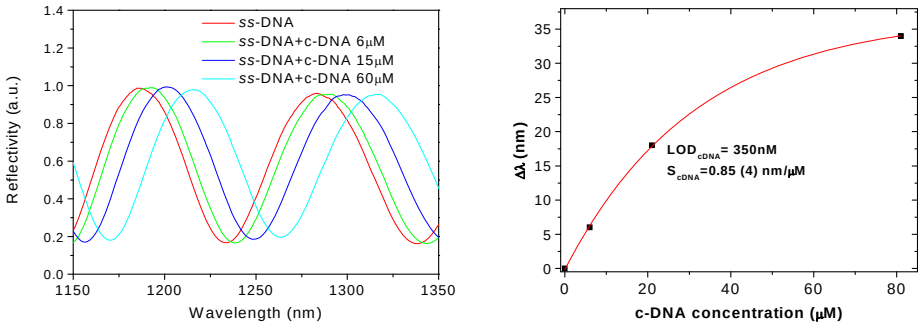


A B

Figura 13: A) spostamento dello spettro di riflessione dovuto all'interazione *ss*DNA-*c*DNA. B) curva Dose-resposta in funzione della concentrazione di *c*DNA.

È stato possibile determinare per ogni coppia sonda-ligando i limiti di rivelazione (LOD) del nostro dispositivo e la sensibilità (S) di misura dello stesso.
Di seguito è riportata la tabella con i valori di concentrazione per le sonde ed i valori di LOD ed S calcolati secondo la metodologia IUPAC (IUPAC Compendium of Analytical Nomenclature, Definitive Rules, 3d Edition, Section 10.3.3.3.14 "Limit of Detection",1997).

| ***Sonda*** | ***Concentrazione*** | ***Ligando*** | ***Controllo negativo*** | ***LOD*** | ***S*** |
|---|---|---|---|---|---|
| ***DNA*** | 60 μM | *c*DNA | *nc*DNA | 350nM | 0.85 nm/μM |
| ***GlnBP*** | 1mM | Gln | Glucosio | 9nM | $3*10^{-2}$nm/nM |
| ***GlnBP*** | 1mM | Gliadina | Prolamina del riso | 670pM | 448 nm/μM |
| ***TMBP*** | 7.5 μM | Glucosio | Gln | 10 μM | 0.03 nm/μM |

**Integrazione del silicio poroso in un *lab-on-chip* (J1, J7, J9, J13, J15)**
La realizzazione di sistemi multifunzionali complessi ove circuiti e componenti elettronici ed ottici, ed elementi di sensing coesistono e operano sinergicamente, è di importanza strategica in diversi settori (produzione-automazione, trasporti, medicina, biochimica, sicurezza e ambiente). La diffusione di tali sistemi multifunzionali, in grado di operare nei più svariati ambienti, anche potenzialmente pericolosi, e che svolgono molteplici funzioni di monitoraggio e di diagnostica, presuppone una drastica riduzione dei costi ed un significativo incremento della loro affidabilità.
L'attività di ricerca relativa a quest'ultima fase del lavoro di tesi è stata volta alla progettazione, realizzazione e caratterizzazione di microsistemi dotati di funzionalità di trasduzione ottica, basati sulle tecnologie di fabbricazione del silicio e dei materiali tecnologicamente compatibili. Poiché la produzione di microsensori ottici, integrabili su chip con altri componenti optoelettronici e microfluidici, necessita della compatibilità con i processi ed i circuiti microelettronici, è stato affrontato il problema dell'integrazione dell'elemento sensibile in silicio poroso in un microsistema ottico in cui tutte le funzioni (alimentazione, analisi, spurgo, e così via) per il funzionamento del trasduttore sono miniaturizzate in un microdispositivo.
Per la realizzazione del dispositivo sono state ottimizzate alcune delle tecniche classiche della microelettronica e delle microlavorazioni, quali gli attacchi anisotropi in KOH, la fotolitografia e gli attacchi acidi del vetro.
È stato inoltre definito un processo di incollaggio anodico "*anodic bonding*" per sigillare il silicio con vetro trasparente compatibilmente con le caratteristiche del silicio poroso.
Il silicio poroso infatti per la sua morfologia spugnosa è abbastanza fragile dal punto di vista meccanico; inoltre la sua superficie idrogenata tende ad ossidarsi facilmente alle temperature tipiche dell'"*anodic bonding*" (400-800 °C) e poiché l'ossido cresce per un

60% al di sopra della superficie occupa parte dei pori con conseguente perdita di superficie specifica e quindi di sensibilità.
Una sperimentazione dedicata ha permesso di stabilire la temperatura minima (250 °C) ed il tempo necessario (2 min.) per ottenere un processo tale da sigillare efficacemente il dispositivo con il vetro. Lo schema del dispositivo realizzato, insieme con il flusso di processo per la fabbricazione, è mostrato in Figura 14*a*, mentre in Figura 14*b* è riportata una fotografia del microsistema su banco ottico.

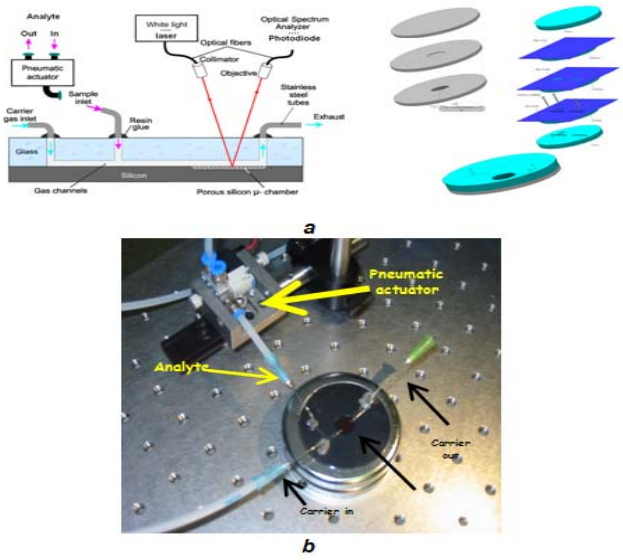


Figura 14: a) Schema del microsistema ottico e flusso di processo per la fabbricazione; *b)* fotografia del microsistema su banco ottico

L'utilizzo di un microsistema di questo tipo riduce enormemente i tempi di risposta del dispositivo la cui durata è essenzialmente dovuta alla diffusione delle specie biochimiche da analizzare all'interno della camera di test dove si trova l'elemento sensibile. Risultati ancora migliori possono essere ottenuti alimentando il sensore con un attuatore pneumatico: il fluido da analizzare, trasportato da un flusso inerte, arriva sul trasduttore solo in determinati intervalli di tempo che possono essere resi piccoli a piacere.
La realizzazione di una matrice di elementi trasduttori richiede la messa a punto di un processo fotolitografico ed uno di attacco per la definizione delle strutture micrometriche. La fotolitografia (come si vede in Figura 15) è quel processo che consente il trasferimento del disegno da realizzare sul silicio da una maschera ad un sottile strato di materiale sensibile alla radiazione (*resist*), che ricopre la superficie del substrato.

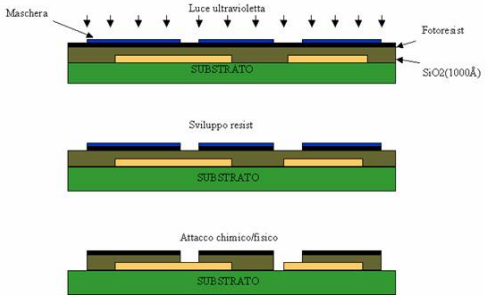


Figura 15: Schema del processo fotolitografico

Una delle tecniche base per la microlavorazione del silicio è quella che utilizza soluzioni acquose alcaline. Comunemente l'attacco umido anisotropo include soluzioni acquose di KOH, miscele di KOH e IPA (alcol isopropilico), oppure EDP (Etilendiammina e Pirocatecolo). Tali soluzioni rendono possibile l'etching del silicio, il quale viene attaccato con differenti velocità nelle varie direzioni cristallografiche.

Di fondamentale importanza è la scelta della maschera fotolitografica da utilizzare durante l'attacco, tenendo conto anche della velocità di incisione da parte della soluzione alcalina sullo strato di mascheramento. Per gli attacchi in KOH si usano generalmente maschere di nitruro di silicio, che non sono attaccabili, diossido di silicio che sono incise con una velocità di 1.4 nm/min e silicio di tipo p che offrono una riduzione sul silicio lievemente drogato della velocità di incisione tra 10:1 e 100:1, a seconda delle concentrazioni delle soluzioni e dalla temperatura del processo.
Per la realizzazione di array di microvaschette con un volume di 10 μl, si è utilizzato una maschera di nitruro di silicio spessa 535 nm ed una soluzione acquose di KOH al 33% in peso alla temperatura di 80 ° C per 160 min.
Il patterning, tuttavia, di campioni di PSi è fortemente limitato. La realizzazione del poroso richiede il contatto del campione con una soluzione HF in flusso di corrente, condizioni molto aggressive per le maschere litografiche comunemente utilizzate. È stato, pertanto, messo a punto e caratterizzato un processo fotolitografico atto a produrre una maschera protettiva da potersi utilizzare per un attacco elettrochimico. La definizione dei parametri di processo finalizzati alla realizzazione della maschera, dalla fotolitografia alla deposizione di film sottili, sono stati di estrema importanza, essendo questi dei processi tecnologici estremamente sensibili all'ambiente nel quale sono effettuati (variazioni anche minime nelle condizioni di temperatura, pressione ed umidità e la presenza di particelle volatili non desiderate minano la riuscita dell'operazione), si è scelto di lavorare in clean room, un laboratorio ad ambiente controllato e depolverizzato.
Partendo da lavori riportati in letteratura è stata deposta e poi fotolitografata una maschera di nitruro di silicio. Le maschere composte da specie al nitruro sono state scelte poiché offrono una buona resistenza all'attacco a fronte di un basso costo di produzione ed un'elevata risoluzione per quel che riguarda il design del substrato. Il campione è stato ricoperto da uno strato di nitruro di silicio, depositato tramite deposizione chimica in fase vapore assistita dal plasma (PECVD), come maschera per l'attacco elettrochimico. Lo stesso è stato poi processato al fine di ottenere il design desiderato. Sono stati messi a punto i parametri di processo per la deposizione regolando opportunamente flussi di silano e ammoniaca.
Le maschere realizzate avevano 400 fori di 200μm di diametro, spaziati tra di loro in entrambe le direzioni di 600μm. È stato quindi condotto l'attacco elettrochimico per ottenere monostrati da 500 nm (spessore minimo per un'analisi all'ellissometro) con porosità del 50% utilizzando una J pari a 50mA/cm$^2$. Una foto dell'array realizzato, acquisita al microscopio ottico è riportata in Figura 16.

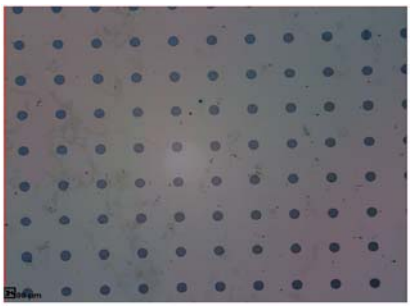

Figura 16: Immagine dell'array di monostrati in PSi acquisita al microscopio ottico: ingrandimento 1.25X

L'analisi riflettometrica, come già descritto, prevede l'utilizzo di una sorgente di luce bianca, da far incidere perpendicolarmente sul campione, ed un analizzatore ottico di spettro, al quale inviare la luce riflessa dal campione stesso. Questa connessione al campione avviene grazie ad una fibra ottica detta 'ad Y' l'unica che strutturalmente ci

consente di inviare luce e convogliare quella riflessa, apparato e spettro ottico di riflessione in Figura 17. La luce, in questo caso, è stata focalizzata sul campione utilizzando un obiettivo 20x, capace di diminuire la focale e restringere lo spot per poter analizzare campioni di poroso di dimensioni micrometriche.

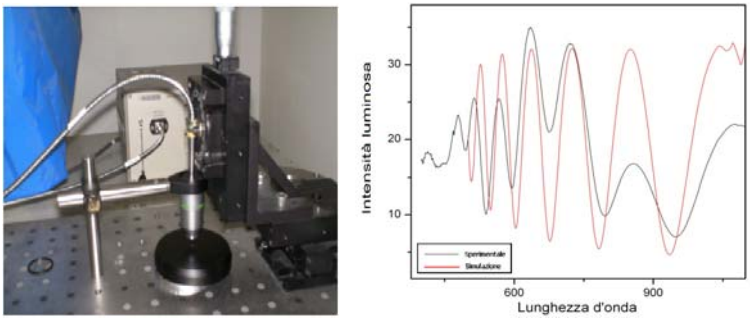


**A** **B**

Figura 17: A)apparato sperimentale utilizzato per misurare gli spettri ottici di riflessione dei campioni dell'array; B) confronto tra lo spettro di riflessione simulato (rosso) e quello sperimentale (nero).

Il dispositivo ottico di array in PSi così realizzato potrà essere applicato in diversi settori, dalla genomica, la post-genomica, la proteomica e le analisi molecolari finalizzate alla diagnostica ad alta automazione per la medicina, la farmacogenomica e l'industria agro-alimentare. Le soluzioni previste porteranno ad un miglioramento significativo del dispositivo in termini di sensibilità, riduzioni dei costi, velocità, predisposizione all'automazione, affidabilità e ripetibilità, in modo da poter monitorare contemporaneamente diversi analiti in miscele complesse.

# Chapter 1
*Porous Silicon*

## Introduction

The development of biochips is a major thrust of the rapidly growing biotechnology industry, which encompasses a very diverse range of research efforts including genomics, proteomics, computational biology, and pharmaceuticals, among other activities. Advances in these areas are giving scientists new methods for unraveling the complex biochemical processes occurring inside cells, with the larger goal of understanding and treating human diseases. At the same time, the semiconductor industry has been steadily perfecting the science of microminiaturization. The merging of these two fields in recent years has enabled biotechnologists to begin packing their traditionally bulky sensing tools into smaller and smaller spaces, onto so-called biochips. These chips are essentially miniaturized laboratories that can perform hundreds or thousands of simultaneous biochemical reactions. Biochips enable researchers to quickly screen large numbers of biological analytes for a variety of purposes, from disease diagnosis to detection of bioterrorism agents.

The development of biochips has a long history, starting with early work on the underlying sensor technology. One of the first portable, chemistry-based sensors was the glass pH electrode, invented in 1922 by Hughes [1]. Measurement of pH was accomplished by detecting the potential difference developed across a thin glass membrane selective to the permeation of hydrogen ions; this selectivity was achieved by exchanges between $H^+$ and SiO sites in the glass. The basic concept of using exchange sites to create permselective membranes was used to develop other ion sensors in subsequent years. For example, a $K^+$ sensor was produced by incorporating valinomycin into a thin membrane [2]. Over thirty years elapsed before the first true biosensor (*i.e.* a sensor utilizing biological molecules) emerged. In 1956, Leland Clark published a paper on an oxygen sensing electrode [3]. This device became the basis for a glucose sensor developed in 1962 by Clark and colleague Lyons which utilized glucose oxidase molecules embedded in a dialysis membrane [4]. The enzyme functioned in the presence of glucose to decrease the amount of oxygen available to the oxygen electrode, thereby relating oxygen levels to glucose concentration. This and similar biosensors became known as enzyme electrodes, and are still in use today.

In 1953, Watson and Crick announced their discovery of the now familiar double helix structure of DNA molecules and set the stage for genetics research that continues to the present day [5]. The development of sequencing techniques in 1977 by Gilbert and Sanger [6] (working separately) enabled researchers to directly read the genetic codes that provide instructions for protein synthesis. This research showed how hybridization of complementary single oligonucleotide strands could be used as a basis for DNA sensing. Two additional developments enabled the technology used in modern DNA-based biosensors. First, in 1983 Kary Mullis invented the polymerase chain reaction (PCR) technique[5], a method for amplifying DNA concentrations. This discovery made possible the detection of extremely small quantities of DNA in samples. Second, in 1986 Hood and coworkers devised a method to label DNA molecules with fluorescent tags instead of radiolabels [7], thus enabling hybridization experiments to be observed optically.

The rapid technological advances of the biochemistry and semiconductor fields in the 1980s led to the large scale development of biochips in the 1990s. At this time, it became clear that biochips were largely a "platform" technology which consisted of several separate, yet integrated components. Figure 1 shows the makeup of a typical biochip platform. The actual sensing component (or "chip") is just one piece of a complete analysis system.

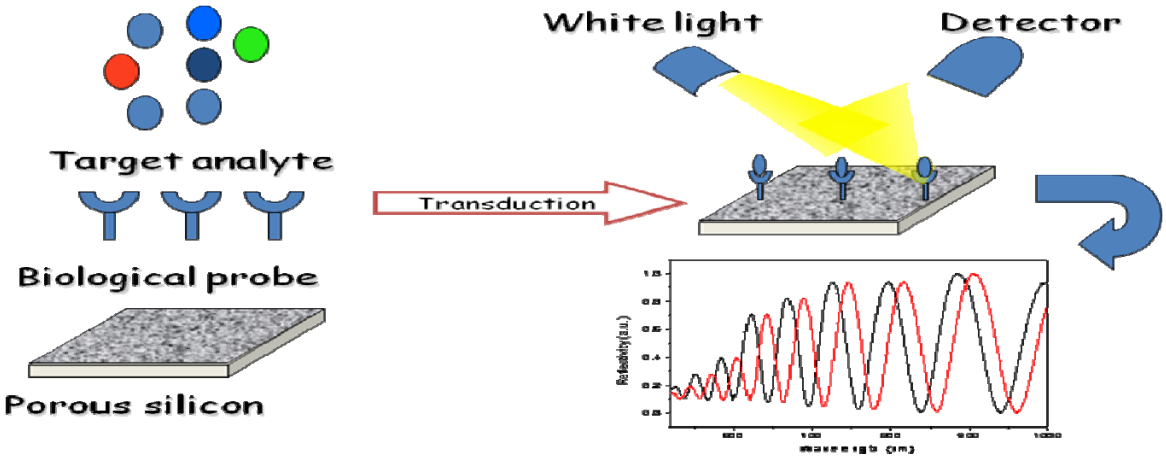


Figure 1: schematic of a biosensor

Transduction must be done to translate the actual sensing event (DNA binding, oxidation/reduction, *etc.*) into a format understandable by a computer (voltage, light intensity, mass, *etc.*), which then enables additional analysis and processing to produce a final, human-readable output. The multiple technologies needed to make a successful biochip — from sensing chemistry, to microarraying, to signal processing — require a true multidisciplinary approach, making the barrier to entry steep. One of the first commercial biochips was introduced by Affymetrix. Their "GeneChip" products contain thousands of individual DNA sensors for use in sensing defects, or single nucleotide polymorphisms (SNPs), in genes such as p53 (a tumor suppressor) and BRCA1 and BRCA2 (related to breast cancer) [8]. The chips are produced using microlithography techniques traditionally used to fabricate integrated circuits (see below).

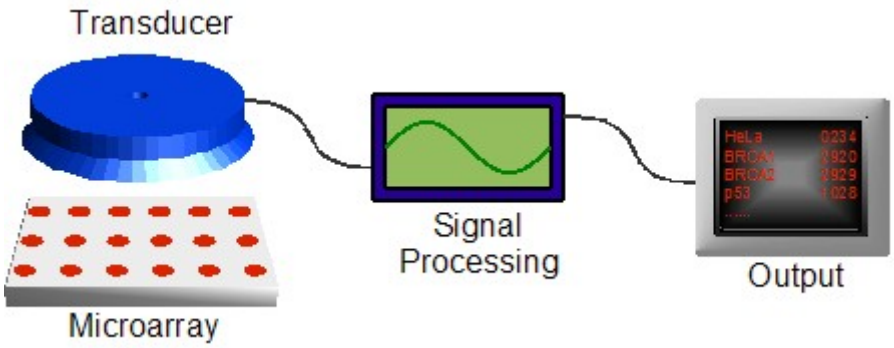


Biochips are a platform that require, in addition to microarray technology, transduction and signal processing technologies to output the results of sensing experiments

Today, a large variety of biochip technologies are either in development or being commercialized. Numerous advancements continue to be made in sensing research that enable new platforms to be developed for new applications. Cancer diagnosis through DNA typing is just one market opportunity. A variety of industries currently desire the ability to simultaneously screen for a wide range of chemical and biological agents, with purposes ranging from testing public water systems for disease agents to screening airline cargo for explosives. Pharmaceutical companies wish to combinatorially screen drug candidates against target enzymes. To achieve these ends, DNA, RNA, proteins, and even living cells are being employed as sensing

mediators on biochips. Numerous transduction methods can be employed including surface plasmon resonance, fluorescence, and chemiluminescence. The particular sensing and transduction techniques chosen depend on factors such as price, sensitivity, and reusability.

Optical transduction is more and more used since photonic devices could be small, lightweight and thus portable due to the integrability of all optical components. Furthermore, optical devices do not require electric contacts. Fluorescence is by far the most used optical signalling method but a wide-use sensor can not be limited by the labelling of the probe nor the analyte, since this step is not always possible.

Reagentless optical biosensors are monitoring devices which can detect a target analyte in a heterogeneous solution without the addition of anything than the sample. In the fields of genomics and proteomics this is a straightforward advantage since it allows real-time readouts and, thus, very high throughoutputs analysis. A label free optical biosensor can be realized by integrating the biological probe with a signalling material which directly transduces the molecular recognition event into an optical signal.

There are many advantages of optical sensing. Optical sensing schemes are sensitive. By measuring differences in wavelengths or times, optical signals can be readily multiplexed. Some optical techniques, such as fluorescence, have intrinsic amplification in which a single label can lead to a million photons. In addition, some optical techniques are zero or “black” background in which the only source of signal is due to the presence of the species being measured, thereby enabling high sensitivity measurements. Finally, optical signals travel in an open path—no wires or other transmitting conduits are necessary. This feature enables remote measurements to be made.

There are a variety of optical sensing transduction mechanisms including:

- Luminescence
- Fluorescence—intensity, lifetime, polarization
- Phosphorescence
- Fluorescence resonance energy transfer
- Absorbance
- Scattering
- Raman-surface enhanced, resonance
- Surface plasmon resonance
- Interference

Each of these techniques may have several variations. Another rubric for classifying optical sensors revolves around the categories of materials, surfaces, and arrays. In the materials field, there is a burgeoning effort in developing new materials for performing optical sensing. Such materials encompass work in the fields of polymers, ceramics, and semiconductors as well as more conventional inorganic and organic materials. These materials can be used as new recognition agents, as supports for immobilizing sensing materials, as materials for concentrating analytes, and as intrinsic optical sensors with integrated functionality including binding and signal transduction. This latter goal of creating materials that integrate binding with optical signal transduction is a major area of interest and investigation.

In the surfaces area, a host of new phenomena are being discovered and employed for biosensing.

It should be noted that there is a growing trend aimed at creating nanoscale devices.

In the past two decades, the biological and medical fields have seen great advances in the development of biosensors and biochips for characterizing and quantifying biomolecules. The biochemistry-based issues may include the characteristics of the recognition molecules in terms of specificity, binding avidity, reversibility of binding, stability under conditions of use and storage, functionality after immobilization, signal generation, biochemical signal amplification, discrimination of specific from nonspecific binding events, reaction time, availability and cost.
Using bioreceptors from biological organisms or receptors that have been patterned after biological systems, scientists have developed new methods of biochemical analysis that exploit the high selectivity of the biological recognition systems [9].
Arrays are being employed for an ever-increasing number of analytes. Ten years ago, the main focus on sensors was specificity and sensitivity. The need to measure multiple parameters was solved by bundling several sensors together in order to multiplex them. Today, arrays with tens of thousands, and even hundreds of thousands of features are commonplace in the DNA microarray field. Most such microarrays use fluorescence signals as the transduction mechanism. The ability to measure so many analytes simultaneously has revolutionized the thinking in sensing in general and optical sensing in particular. It is no longer sufficient in most applications to measure a single analyte as such a measurement captures only part of the information about a complex real-world sample. A variety of interesting and novel methods for preparing arrays have been developed for a wide variety of applications. Arrays also offer the ability to make replicate measurements to minimize false responses and to employ less selective sensing schemes coupled with intelligent processing to remove the requirement for absolute specificity.
Silicon technology is already pervasive in our everyday lives. Silicon 'chips' often help us shop, cook and relax. They are involved in many forms of transport and control most forms of communication at the workplace.
The choice of this thesis for the support material and contemporary for the transducer element fallen on porous silicon.

- *FABRICATION AND CHARACTERIZATION OF POROUS SILICON (PSi) MATERIALS*

The current interest in porous silicon (PSi) results from the demonstration of efficient visible photoluminescence of this material, first reported by Prof. Canham in 1990. However, PSi is not a new material: it was first reported over 40 years ago by Uhlir. During studies of the electropolishing of silicon in aqueous hydrofluoric acid (HF), he observed that the surface often became black, brown or red. More detailed studies were performed by Turner and Archer, but these films were not recognized as being PSi. It was Watanabe et al. who first reported their porous nature. Porous silicon, then, has been investigated for applications in microelectronics, optoelectronics, chemical and biological sensors, and biomedical devices.
The *in vivo* use of porous silicon was first promoted by Leigh Canham, who demonstrated its resorbability and biocompatibility in the mid 1990s. Subsequently, PSi or porous $SiO_2$ (prepared from PSi by oxidation) host matrices have been employed to demonstrate *in vitro* release of the steroid dexamethasone, ibuprofen and many other drugs. The first report of drug delivery from PSi across a cellular barrier was performed with insulin, delivered across monolayers of Caco-2 cells. An excellent review of the potential for use of PSi in various drug delivery applications has recently appeared.

The basic method to fabricate PSi is electrochemical dissolution of single crystalline silicon wafer in a hydrofluoridic acid electrolyte solution. This is obtained by monitoring either the anodic current (galvanostatic) or voltage (potentiostatic).
In general, constant current is preferable as it allows better control of the porosity and thickness. It also provides better reproducibility from sample to sample.
Pore morphology and pore size can be varied by controlling the current density, the type and the concentration of dopant, the crystalline orientation of the wafer, and the electrolyte concentration in order to form macro-, meso-, and micropores. Pore sizes ranging from 1 nm to a few microns can be prepared.
In the simplest setup to fabricate PSi, plates of silicon and Pt are dipped into HF solution and an etching current is applied between these electrodes. The porous layer is formed in the surface of the silicon wafer, which is used as a positive anode. Usually a cathode is made of platinum and the fabrication cell has to be made of HF-resistant material, for example Teflon. Dilute HF solution or ethanolic HF are generally used as electrolytes. Ethanol is added to reduce formation of hydrogen bubbles and to improve the electrolyte penetration in the pores and, thus, uniformity of the PSi layer.
The mechanism of pore formation is not generally agreed upon, but it is thought to involve a combination of electronic and chemical factors. The type of dopant in the original silicon wafer is important because it determines the availability of valence band holes that are the key oxidizing equivalents in the reaction shown in Figure 2.

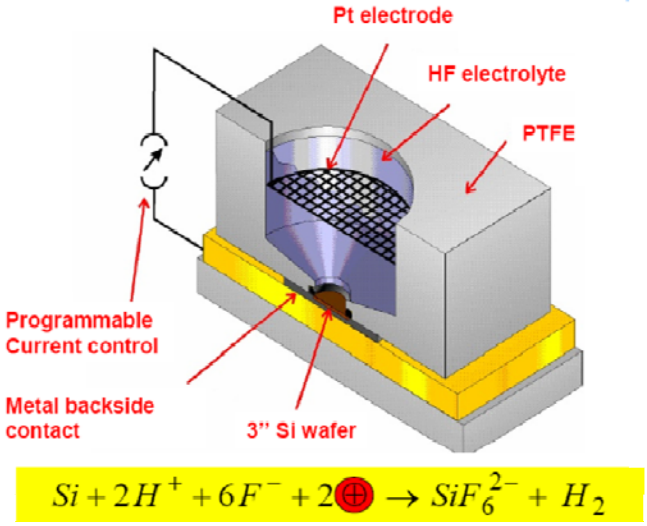


Figure 2: schematic of the etch cell used to prepare porous silicon. The electrochemical half-reactions are shown.

In general the relationships of dopant to morphology can be segregated into four groups based on the type and concentration of the dopant: *n*-type, *p*-type, highly doped *n*-type, and highly doped *p*-type. By "*highly doped*", the dopant levels at which the conductivity behavior of the material is more metallic than semiconducting.
The *n*-type silicon substrate has to be illuminated during anodization to generate photo-excited holes on the surface. For this silicon type wafers, with a relatively moderate doping level, exclusion of valence band holes from the space charge region determines the pore diameter. Quantum confinement effects are thought to limit pore size in moderately *p*-doped material. For both dopant types the reaction is crystal face selective, with the pores propagating primarily in the <100> direction of the single crystal.

A simplified mechanism for the chemical reaction in reported in Figure 3 [10].

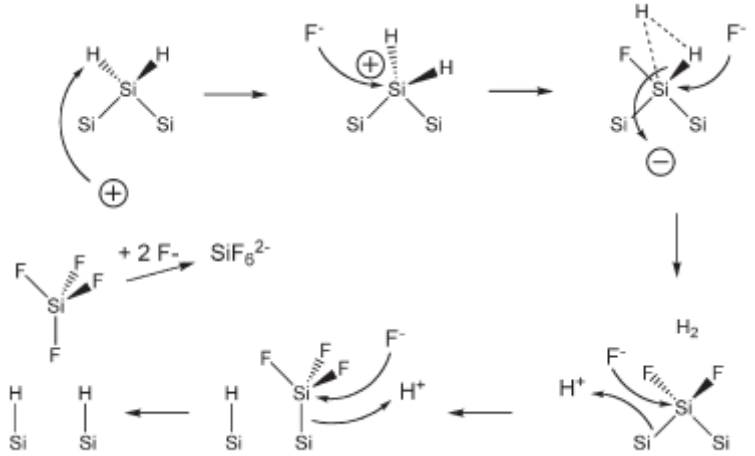


Figure 3: mechanism of silicon oxidation during the formation of porous silicon.

Application of anodic current oxidizes a surface silicon atom, which is then attacked by fluoride. The net process is a 4 electron oxidation, but only two equivalents are supplied by the current source. The other two equivalents come from reduction of protons in the solution by surface $SiF_2$ species. Pore formation occurs as Si atoms are removed in the form of $SiF_4$, which reacts with two equivalents of $F^-$ in solution to form $SiF_6^{2-}$.

The porosity and the thickness of the PSi layers are among the most important parameters which characterize porous silicon. The porosity is defined as the fraction of void within the PSi layer and can be determined easily by weight measurements.

The virgin wafer is first weighted before anodization ($m_1$), then just after anodization ($m_2$) and finally after dissolution of the whole porous layer in a molar NaOH aqueous solution ($m_3$). Uniform and rapid stripping in the NaOH solution is obtained when the PSi layer is covered with a small amount of ethanol which improves the infiltration of aqueous NaOH in the pores. The porosity is given simply by the following equation:

$$P(\%) = \frac{(m1 - m2)}{(m1 - m3)}$$

From these measured masses, it is also possible to determine the thickness of the layer according to the following formula:

$$W = \frac{(m1 - m3)}{S\ x\ d}$$

where d is the density of bulk silicon and S the wafer area exposed to HF during anodization.

The porosity of a growing porous Si layer is proportional to the current density being applied, and it typically ranges between 40 and 80%. Pores form only at the Si/porous Si interface, and once formed, the morphology of the pores does not change significantly for the remainder of the etching process.

However, the porosity of a growing layer can be altered by changing the applied current. The film will continue to grow with this new porosity until the current changes. This feature allows the construction of layered nanostructures simply by

modulating the applied current during an etch. For example, one dimensional photonic crystals consisting of a stack of layers with alternating refractive index can be prepared by periodically modulating the current during an etch.
The ability to easily tune the pore sizes and volumes during the electrochemical etch is a unique property of PSi that is very useful for biological applications. Other porous materials generally require a more complicated design protocol to control pore size, and even then, the available pore sizes tend to span a limited range. With electrochemically prepared PSi, control over porosity and pore size is obtained by adjusting the current settings during the etch. Typically, larger current density produces larger pores. Large pores are desirable when incorporating sizable molecules or drugs within the pores.(Figure 4)

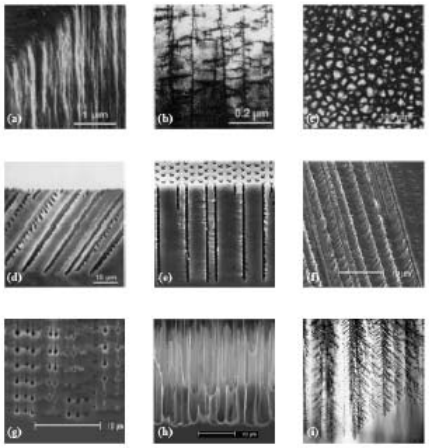

Figure 4: SEM images of typical porous silicon morphologies.

- *Stain etching*

Although the electrochemical anodization is commonly used in the fabrication of PSi, several other fabrication methods have been introduced. One of these methods in a so-called stain etching. The term stain etching refers to the brownish or reddish color of the film of porous Si that is generated on a crystalline silicon material subjected to the process [11]. The stain films are produced by immersion of silicon substrate in HF solution without any electrical bias. This method is even simpler than the previously presented anodization. However, the control of the porosity, layer thickness and pore size of PSi is quite limited. Stain etching in fact is less reproducible than the electrochemical process, although recent advances have improved the reliability of the process substantially [12]. Furthermore, stain etching cannot be used to prepare stratified structures such as double layers or multilayered photonic crystals. However, PSi powders prepared by stain etch are now commercially available (http://vestaceramics.net), and a few additional vendors are poised to enter the market. For the biomedically inclined researcher this eliminates the need to set up a complicated and hazardous electrochemical etching system, and it should stimulate the growth of the field.

- *PSi Photosynthesis*

Another zero-current etching method is photosynthesis. In this approach, silicon substrate is merely illuminated with intense visible light in a HF solution, without electrochemical bias. This is a very interesting method since it allows the fabricating of PSi microstructure without a mask, which is usually used in lithographic methods.

After the etching, the next step to be considered is drying of the PSi material, if a liquid electrolyte has been used. Drying, if the electrolyte in the pores is allowed to evaporate at atmospheric pressure and temperature, may induce cracking and shrinkage. Especially the higher, brittle porosity structures (>75%) often do not have mechanical strength enough to survive the electrolyte evaporation without significant degradation in the structure. This is because the formed liquid vapour interface can generate large capillary stresses. In most cases (porosity <75%), drying of PSi in laboratory air or under nitrogen flush is feasible.
Almost all properties of PSi, such as porosity, porous layer thickness, pore size and shape, as well as microstructure, strongly depend on the fabrication conditions. In the case of anodization, these conditions include HF concentration, chemical composition of electrolyte, current density (and potential), wafer type and resistivity, crystallographic orientation, temperature, time, electrolyte stirring, illumination intensity, and wavelength, etc. Thus, a complete control of the fabrication is complicated and all possible parameters should be taken into account. Fortunately, some of these parameters also depend on each other.
The as-anodized PSi is hydrogen terminated consisting of Si–H, Si–$H_2$, and Si–$H_3$ hydrides. The main impurity observed in PSi is oxygen. Some other minor impurities like carbon and fluorine are also commonly detected shortly after the fabrication. Instead of being real impurities from the anodization process, detected impurities are mainly adsorbed during the storage at ambient or laboratory air. For various applications, the non reactivity of the material is of utmost importance and the need to replace the poorly stable hydrogen termination of the as anodized PSi is obvious.
Already in 1965, Beckmann found out that Psi films were clearly aged when they were stored at ambient air for a long period.[13] This aging is mainly due to the native oxidation of PSi, similar to observations with Si wafers. PSi films slowly oxidized in ambient air depending on the environmental conditions, for example, humidity, temperature, composition of air, etc. Consequently, both the structural and optical properties were continuously changed after storage. Although the aging has been known for a long time and its effects on the properties of PSi have been continuously studied and reported, some authors do not specify the age of their samples.

- *Biocompatibility*

Before 1995, few papers on Si biocompatibility and none on PSi biocompatibility were published, [14]but after the first biocompatibility report by Canham, [15]a lot of work in this field of PSi research has been done. Most of these papers deal with in vitro studies, including calcification, [15-17] cell adhesion and culturing, [18,19]neural networks, protein adsorption, [20-22] and biodegradability studies, [23,24] but also some in vivo assessments of tissue compatibility have been carried out. [25]

Above it was defined that the interaction between an analyte and a biological recognition system is normally detected in biosensors by the transducer element which converts the molecular event into a measurable effect. Due to its sponge-like structure, PSi is an almost ideal material as a transducer: its surface has a specific area of the order of 200 $m^2$ $cm^{-3}$ – 500 $m^2$ $cm^{-3}$, so that a very effective interaction with liquid or gaseous substances is assured. Moreover, PSi is completely compatible with standard IC processes. Therefore, it could usefully be employed in the so-called smart sensors [26]. Recently, lot of experimental work, exploiting the worth noting properties of porous silicon (PSi) in chemical and biological sensing, has been reported [27,28].

PSi optical sensors are based on changes of photoluminescence or reflectivity when exposed to the target analytes which substitute the air into the PSi pores. The effect depends on the chemical and physical properties of each analyte, so that the sensor can be used to recognize the pure substances. Due to the sensing mechanism, these kinds of devices are not able to identify the components of a complex mixture. In order to enhance the sensor selectivity through specific interactions, we have to chemically or physically modify the PSi surface. The common approach is to create a covalent bond between the porous silicon surface and the biomolecules which specifically recognize the target analytes [29].
The reliability of the biosensor strongly depends on the functionalization process: how fast, simple, homogenous and repeatable it is. This step is also very important for the stability of the sensor.
Immediately after silicon electrochemically etched, the surface is covered with reactive hydride species. These chemical functionalities provide a versatile starting point for various reactions that determine the dissolution rate in aqueous media, allow the attachment of biological probes. The two most important modification reactions are chemical oxidation and grafting of Si-C species. In this way the substitution of the Si-H bonds with these ones guarantees a much more stable surface from the thermodynamic point of view.
The integration of sensitive elements into complex microsystems, i.e. lab on chip or micro-total-analysis systems, is of straightforward interest, especially for the miniaturisation of each component. This step is never a trivial one: the fabrication process often requires high temperatures and mechanical stresses which can damage or even destroy the bio- or chemo- sensitive transducer structures.
The anodic bonding (AB) is a standard IC fabrication technique which is widely used in microfluidic due to a wide spectrum of advantages among which the hermetic sealing [30]. Due to the good bonding quality, glass transparency, technological cleanness and high passivity to most of chemicals and biological substances, AB is also commonly exploited in the fabrication of lab-on-chip devices. The compatibility of this primary integration technique with highly demanding sensing micro-components plays a basic role in view of the realization of lab-on-chip devices.
Testing and demonstrating the porous silicon capabilities as a useful functional material in the optical transduction of biochemical interactions is only the first action in the realisation of an optical biochip based on this nanostructured material. In this case, all the fabrication processes should be compatible with the utilisation of biological probes and the feasibility of such devices must be proven. This means that the standard integrated circuit micro-technologies should be modified and adapted to this new field of application in order to preserve the stability of the transducer element and all the biological components (probes and targets). The porous silicon low cost technology could thus provide a link between the conventional CMOS technology and the photonic devices in the realization of the so-called smart sensors and biochips. A very strong interdisciplinary approach is required to match and resolve all the technological problems.
The final objective of this thesis is to design and fabricate different resonant optical structures, integrate them into a simple lab-on-chip devices based on the porous silicon nanotechnology. Some porous silicon surface modification strategies in order to realize an optical biosensor were exploited; the target was the fabrication of sensitive label-free biosensors, which are highly requested for applications in high throughput drug monitoring and diseases diagnostics, unlabeled analytes require in fact easy sample preparation.

**Materials and Methods: Porous Silicon' production calibration**

Today, the electrochemical etching is a standard method to fabricate nanostructured porous silicon: a proper choice of the applied current density, the electrolyte composition, and the silicon doping allow precise control over the morphology and, consequently, on the physical and chemical properties of the porous silicon structure. Computer controlled electrochemical etching processes are exploited for the realization of porous silicon films of controlled thickness and porosity (defined as the percentage of void in the silicon volume).

Nanoporous, mesoporous and macroporous structures can be achieved, with pore size ranging from few nanometers up to microns. Moreover, since the etching process is self-stopping, it is possible to fabricate with a single run process multilayer stacks made of single layers of different porosity. The dielectric properties of each PSi layer, and in particular its refractive index *n*, can be namely modulated between those of crystalline silicon (*n = 3.54*, porosity = 0) and air (*n= 1*, porosity = 100 %); so that alternating high and low porosity layers, lot of photonic structures, such as Fabry-Perot interferometers, omni-directional Bragg reflectors, optical filters based on microcavities, and even complicated quasi-periodic sequences (Thue-Morse) can be simply realized, as it is shown in Figure 5.

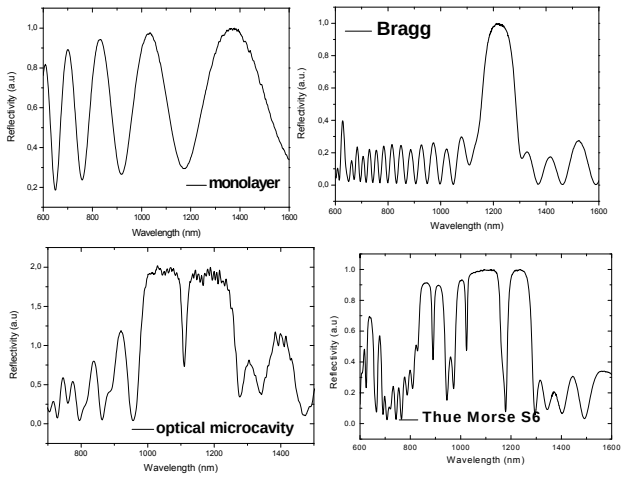


Figure 5. Experimental reflectivity spectra of different PSi optical structures.

In this study Fabry-Perot single layer, Bragg mirrors, Thue Morse and optical microcavities have been used as sensors.

The porous silicon layer was obtained by electrochemical etching in a HF-based solution at room temperature. The substrate used was a highly doped $p^+$-silicon, <100> oriented, 0.01 Ω cm resistivity, 400 μm thick. Before anodization the substrate was placed in HF solution to remove the native oxide. With this substrate we can obtain mesoporous layers, with a pore average dimension of about 50 nm. In figure 6 SEM images are reported.

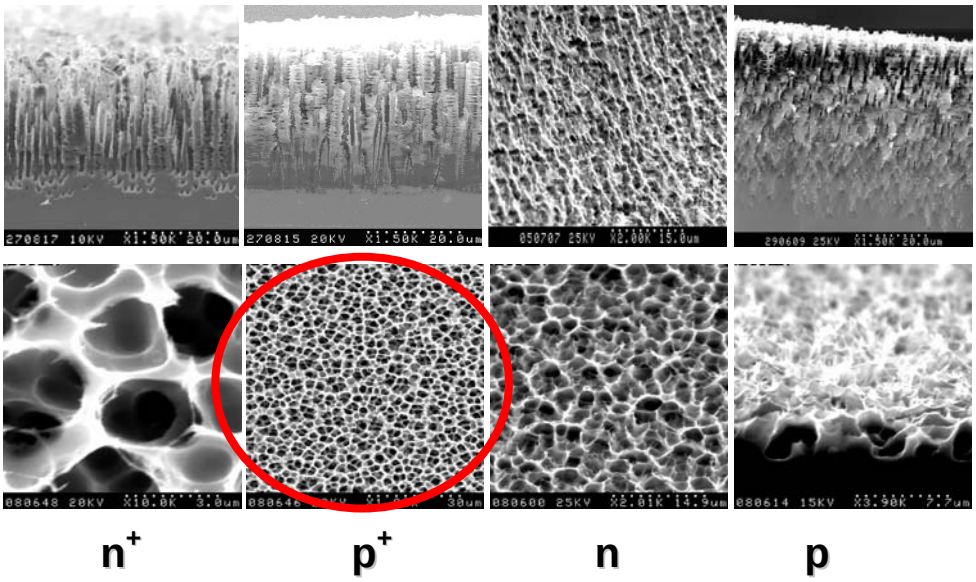


Figure 6. SEM images of different PSi morphologies. The substrate p+ type is the chosen for this work.

The first step of this thesis work was to set the parameters to realize and control the porous silicon fabrication process.
It was checked for the best HF concentration in ethanol solution (HF : EtOH 1:1 and 3:7). The calibration curve for establish the etch rate for each current density and the layer porosity were performed for each HF solution. In Figure 7 the two calibrations curves are reported to clarify.

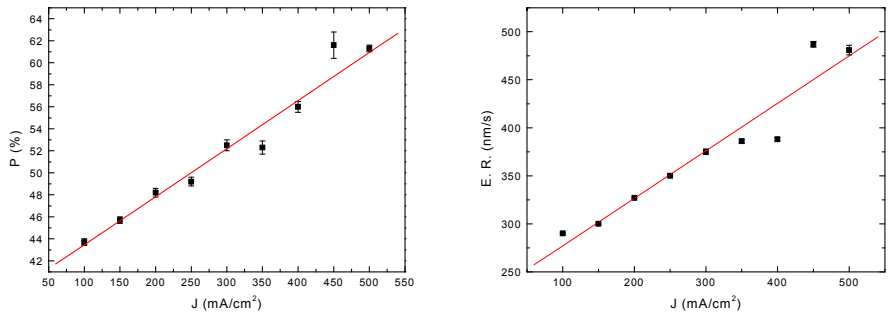


A

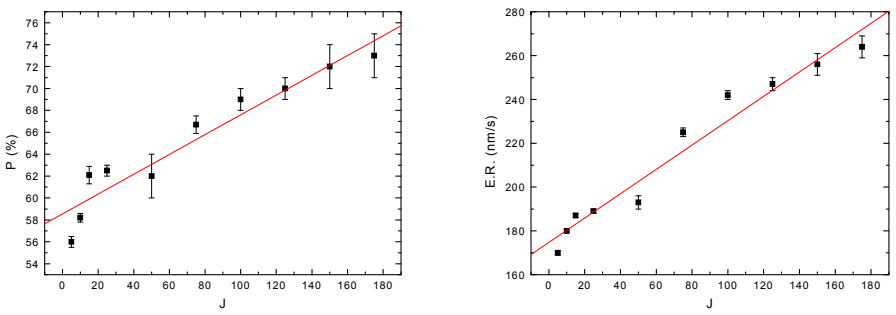


B

Figure 7. Silicon wafer: p+ type, <100> orientation, 8-12 mW cm resistivity. A) Etching solution: HF/EtOH=50/50; B) Etching solution: HF/EtOH=30/70.

The morphology of the porous silicon layers was investigated by variable angle spectroscopic ellipsometer (UVISEL, Horiba-Jobin-Yvon) and scanning electron microscope (SEM-FEG Gemini 300, Carl Zeiss).
Both the analytical techniques have showed the presence of a top layer on the porous silicon structure of thickness between 20 nm and 100 nm and porosity of 20-40 % due to hydrogen contamination of the silicon wafer [31]. Such film prevents not only the pores from filling but also any biochemical interaction with the hydrogenated porous silicon surface after the etching process. For sensing purposes it is therefore mandatory to avoid the formation of the parasitic film by thermal treating the wafer at 300 °C in nitrogen atmosphere before the electrochemical etch [32].
In figure 8 a cross section SEM image of the PSi top surface is reported. The thin low porosity layer on the top of the porous silicon device is well evident. In the thermal treated silicon wafer, this top layer is absent. The same result is confirmed by ellipsometric measurements.

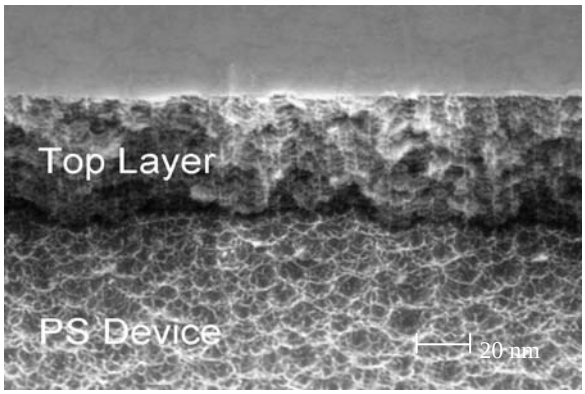


Figure 8: Cross section scanning electron microscopy image of a porous silicon layer.

Due to the nanostructured nature of PSi, it is essential to improve the pore infiltration of biomolecular probes: to this aim, the device was optimized employing a strong base post etch process. By immersing the device in an aqueous ethanol solution, containing millimolar concentration of KOH, for 15 min. This treatment produces an increase of about 15-20% the porosity without affecting the optical quality of the device [33]. The presence of Si-H bonds on the porous silicon surface has been monitored by means of infrared spectroscopy with a Fourier transform spectrometer (FT-IR Nicolet Nexus) [33].
The fresh etched porous silicon device shows the characteristic peaks of Si-H bonds at 910 $cm^{-1}$ and 2100 $cm^{-1}$. The KOH post-etch treatment used to increase the porosity and to improve the pore infiltration by biological solutions, unfortunately removes most of these bonds and oxidizes the PSi. To restore the Si-H bonds the porous silicon device were rinsed in a low concentration HF-based solution (5 mM) for 30 s.
Figure 9 shows the FT-IR spectrum of a porous silicon microcavity after KOH and HF treatments. The Si-H bonds, removed by KOH, are present again and the silicon dioxide fingerprint (at 1050-1100 $cm^{-1}$) disappears.

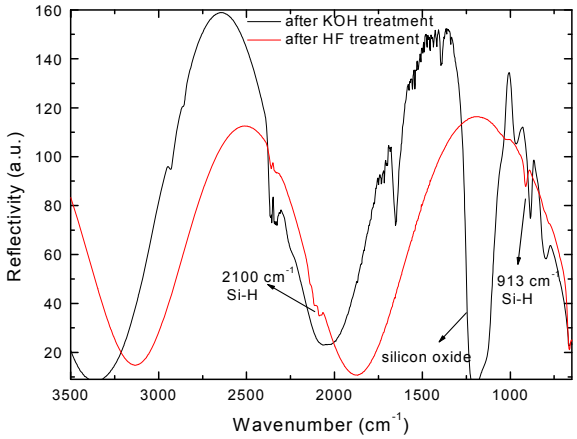


Figure 9: FT-IR spectrum of a porous silicon microcavity after KOH and HF post-etch treatments.

The experimental set-up (see Figure 10) to characterize the PSi devices from an optical point of view is very simple: a tungsten lamp (400 nm < λ < 1800 nm) inquired, through an optical fiber and a collimator, the sensor closed in a glass vial which can be fluxed by liquids or gases. The reflected beam is collected by an objective, coupled into a multimode fiber, and then directed in an optical spectrum analyser (Ando, AQ6315A). The reflectivity spectra had been measured with a resolution of 0.2 nm.

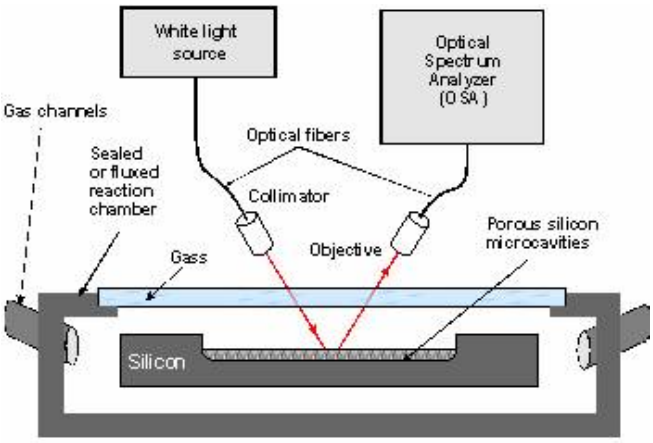


Figure 10: optical set-up

In Figure 11 the optical reflectivity (as explicative example) spectra of a porous silicon layer as-etched and post KOH and HF treatments are reported, in order to show that the optical response of the devices is not affected by the strong chemical treatments.

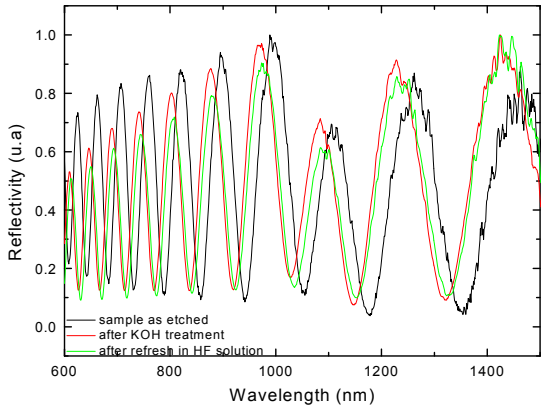


Figure 11: Reflectivity optical spectra of the porous silicon layer after KOH and HF treatments.

In this chapter, are presented some experimental results about sensing of chemical substances, flammable and toxic organic solvents and also some hydrocarbons, using several porous silicon optical structures with different pores structures.

## References


1. Hughes 1922. *J. Amer. Chem. Soc*. *44*, 2860.
2. J.B. Schulz, M. Weller and T. Klockgether, *J. Neurosci*. 1996, *16* : 4696–4706
3. L.C. Clark, *Trans. Am. Soc. Art. Int. Org.* 1956 *2*, 41–52.
4. L.C. Clark Jr. and C. Lyons, *Ann. NY Acad. Sci.* 1962, *102:* 29–45.
5. Kubisiak, T.L., Nelson, C.D., Nowak, J., and Friend, A.L. J. Sustain. For. 2000, 10, 69-78.
6. Sanger F, Air GM, Barrell BG, Brown NL, Coulson AR, Fiddes CA, Hutchison CA, Slocombe PM, Smith M. *Nature.* 1977 Feb 24;265(5596):687–695
7. L.M. Smith, J.Z. Sanders, R.J. Kaiser, P. Hughes, C. Dodd, C.R. Connell, C. Heiner, S.B.H. Kent and L.E. Hood. Nature (London) 321 1986, pp. 674–679
8. Ward I.M. and Chen,J. 2001 *J. Biol. Chem.*, 276:, 47759–47762
9. Sadana A 2002 Engineering Biosensors (San Diego, CA: Academic)
10. V. Lehmann, U. Gosele, *Appl. Phys. Lett*. 1991 *58:* 856–858.
11. R.J. Archer, *J. Phys. Chem. Solids* 1960 *14:* 104–110.
12. E.A. de Vasconcelos, E.F. da Silva, B. dos Santos, W.M. de Azevedo, J.A.K. Freire, *Phys. Status Solidi A—Appl. Mat.* 2005 *202* : 1539–1542.
13. Beckmann KH. 1965. *Surf Sci* 3:314–332.
14. Canham LT, Aston R. 2001. *Phys World* 14: 27–31.
15. Canham LT. 1995. Bioactive silicon structure fabrication through nanoetching techniques. *Adv Mater* 7:1033–1037.
16. Canham LT. 1997. Biomedical applications of porous silicon. In: Canham LT, editor. Properties of porous silicon. EMIS Datareview series No 18. London: INSPEC. pp 371–376.
17. Canham LT, Reeves CL, King DO, Branfield PJ, Crabb JG, Ward MCL. 1996. Bioactive polycrystalline silicon. Adv Mater 8:850–852.
18. Bayliss SC, Buckberry LD, Harris PJ, Tobin M. 2000. Nature of the silicon-animal cell interface. J Porous Mater 7:191–195.
19. Bayliss SC, Heald R, Flecther R, Buckberry LD. 1999. The culture of mammalian cells on nanostructured silicon. Adv Mater 11:318–321.
20. Karlsson LM, Tengvall P, Lundstrom I, Arwin H. 2003. Adsorption of human serum albumin in porous silicon gradients. Phys Stat Sol (a) 197: 326–330.
21. Karlsson LM, Tengvall P, Lundstrom I, Arwin H. 2003. Penetration and loading of human serum albumin in porous silicon layers with different size and thicknesses. J Colloid Interface Sci 266:40–47.
22. Prestidge CA, Barnes TJ, Mierczynska-Vasilev A, Kempson I, Peddie F, Lau CH, Barnett C. 2007. Peptide and protein loading into porous silicon wafers. Phys Stat Sol (a) In press.

23. Anderson SHC, Elliot H, Wallis DJ, Canham LT, Powell JJ. 2003. Dissolution of different forms of partially porous silicon wafers under simulated physiological conditions. Phys Stat Sol (a) 197: 331–335.
24. Canham LT, Reeves CL, Newey JP, Houlton MR, Cox TI, Buriak JM, Stewart MP. 1999. Derivatized mesoporous silicon with dramatically improved stability in simulated human blood plasma. Adv Mater 11:1505–1507.
25. Bowditch AP, Waters K, Gale H, Rice P, Scott EAM, Canham LT, Reeves CL, Loni A, Cox TI. 1999. In-vivo assessment of tissue compatibility and calcification of bulk and porous silicon. Mat Res Soc Symp Proc 536:149–154.
26. De Stefano L., Moretti L., Rendina I., Rossi A. M., Tundo S. (2004), “Smart optical sensors for chemical substances based on porous silicon technology”, Appl. Opt. 43, No. 1, 167-172.
27. De Stefano L., Moretti L., Rossi A. M., Rocchia M., Lamberti A., Longo O., Arcari P., Rendina I., (2004), “Optical sensors for vapors, liquids, and biological molecules based on porous silicon technology”, IEEE Trans. Nanotech. Vol. 3 n. 1, 49-54.
28. Dancil K.-P. S., Greiner D. P., and Sailor M. J. (1999), “A Porous Silicon Optical Biosensor: Detection of Reversible Binding of IgG to a Protein A-Modified Surface”, J. Am. Chem. Soc. 121, 7925-7930.
29. Hart B. R., Letant S. E., Kane S. R., Hadi M. Z., Shields S. J. and Reynolds J. G. (2003), “New method for attachment of biomolecules to porous silicon”, Chem. Comm., 322-323.
30. Ljibisa Ristic, Sensors Technology and Devices, pp. 207, 1994.

31. Gaillet M., Guendouz M., Ben Salah M., Le Jeune B., Le Brun G., Thin Solid Film 455-456, 410 (2004).
32. V. Chamard, G. Dolino and F. Muller, J. Appl. Phys. 84, 6659 (1998).
33. Socrates G., Infrared and Raman characteristic Group Frequencies (Wiley, England 2001).

## Thue-Morse: aperiodic multilayers made of porous silicon

This section is aimed at the optimization of the fabrication process and the characterization of the Thue-Morse $S_0$-$S_7$ sequences by using the PSi technology.

phys. stat. sol. (c) **4**, No. 6, 1966–1970 (2007) / **DOI** 10.1002/pssc.200674342

# Optical properties of porous silicon Thue-Morse structures

**Luca De Stefano**[*, 1], **Ilaria Rea**[1], **Lucia Rotiroti**[1], **Luigi Moretti**[2], and **Ivo Rendina**[1]

[1] Institute for Microelectronics and Microsystems, National Council of Research, Via P. Castellino 111, 80131 Naples, Italy
[2] DIMET "Mediterranea" University of Reggio Calabria, Località Feo di Vito, 89060 Reggio Calabria, Italy

Received 17 March 2006, revised 15 September 2006, accepted 15 November 2006
Published online 9 May 2007

**PACS** 42.70.Qs, 78.66.Db, 78.67.–n, 81.05.Rm

Dielectric aperiodic Thue-Morse structures up to 128 layers have been realized by the porous silicon technology. Normal incidence reflectivity measurements have been performed to investigate the photonic properties of the devices. A partial photonic band gap region, centered at 1100 nm and 70 nm wide has been observed for the $S_6$ and $S_7$ Thue-Morse structures. The $S_6$ multilayer has been studied as sensor device on exposure to several chemical substances.

© 2007 WILEY-VCH Verlag GmbH & Co. KGaA, Weinheim

## 1 Introduction

In recent years, dielectric photonic band gap (PBG) structures have attracted great attention for their property to forbid the propagation of the light at fixed wavelengths and the possibility to realize an all-optical integrated circuit which is the basic element of the optical computer [1, 2]. The simplest, one dimensional PBG structure is the Bragg mirror which is made of alternating layers of high ($n_H$) and low ($n_L$) refractive index, whose thicknesses satisfy the Bragg relation $2(n_Hd_H+n_Ld_L) = \lambda_Bm$ where m is the order of the Bragg condition. Lot of theoretical and experimental studies on these periodic structures have shown that they are characterized by the presence of only one degenerate PBG in a period of the reciprocal space, even if it can be omnidirectional [3]. On the contrary, multiple PBGs are typical of aperiodic structures. The main example of 1D aperiodic multilayer is given by the Thue-Morse sequence which can be obtained alternating high (A) and low (B) refractive index layers following the substitution rules A→AB and B→BA [4]. The lower-orders of the Thue-Morse sequence are: $S_0$=A, $S_1$=AB, $S_2$=ABBA, $S_3$=ABBABAAB, $S_4$=ABBABAABBAABABBA, and so on. Dielectric Thue-Morse multilayers have been already demonstrated using $Si/SiO_2$ and $TiO_2/SiO_2$ as high/low refractive index materials [5, 6] and recently also in porous silicon (PSi) [7]. In this study we have fabricated and characterized the Thue-Morse $S_0$-$S_7$ sequences by using the PSi technology. The PSi is a very attractive material due to the possibility of realize in only one process multilayered structures that exploit a high quality optical response. PSi is obtained by the electrochemical etching of crystalline silicon in a hydrofluoridric acid (HF) based solution. The porosity and the thickness of a single layer are linear functions of the current density and the anodization time for a fixed doping level of the silicon wafer and HF concentration. The refractive index of the PSi film depends on its porosity, and can be calculated in the frame of several effective medium approximations, like the Bruggemann or Maxwell-Garnett models [8]. Moreover, the PSi is an ideal material for sensing applications because it is characterized by a very large specific surface area (200-500 $m^2$ $cm^{-3}$), so that an effective interaction with several substances is assured.

[*] Corresponding author: e-mail: luca.destefano@na.imm.cnr.it, Phone: +390816132375, Fax: +390816132598



© 2007 WILEY-VCH Verlag GmbH & Co. KGaA, Weinheim

## 2 Materials and methods

A highly doped $p^+$-silicon, <100> oriented, 0.01 Ω cm resistivity, 400 μm thick was used as substrate to realize the Thue-Morse structures. Samples were fabricated in dark light at room temperature using a solution of 30% volumetric fraction of aqueous HF (50% wt) and 70% of Ethanol. Before anodization, we have removed the thin film of native oxide from the silicon wafer by rapid rinsing it in a diluted HF solution. High porosity layers, with an average refractive index $n_H \cong 1.3$ and a thickness $d \cong 135$ nm, were obtained applying a current density of 150 mA/cm$^2$ for 0.88 s. Low porosity layers, with an effective refractive index $n_L \cong 1.96$ and a thickness of $d \cong 90$ nm, were obtained with a current density of 5 mA/cm$^2$ for 0.53 s. The thickness $d$ of each layer was designed to satisfy the Bragg condition $dn = \lambda_B/4$ where $n$ is the average refractive index and $\lambda_B$=700 nm. Thicknesses and porosities have been estimated by variable angle spectroscopic ellipsometry measurements on the single PSi layers.
An Y optical reflection probe (Avantes), connected to a white light source and to an optical spectrum analyzer (Ando, AQ6315A), has been used for the reflectivity measurements at normal incidence. The reflectivity spectra were measured between 600 and 1600 nm with a resolution of 0.2 nm.
Reflectivity measurements on exposure to volatile substances have been performed in a steel test chamber equipped with an optical access through a quartz window and in/out channels for gas feeding.

## 3 Results and discussion

A scheme of the porous silicon Thue-Morse sequences realized is reported in Fig. 1: the number of the layers increases, as $2^n$ where $n$ is the Thue-Morse order, while the thickness of the devices is $d_{Sn} = 2d_{Sn-1}$ for n > 1. The realized samples $S_0$-$S_7$ have thicknesses spanning the range between 0.135 μm and 14.4 μm.

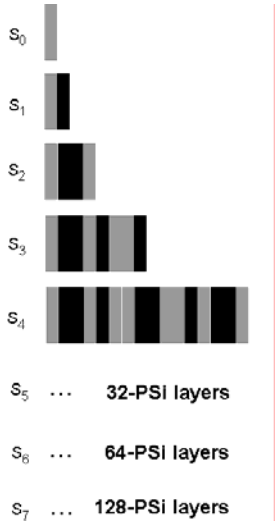


**Fig. 1** Scheme of the porous silicon Thue-Morse sequences realized and characterized in the present work.

In Figs. 2 and 3 the experimental (solid line) and calculated (dash line) normal incidence reflectivity spectra are reported for $S_3$ (2-a), $S_4$ (2-b), $S_5$ (2-c), $S_6$ (3-d), and $S_7$ (3-e) Thue-Morse structures which are constituted by 8, 16, 32, 64 and 128 layers, respectively. The reflectivity spectra have been reproduced by a transfer matrix method [9] including the wavelength dispersion of silicon. At the increasing of the layers number we can observe a worsening of the agreement between the experimental and calcu-

 © 2007 WILEY-VCH Verlag GmbH & Co. KGaA, Weinheim

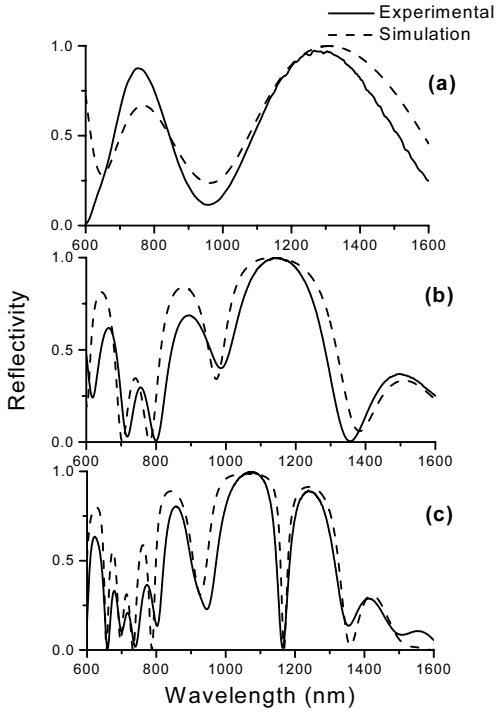


**Fig. 2** Experimental (solid line) and calculated (dashed line) normal incidence reflectivity spectra for $S_3$ (a), $S_4$ (b) and $S_5$ (c) Thue-Morse structures.

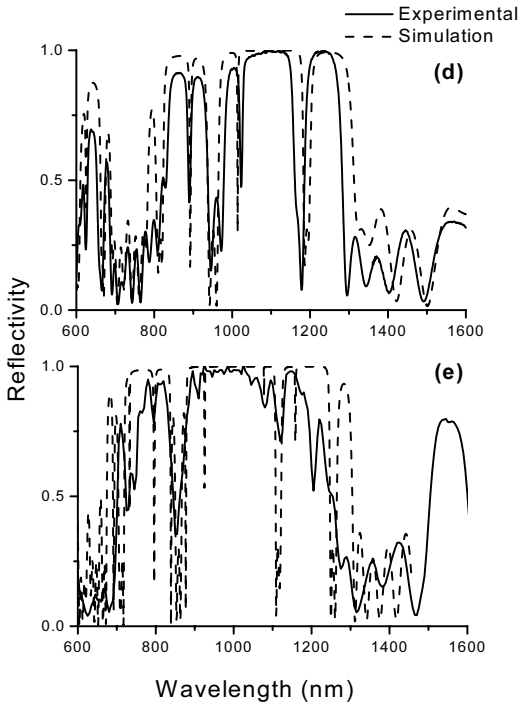


**Fig. 3** Experimental (solid line) and calculated (dashed line) normal incidence reflectivity spectra for $S_6$ (d) and $S_7$ (e) Thue-Morse structures.

lated spectra. This effect is due to small porosity and thickness dishomogeneities of the deeper layers, and to scattering losses, caused by interfaces roughness. The spectrum of $S_3$ Thue-Morse is characterized by two band gaps separated by a transmission peak at 1000 nm. At the increasing of the order of Thue-Morse sequence, the photonic band gap splits and very narrow transmission peaks appear. This is a well known effect due to the random nature of the aperiodic Thue-Morse: the eigenstates, i.e. the stationary configurations of the electromagnetic field, are more localized respect to the periodic and quasi-periodic geometrical structures, such as the Bragg and the Fibonacci geometries, respectively [10].

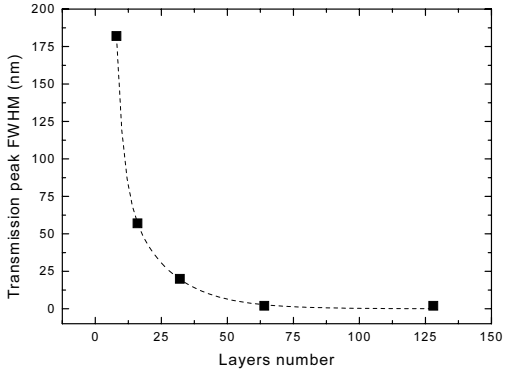


**Fig. 4** Full width at half maximum of the transmission peaks in the experimental reflectivity spectra of S3-S7 sequences.

© 2007 WILEY-VCH Verlag GmbH & Co. KGaA, Weinheim 

The Fig. 4 reports the full width at half maximum (FWHM) of the transmission peaks present in the reflectivity stop bands spectra of the $S_3$-$S_7$ Thue-Morse structures: on increasing the number of the layers the peak width decreases exactly as an exponential function ($R^2 = 0.998$).
The presence of resonant peaks in the reflectivity spectrum suggests the use of such porous structures as optical transducers for gas and liquid monitoring. The $S_6$ Thue-Morse structure has been investigated as sensor device on exposure to several vapors [11, 12]. The gaseous substances penetrate into the nanometric pores, substituting the air. The average refractive indexes of the layers change, so that the reflectivity spectrum of the device shifts towards higher wavelengths. In Figure 5 the red-shift of the $S_6$ structure transmission sharp peak at 1000 nm is reported as a function of the refractive index of each volatile substance. A linear response is observed and a sensitivity of 530 (50) nm/RIU (Refractive Index Unit) can be estimated.

**Table 1** Central wavelength and width of the photonic and fractal theoretical stop band.

| TM Structure | PBG | | I FBG | | II FBG | |
|---|---|---|---|---|---|---|
| | λ (nm) | Width (nm) | λ (nm) | Width(nm) | λ (nm) | Width (nm) |
| $S_3$ | 766 | 161 | 1307 | 452 | 0 | 0 |
| $S_4$ | 880 | 149 | 1138 | 324 | 0 | 0 |
| $S_5$ | 840 | 111 | 1060 | 210 | 1240 | 146 |
| $S_6$ | 870 | 114 | 1084 | 218 | 1250 | 112 |
| $S_7$ | 813 | 119 | 1029 | 230 | 1216 | 125 |

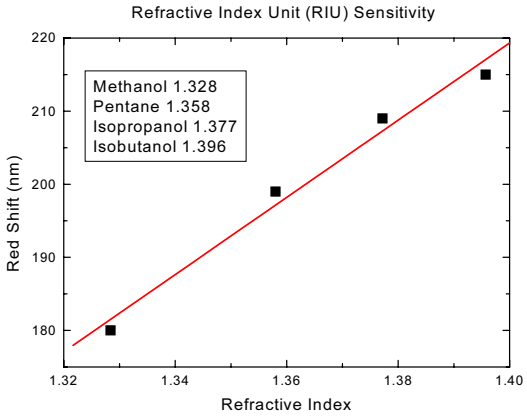


**Fig. 5** Red-shift of the S6 structure transmission peak at 1000 nm versus the refractive index of vapor substances.

## 4 Conclusions

In conclusion, in this work we have reported the fabrication and the optical characterization of aperiodic Thue-Morse structures up to 128 layers based on PSi technology. The multilayers are relatively easy to realize and exploit a high quality optical response. A splitting of photonic band gap is observed at the increasing of the Thue-Morse order. A partial photonic band gap region, centered at 1100 nm and 70 nm wide was observed for the $S_6$ and $S_7$ Thue-Morse structures. The PSi Thue-Morse structures can be also successfully used as sensor devices due to their characteristic properties.


© 2007 WILEY-VCH Verlag GmbH & Co. KGaA, Weinheim

## References

[1] E. Yablonovitch, Phys. Rev. Lett. **58**, 2059 (1987).
[2] S. John, Phys. Rev. Lett. **58**, 2486 (1987).
[3] V. Agarwal and J. A. del Rio, Appl. Phys. Lett. **82**, 1512 (2003).
[4] M. Dulea, M. Severin, and R. Riklund, Phys. Rev. B **42**, 3680 (1990).
[5] L. Dal Negro, M. Stolfi, Y. Yi, J. Michel, X. Duan, L. C. Kimerling, J. LeBlanc, and J. Haavisto, Appl. Phys. Lett. **84**, 5186 (2004).
[6] F. Qui, R. W. Peng, X. Q. Huang, X. F. Hu, Mu Wang, A. Hu, S. S. Jiang, and D. Feng, Europhys. Lett. **68**, 658 (2004).
[7] M. E. Mora-Ramos, V. Agarwal, and J. A. Soto Urueta, Microelectron. J. **36**, 413 (2005).
[8] R. W. Hardeman, M. I. J. Beale, D. B. Gasson, J. M. Keen, C. Pickering, and D. J. Robbins, Surf. Sci. **152/153**, 1051 (1985).
[9] M. A. Muriel and A. Carballar, IEEE Photon. Technol. Lett. **9**, 955 (1997).
[10] X. Jiang, Y. Zhang, S. Feng, K. Huang, Y. Yi, and J. D. Joannopoulos, Appl. Phys. Lett. **86**, 201110 (2006).
[11] P. A. Snow, E. K. Squire, P. St. J. Russell, and L. T. Canham, J. Appl. Phys. **86**, 1781 (1999).
[12] L. De Stefano, I. Rendina, L. Moretti, S. Tundo, and A. M. Rossi, Appl. Opt. **43**, 167 (2004).

© 2007 WILEY-VCH Verlag GmbH & Co. KGaA, Weinheim 

## Optical sensing of chemical compounds using porous silicon devices

In this section are presented some very interesting results about the detection of chemical compounds by using porous silicon optical devices. Some porous silicon structures, were exposed to several substances of environmental interest: the detection in aqueous and humic solutions of a common pesticide and organic compounds. Very large red shifts of the reflectivity spectra, due to changes in the average refractive index, have been observed.

**Introduction to the sensing mechanism**

In this section, are presented optical sensors, based on porous silicon (PSi) technology for liquid and vapour detection. Optical sensors for chemical contaminants can adopt a spectroscopic method (usually in the IR region where gas absorption spectra have specific signatures), or measure the changes in some physical properties (colour, refractive index, photoluminescence, fluorescence and so on) due to the interaction between the substances under investigation and the sensor itself [1, 2]. From this point of view, PSi is a very interesting material due to its large specific surface area (on the order of 500 $m^2/cm^3$) which is a great advantage in gas sensing applications, so that this technology has been extensively studied in this field. When the PSi is exposed to vapours, or dip in liquid substances, a repeatable and completely reversible change in the reflectivity spectrum is observed. In fact, the substitution of air in the pores by the organic molecules causes an increasing of the average refractive index of the device, shifting towards longer wavelengths its characteristic reflectivity spectrum.

In a first optical characterization, it was followed the approach of Sailor et al. [3] choosing the simple case of a single layer of porous silicon as transducer device. Figure 1 shows a typical reflectivity spectrum (before and after chemical infiltration) from a PSi layer under white light illumination.

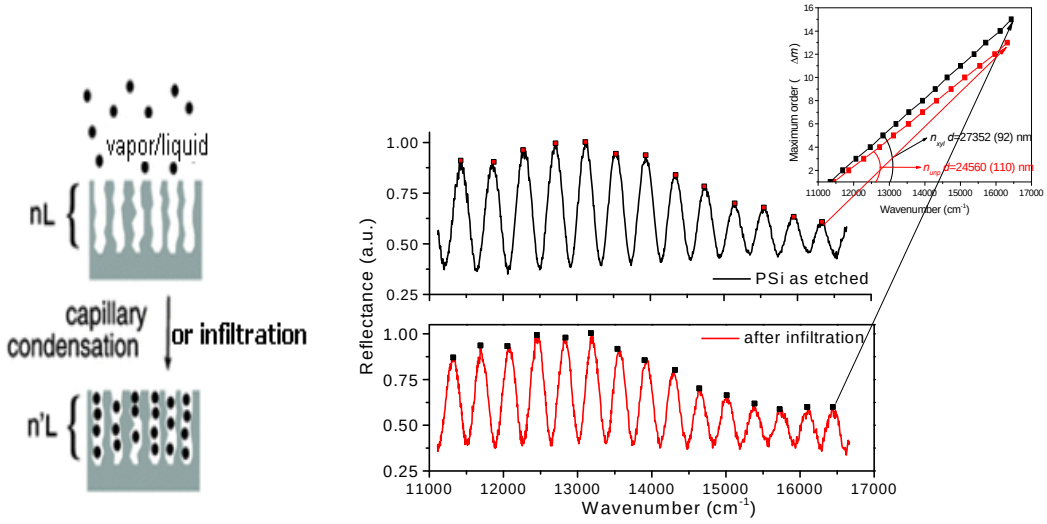


Figure 1. Reflectivity spectrum of PSi layer. In the inset the *m*-order peak are plotted as function of the wavenumber.

From the optical point of view, this structure is an optical Fabry-Perot interferometer, so that the maxima in the reflectivity spectrum appear at wavelengths $\lambda_m$ which satisfy the fallowing relationship:

$$m = 2nd / \lambda_m \tag{1}$$

where *m* is an integer, *d* is the film thickness and *n* is the average refractive index of the layer [4, 5].

If it's assumed that the refractive index is independent on the wavelength over the considered range, the maxima are equally spaced in the wavenumber (1/λm). When the maximum order *m* is plotted as a function of the wavenumber, each point lies on a straight

line which slope is the optical path *nd*, as it is shown in the inset of Figure 1. When the PSi layer is exposed to vapors, or dip in the liquid phase of the same substance, the substitution of air into the pores by its molecules causes a fringes shift in wavelength, which corresponds to a change in the optical path *nd*. Since the thickness *d* is fixed by the physical dimension of the PSi matrix, the variation is clearly due to changes in the average refractive index. In the case of vapors and gases, the filling liquid phase is due to the capillary condensation phenomenon, which is regulated from the Kelvin equation:

$$K_B T_{\rho_l} \ln(p_{sat} / p) = 2\gamma_{\mathrm{lg}} \cos\theta / R \tag{2}$$

where $\rho_l$ is the density of the liquid phase, $\gamma_{lg}$ is the liquid-gas surface tension coefficient at room temperature $T$, $R$ is the radius of the pores, $p/p_{sat}$ is the relative vapour pressure into the pores, and $\theta$ is the contact angle [6].
A quantitative model taking into account the optical path increase can be realized by applying the Bruggemann effective medium approximation theory. The relation between the volume fraction of each medium and its dielectric constant can be written as:

$$(1-p)\left(\frac{\varepsilon_{Si}-\varepsilon_p}{\varepsilon_{Si}+2\varepsilon_p}\right)+(p-V)\left(\frac{\varepsilon_{air}-\varepsilon_p}{\varepsilon_{air}+2\varepsilon_p}\right)+V\left(\frac{\varepsilon_{ch}-\varepsilon_p}{\varepsilon_{ch}+2\varepsilon_p}\right)=0 \tag{3}$$

where $p$, $V$, $\varepsilon_{si}$, $\varepsilon_{air}$, $\varepsilon_{ch}$ and $\varepsilon_p$ are the layer porosity, the layer liquid fraction (LLF), the dielectric constants of silicon, air, chemical substance and porous silicon, respectively [7].

## References


1. P. A. Snow, E. K. Squire, P. St. J. Russel, and L. T. Canham, Vapor sensing using the optical properties of porous silicon Bragg mirrors, J. Appl. Phys. 86, (1999) 1781-1784.
2. V. S. Y. Lin, K. Motesharei, K. P. S. Dancil, M. J. Sailor, and M. R. Ghadiri, A porous silicon-based optical interferometric biosensor, Science 278, (1997) 840-843.
3. Gao, J.; Gao, T.; Sailor, M.J. Porous-silicon vapor sensor based on laser interferometry. Appl. Phys. Lett. 2000, 77, 901-903.
4. Lin, V. S.-Y.; Motesharei, K.; Dancil, K.-P. S.; Sailor, M. J.; Ghadiri, M. R. A porous silicon-based optical interferometric biosensor. Science 1997, 278, 840-843.
5. Anderson, M. A.; Tinsley-Brown, A.; Allcock, P.; Perkins, E. A.; Snow, P.; Hollings, M.; Smith, R. G.; Reeves, C.; Squirrell, D. J.; Nicklin, S.; Cox; T. I. Sensitivity of the optical properties of porous silicon layers to the refractive index of liquid in the pores. Phys. Stat. Sol. A 2003, 197, 528-533.
6. Neimark, V.; Ravikovitch, P. I. Capillary condensation in MMS and pore structure characterization. Microporous Mesoporous Mater. 2001, 44-45, 697-707.
7. Spanier, J. E.; Herman, I. P. Use of hybrid phenomenological and statistical effective-medium theories of dielectric functions to model the infrared reflectance of porous SiC films. Phys. Rev. B 2000, 61, 10437-10450.

phys. stat. sol. (c) **4**, No. 6, 1941–1945 (2007) / **DOI** 10.1002/pssc.200674336

# Quantitative measurements of hydro-alcoholic binary mixtures by porous silicon optical microsensors

**Luca De Stefano**[*1], **Lucia Rotiroti**[1], **Ilaria Rea**[1], **Luigi Moretti**[2], and **Ivo Rendina**[1]

[1] Institute for Microelectronics and Microsystems, National Council of Research, Via P. Castellino 111, 80131 Naples, Italy
[2] DIMET – "Mediterranea" University of Reggio Calabria, Località Feo di Vito, 89060 Reggio Calabria, Italy

Received 17 March 2006, revised 15 September 2006, accepted 15 November 2006
Published online 9 May 2007

**PACS** 07.07.Df, 81.05.Rm, 81.70.Jb

In this communication, we present a simple, completely reversible and well performing optical microsensor for the quantitative determination in liquid hydro-alcoholic binary mixtures, based on the simple and low cost porous silicon (PSi) nanotechnology. In our sensor device, the transducer element is a PSi optical microcavity (PSMC) which is constituted by a Fabry-Pérot layer between two distributed Bragg reflectors. When the device is exposed to the mixture, the partial substitution of air in the pores changes the average refractive index of PSMC, causing a red shift of its reflectivity spectrum, characteristic of the concentration of each component. We have characterized, in the 0-100% composition range, three hydro-alcoholic binary mixtures (water-Ethanol, water- Methanol and water- Isopropanol) which exhibit very different behaviour.

© 2007 WILEY-VCH Verlag GmbH & Co. KGaA, Weinheim

## 1 Introduction

Hydro-alcoholic mixtures are largely used in the food industry: for example, the monitoring of the DI water-Ethanol compound is of extreme importance since it determines the alcoholic volume content of the most common beverages such as wines, beers, liquors and spirits. The standard methods, prescribed for the quantitative determination of the alcohol concentration, suffer some drawbacks since they require professional laboratories with specialized personnel, and expensive equipment, such as the HPLC, and sometimes also the sample pre-treatment. These procedures cannot be applied on line and are useless for fast routine analyses. The optical sensors offer a very attractive solution in the realization of analytical devices: they could exhibit high sensitivity, fast response, small dimensions, low cost and also the possibility of remote sensing.

PSi based optical sensors have recently gained a well established place among the optical monitoring devices due to the peculiar physical properties of this material. PSi is very cheap to produce, fully integrable with the standard silicon technology, moreover its high surface area assures a strong and fast interaction with liquid or vapor substances. On these bases, several applications of PSi monolayer and multilayer structures have been recently considered in biological and chemical sensing [1–3, 9]. A step beyond the optical identification of a pure substance is the quantitative determination of the components concentrations in a mixture. When the PSi device is exposed to a liquid or gaseous solution, a change in the optical reflectivity spectrum can be observed due to the partial substitution of air in the pores by a liquid phase, due to the direct infiltration or to the capillary condensation, which increases the average

[*] Corresponding author: e-mail: luca.destefano@na.imm.cnr.it, Phone +390816132375, Fax +390816132598

© 2007 WILEY-VCH Verlag GmbH & Co. KGaA, Weinheim

refractive index. This phenomenon depends on both the refractive index of the liquid phase but also on the filling factor, i.e. how it penetrates into the spongy structure of the PSi. The dependence of the result on two parameters permits to resolve a binary mixture with only one optical measurement [4]. Our group has already published some quantitative results on gaseous and liquid binary mixtures, obtained by using PSi based resonant optical sensors. In particular, we have characterized the sensor response on exposure to vapors of several volatile compounds (Iso-propanol/Ethanol, Iso-propanol/Methanol, Xylene/Methanol), and after the interaction with liquid solutions of pesticides in water and humic acid [5–7]. We present here an all-optical PSi based chemical sensor for quantitative determination in liquid hydro-alcoholic binary mixtures.

## 2 Material and methods

The optical transducer we used in our experiments is a λ/2 Fabry-Pérot layer enclosed between two Bragg reflectors; each one fabricated by alternating seven layers with high (low) and low (high) refractive indices (porosities). This PSi multilayer structure is an optical microcavity (PSMC), electrochemically etched by a HF-based solution on a highly doped $p^+$-silicon, <100> oriented, 0.01 Ω cm resistivity, and 400 μm thick. A current density of 350 mA/cm$^2$ for 0.6 sec was applied to obtain the high refractive index layer, with a porosity of 62 %, while one of 50 mA/cm$^2$ was applied for 0.8 sec for the low index layer, with a porosity of 42 %. The Fabry-Pérot is a low refractive index layer. This structure has a characteristic resonance peak at 1110 nm in the middle of a 271 nm stop band. The infiltration of the aqueous solution into the spongy structure could be problematic since the PSi surface as etched is highly hydrophobic due to the presence of Si-H bonds. In order to assure an efficient interaction it is necessary to make this surface hydrophilic by a thermal oxidation process (at 900 °C for 45 minutes).

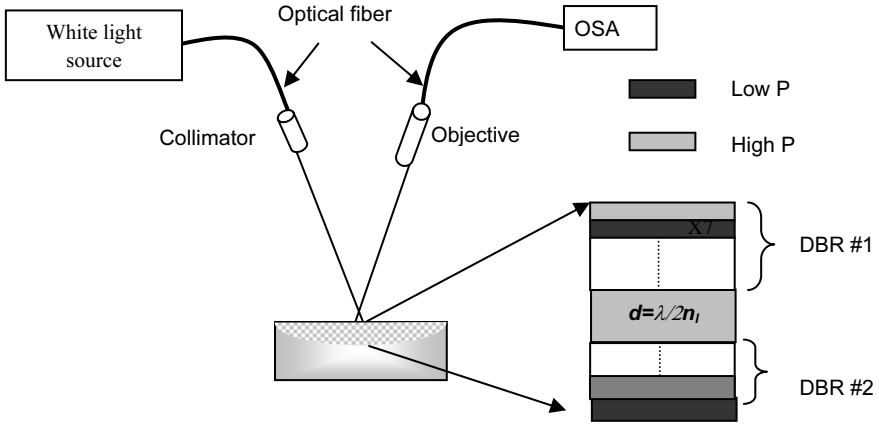


**Fig. 1** The experimental optical set-up: the sample was illuminated by a collimated white source; the output signal was directed in an optical spectrum analyzer and it was measured over the range 1000-1050 nm with a resolution of 0.2 nm.

We studied the resonance peak shift on exposure to the liquid mixtures as a function of the alcohols concentration in the de-ionized water (DI). To avoid some lens effect, we placed a drop (20 μL) of the solution on the PSi surface and covered it by a thin transparent glass. In Fig. 1 the experimental set-up used to measure the reflectivity spectrum is reported. When the liquid penetrated into the PSMC, a change in the cavity reflectivity spectrum was observed: the partial substitution of air by liquid in the

© 2007 WILEY-VCH Verlag GmbH & Co. KGaA, Weinheim 

pores of each layer increases the average refractive index of the microcavity and, consequentially, generates a red-shift of the reflectivity spectrum. Measurements are stored when equilibrium conditions are reached, i.e. when the signal does not change any more in time.

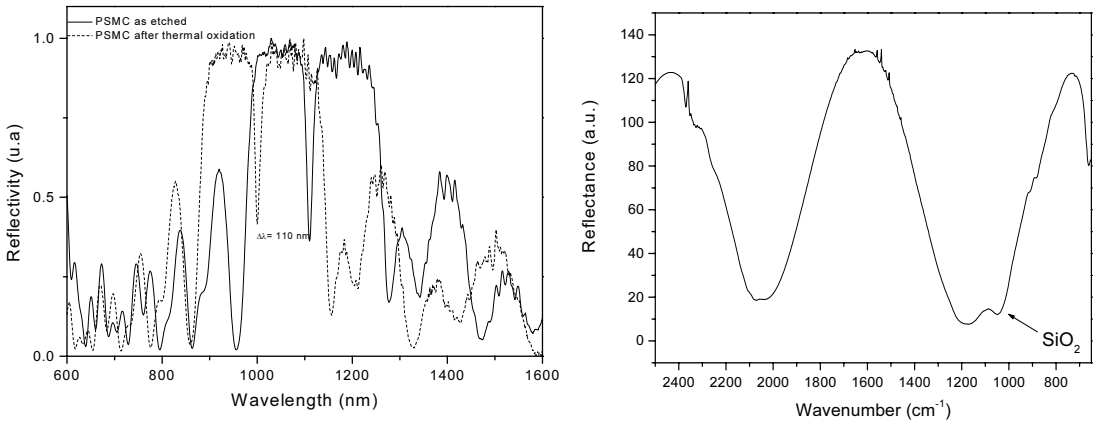


**Fig. 2** The optical spectrum of the PSMC before and after the thermal oxidation and the infrared spectrum after thermal treatment.

## 3 Experimental results

The optical and infrared spectra of the device before and after the oxidation are reported in Fig. 2. The microcavity has a FWHM of 12 nm and the thermal oxidation causes a blue shift of the reflectivity spectrum of 110 nm. The optical quality of the PSi response is preserved after the thermal treatment. In the infrared spectrum is well evident the presence of the characteristic peaks of Si-O-Si bonds at about 1000-1100 $cm^{-1}$ and the absence of the Si-H bonds at 2100 $cm^{-1}$.

In a recent paper[5], we have already used a very simple method, common in the analytical chemistry, for the quantitative determinations of binary mixtures: the External Standard Method. The calibration curves can be obtained by measuring the physical parameter under monitoring, such as the infrared absorption at

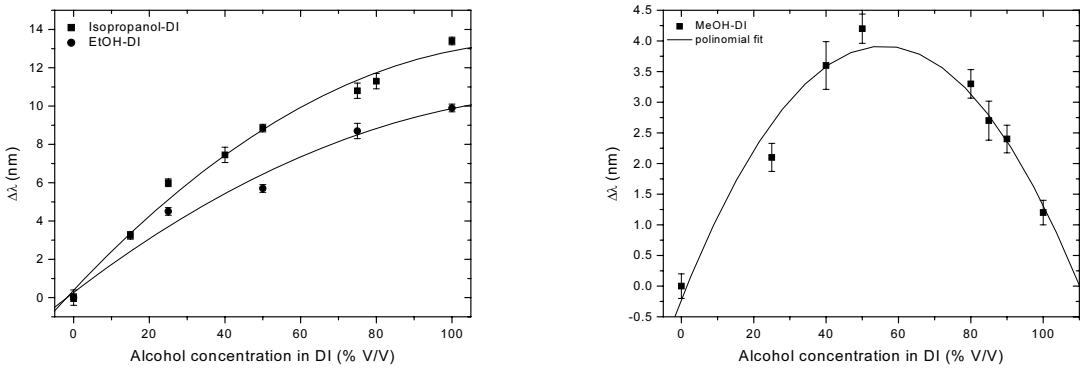


**Fig. 3** The calibration curves in case of three binary mixtures (Iso-propanol/DI, Ethanol/DI and Methanol/DI).


© 2007 WILEY-VCH Verlag GmbH & Co. KGaA, Weinheim

a fixed wavelength or the optical intensity, while the content of one component varies between 0 and 100%, volume by volume (V/V). Also in the case under study, the calibration curves have been obtained by plotting the peak shifts measured as a function of the volume percentage of one component in the binary mixtures.

The results are shown in Fig. 3. The errors on the experimental points are the standard deviations on three to five measurements, using the same chip and the same hydro-alcoholic solution. There is a well evident dissimilarity respect to the linear behaviour of the optical response obtained on exposure to the vapours of the volatile binary compounds. Of course, even if the calibration curves are not linear, the unknown concentrations of the characterized mixtures can be still quantitatively determined with a single measurement of the peak shift: the volume concentrations of both the components can be picked out from the interpolation of the experimental data. Moreover, while the Isopropanol and Ethanol-DI mixtures shifts follow a slow parabolic behaviour, the Methanol-DI mixture exhibits a very different response. The main difference is that a 50 % solution of Methanol in DI causes a larger shift than both the pure substances. An explanation to the shape of the $\Delta\lambda$ curves can be found in the behaviour of the mixtures refractive indexes as a function of the alcohol concentration [8], shown in Fig. 4. In all the cases, the peak shift strictly follows the behaviour of the refractive index binary mixture. The anomalous shape of the Methanol-DI mixture can be ascribed to the higher dipole moment of its constituent: due to a strong dipolar interaction this hydro-alcoholic mixture could exhibit a denser optical phase respect to the two pure substances [8].

The time-resolved measurements have shown that sensor dynamic is of order of few seconds, also depending on geometrical characteristic of the experimental set-up [3]. Moreover, the phenomenon is completely reversible and reproducible, so that the transducer PSi element can be reusable several times.

As a practical application of this study, we have tried to use the PSMC to determine the alcohol content of a red wine (Aglianico del Taburno, DOC). To this aim, we have diluted the wine, with a declared alcohol content of 12% V/V, in DI water and we have measured the calibration curve up to this value. From the graph in Fig. 3, we expected a linear behavior, due to the small range of Ethanol concentration in the wine. In Fig. 5, we have reported the wine calibration curve together with the first order approximation of the Ethanol-DI calibration curve of Fig. 3. The two curves are both linear but they have different slopes: in particular, the Ethanol-DI curve underestimates the wine percentage content. This is also a

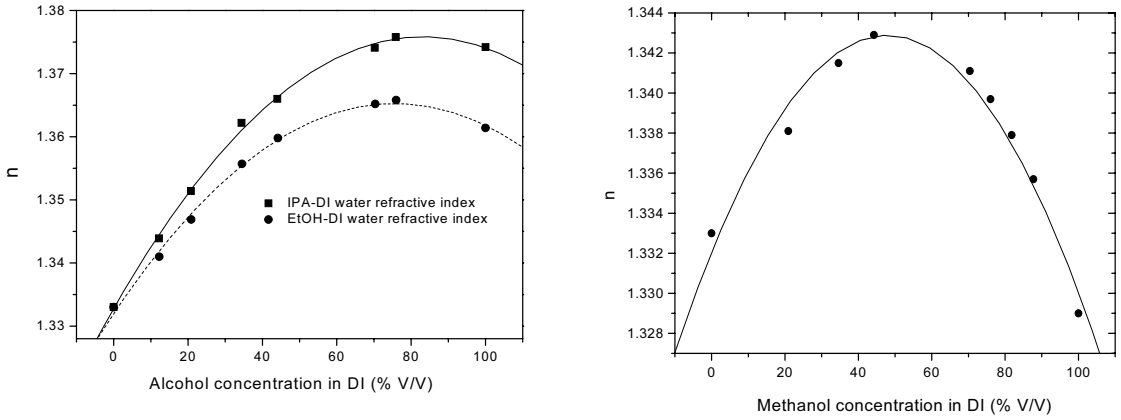


**Fig. 4** The mixtures refractive indexes as a function of the alcohol concentration in DI.

somewhat expected result: in fact the wine is a very complex mixture where Ethanol and water are the main constituents but many other volatile organic compounds are present. Nevertheless, we believe that

© 2007 WILEY-VCH Verlag GmbH & Co. KGaA, Weinheim 

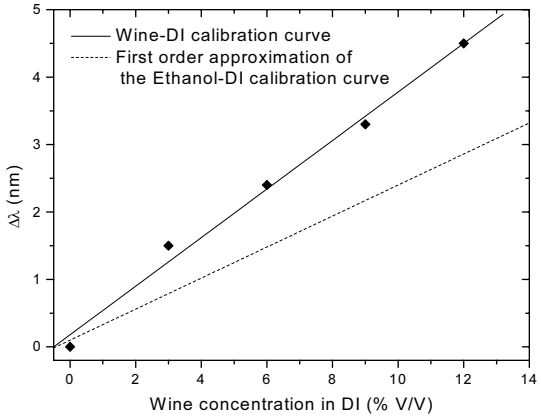


**Fig. 5** The calibration curve in case of wine-DI water solution.

the measurement technique could be improved, perhaps by time-resolved procedures, in order to give more precise results.

## 4 Conclusion

We have presented a simple and well performing optical microsensor for quantitative determination in liquid mixtures, based on the simple and low cost porous silicon nanotechnology. The device is a micro-cavity structure that is directly realized on the silicon chip by electrochemical etching. The fabrication process is compatible with silicon microelectronic and micro machining technologies, so that the sensors could be monolithically integrated with microelectronic circuits, or be part of a micro-optical-system. In terms of the measurement resolution, the resonant cavity enhanced operation of the proposed sensor offers very good performances: the interaction between the porous silicon microcavity and the external mixtures detunes the optical microcavity inducing large shifts of its resonant peak wavelength.

## References

[1] P. A. Snow, E. K. Squire, P. St. J. Russel, and L. T. Canaham, J. Appl. Phys. **86**, 1781 (1999).
[2] V. S. Y. Lin, K. Motesharei, K. P. S. Dancil, M. J. Sailor, and M. R. Ghadiri, Science **278**, 840 (1997).
[3] L. De Stefano, I. Rendina, L. Moretti, A.M. Rossi, Sens. Actuators B **100**, 168 (2004).
[4] C.K. Ho, M.T. Itamura, M. Kelley, and R.G. Hughes, Review of Chemical Sensors for In-situ Monitoring of Volatile Contaminants, Sandia Report SAND2001-0643, Sandia National Laboratories, 2001.
[5] L. De Stefano, I. Rendina, L. Moretti, and A.M. Rossi, phys. stat. sol. (a) **201**, 1011 (2004).
[6] L. De Stefano, L. Moretti, I. Rendina, and L. Rotiroti, Sens. Actuators B **111/112**, 522 (2005).
[7] L. Rotiroti, L. De Stefano, L. Moretti, A. Piccolo, I. Rendina, and A. M. Rossi, Biosens. Bioelectron. **20**, 2136 (2005).
[8] Handbook of Chemistry and Physics, 68th ed. (CRC Press, Boca Raton, 1987/1988).
[9] L. De Stefano, I. Rea, I. Rendina, L. Rotiroti, M. Rossi, and S. D'Auria phys. stat. sol. (a) **203**, 886 (2006).

 © 2007 WILEY-VCH Verlag GmbH & Co. KGaA, Weinheim

# Chapter 2

*Chemical and Biological functionalization of Porous Silicon surface*

**Introduction: Porous Silicon surface chemical functionalization**

Biosensors are nowadays technological hot topics due to the possible applications in fields of social interest such as medical diagnostic and health care, monitoring of environmental pollutants, homeland and defence security [1].

Reagentless optical biosensors are monitoring devices which can detect a target analyte in a heterogeneous solution without the addition of anything than the sample. In the fields of genomics and proteomics this is a straightforward advantage since it allows real-time readouts and, thus, very high throughoutputs analysis. A label free optical biosensor can be realized by integrating the biological probe with a signalling material which directly transduces the molecular recognition event into an optical signal.

PSi is also very used as photonic material due to the possibility of fabricating high quality optical structures, either as single layers, like Fabry-Perot interferometers [2], or multilayers, such as Bragg [3] or rugate filters [4]. A key feature for a recognition transducer is a large surface area: PSi has a porous structure with a specific area up to 200 – 500 $m^2$ $cm^{-3}$, so that it can be very sensitive to the presence of biochemical species which penetrate inside the pores. Unfortunately, the surface of the "as etched" PSi is highly hydrophobic due to the Si-H bonds so that aqueous solution can not infiltrate the sponge like matrix. A proper passivation process must be applied to stabilise the surface and to covalently link the bioprobe [5].

- *Hydrosilylation to produce Si-C bonds*

Interesting results on the chemical derivatization of PSi were reported before 1998, but the problem was the low treatment efficiency and, thus, the remaining instability. Especially, the groups of Mike Sailor (Department of Chemistry and Biochemistry University of California, San Diego), Jean-Noel Chazalviel (Palaiseau Polytechnical Institute, France), and Jillian Buriak (Department of Chemistry, University of Alberta, and the National Institute for Nanotechnology) studied different possible treatments for the PSi surface modifications with Si–C bonds.

Their work finally led to the derivatized PSi surface, in which the Si–H bonds were replaced with Si–C bonds using hydrosilylation of alkenes or alkynes on the PSi surface. The group of Buriak introduced three different approaches to obtain the chemically derivatized PSi surface: Lewis acid mediated hydrosilylation [6,7] white light-promoted hydrosilylation [8,9] and cathodic electrografting [10].

Carbon directly bonded to silicon yields a very stable surface species. First recognized by Chidsey and coworkers [11], Si–C bonded species possess greater kinetic stability relative to Si–O due to the low electronegativity of carbon. Silicon can readily form 5- and 6-coordinate intermediates, and an electronegative element such as oxygen enhances the tendency of silicon to be attacked by nucleophiles. Si–C bonds are usually formed on hydride-terminated porous Si surfaces by hydrosilylation (Figure 1). Hydrosilylation involves reaction of an alkene (usually terminal) or alkyne with a Si–H bond. On porous Si, the reaction can be thermal [12], photochemical [13], or Lewis acid catalyzed [14].

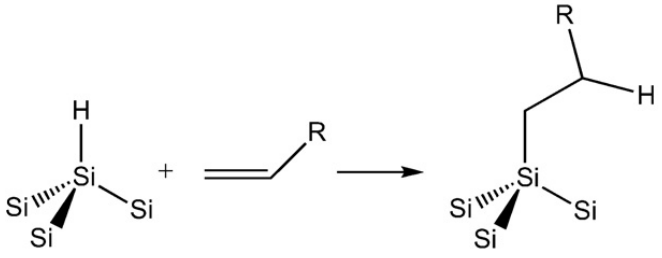


Figure 1: mechanism of PSi functionalization by nucleophilic substitution.

Thermal hydrosilylation provides a means to place a wide variety of organic functional groups on a crystalline Si or porous Si surface. The main requirement of the reaction is that the silicon surface contains Si–H species so they can react with a terminal alkene on the organic fragment. Thus it is important to use freshly etched porous Si and to exclude oxygen and water from the reaction mixture.

- *Chemical grafting of Si-C bonds*

As an alternative to hydrosilylation, covalently attached layers can be formed on porous Si surfaces using Grignard (figure 2) and alkyl- or aryllithium reagents [15]. Because of their ease of application and dramatic improvements in stability, hydrosilylation grafting of alkyl halides are useful reactions for the preparation of biointerfaces.

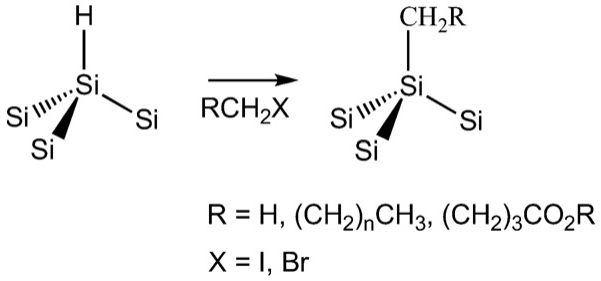


Figure 2: mechanism of PSi functionalization by Grignard reactive.

It is important to note that porous Si modification reactions do not provide 100% surface coverage; they merely decorate the surface with the functional group. Thus infrared spectra show a large amount of surface Si–H groups remaining after hydrosilylation or grafting reaction.
It is still an open question as to why the modification reactions impart such stability to the material. The stability probably derives from a combination of two factors: the Si–C bond is kinetically inert due to the low electro negativity of carbon and the attached organic species (typically a hydrocarbon chain 8 or more carbons long) is sufficiently hydrophobic that aqueous nucleophiles are excluded from the vicinity of their Si atom target. Reaction of porous Si with gas phase acetylene generates highly carbonized porous Si that is possibly the most stable form of Si–C modified porous Si [16]. This material is referred to as thermally carbonized PSi. It has been extensively investigated by Salonen at Department of Physics of University of Turku, (Turku, Finland) and coworkers, with many publications of relevance to drug loading and delivery [17].

- *Conjugation of bio molecules to modified PSi*

Carbon grafting stabilizes porous Si against dissolution in aqueous media, but the surface must still avoid the non-specific binding of proteins and other biological species.
The oxides of porous Si are easy to functionalize using conventional silanol chemistries. When small pores are present (as with p-type samples), trialkoxysilanes [$(RO)_3Si–R'$] can be employed as surface linkers [18].
Whereas Si–C chemistries are robust and versatile, chemistries involving Si–O bonds represent an attractive alternative for two reasons.
First, the timescale in which highly porous $SiO_2$ is stable in aqueous media is consistent with many short-term biomolecular recognitions applications: typically 20 min to a few hours. Second, a porous $SiO_2$ sample that contains no additional stabilizing chemistries is less likely to produce toxic or antigenic side effects.

- *Oxidation of porous silicon*

With its high surface area, porous silicon is particularly susceptible to air or water oxidation. The simplest way to stabilize PSi is obviously a partial oxidation. A few hours even at quite mild conditions, around 300°C, cause mainly the so called back-bond oxidation of PSi [19]. The oxygen atoms selectively attack the back-bonds of the surface Si atoms instead of replacing hydrogen atoms. The oxygen bridges formed between the surface Si atoms and the second atomic Si layer expand the local atomic structure by 30%, causing a slight decrease in the pore diameter. In addition to the increased stability, the oxidation at 300°C also changes the surface from hydrophobic to hydrophilic, which is important in many biological applications under physiological conditions. Increased temperature also increases the extent of oxidation leading to completely oxidized PSi at around 900–1000°C [20]. Due to the structural expansion, the pore diameter and porosity are dependent on the extent of oxidation, and a drastic drop in the specific surface area has been observed in PSi oxidized around 600°C [21].

Once oxidized, Si-O bonds are easy to prepare on porous silicon by oxidation, and a variety of chemical or electrochemical oxidants can be used. There are also many other techniques to oxidize PSi, such as anodic oxidation, [22,23] photo-oxidation, [24-26] and chemical oxidation. Like the thermal oxidation, the chemical oxidation is quite simple, in which PSi is oxidized with inorganic or organic agents. [27-31]

Milder chemical oxidants, such as dimethyl sulfoxide (DMSO), or piranha solutions ($H_2SO_4/H_2O_2$ 7:3) can also be used for this reaction. Mild oxidants are sometimes preferred because they can improve the mechanical stability of highly porous Si films, which are typically quite fragile. The mechanical instability of PSi is directly related to the strain that is induced in the film as it is produced in the electrochemical etching process, and the volume expansion that accompanies thermal oxidation can also introduce strain. Electrochemical oxidation, in which a porous Si sample is anodized in the presence of a mineral acid such as $H_2SO_4$, yields a fairly stable oxide. Mild chemical oxidants presumably attack PSi preferentially at Si–Si bonds that are the most strained, and hence most reactive.

Aqueous solutions of bases such as KOH can also be used to enlarge the pores after etching [32]. Oxidation imparts hydrophilicity to the porous structure, enabling the binding and adsorption of hydrophilic biomolecules within the pores.

## References


1. *Optical Biosensors*, Eds. F.S. Ligler and C.A. Rowe Taitt, Elsevier, Amsterdam, The Netherlands, **2004**.
2. Dancil, K. -P. S.; Greiner, D. P.; Sailor, M. J., A Porous Silicon Optical Biosensor: Detection of Reversible Binding of IgG to a Protein A-Modified Surface, *J. Am. Chem. Soc.* **1999,** *121*, 7925-7930.
3. Snow, P. A.; Squire, E. K.; Russel, P. St. J.; Canham, L. T., Vapor sensing using the optical properties of porous silicon Bragg mirrors, *J. Appl. Phys.* **1999,** *86*, 1781-1784.
4. Lorenzo, E.; Oton, C. J.; Capuj, N. E.; Ghulinyan, M.; Navarro-Urrios, D.; Gaburro, Z.; Pavesi, L., Porous silicon-based rugate filters, *Appl. Opt.* **2005,** *44*, 5415-5421.
5. Ouyang, H.; Chrtistophersen, M.; Viard, R.; Miller, B. L.; Fauchet, P. M., Macroporous silicon microcavities for macromolecule detection, *Adv. Funct. Mater*. **2005,** *15*, 1851-1859**.**
6. Buriak JM, Allen MJ. 1998. Lewis acid mediated functionalization of porous silicon with substituted alkenes and alkynes. J Am Chem Soc 120: 1339–1340.
7. Buriak JM, Sterward MP, Geders TW, Allen MJ, Choi HC, Smith J, Raftery D, Canham LT. 1999. Lewis acid mediated hydrosilylation porous silicon surfaces. J AmChem Soc 121:11491–11502.
8. Stewart MP, Buriak JM. 1998. Photopatterned hydrosilylation on porous silicon. Angew Chem Int Ed 37:3257–3260.
9. Stewart MP, Buriak JM. 2001. Exciton-mediated hydrosilylation on photoluminescent nanocrystalline silicon. J Am Chem Soc 123:7821–7830.

10. Robins EG, Stewart MP, Buriak JM. 1999. Anodic and cathodic electrografting of alkynes on porous silicon. Chem Comm 24:2479–2480.
11. M.R. Linford, C.E.D. Chidsey, Alkyl monolayers covalently attached to silicon surfaces, J. Am. Chem. Soc. 115 (1993) 12631–12632.
12. R. Boukherroub, J.T.C. Wojtyk, D.D.M. Wayner, D.J. Lockwood, Thermal hydrosilylation of undecylenic acid with porous silicon, J. Electrochem. Soc. 149 (2002) 59–63.
13. M.P. Stewart, J.M. Buriak, Photopatterned hydrosilylation on porous silicon, Angew. Chem. Int. Ed. Engl. 37 (1998) 3257–3260.
14. J.M. Buriak, Organometallic chemistry on silicon and germanium surfaces, Chem. Rev. 102 (2002) 1272–1308.
15. J. Terry, M.R. Linford, C. Wigren, R.Y. Cao, P. Pianetta, C.E.D. Chidsey, Alkylterminated Si(111) surfaces: a high-resolution, core level photoelectron spectroscopy study, J. Appl. Phys. 85 (1999) 213–221.
16. M. Bjorkqvist, J. Salonen, E. Laine, L. Niinisto, Comparison of stabilizing treatments on porous silicon for sensor applications, Phys. Status Solidi A—Appl. Res. 197 (2003) 374–377.
17. A.M. Kaukonen, L. Laitinen, J. Salonen, et al., Enhanced in vitro permeation of furosemide loaded into thermally carbonized mesoporous silicon (TCPSi) microparticles, Eur. J. Pharm. Biopharm. 66 (2007) 348–356
18. A. Janshoff, K.P.S. Dancil, C. Steinem, et al., Macroporous p-type silicon Fabry– Perot layers. Fabrication, characterization, and applications in biosensing, J. Am. Chem. Soc. 120 (1998) 12108–12116.
19. Salonen J, Lehto VP, Laine E. 1997. Thermal oxidation of free-standing porous silicon films. Appl Phys Lett 70:637–639.
20. Canham LT. 1997. Chemical composition of intentionally oxidized porous silicon. In: Canham LT, editor. Properties of porous silicon. EMIS Datareview series No 18. London: INSPEC. pp 158– 162.
21. Halimaoui A. 1995. Porous silicon: Material processing, properties and applications. In: Vial JC, Derrien J, editors. Porous silicon science and technology. France: Springer-Verlag. pp 33–52.
22. Herino R. 1995. Luminescence of porous silicon after electrochemical oxidation. In: Vial JC, Derrien J, editors. Porous silicon science and technology. France: Springer-Verlag. pp 53–66.
23. Mulloni V, Pavesi L. 2000. Electrochemically oxidized porous silicon microcavities. Mat Sci Eng B 69–70:59–65.
24. Tischler MA, Collin RT, Stathis JH, Tsang JC. 1992. Luminescence degradation in porous silicon. Appl Phys Lett 60:639–641.
25. Salonen J, Lehto VP, Laine E. 1999. Photo-oxidation studies of porous silicon using microcalorimetric method. J Appl Phys 86:5888–5893.
26. Gole JL, Dixon DA. 1998. Evidence for oxide formation of the single and multiphoton excitation of a porous silicon surface or silicon ‘‘nanoparticles’’. J Appl Phys 83:5985–5991.
27. Song JH, Sailor MJ. 1999. Chemical modification of crystalline porous silicon surfaces. Comments Inorg Chem 1-3:69–84.
28. Nakajima A, Itakura T, Watanabe S, Nakayama N. 1992. Photoluminescence of porous Si, oxidized and then deoxidized chemically. Appl Phys Lett 61:46–48.
29. Rao BVRM, Basu PK, Biswas JC, Lahiri SK, Ghosh S, Bose DN. 1996. Large enhancement of photoluminescence from porous silicon films by post-anodization treatment in boiling hydrogen peroxide. Solid State Comm 97:417–418.
30. Yin F, Li XP, Zhang ZZ, Xiao XR. 1997. Investigations on the surface reactivity of luminescent porous silicon. Appl Surf Sci 119:310–312.
31. Salonen J, Lehto VP, Laine E. 1997. The room temperature oxidation of porous silicon. Appl Surf Sci 120:191–198.
32. L. A. De Louise and B. L. Miller, Mat. Res. Soc. Symp. Proc. **782**, A5.3.1 (2004).

# DNA Optical Detection Based on Porous Silicon Technology

This section is aimed at the optimization of the functionalization process investigating also the role of thickness and porosity of the PSi chip, the time exposure to ultraviolet (UV) light and also the concentration of the *ss*DNA solution.

*In collaboration with Prof. P. Arcari of University of Naples “Federico II”, Italy*

*Sensors* **2007**, *7*, 214-221

**sensors**

**ISSN 1424-8220**
© 2007 by MDPI
www.mdpi.org/sensors

*Full Research Paper*

# DNA Optical Detection Based on Porous Silicon Technology: from Biosensors to Biochips

**Luca De Stefano [1,*], Paolo Arcari [2], Annalisa Lamberti [2], Carmen Sanges [2], Lucia Rotiroti [1,3], Ilaria Rea [1, 4] and Ivo Rendina [1]**

[1] Institute for Microelectronics and Microsystems – Unit of Naples – National Council of Research, Via P. Castellino 111, 80131 Napoli, Italy (E-mail: luca.destefano@na.imm.cnr.it)

[2] Department of Biochemistry and Medical Biotechnologies, University of Naples "Federico II", Via S. Pansini 5, 80131 Napoli, Italy.

[3] Department of Organic Chemistry and Biochemistry, University of Naples "Federico II", Via Cinthia, 80128 Napoli, Italy

[4] Department of Physical Sciences, University of Naples "Federico II", Via Cinthia, 80126 Naples, Italy

* Author to whom correspondence should be addressed. E-mail: luca.destefano@na.imm.cnr.it

*Received: 15 February 2007 / Accepted: 26 February 2007 / Published: 28 February 2007*

---

**Abstract:** A photochemical functionalization process which passivates the porous silicon surface of optical biosensors has been optimized as a function of the thickness and the porosity of the devices. The surface modification has been characterized by contact angle measurements. Fluorescence measurements have been used to investigate the stability of the DNA single strands bound to the nanostructured material. A dose-response curve for an optical label-free biosensor in the 6-80 μM range has been realized.

**Keywords:** Optical Biosensors, Porous Silicon, Biochip.

---

## 1. Introduction

Biosensors are nowadays technological hot topics due to the possible applications in social interest fields such as medical diagnostic and health care, monitoring of environmental pollutants, home and defence security [1]. Besides the signal generated by the sensing device, the biosensor is constituted by the molecular recognition element and the transducer material. The molecular recognition element can be a biological molecule, such as DNA single strand, proteins, enzymes, or a biological system, such as

membrane, cell, and tissues: in this way, the sensing mechanism takes advantage of the natural sensitivity and specificity of the biomolecular interactions. Optical transduction is more and more used since photonic devices could be small, lightweight and thus portable due to the integrability of all optical components. Furthermore, optical devices do not require electric contacts. Fluorescence is by far the most used optical signalling method but a wide-use sensor can not be limited by the labelling of the probe nor the analyte, since this step is not always possible [2]. Reagentless optical biosensors are monitoring devices which can detect a target analyte in a heterogeneous solution without the addition of anything than the sample. In the fields of genomics and proteomics this is a straightforward advantage since it allows real-time readouts and, thus, very high throughoutputs analysis. A label free optical biosensor can be realized by integrating the biological probe with a signalling material which directly transduces the molecular recognition event into an optical signal. Recently, lot of theoretical and experimental work, concerning the worth noting properties of nanostructured porous silicon (PSi) in chemical and biological sensing, has been reported, showing that, due to its morphological and physical properties, PSi is a very versatile sensing platform [3, 4]. PSi is an available, low cost material, completely compatible with VLSI and micromachining technologies, so that it could usefully be employed in the fabrication of micro-opto-electric-mechanical system and smart sensors. PSi is also very used as photonic material due to the possibility of fabricating high quality optical structures, either as single layers, like Fabry-Perot interferometers [5], or multilayers, such as Bragg [6] or rugate filters [7]. A key feature for a recognition transducer is a large surface area: PSi has a porous structure with a specific area up to 200 – 500 $m^2$ $cm^{-3}$, so that it can be very sensitive to the presence of biochemical species which penetrate inside the pores. Unfortunately, the surface of the "as etched" PSi is highly hydrophobic so that aqueous solution can not infiltrate the sponge like matrix. A proper passivation process must be applied to stabilise the surface and to covalently link the bioprobe [8]. The development of PSi based biosensor arrays critically depends on the surface functionalization process and how it is compatible with the microfabrication technologies. In a recently published article, we have exploited a photochemical functionalization process of the PSi surface to covalently bind DNA single strands (*ss*DNA) and we have also demonstrate that the device works as an all optical biosensor for *ss*DNA-*c*DNA interactions [9]. In the present work, we have optimised the functionalization process by investigating the role of thickness and porosity of the PSi chip, the time exposure to ultraviolet (UV) light and also the concentration of the *ss*DNA solution. Fluorescent measurements have been used to test the chip stability against the washing in aqueous solutions.

## 2. Experimental Section

In this study we used as optical transducer a porous silicon layer of fixed thickness and porosity: from an optical point of view, this structure acts as a Fabry-Perot interferometer. To study the influence of porous silicon physical parameters, we have fabricated several layers, obtained by electrochemical etch in a HF/EtOH (3:7) solution, at room temperature and dark light. Highly doped $p^+$-silicon, <100> oriented, 0.005 Ω cm resistivity, 400 μm thick was used. The PSi samples were characterised by variable angle spectroscopic ellipsometry [10]. Etching times and anodic current densities have been reported in Table 1.

**Table 1.** PSi layers physical characteristics and fabrication parameters.

| Current Density ($mA/cm^2$) | Porosity (%) | Etch Rate (nm/s) | Thickness (μm) | Etch Time (s) |
|---|---|---|---|---|
| 50 | 60 | 193 | 2.0 | 10.4 |
| | | | 4.0 | 20.7 |
| | | | 6.0 | 31.1 |
| 125 | 70 | 247 | 2.0 | 8.1 |
| | | | 4.0 | 16.2 |
| | | | 6.0 | 24.3 |
| 150 | 80 | 137 | 2.0 | 14.6 |
| | | | 4.0 | 29.2 |
| | | | 6.0 | 43.8 |

The photo-activated chemical modification of PSi surface was based on the UV exposure of a solution of alkenes which bring some carboxylic acid groups. The PSi chip has been pre-cleaned in an ultrasonic acetone bath then washed in deionized water. After dried in $N_2$ stream, it has been immediately covered with 10% N-hydroxysuccinimide ester (UANHS) solution in $CH_2Cl_2$. The UANHS was house synthesised as described in literature [11]. This treatment results in covalent attachment of UANHS to the porous silicon surface. The chip was then washed in dichloromethane in an ultrasonic bath for 10 min to remove any adsorbed alkene from the surface. The carboxyl-terminated monolayer covering the PSi surface works as a reactive substrate for the chemistry of the subsequent attachment of the DNA sequences. DNA single strands in a HEPES solution 10mM (pH=7.5) have been incubated overnight.

FT-IR spectroscopy (Thermo - Nicholet NEXUS) has been used to verify the efficiency of the reaction. After the chemical functionalization we have also quantitatively measured the efficiency of the binding between the DNA and the porous silicon surface using a fluorescent DNA probe (5'GGACTTGCCCGAATCTACGTGTCCA3', Primm) labelled with a proper chromophore group (Fluorescein CY3.5, the absorption peak is at 581 nm and the emission is at 596 nm). Fluorescence images were recorded by a Leica Z16 APO fluorescence macroscopy system. The fluorescent chips have been dialyzed overnight, first in water and then in a HEPES solution, at room temperature to assess the binding between the bioprobe and the PSi surface.

Contact angle measurements have been performed by using a KSV Instruments LTD CAM 200 Optical Contact Angle Meter.

The reflectivity measurements have been performed by a very simple experimental set-up: a tungsten lamp (400 nm < $\lambda$ < 1800 nm) illuminates, through an optical fiber and a collimator, the sensor and the reflected beam is collected by an objective, coupled into a multimode fiber, and then directed in an optical spectrum analyser (Ando, AQ6315A). The reflectivity spectra have been measured with a resolution of 0.5 nm.

## 3. Results and Discussion

Infrared spectroscopy is a powerful tool in surfaces characterisation: it is fast, accurate and could also performe quantitative determinations. We have investigated all the PSi monolayers before and after the photochemical passivation process since we were worried about the functionalization efficiency of thicker samples. A thicker layer can adsorb more bioprobes than a thinner one but the UV exposure could also be less effective, due to light absorption by PSi at those frequencies. Our measurements demonstrate that up to 6 μm thick PSi monolayer, a complete passivation and functionalization of the surface can be obtained by exposing for a sufficiently long time the sample: in Figure 1A are shown the FT-IR spectra of the PSi monolayer as etched and after three different times of exposure to UV light.

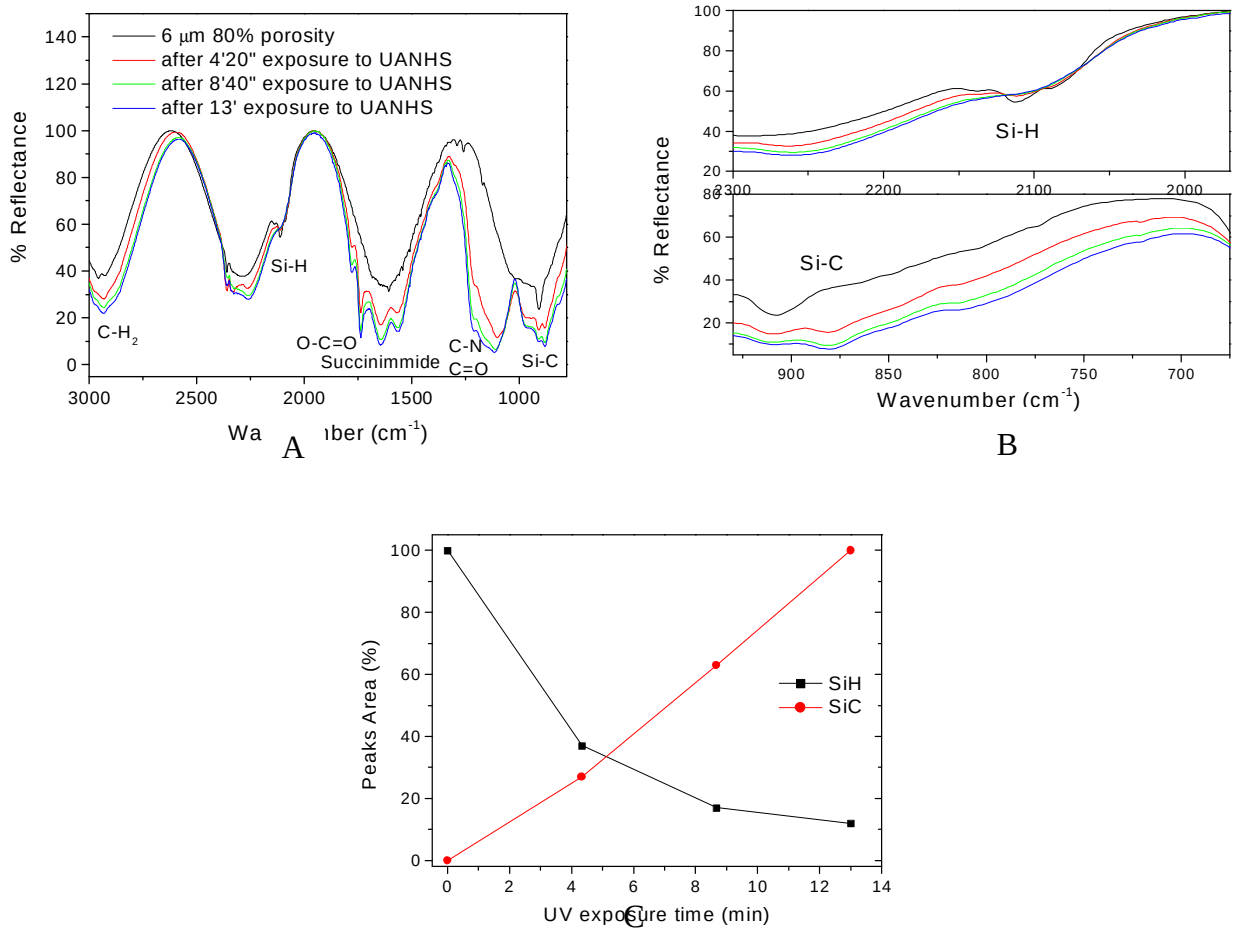


**Figure 1.** A) FT-IR spectra of the PSi monolayer as etched and after three different times of exposure to UV light. B) Particulars of the Si-H bond and Si-C bond peaks at 2100 and 880 $cm^{-1}$, respectively. C) Peaks area as function of the exposure time: the reaction yield increases monotonically with the exposure time.

The characteristic peaks of the Si-H bonds (at 2100 $cm^{-1}$) progressively disappear while the amide I band (at 1634 $cm^{-1}$) and the Si-C peak (at 880 $cm^{-1}$) become more and more evident. Figure 1B is an enlargement of the characteristic peaks of these resonances. The reaction yield increases quite monotonically with the exposure time, as it can be seen in Figure 1C. Thinner samples can be functionalised in faster exposure times, but the overall volume available to adsorb bioprobes is drastically reduced.

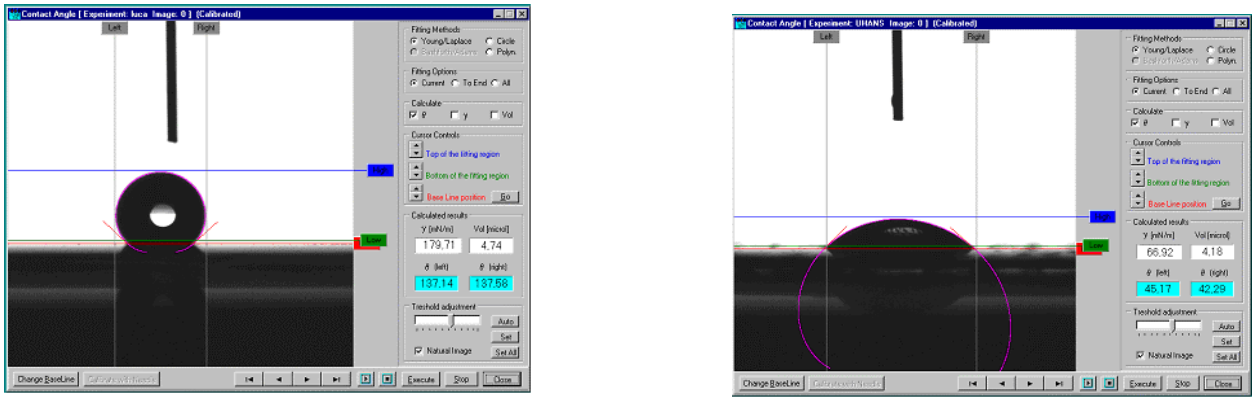

**A** **B**

**Figure 2.** Characterisation of the PSi surface by contact angles measurements. A) The PSi as etched shows a clearly hydrophobic behaviour. B) After the passivation process the PSi surface is hydrophilic thus allowing the penetration of biological solution.

The surface passivation is also well evident by contact angle measurements: the hydrogenated PSi surface is highly hydrophobic, due to the presence of the Si-H bonds, so that a drop of deionised water exploits a high surface tension which prevents its diffusion in the pores. This behaviour is well depicted in Figure 2A: the contact angle is 137±1 degree, averaging the left and right values of three different drops having the same volumes, and the estimated surface tension is 179 mN/m. After the photoreaction with the UANHS, the Si-H bonds are replaced by the Si-C bonds and the PSi surface shows a hydrophilic behaviour, as shown in Figure 2B: the drop spreads on the surface and the contact angle drastically decreases to 43±3 degree and also the surface tension is lowered to 67 mN/m. In this condition, an aqueous solution can be infiltrated in the nanostructured layer.

To test the stability of the covalent bonding between the organic linker layers, which homogeneously cover the PSi surface, and the biological probes we have used a fluorescent DNA single strand as an optical tracer. After the chemical bonding of the labelled *ss*DNA, the chip was observed by the fluorescence macroscopy system. Under the light of the 100W high-pressure mercury source, we have found a high and homogeneous fluorescence on the whole chip surface which still remains bright even after two overnight dialysis washings in a HEPES solution and in deionised water, as it can be seen in Figures 3 A, B, and C. We have also studied the yield of the chemical functionalization by spotting different concentrations of the fluorescent *ss*DNA and measuring the fluorescence intensities of the images before and after the washings. The results reported in Figure 4 confirm the qualitative findings of Figure 3: the fluorescent intensities decrease but remain of the same order of magnitude. From this

graph we can also estimate the concentration of the DNA probe which saturates the binding sites available.

The PSi optical biosensors measure the change in the average refractive index of the device: when a bioconjugation event takes place, the refractive index of the molecular complex changes and the interference pattern on output is thus modified. The label free optical monitoring of the *ss*DNA-*c*DNA hybridization is simply the comparison between the optical spectra of the porous silicon layer after the UANHS and probe immobilization on the chip surface and after its hybridization with the *c*DNA. Each step of the chip preparation increases the optical path in the reflectivity spectrum recorded, due to the substitution of the air into the pores by the organic and biological compounds. The interaction of the *ss*DNA with its complementary sequence has been detected as a fringes shift in the wavelengths, which corresponds to a change in the optical path. Since the thickness *d* is fixed by the physical dimension of the PSi matrix, the variation is clearly due to changes in the average refractive index.

**A** **B** **C**

**Figure 3**: A) Fluorescence of the chip surface after the binding of the labelled *ss*DNA; B) after the overnight dialysis in HEPES solution; C) after the overnight dialysis in deionised water.

In Figure 5A the reflectivity spectra of the PSi layer for different *c*DNA concentration are reported, while in Figure 5B a dose-response curve is reported. A control measurement has been made using a *nc*DNA sequence: a very small shift (less than 2 nm) has been recorded in the reflectivity spectrum respect to the one obtained after the probe linking.

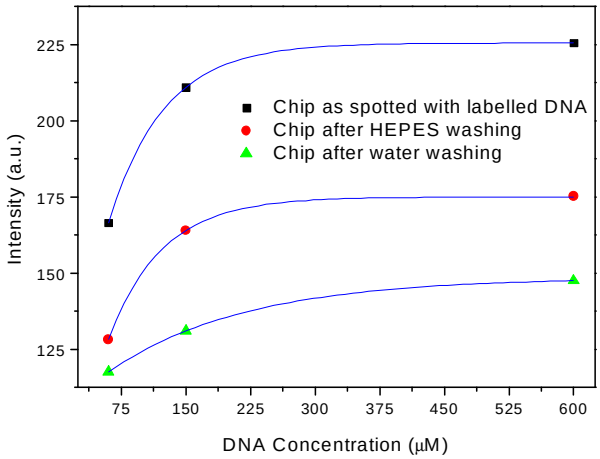


**Figure 4.** Fluorescence intensities of the chip surface after the binding of the labelled *ss*DNA and the two overnight dialysis as a function of the *c*DNA concentration.

The sensor response has been fitted by a monoexponential growth model, $y=A-Be^{-kx}$, where $A$ is the offset, $B$ the amplitude, $k$ the rate and $y'=Bk$ the limiting sensitivity, i.e. the sensitivity in the limit of zero ligand concentration. In this case, we obtained for this parameter the value of 1.1 (0.1) nm/μM, which corresponds to a limit of detection of 90 nM for a system able to detect a wavelength shift of 0.1 nm.

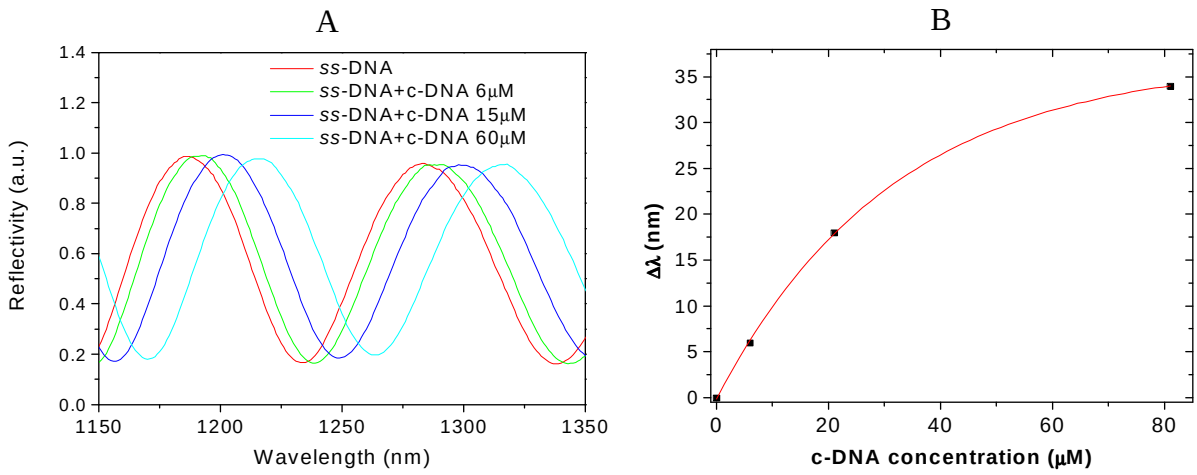


**Figure 5.** A) Fringes shifts due to *ss*DNA-*c*DNA interaction. B) Dose-response curve as a function of the cDNA concentration.

In conclusions, we have optimized the PSi surface functionalization process by investigating the role of chip thickness and porosity, on exposure to ultraviolet (UV) light for different times interval and also for different concentration of the *ss*DNA probe. Fluorescent measurements have confirmed the chip stability against the washing in aqueous solutions. These results will be very useful in the design and realisation of a PSi based label free optical biochip.

## Acknowledgements

Authors wish to acknowledge dr. Andrea M. Rossi of National Institute of Metrological Research, Turin, Italy, for helpful discussions and Prof. N. Scaramuzza and dr. M. Giocondo of University of Calabria, Cosenza, Italy, for contact angle measurements. This work is partially supported by the FIRB Italian project RBLA033WJX_005.

## References and Notes

1. *Optical Biosensors*, Eds. F.S. Ligler and C.A. Rowe Taitt, Elsevier, Amsterdam, The Netherlands, **2004**.
2. Salitermkan, S. S. *Fundamentals of BioMEMS and Medical Microdevices*; Wiley-Interscience, SPIE PRESS (Bellingham, Washington USA), **2006.**
3. Lin, V. S. Y.; Motesharei, K.; Dancil, K. P. S.; Sailor, M. J.; Ghadiri, M. R., A porous silicon-based optical interferometric biosensor, *Science* **1997,** *278*, 840-843.

4. De Stefano, L.; Moretti, L.; Rendina, I.; Rossi, A. M., Time-resolved sensing of chemical species in porous silicon optical microcavity, *Sensor and Actuators B* **2004,** *100*, 168-172.
5. Dancil, K. -P. S.; Greiner, D. P.; Sailor, M. J., A Porous Silicon Optical Biosensor: Detection of Reversible Binding of IgG to a Protein A-Modified Surface, *J. Am. Chem. Soc.* **1999,** *121*, 7925-7930.
6. Snow, P. A.; Squire, E. K.; Russel, P. St. J.; Canham, L. T., Vapor sensing using the optical properties of porous silicon Bragg mirrors, *J. Appl. Phys.* **1999,** *86*, 1781-1784.
7. Lorenzo, E.; Oton, C. J.; Capuj, N. E.; Ghulinyan, M.; Navarro-Urrios, D.; Gaburro, Z.; Pavesi, L., Porous silicon-based rugate filters, *Appl. Opt.* **2005,** *44*, 5415-5421.
8. Ouyang, H.; Chrtistophersen, M.; Viard, R.; Miller, B. L.; Fauchet, P. M., Macroporous silicon microcavities for macromolecule detection, *Adv. Funct. Mater*. **2005,** *15*, 1851-1859**.**
9. De Stefano, L.; Rotiroti, L.; Rea, I.; Rendina, I.; Moretti, L.; Di Francia, G.; Massera, E.; Lamberti, A.; Arcari, P.; Sangez, C., Porous silicon-based optical biochips, *Journal of Optics A: Pure and Applied Optics* **2006,** *8*, S540-S544.
10. Wongmanerod, C.; Zangooie, S.; Arwin, H., Determination of pore size distribution and surface area of thin porous silicon layers by spectroscopic ellipsometry, *Applied Surface Science* **2001**, *172*, 117-125.
11. Yin, H.B.; Brown, T.; Gref, R.; Wilkinson, J.S.; Melvin, T., Chemical modification and micropatterning of Si(100) with oligonucleotides, *Microelectronic Engineering* **2004,** *73-74*, 830-836.

© 2007 by MDPI (http://www.mdpi.org). Reproduction is permitted for noncommercial purposes.

## Examples of optical biosensors for the detection of analytes of clinical, industrial, and home security interest.

This section is aimed at the characterization of a PSi device functionalized with some proteins and enzymes.
It was studied that Glutamine-binding protein (GlnBP) from *Escherichia coli* specifically binds Glutamine and a wheat gliadin peptide (mainly responsible of inducing celiac disease), and that acetylcholinesterase (AChE) activity can be inhibited with organophosphorous pesticides, nerve agents and nitro-aromatic compounds, very dangerous substances.

*In collaboration with Dr. S. D'Auria from Institute for Protein Biochemistry, National Council of Research, Italy*

research articles Journal of proteome research

# Glutamine-Binding Protein from *Escherichia coli* Specifically Binds a Wheat Gliadin Peptide Allowing the Design of a New Porous Silicon-Based Optical Biosensor†

**Luca De Stefano,‡ Mauro Rossi,§ Maria Staiano,|| Gianfranco Mamone,§ Antonoietta Parracino,|| Lucia Rotiroti,‡ Ivo Rendina,‡ Mosè Rossi,|| and Sabato D'Auria*,||**

*Institute for Microelectronics and Microsystems, CNR, Naples, Italy, Institute of Food Sciences, CNR, Avellino, Italy, and Institute of Protein Biochemistry, CNR, Naples, Italy*

**Received January 20, 2006**

In this work, the binding of the recombinant glutamine-binding protein (GlnBP) from *Escherichia coli* to gliadin peptides, toxic for celiac patients, was investigated by mass spectrometry experiments and optical techniques. Mass spectrometry experiments demonstrated that GlnBP binds the following amino acid sequence: XXQPQPQQQQQQQQQQQQL, present only into the toxic prolamines. The binding of GlnBP to gliadin suggested us to design a new optical biosensor based on nanostructured porous silicon (PSi) for the detection of trace amounts of gliadin in food. The GlnBP, which acts as a molecular probe for the gliadin, was covalently linked to the surface of the PSi wafer by a proper passivation process. The GlnBP−gliadin interaction was revealed as a shift in wavelength of the fringes in the reflectivity spectrum of the PSi layer. The GlnBP, covalently bonded to the PSi chip, selectively recognized the toxic peptide. Finally, the sensor response to the protein concentration was measured in the range 2.0−40.0 $\mu$g/L and the sensitivity of the sensor was determined.

**Keywords:** gliadin • optical biosensors • porous silicon • celiac disease

There is a strong need for integrated and automated bioanalytical systems in medical, food, agricultural, environmental, and defense testing. Now, the main market is shared between blood glucose, pregnancy, antibody-based infectious diseases, and biological warfare agent detection.[1] The interaction between an analyte and a biological recognition system is normally detected in biosensors by the transducer element which converts the molecular event into a measurable effect, such as an electrical or optical signal. Because of its spongelike structure, porous silicon (PSi) is an almost ideal material as a transducer: its surface has a specific area of the order of 200−500 $m^2\ cm^{-3}$, so that a very effective interaction with liquid or gaseous substances is assured.[2,3] PSi optical sensors are based on changes of photoluminescence or reflectivity when exposed to the target analytes which substitute the air into the PSi pores.[4] The effect depends on the chemical and physical properties of each analyte, so that the sensor can be used to recognize the pure substances. Because of the sensing mechanism, these kinds of devices are not able to identify the components of a complex mixture. To enhance the sensor selectivity through specific interactions, some researchers have proposed to chemically or physically modify the PSi surface; the common approach is to create a covalent bond between the porous silicon surface and the biomolecules which specifically recognize the unknown analytes.[5−7] Among different probes of biological nature, ligand-binding proteins are particularly good candidates in designing highly specific biosensors for small analytes; in particular, the glutamine-binding protein (GlnBP) from *Escherichia coli* is a monomeric protein composed of 224 amino acid residues (26 kDa) responsible for the first step in the active transport of L-glutamine across the cytoplasm membrane. The GlnBP consists of two similar globular domains, the large domain (residues 1−84 and 186−224) and the small domain (residues 90−180), linked by two peptides. The deep cleft formed between the two domains contains the ligand-binding site. The GlnBP binds L-glutamine with a dissociation constant $K_d$ of $5 \times 10^{-9}$ M[8] as well as polyglutamine residues. In this study, we show that GlnBP is able to bind with high affinity the amino acid sequences present in the gliadin allowing the design of a new reagentless microsensor for the optical interferometric detection of gliadin based on a chemically modified porous silicon nanostructured surface covalently linking the GlnBP. The gliadin by the wheat gluten is mainly responsible of inducing celiac disease, an inflammatory disease of the small intestine affecting genetically susceptible people.[9] Presently, a strict gluten-free lifelong diet is mandatory for celiac patients for both intestinal mucosal recovery and prevention of complicating conditions such as lymphoma. However, dietary compliance has been shown to

† The authors wish to dedicate this work to the memory of Prof. Arturo Leone, Director of the Institute of Food Sciences, CNR, Avellino, Italy.

* Addess correspondence to Dr. Sabato D'Auria, Institute of Protein Biochemistry, Consiglio Nazionale delle Ricerche, Via Pietro Castellino 111, 80131 Naples, Italy. Fax, +39-0816132277; e-mail, s.dauria@ibp.cnr.it.

‡ Institute for Microelectronics and Microsystems, CNR.

§ Institute of Food Sciences, CNR.

|| Institute of Protein Biochemistry, CNR.

10.1021/pr0600226 CCC: $33.50 © 2006 American Chemical Society



Published on Web 03/21/2006

be poor in most patients mainly because of inadvertent gluten consumption. From this point of view, a very sensitive assay for detection of toxic components of prolamins in food represents a perspective worth pursuing. Furthermore, the gliadin is a mixture of many proteins.[10] This observation highlighted the difficulties in identifying sequences useful for developing an immunoassay addressed toward the toxic portions of gliadin. The obtained results show that, even if the protein is blocked on the PSi surface, the GlnBP can strongly bind the substrate and work as a molecular probe for the detection of gliadin.

## Materials and Methods

**Materials.** All the chemicals used were commercial samples of the purest quality.

**Protein Purification.** The recombinant glutamine-binding protein from *E. coli* was prepared and purified according to D'Auria et al.[7] The protein concentration was determined by the method of Bradford[11] with bovine serum albumin as standard on a double beam Cary 1E spectrophotometer (Varian, Mulgrade, Victoria, Australia).

**Mass Spectrometry Analysis.** MALDI-TOF experiments were carried out on a PerSeptive Biosystems (Framingham, MA) Voyager DE-PRO instrument equipped with a $N_2$ laser (337 nm, 3 ns pulse width). Each spectrum was taken with the following procedure: 1 $\mu$L-aliquot of sample was loaded on a stainless steel plate together with 1 $\mu$L of matrix α-cyano-4-hydroxycinnamic acid (10 mg in 1 mL of aqueous 50% acetonitrile). Mass spectrum acquisition was performed in both positive linear and reflectron mode by accumulating 200 laser pulses. The accelerating voltage was 20 kV. External mass calibration was performed with mass peptide standards (SIGMA). Tandem mass spectrometry (MS/MS) data for the extracted peptides were obtained using a Q-STAR mass spectrometer (Applied Biosystems) equipped with a nanospray interface (Protana, Odense, Denmark). Dried samples were resuspended in 0.1% TFA, desalted using Zip-Tip C18 microcolumns (Millipore), and sprayed from gold-coated, 'medium length' borosilicate capillaries (Protana). The capillary voltage used was 800 V. Doubly charged ion isotopic cluster was selected by the quadrupole mass filter (MS1) and then induced to fragment by collision. The collision energy was 30−40 eV, depending on the size of the peptide. The collision-induced dissociation was processed using Analyst 5 software (Applied Biosystems). The deconvolution MS/MS was manually interpreted with the help of the Analyst 5 software.

**Porous Silicon Chip Preparation and GlnBP Immobilization.** Proof of PSi in biosensing has been experimentally demonstrated in a variety of sensors devices, including rugate filters, Bragg filters, single-layer films, and protein and DNA microarray, due to the large internal surface area which depending upon depth can easily be over 1000 times that of a planar surface of equal diameter, thus, enabling the immobilization of large amounts of selective receptors.[12−14] However, for the device to function effectively, the porous morphology should enable homogeneous diffusion everywhere in the matrix. In the case of porous silicon, the porosity, determined by pore size and distribution, is tunable over a rather wide range by properly setting the fabrication parameters, that is, current density, etching time, etching solution, and wafer type. It is therefore possible to optimize the porous matrix structure to achieve maximum diffusion and maintain high level optical features. Previous ellipsometric characterization has shown that the surface of the porous silicon layer as prepared could be covered by a 100−200 nm thin parasitic film of very low porosity (<20%) due to hydrogen contamination of the silicon wafer.[15] Such film prevents not only the pores from filling but also any biochemical interaction with the porous silicon surface after the etching process. For sensing purposes, it is therefore mandatory to avoid the formation of the parasitic film by thermally treating the wafer at 300 °C in a nitrogen atmosphere before the electrochemical etch.[16]

In our experiments, we used a porous silicon Fabry-Perot film, which optically acts as an interferometer fabricated by electrochemical etching of $p^+$-type (100) crystalline silicon (resistivity 8−12 mΩ cm) in HF/EtOH (30:70) solution. The etching current had a value of 150 mA/cm$^2$ and was applied for 73 s. The layer thickness was about 10 $\mu$m, and the porosity was about 70% (values estimated by fitting the optical reflectivity data). The electrochemical dissolution process leaves nanodimensional residues into the channels which partially fill the pores in the layers and prevent a homogeneous diffusion of biological solutions. To remove the nanostructures and improve pore infiltration of biomolecular probe-target systems, we used a KOH post-etch process elsewhere described.[17] The optical setup required for our sensing experiments was very simple: a tungsten lamp (400 nm < $\lambda$ < 1800 nm) stimulated the sensor, through an optical fiber and a collimator. The reflected beam was collected by an objective, coupled into a multimode fiber, and then directed in an optical spectrum analyzer (Ando, AQ6315A). The reflectivity spectra, measured with a resolution of 0.1 nm, exhibited many fringes in the wavelength range between 900 and 1200 nm. The solutions containing the molecular probe and the analyte were directly spotted on the sensor surface.

Procedures for the immobilization of biomolecules on porous silicon are usually based on a chemistry which involves the silanization of the oxidized PSi surface.[18] A promising, recently proposed alternative is that exploiting the reaction of acids molecules with the hydrogen-terminated porous silicon surface to obtain a more stable organic layer covalently attached to the PSi surface through Si−C bonds.[19] In particular, we exploited a photoactivated modification of PSi surface based on the UV exposure of a solution of alkenes functionalized with carboxylic acid groups. After it was ultrasonically cleaned in acetone for 10 min, the PSi chip was washed with deminerilized (demi) water and dried in $N_2$ stream and immediately covered with a 10% *N*-hydroxysuccinimide ester (UANHS) solution in $CH_2Cl_2$. The chip was exposed to a UV lamp (500 W, 40 $\mu$W/cm$^2$ measured) for 45 min. The UANHS was synthesized in-house as described.[19] This treatment resulted in covalent attachment of UANHS to the porous silicon surface following the reaction showed in Figure 1. After the photoreaction, the chip was washed by dichloromethane in an ultrasonic bath three times for 5 min and rinsed with acetone to remove any adsorbed alkene from the surface. The carboxyl-terminated surface obtained acts as a substrate for the chemistry of the subsequent attachment of the protein.

Gliadin and rice prolamins were extracted from flours with 60% (v/v) aqueous ethanol by magnetic stirring for 30 min at 50 °C. The suspensions were centrifuged for 20 min at 15 000*g* at room temperature. The supernatants were freeze-dried; prolamins were subsequently dissolved in 0.2 N HCl and incubated with pepsin (1:100 enzyme/substrate ratio) for 2 h at 37 °C; then, the pH was adjusted to 8.0 and trypsin added (enzyme/substrate ratio of 1:100). After a 2.0-h incubation at

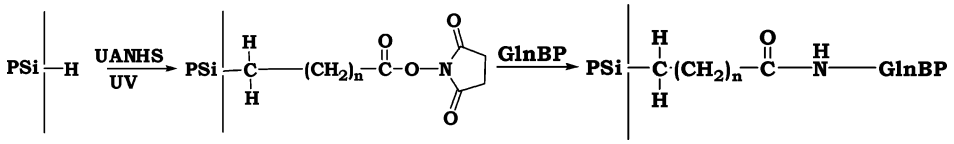


**Figure 1.** Photoinduced reaction used to link GlnBP to the PSi chip surface.

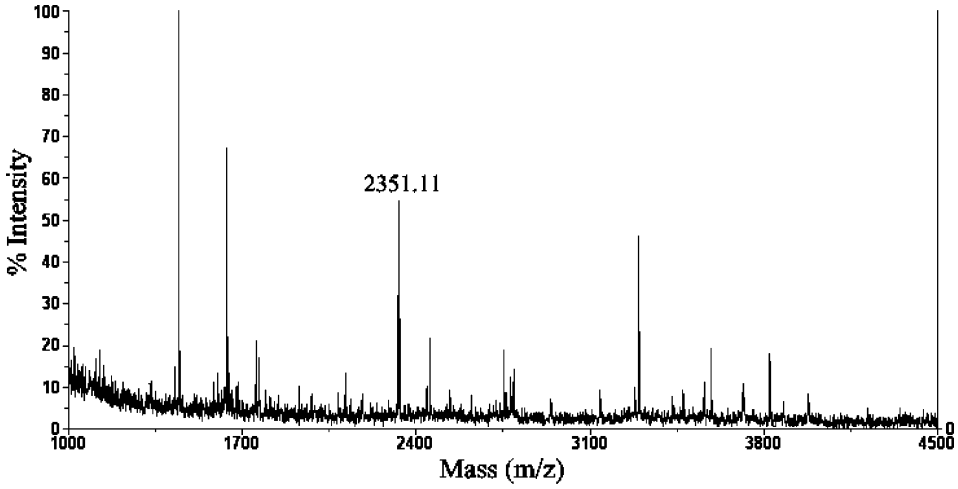


**Figure 2.** MALDI-TOF spectrum of gliadin digest bound to GlnBP. The amino acid sequence of $MH^+$ 2351.11 was determined by nanoESI−MS/MS.

37 °C, the reaction was stopped by heating for 5 min; the peptic-tryptic (PT) digest was freeze-dried and stored at −20 °C.

A solution of homogeneous 2.0 mg/mL GlnBP in 1.0 mL of 0.1 M bicarbonate buffer, pH 9.0, was mixed with 10 $\mu$L of rodhamine (Molecular Probes) solution in *N*,*N*-dimethylformamide (DMF) (1.0 $\mu$g of rodhamine/100 $\mu$L of DMF). The reaction mixture was incubated for 1.0 h at 30 °C, and the labeled protein was separated from the unreacted probe by passing over a Sephadex G-25 column equilibrated in 50 mM phosphate buffer and 100 mM NaCl, pH 7.0.

The immobilization of GlnBP was carried out by applying 50 $\mu$L of a 1 mg/mL solution prepared in 100 mM PBE buffer at pH 6.5 to each chip. The chips were incubated at −4 °C for 1.0 h. After the reaction, the excess of reagent was removed and the wafers were extensively washed at room temperature by PBE buffer.

To assess the protein penetration into the pores, we spotted 20 $\mu$L of 1.0 mM sodium bicarbonate buffer containing the dye-labeled protein onto the porous silicon chip. This chip was observed by a confocal microscopy system.

## Results and Discussion

GlnBP is a monomeric protein that binds glutamine (Gln) and poly-Gln residues with high affinity.[7,8] Since gluten proteins are rich in Gln residues, we questioned if GlnBP was able to bind amino acid sequences present in gluten proteins such as gliadin, a protein toxic for celiac patients. To check it, GlnBP was covalently bound to a CNBr-activated Sepharose 4B resin according to the manufacturer's instructions (Amersham Biosciences Europe GmbH, Cologno Monzese, Italy) and a gliadin PT digest was passed through the column. The column was washed with 3 vol of phosphate buffer saline, and the peptide(s) bound to GlnBP were eluted with 0.2 M glycine/HCl, pH 3.0. The eluted fractions were utilized for mass spectrometric experiments.

MALDI-TOF analysis on the isolated gliadin digest gave a complex peptide profile, which was difficult to rationalize due to the high sequence variability among the components of the gliadin fraction (Figure 2). In fact, the main difficulty in gliadin structural analysis lies in high protein heterogeneity owed to numerous duplications, and subsequent divergences of the gliadin multigene family encoding a polymorphic set of polypeptides. To identify the derived PT peptides, the gliadin sequences in the eluted fraction were analyzed by MS/MS experiments. Figure 3 shows the nanoESI−MS/MS spectrum of the triply charged ion at $m/z$ 784.37 ($MH^+$ = 2351.11 Da), corresponding to the sequence XXQPQPQQQQQQQQQQQL (X indicates an unidentified residue) corresponding to that of wheat α-gliadin (Swiss-Prot, accession number Q9ZP09) with only the last 13 amino acid residues of peptide.

The two amino acid residues located at the peptide N-teminal, corresponding to the "*b2*" fragment, were not exactly identified (Figure 3). In particular, since the "*b2*" fragment is 232.08 Da, the first two amino acid residues could be either Met−Thr or Thr−Met. For this reason, we preferred to indicate them as XX.

This result prompts us to develop a new methodology for sensing toxic sequences for celiac patients. First, we immobilized GlnBP to a porous silicon wafer and tested the strength of the covalent bond between the labeled GlnBP and the porous silicon surface by washing the chip in a demi-water flux. In Figure 4, a confocal microscopy image of the PSi chip under a He−Ne laser beam irradiation is shown. We found that the fluorescence is very high and homogeneous on the whole surface. We also checked, by Fourier transformed infrared (FT-IR) spectroscopy, that the PSi surface covered by the protein shows a good stability toward aqueous oxidation: after the water treatment, the characteristic peak of Si−O−Si bonds did not appear in the FT-IR spectrum. In the presence of gliadin PT, GlnBP undergoes a large conformational change in its global structure to accommodate the ligand inside the binding

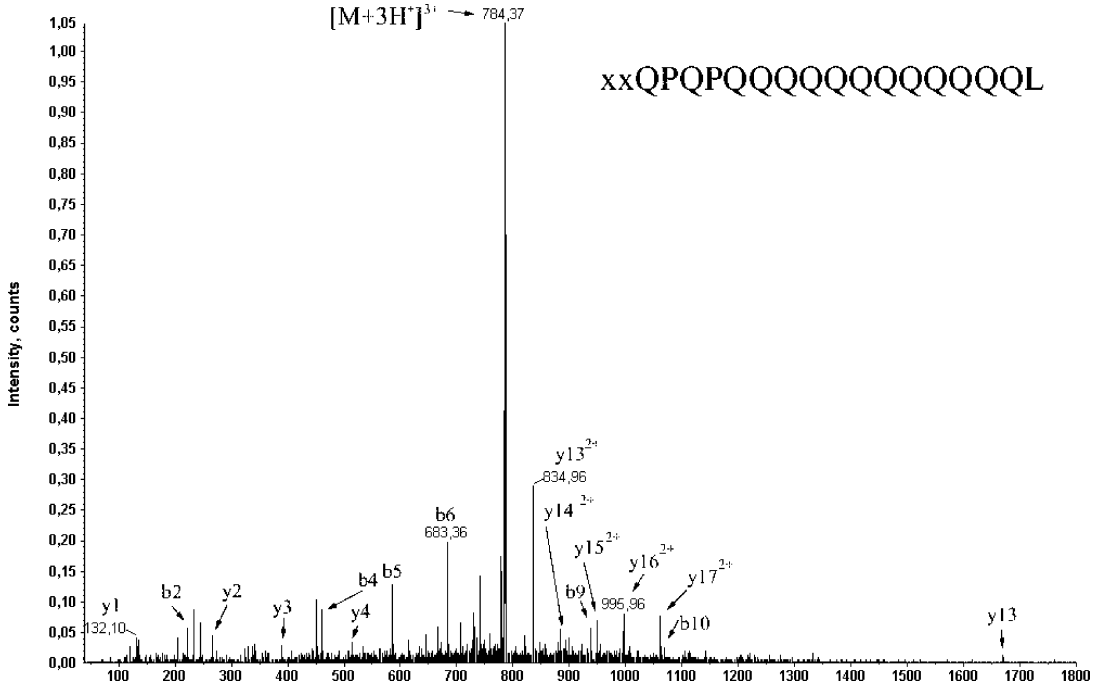


**Figure 3.** MS/MS spectra of triple ion charged 784.37 ($M = 2351.11$ Da).

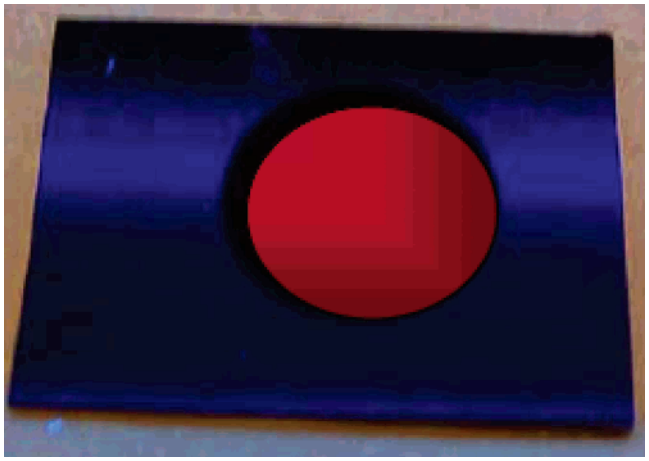

**Figure 4.** Confocal microscopy image of the PSi chip after immobilization of rodhamine-labeled GlnBP.

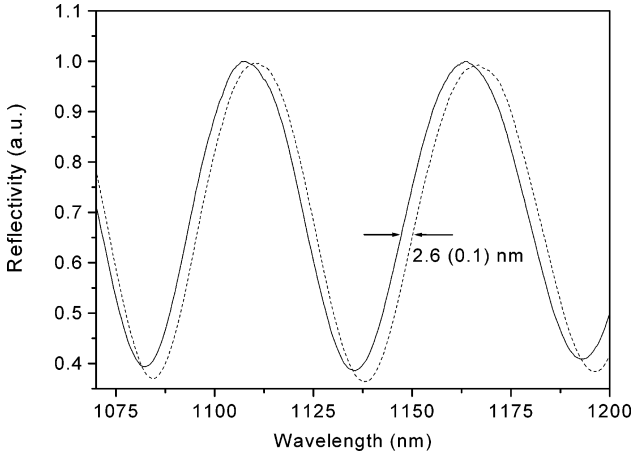


**Figure 5.** Fringes' shift due to protein−protein interaction. Continuous curve, porous silicon and GlnBP; dashed curve, porous silicon, GlnBP, and PT-gliadin. Wavelength shift between the continuous curve and the dashed curve is 2.6 (0.1) nm.

site. The ligand-binding event was detected as a fringe shift in wavelength, which corresponds to a change in the optical path *nd*. Since the thickness *d* is fixed by the physical dimension of the PSi matrix, the variation is clearly due to changes in the average refractive index.

The experimental measurement to detect the binding of gliadin to GlnBP is a two-step procedure: first, we registered the optical spectrum of the porous silicon layer after the GlnBP absorption on the chip surface and, then, after the PT-gliadin solution has been spotted on it. The organic material excess was removed by further rinses in the buffer solution. In Figure 5, the shifts induced in the fringes of the reflectivity spectrum are reported. A well-defined red-shift of 2.6 ± 0.1 nm all over a wide range of wavelengths, due to protein−ligand interaction, was registered. Control experiments were made by using two different solutions containing nontoxic peptides produced following a peptic-tryptic digestion of zein, the corresponding prolamines from corn, and rice prolamines, that represent safe cereals for celiac patients; the fringes' shift in the reflectivity spectrum, with respect to the one obtained after the GlnBP absorption on the chip surface, was undetectable ($\Delta\lambda < 0.1$ nm) in each single measurement.

We also measured the signal response to the protein concentration after the ligand interaction. Figure 6 shows the dose−response curve as a function of the PT-gliadin concentration. Since the sensor displays a linear response between 2.0 and 8.0 $\mu$M, it is possible to calculate the sensitivity of the optical interferometer to the concentration of PT-gliadin by estimating the slope of the curve: $s_{Gli} = 421$ (13) nm/$\mu$M. The sensor response saturates approximately at 35 $\mu$M, which means that about 45% of the spotted proteins have bound the respective peptide.

The rationale of the proposed strategy is that gluten proteins (gliadins and glutenins) are characterized by a high content of glutamine (Gln) residues and, consequently, they represent a

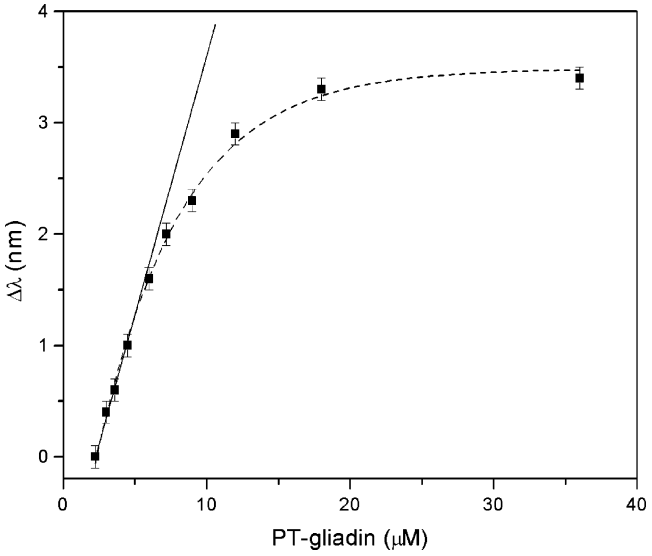


**Figure 6.** Dose−response curve. Optical variations as a function of the PT-gliadin concentration.

substrate for the GlnBP. As a consequence, the relevance of these results for the topic of gluten determination has been addressed. The detection of residual gluten in food is fundamental for celiacs patients. Among toxic prolamins, gliadin has been very well characterized. Gliadin is a mixture of many proteins;[10] biochemical analysis revealed the existence of a relationship among the various constituents, so gliadin fractions have been grouped in three classes named α, $\gamma$, and $\omega$ gliadins.[20] To date, several immuno-active gliadin peptides in the celiac population have been identified.[21,22] Some of these epitopes are encompassed in a 33-mer gliadin peptide found to be resistant to digestion by gastric and pancreatic enzymes.[22] It is noteworthy that most of these T-cell epitopes were recognized following deamidation catalyzed by tissue transglutaminase (tTG), in which some specific glutamine residues were converted to glutamic acid.[23] Moreover, T-cell epitopes cluster in regions that are rich in proline residues.[24] Taken together, these observations highlighted the difficulties in identifying sequences useful for developing immunoassays addressed toward the toxic portions of gliadin. Ideally, a method to determine gliadin should be applicable in a wide range of food, irrespective of processing, and should be directly related with toxicity. Until now, none of the produced methods were considered to be fully satisfactory.[25,26] On the other hand, the use of reducing agents, that are present in the proposed solvent, can improve the extraction of prolamines but affect their immunochemical quantification.[27] From this point of view, our method can potentially work also in reducing conditions, thus, overcoming the problem related to prolamin extraction.[28]

In conclusion, in this work, we have presented useful data for the development of an optical protein microsensor, based on porous silicon nanotechnology, for an easy and rapid detection of gliadin. The porous silicon matrix is demonstrated to be very useful as transducer material in this kind of biosensor: its highly specific area ensures good sensitivities in organic molecules sensing, and at the same time, it supplies a fast and easy readable optical response. Even if the GlnBP is covalently bonded to the PSi surface, due to a proper functionalization process, it still selectively recognizes the target analyte with an overall efficiency of 45%. Genetic manipulation experiments for improving the protein affinity to PT-gliadin are in progress.

Abbreviations: GlnBP, glutamine-binding protein; Gln, glutamine; PSi, porous silicon; MS/MS, tandem mass spectrometry; nanoESI, nanospray electrospray ionization.

**Acknowledgment.** This project was realized in the frame of the CRdC-ATIBB and CRdc-NTP POR UE-Campania Mis 3.16 activities and in the frame of the CNR Commessa "Diagnostica avanzata ed alimentazione".

## References

(1) Lee, T. M.; Hsing, I. *Anal. Chim. Acta* **2005**, *530*, 143−153.
(2) Arrand, H. F.; Loni, A.; Arens-Fischer, R.; Kruger, M. G.; Thoenissen, M.; Lueth, H.; Kershaw, S.; Vorazov, N. N. *J. Lumin.* **1999**, *80*, 119−123.
(3) Chamard, V.; Dolino, G.; Muller, F. *J. Appl. Phys.* **1998**, *84*, 6659−6666.
(4) *Properties of Porous Silicon*; Canham, L., Ed.; IEE Inspec: London, 1997.
(5) Dancil, K.-P. S.; Greiner, D. P.; Sailor, M. J. *J. Am. Chem. Soc.* **1999**, *121*, 7925−7930.
(6) Dattelbaum, J. D.; Lakowicz, J. R. *Anal. Biochem.* **2001**, *291*, 89−95.
(7) D'Auria, S.; Scirè, A.; Varriale, A.; Scognamiglio, V.; Staiano, M.; Ausili, A.; Rossi, M.; Tanfani, F. *Proteins* **2005**; *58*, 80−87.
(8) Kuznetsova, I. M.; Stepanenko, O. V.; Turoverov, K. K.; Staiano, M.; Scognamiglio, V.; Rossi, M.; D'Auria, S. *J. Proteome Res.* **2005**, *4*, 417−423.
(9) Maki, M.; Collin, P. *Lancet* **1997**, *349*, 1755−1759.
(10) Platt, S. G.; Kasarda, D. D. *Biochim. Biophys. Acta* **1971**, *243*, 407−415.
(11) Bradford, M. M. *Anal. Biochem.* **1976**, *72*, 248−254.
(12) De Stefano, L.; Moretti, L.; Rendina, I.; Rossi, A. M.; Tundo, S. *Appl. Opt.* **2004**, *43*, 167−172.
(13) De Stefano, L.; Moretti, L.; Rossi, A. M.; Rocchia, M.; Lamberti, A.; Longo, O.; Arcari, P.; Rendina, I. *IEEE Trans. Nanotech.* **2004**, *3*, 49−54.
(14) Gao, J.; Gao, T.; Sailor, M. J. *Appl. Phys. Lett.* **2000**, *77*, 901−903.
(15) Gaillet, M.; Guendouz, M.; Ben Salah, M.; Le Jeune, B.; Le Brun, G. *Thin Solid Films* **2004**, *455−456*, 410−416.
(16) Chamard, V.; Dolino, G.; Muller, F. *J. Appl. Phys.* **1998**, *84*, 6659.
(17) DeLouise, L. A.; Miller, B. L. *Mater. Res. Soc. Symp. Proc.* **2004**, *782*, A5.3.1.
(18) Hart, B. R.; Letant, S. E.; Kane, S. R.; Hadi, M. Z.; Shields, S. J.; Reynolds, J. G. *Chem. Commun.* **2003**, 322−323.
(19) Yin, H. B.; Brown, T.; Gref, R.; Wilkinson, J. S.; Melvin, T. *Microelectron. Eng.* **2004**, *73−74*, 830−836.
(20) Wieser, H.; Mödl, A.; Seilmeier, W.; Belitz, H. D. *Z. Lebens. -Unters. Forsch.* **1987**, *185*, 371−378.
(21) Vader, L. W.; de Ru, A.; van der Wal, Y.; Kooy, Y. M. C.; Benckhuijsen, W.; Merin, M. L.; Wouter Drijfhout, J. W.; van Veelen, P.; Koning, F. *J. Exp. Med.* **2002**, *195*, 643−649.
(22) Van de Wal, Y.; Kooy, Y. M.; van Veelen, P. A.; Pena, S. A.; Mearin, L. M.; Molberg, O.; Lundin, K. E.; Sollid, L. M.; Mutis, T.; Benckhuijsen, W. E.; Drijfhout, J. W.; Koning, F. *Proc. Natl. Acad. Sci. U.S.A.* **1998**, *95*, 10050−10054.
(23) Shan, L.; Molberg, O. *Science* **2002**, *297*, 2275−2279.
(24) Molberg, O.; McAdam, S. N.; Korner, R.; Quarsten, H.; Kristiansen, C.; Madsen, L.; Fugger, L.; Scott, H.; Noren, O.; Roepstorff, P.; Lundin, K. E.; Sjostrom, H.; Sollid, L. M. *Nat. Med.* **1998**, *4*, 713−717.
(25) Arentz-Hansen, H.; McAdam, S. N.; Molberg, O.; Fleckenstein, B.; Lundin, K. E.; Jorgensen, T. J.; Jung, G.; Roepstorff, P.; Sollid, L. M. *Gastroenterology* **2002**, *123*, 803−809.
(26) Skerrit, J. H.; Hill, A. S. *J. Agric. Food Chem.* **1990**, *38*, 1771−1778.
(27) Sorell, L.; Lopez, J. A.; Valdes, I.; Alfonso, P.; Camafeita, E.; Acevedo, B.; Chirdo, F.; Gavilondo, J.; Mendez, E. *FEBS Lett.* **1998**, *439*, 46−50.
(28) Margheritis, A. I.; Dona, V. V.; Fossati, C. A.; Chirdo, F. G. *Proceedings of the 17*th *Meeting of the Working Group on Prolamin Analysis and Toxicity*, London, U.K., October 3−6, 2002; Verlag Wissenschaftliche Scripten, Zwickau.

PR0600226

INSTITUTE OF PHYSICS PUBLISHING JOURNAL OF PHYSICS: CONDENSED MATTER

J. Phys.: Condens. Matter **18** (2006) S2019–S2028 doi:10.1088/0953-8984/18/33/S17

# Nanostructured silicon-based biosensors for the selective identification of analytes of social interest

**Sabato D'Auria[1,4], Marcella de Champdoré[1], Vincenzo Aurilia[1], Antonietta Parracino[1], Maria Staiano[1], Annalisa Vitale[1], Mosè Rossi[1], Ilaria Rea[2], Lucia Rotiroti[2], Andrea M Rossi[3], Stefano Borini[3], Ivo Rendina[2] and Luca De Stefano[2]**

[1] Institute of Protein Biochemistry, CNR, Via Pietro Castellino, 111 80131 Naples, Italy
[2] Institute for Microelectronics and Microsystems, CNR—Department of Naples, Via Pietro Castellino 111, 80131 Naples, Italy
[3] Istituto Nazionale di Ricerca Metrologica—INRIM, Via Strada delle Cacce 91, 10100 Turin, Italy

E-mail: s.dauria@ibp.cnr.it

Received 13 January 2006
Published 4 August 2006
Online at stacks.iop.org/JPhysCM/18/S2019

**Abstract**

Small analytes such as glucose, L-glutamine (Gln), and ammonium nitrate are detected by means of optical biosensors based on a very common nanostructured material, porous silicon (PSi). Specific recognition elements, such as protein receptors and enzymes, were immobilized on hydrogenated PSi wafers and used as probes in optical sensing systems. The binding events were optically transduced as wavelength shifts of the porous silicon reflectivity spectrum or were monitored via changes of the fluorescence emission. The biosensors described in this article suggest a general approach for the development of new sensing systems for a wide range of analytes of high social interest.

(Some figures in this article are in colour only in the electronic version)

## 1. Introduction

For many decades, scientists have recognized the power of incorporating biological principles and molecules into the design of artificial devices. Biosensors, an amalgamation of signal transducers and biocomponents, play a prominent role in medicine, food, and processing technologies. Compactness, portability, high specificity, and sensitivity represent some reasons why biosensors are considered as holding promise, with high potential for replacing current analytical practice [1].

[4] Address for correspondence: Institute of Protein Biochemistry, Italian National Research Council, Via Pietro Castellino, 111-80131 Naples, Italy.

 © 2006 IOP Publishing Ltd Printed in the UK 

Fluorescence detection is the dominant analytical approach in medical testing, biotechnology, and drug discovery. Starting in the 1980s the first chemically synthesized fluorescence probes for specific analytes became available. However, the development of probes for complex analytes present in biological specimens cannot be approached via chemical synthesis alone [2–4]. In fact, the number of potential ligands specifically recognized by different proteins is very large and ranges from small molecules to macromolecules (including proteins themselves). The advantages of using proteins as components of biosensors are many and include relatively low costs in design and synthesis, the fact that proteins are, at least in general, soluble in water, and finally, with the progress of molecular genetics, the possibility of improving/changing some of the properties of the proteins by genetic manipulation [5, 6].

Recently, a lot of experimental work exploiting the properties of porous silicon (PSi) in chemical and biological sensing has been reported [7, 8]. PSi is an almost ideal material as a transducer due to its porous structure, with a hydrogen terminated surface, having a specific area of the order of 200–500 $m^2$ $cm^{-3}$, so a very effective interaction with several adsorbates is ensured. Moreover, PSi is an available and low cost material, completely compatible with standard IC processes, and a useful component of so-called smart sensors [9]. The PSi is fabricated by the electrochemical etching of a silicon (Si) wafer in a hydrofluoridic acid solution. It is well known that the porous silicon 'as etched' has an Si–H terminated surface due to the Si dissolution process [10]. PSi optical sensors are based on changes of photoluminescence or reflectivity upon exposure to the target analytes [11, 12], which replace the air in the PSi pores. The optical changes depend on the chemical and physical properties of the bound analyte. As a consequence, these devices cannot be used for the identification of analytes in a complex mixture. In order to enhance the sensor selectivity, it is possible to utilize PSi wafer as substrate for the covalent immobilization of biomolecules, such as proteins, enzymes, and antibodies, that are able to recognize target analytes in a complex matrix [13–20].

In this paper, we report new findings of relevance to the design of advanced biosensors obtained by a multidisciplinary group of scientists, for the optical detection of analytes of social interest such as glucose, ammonium nitrate, and glutamine.

## 2. Glucose detection

Close control of blood glucose is essential to avoid the long term adverse consequences of elevated blood glucose, including neuropathies, blindness, and other consequences [21]. Non-invasive measurements of blood glucose have been a long-standing research target because they would allow the development of a variety of devices for diabetic health care, including continuous painless glucose monitoring, control of an insulin pump, and warning systems for hyperglycaemic and hypoglycaemic conditions. Hypoglycaemia is a frequent occurrence in diabetics, and can result in coma or death. The acute and chronic problems of diabetics and hypoglycaemia can be ameliorated by continuous monitoring of blood glucose. At present, the only reliable method for measuring blood glucose is via a finger prick and subsequent glucose measurement, typically using glucose oxidase. This procedure is painful and even the most compliant individuals, with good understanding and motivation for glucose control, are not willing to prick themselves more than several times per day. These medical needs have fostered intensive efforts to develop sensors for glucose [22, 23]. The absence of a suitable non-invasive glucose measurement has fostered decades of research, little of which has however resulted in simpler and/or improved glucose monitoring. Included in this effort is the development of fluorescence probes specific for glucose, typically based on boronic acid chemistry [24, 25]. An alternative approach to glucose sensing using fluorescence is based on proteins which bind glucose. Optical detection of glucose appears to have had its origin

in the promising studies of Schultz and co-workers [26, 27], who developed a competitive glucose assay which does not require substrates and does not consume glucose. This assay used fluorescence resonance energy transfer (FRET) between a fluorescence donor and an acceptor, each covalently linked to concanavalin A (ConA) or dextran. In the absence of glucose the binding between ConA and dextran resulted in a high FRET efficiency. The addition of glucose resulted in its competitive binding to ConA, displacement of ConA from the labelled dextran, and a decrease in FRET efficiency. These results generated considerable enthusiasm for fluorescence sensing of glucose [28]. The glucose–ConA system was also studied by other labs. They identified several problems, namely that the system was only partially reversible upon addition of glucose, and that it became less reversible with time and showed aggregation [29]. For this reason, the use of other glucose-binding proteins as sensors was explored by several research groups [30–35]. If a reliable fluorescence assay for glucose could be developed, then the robustness of lifetime-based sensing [36] could allow development of a minimally invasive implantable glucose sensor, or of a sensor which uses extracted interstitial fluid. The lifetime sensor could measure glucose concentration through the skin [37] using a red laser diode or light emitting diode (LED) device as the light source. These devices are easily powered with batteries and can be engineered into a portable device. An implantable sensor can be expected to report on blood glucose because tissue glucose closely tracks blood glucose with a 15 min time lag [38].

Glucose oxidase (GO) (EC 1.1.3.4) from *Aspergillus niger* catalyses the conversion of $\beta$-D-glucose and oxygen to D-glucono-1,5-lactone and hydrogen peroxide. It is a flavoprotein, highly specific for $\beta$-D-glucose, and is widely used to estimate glucose concentration in blood or urine samples through the formation of coloured dyes [39]. Because glucose is consumed, this enzyme cannot be used as a reversible sensor. We extended the use of GO under conditions where no reaction occurs. In particular, in order to prevent glucose oxidation, we removed the FAD cofactor which is strictly required for the reaction.

The absorbance spectrum of apo-GO shows the characteristic shape of the coenzyme-free proteins, with an absorbance maximum at 278 nm due to the aromatic amino acid residues. The absence of absorption at wavelengths above 300 nm indicates that the FAD has been completely removed. The fluorescence emission spectrum of apo-GO at room temperature upon excitation at 298 nm displays an emission maximum at 340 nm, which is characteristic of partially shielded tryptophan residues. The addition of 20 mM glucose to the enzyme solution resulted in a quenching of about 18% of the tryptophanyl fluorescence emission (data not shown). This result indicates that the apo-GO is still able to bind glucose. The observed fluorescence quenching may be mainly ascribed to the tryptophanyl residue 426. In fact, as shown by x-ray analysis and molecular dynamics simulations, the glucose-binding site of GO is formed by Asp 584, Tyr 515, His 559 and His 516. Moreover, Phe 414, Trp 426 and Asn 514 are in locations where they might form additional contacts with glucose [40].

The intrinsic fluorescence of proteins is usually not useful for clinical sensing because of the need for complex or bulky light sources and because of the presence of numerous proteins in most biological samples. ANS is known to be a polarity-sensitive fluorophore which displays an increased quantum yield in low polarity environments. Additionally, ANS frequently binds to proteins with an increase in intensity. We examined the effects of GO on the emission intensity of ANS. Addition of apo-GO to an ANS solution resulted in an approximate 30-fold increase in the ANS fluorescence intensity. Importantly, the intensity of the ANS emission was sensitive to glucose, decreasing by approximately 25% upon glucose addition. The ANS was not covalently bound to the protein. That addition of glucose results in a progressive decrease in the ANS fluorescence intensity suggests that the ANS is being displaced into a more polar environment upon glucose binding. The decreased ANS intensity occurred with a glucose-

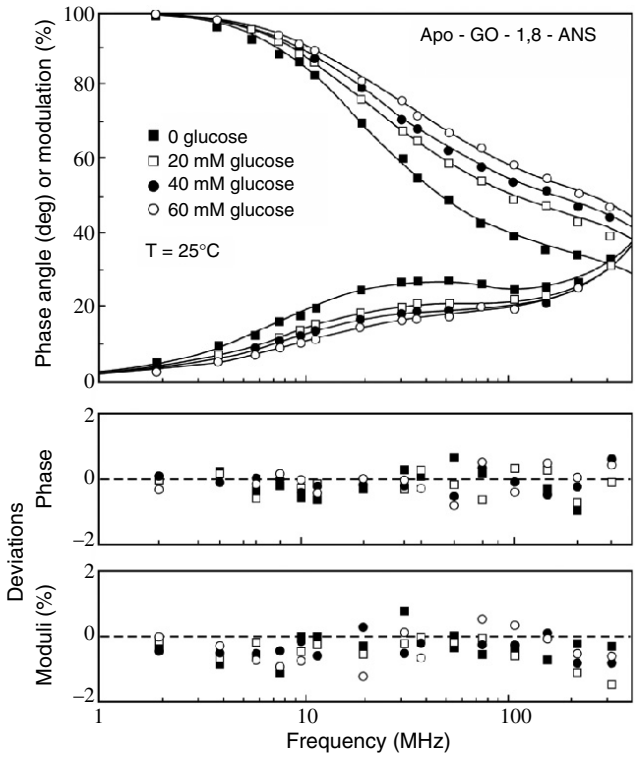


**Figure 1.** Frequency domain intensity decays of 1,8-ANS-glucose oxidase at different concentrations of glucose. Excitation was at 335 nm while the emission was observed through interference filter 535/50 nm with two Corning 3–71 cut-off filters.

binding constant near 10 mM, which is comparable to the $K_D$ of the holo-enzyme. The fact that the binding affinity has not changed significantly may imply that the binding is still specific to glucose. Intensity decays of ANS-labelled apo-GO in the presence of glucose were studied by frequency domain fluorometry. Addition of glucose shifts the frequency responses to higher frequencies, which is due to a decreased ANS lifetime (figure 1). The shorter lifetime of ANS apo-GO in the presence of glucose is again consistent with the suggestion that glucose displaces the ANS to a more polar environment. The mean lifetime decreases by over 40% upon addition of glucose. These results demonstrate that apo-glucose oxidase, when labelled with suitable fluorophores, can serve as a protein sensor for glucose.

## 3. Explosive detection

Organophosphorous pesticides, nerve agents and nitro-aromatic compounds are very dangerous substances which can be used against civil or military objectives. Recently, Bourne and colleagues have demonstrated the mechanism of inhibition, at molecular level, of the acetylcholinesterase (AChE) with several inhibitor molecules [41]. The peripheral anionic site on AChE, located at the active centre gorge entry (figure 2), encompasses overlapping binding sites for allosteric activators and inhibitors; yet, the molecular mechanisms coupling this site to the active centre at the gorge base to modulate catalysis remain unclear. The peripheral site

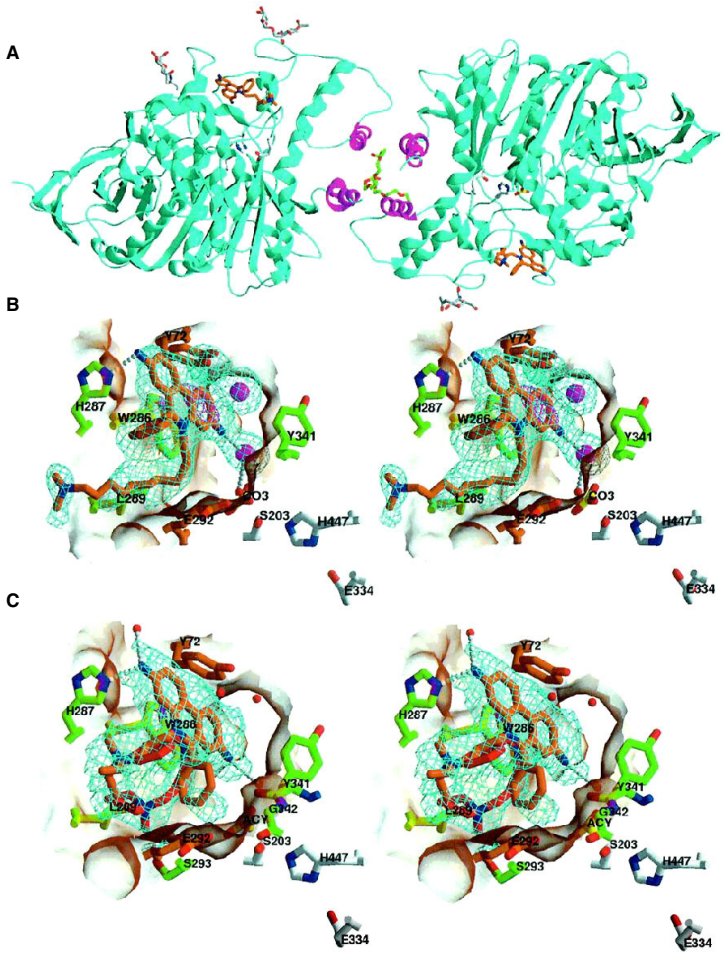


**Figure 2.** Structures of the DI–mAChE and PI–mAChE complexes. (A) Ribbon diagram of the mAChE dimer (cyan, with the four-helix bundle in magenta) bound to DI (orange bonds, blue nitrogen and red oxygen atoms). The carbohydrate moieties linked to residues Asn 350 and Asn 464 in both subunits are displayed as grey bonds and coloured spheres. The side chains of the catalytic triad residues, Ser 203, Glu 334, and His 447, are shown as white bonds in the two dimer subunits. The PEG molecule bound at the centre of the four-helix bundle and the carbonate molecule bound to Ser 203 are shown as grey (green) and light grey (yellow) bonds, respectively. (B) Close-up stereo view of the DI molecule (coloured as in A) bound to the PAS, with the 2.35 Å resolution omit $F_o - F_c$ electron density map contoured at $3.5\sigma$ (cyan) and $7.5\sigma$ (blue); the coordinates of this region were omitted and the protein coordinates were refined by simulated annealing before the phase calculation. The interacting side chains of mAChE residues His 287 and Leu 289, located in the loop region connecting helices $\alpha^3_{6,7}$ and $\alpha^4_{6,7}$, and of residues Trp 286 and Tyr 341 at the gorge entrance, are displayed as grey (green) bonds; those of mAChE residues Tyr 72 and Glu 292, whose respective mutations as methionine and lysine in BgAChE abolish PI binding (see figure 6), are highlighted in light grey (orange). The chloride ions and solvent molecules are shown as pink and red spheres, respectively. The catalytic triad residues, Ser 203, Glu 334, and His 447, and the carbonate molecule (bottom) are shown as white and light grey (orange) bonds, respectively. Hydrogen bonds between mAChE and the DI molecule are shown as white dotted lines. (C) Close-up stereo view of the PI molecule (coloured as for DI) bound to the PAS, with the 2.35 Å resolution omit $F_o - F_c$ electron density map contoured at $3.5\sigma$ (cyan). The PI phenyl and diethylmethylammonio moieties, which show alternative positions in the structure, are displayed as red and orange bonds. The mAChE side chains interacting with the PI molecule are displayed as grey (green) and light grey (orange) bonds as in (B). The mAChE molecular surfaces buried at the DI–mAChE (B) and PI–mAChE (C) complex interfaces are displayed in transparency.

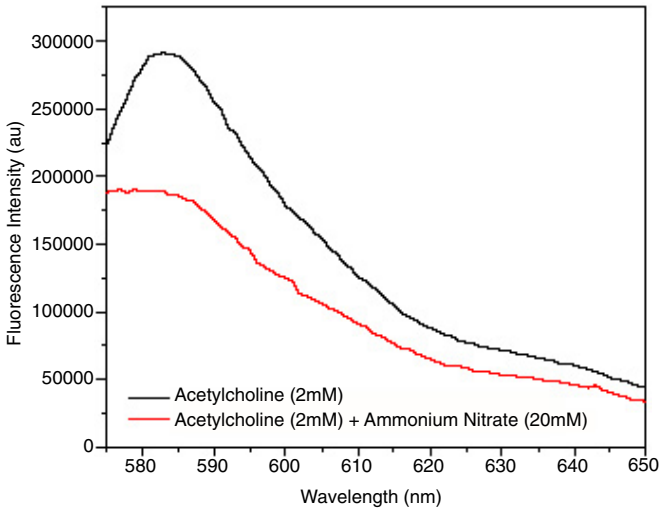


**Figure 3.** Fluorescence emission spectra of AChE immobilized on Psi, in the absence and in the presence of ammonium nitrate.

has also been proposed to be involved in heterologous protein associations occurring during synaptogenesis or upon neurodegeneration [42].

A crystal form of mouse AChE, combined with spectrophotometric analyses of the crystals, allowed us to obtain unique structures of AChE with a free peripheral site, and as three complexes with peripheral site inhibitors: the phenylphenanthridinium ligands, decidium and propidium, and the pyrogallol ligand, gallamine, at 2.20–2.35 Å resolution [43]. Comparison with structures of AChE complexes with the peptide fasciculin or with organic bifunctional inhibitors unveiled new structural determinants contributing to ligand interactions at the peripheral site, and permitted a detailed topographic delineation of this site [44]. These structures provide templates for designing compounds directed to the enzyme surface that modulate specific surface interactions controlling catalytic activity and non-catalytic heterologous protein associations. Since several dangerous substances inhibit AChE activity, first responders and personnel at risk for exposure to these compounds need sensor systems that operate in real time and are reliable, cost-effective, compact, portable, and sensitive [45].

AChE was immobilized on a porous silicon chip by applying 50 $\mu$l of a 1 mg ml$^{-1}$ solution prepared in 100 mM PBE buffer at pH 6.5 to each chip. The chip was incubated at 4 °C overnight. After the reaction, the excess of reagent was removed and the wafers were extensively washed at room temperature with PBE buffer. The AChE activity was monitored by using the Amplex® Red Acetylcholine/Acetylcholinesterase Assay Kit, by following the fluorescence variations at 590 nm.

In figure 3, we report the fluorescence emission in the absence and in presence of ammonium nitrate. As we can see, the presence of ammonium nitrate results in a quenching of the fluorescence emission of about the 39%, indicating the effectiveness of the optical biosensor for the detection of the basic compound of common explosives.

## 4. Glutamine detection

Glutamine (Gln) is an important energy and nitrogen source used in the culturing of eukaryotic cells [46, 47]. Since the catabolism of glutamine leads to the build-up of ammonia which may

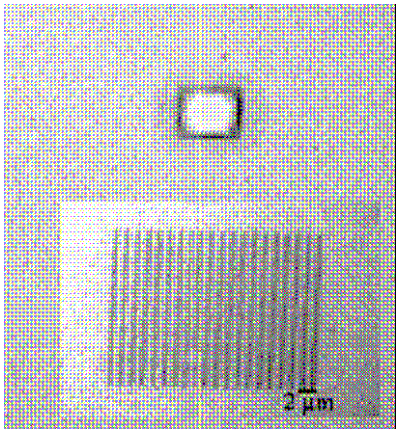


**Figure 4.** Optical microscope image of a PSi chip spotted by a labelled protein after electronic beam irradiation under laser light excitation. The bright area due to the protein fluorescence is clearly evident. The inset shows the nanometric resolution of the pattern produced.

become toxic to the growing culture and thus inhibit growth [48, 49], monitoring glutamine concentrations throughout the growth cycle is an important process. Biosensors available for glutamine are based on immobilized glutaminase [50, 51]. Complications in the determination of glutamine using this type of enzymatic biosensor arise due to the high degree of chemical similarity to glutamate as well as other amino acids. Consequently, additional proteins and electrodes must be added to take into account the interfering signals.

The *Escherichia coli* periplasmic space contains a diverse group of binding proteins whose main function is to present various molecules, such as sugars, amino acids, peptides, and inorganic ions, for transport into the cell [52]. Glutamine-binding protein (GlnBP) from *E. coli* is a monomeric protein composed of 224 amino acid residues (26 kDa) responsible for the first step in the active transport of L-glutamine across the cytoplasmic membrane [53, 54]. Of the naturally occurring amino acids, only glutamine is bound by GlnBP, with a $K_d$ of $3 \times 10^{-7}$ M [54]. The protein consists of two similar globular domains linked by two peptide hinges, and x-ray crystallographic data indicate that the two domains undergo large movements upon ligand binding. The changes in global structure of GlnBP following the Gln binding make it a good candidate for serving as the basis for new biosensor design.

We detected the molecular binding between the GlnBP from *Escherichia coli* and Gln by means of an interferometric microsensor based on the utilization of unmodified porous silicon as solid support for the chip preparation. The sensor operates by measurement of the Fabry–Perot fringes in the wavelength reflection spectrum from the porous silicon layer. The ligand binding was detected as a fringe shift in wavelength, corresponding to a refractive index change. We developed a three-step procedure for the Gln detection. In particular, firstly we registered the optical spectrum of the porous silicon layer as etched; then we repeated the measurement after the GlnBP absorption on the chip surface, and, finally, a Gln solution was spotted on it. Figure 3 shows the shifts induced by each step in the fringes, due to protein–ligand interaction. Figure 4 shows how effective the linking between the protein and the PSi surface is after electron beam irradiation: the bright area is emitted as a spot on an irradiated PSi area and photographed by an optical microscope under laser ($Ar^+$) excitation after several rinses in demi-water. The real nanometric resolution of this functionalizing method is clearly visible. The graft effect is due to the desorption of surface hydrogen atoms which is provoked by the

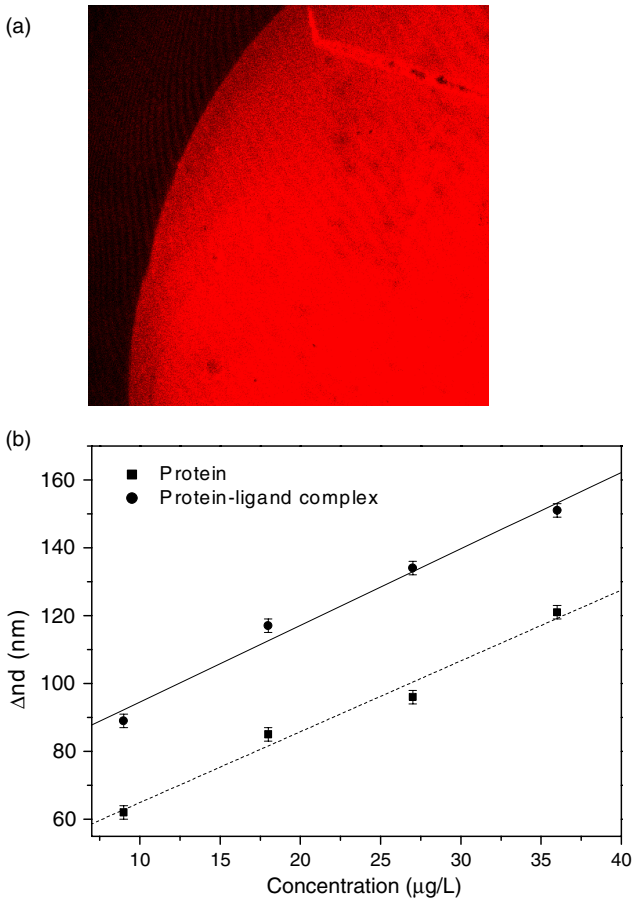


**Figure 5.** (a) Confocal microscopy image of the PSi chip infiltrated with the labelled GlnBP after dialysis in demi-water. (The fluorescence emitted by rhodamine-labelled GlnBP covalently bounded to the photochemically modified PSi surface is registered by a confocal microscope under laser beam (He–Ne) exposure.) (b) Dose–response curve as a function of the concentration of the protein and the Gln–GlnBP complex.

electron beam. The naked surface is thus covered by silicon radicals which strongly react with the proteins. In figures 5(a) and (b) the features of an optical biosensor are presented. In particular, the fluorescence emitted by rhodamine-labelled GlnBP immobilized on the photochemically modified PSi surface is shown in figure 5(a). We also measured the change in the optical path of the PSi layer due to the protein concentration before and after the interaction of the ligand. Figure 5(b) shows the dose–response curve as a function of the concentration of GlnBP and the complex GlnBP–Gln. In this curve, each point represents the average of three independent measurements and the error bars represent the standard deviations. In the protein concentration range investigated, the sensor exhibits a linear response ($R^2 = 0.99$) and it is possible to determine the sensitivity of the optical interferometer to the organic matter by estimating the slopes of the two curves: $s_{\text{prot}} = 21(1)$ nm $\mu g^{-1}$ l and $s_{\text{comp}} = 23(1)$ nm $\mu g^{-1}$ l for the protein and complex, respectively. As expected, the relative distance between the two curves is constant, the protein–complex ratio being always 1:1.

## 5. Conclusions

This paper reviews examples of optical biosensors for the detection of analytes of clinical, industrial, and home security interest. The biosensors described, based on porous silicon nanotechnology, may represent a model for designing advanced optical arrays (lab-on-a-chip) for simultaneously determining analytes of social interest.

## Acknowledgments

This work was supported by CRdC-ATIBB POR UE-Campania Mis 3.16 activities (SD, MR) and by the CNR Commessa Diagnostica avanzata ed alimentazione (SD).

## References

[1] Wolfbeis O S 2000 *Anal. Chem.* **72** 81R–89R
[2] Lakowicz J R 1995 *Proc. SPIE* **2388** 598
[3] Spichiger-Keller U E 1998 *Chemical Sensors and Biosensors for Medical and Biological Applications* (New York: Wiley–VCH) p 313
[4] Verkman A S, Sellers M C, Chao A C, Leung T and Ketcham R 1989 *Anal. Biochem.* **178** 355–61
[5] Tsien R Y, Rink T J and Poenie M 1985 *Cell Calcium* **6** 145–57
[6] Romoser V A, Hinkle P M and Persechini A 1997 *J. Biol. Chem.* **272** 13270–4
[7] Dancil K-P S, Greiner D P and Sailor M J 1999 *J. Am. Chem. Soc.* **121** 7925–30
[8] Arrand H F, Loni A, Arens-Fischer R, Kruger M G, Thoenissen M, Lueth H, Kershaw S and Vorazov N N 1999 *J. Lumin.* **80** 119–23
[9] Gao J, Gao T and Sailor M J 2000 *Appl. Phys. Lett.* **77** 901–3
[10] De Stefano L, Moretti L, Rossi A M, Rocchia M, Lamberti A, Longo O, Arcari P and Rendina I 2004 *IEEE Trans. Nanotech.* **3** 49–54
[11] De Stefano L, Moretti L, Rendina I, Rossi A M and Tundo S 2004 *Appl. Opt.* **43** 167–72
[12] Mulloni V and Pavesi L 2000 *Appl. Phys. Lett.* **76** 2523
[13] D'Auria S, Di Cesare N, Staiano M, Gryczynski Z, Rossi M and Lakowicz J R 2001 *Anal. Biochem.* **303** 138–44
[14] D'Auria S and Lakowicz J R 2001 *Curr. Opin. Biotechnol.* **12** 99–104
[15] D'Auria S, Rossi M, Gryczynski I, Gryczynski Z and Lakowicz J R 2000 *Anal. Biochem.* **283** 83–8
[16] D'Auria S, Di Cesare N, Gryczynski Z, Gryczynski I, Rossi M and Lakowicz J R 2000 *Biochem. Biophys. Res. Commun.* **274** 727–31
[17] D'Auria S, Rossi M, Hermann P and Lakowicz J R 2000 *Biophys. Chem.* **84** 167–76
[18] Staiano M, Bazzicalupo P, Rossi M and D'Auria S 2005 *Mol. BioSyst.* **1** 354–62
[19] Borini S, D'Auria S, Rossi M and Rossi A M 2005 *Lab Chip.* **5** 1048–52
[20] Scognamiglio V, Staiano M, Rossi M and D'Auria S 2004 *J. Fluoresc.* **14** 491–8
[21] The Diabetes Control and Complications Trial Research Group 1993 *N. Engl. J. Med.* **329** 977–86
[22] Roe J N and Smoller R 1998 *Crit. Rev. Ther. Drug Carrier Syst.* **15** 199–241
[23] Wang J, Chatrathi M P, Tian B and Polsky R 2000 *Anal. Chem.* **72** 2514–8
[24] James T D, Limaane P and Shinkai S 1996 *Chem. Commun.* 281–8
[25] Tong A-J, Yamauchi A, Hayashita T, Zhang Z-Y, Smith B D and Teramae N 2001 *Anal. Chem.* **73** 1530–6
[26] Schultz J, Mansouri S and Goldstein I J 1982 *Diabetes Care* **5** 245–53
[27] Meadows D and Schultz J S 1988 *Talanta* **35** 145–50
[28] Russell R J and Pishko M V 1999 *Anal. Chem.* **71** 3126–32
[29] Lakowicz J R and Maliwal B P 1993 *Anal. Chim. Acta* **271** 155–64
[30] Tolosa L, Gryczynski I, Eichhorn L R, Dattelbaum J D, Castellano F N, Rao G and Lakowicz J R 1999 *Anal. Biochem.* **267** 114–20
[31] D'Auria S, Herman P, Rossi M and Lakowicz J R 1999 *Biochem. Biophys. Res. Commun.* **263** 550–3
[32] Marvin J S and Hellinga H W 1998 *J. Am. Chem. Soc.* **120** 7–10
[33] Giuliano K A and Taylor D L 1998 *TIB Tech.* **16** 135–40
[34] Wilson G S and Hu Y 2000 *Chem. Rev.* **100** 2693–704
[35] Schalkhammer T, Lobmaier C, Ecker B, Wakolbinger W, Kynclova E, Hawa G and Pittner F 1994 *Sensors Actuators* B **18/19** 587–91

[36] Szmacinski H and Lakowicz J R 1995 *Sensors Actuators* B **29** 15–24
[37] Bambot S B, Rao G, Romauld M, Carter G M and Lakowicz J R 1995 *Biosens. Bioelectron.* **10** 643–52
[38] Velho G, Froguel P, Thevenot D R and Reach G 1988 *Diab. Nutr. Metab.* **3** 227–33
[39] Menstein D J, Pai E F, Schopfer L M and Massey V 1986 *Biochemistry* **25** 6807–16
[40] Hecht H J, Kalisz H M, Hendle J, Schmid R D and Schmburg D 1993 *J. Mol. Biol.* **229** 153–72
[41] Bourne Y, Kolb H C, Radic Z, Sharpless K B, Taylor P and Marchot P 2004 *Proc. Natl Acad. Sci. USA* **101** 1449–54
[42] Bourne Y, Radic Z, Kolb H C, Sharpless K B, Taylor P and Marchot P 2005 *Chem. Biol. Interact.* **157/158** 159–65
[43] Bourne Y, Taylor P, Radic Z and Marchot P 2003 *EMBO J.* **22** 1–12
[44] Tai K, Shen T, Henchman R H, Bourne Y, Marchot P and McCammon J A 2002 *J. Am. Chem. Soc.* **124** 6153–61
[45] White B J, Legako J A and Harmon H J 2003 *Biosens. Bioelectron.* **18** 729–34
[46] Thomas J N 1986 *Mammalian Cell Technology* ed W G Thilly (Boston, MA: Butterworth) pp 109–30
[47] Zielke H R, Zielke C L and Ozand P T 1984 *Fed. Proc.* **43** 121–5
[48] Ozturk S S and Palsson B O 1990 *Biotechnol. Prog.* **6** 121–8
[49] Oh G S, Izuishi T, Inoue T W and Yoshida T J 1996 *J. Ferment. Bioeng.* **81** 329–36
[50] Sorochinskii V V and Kurganov B I 1997 *Appl. Biochem. Microbiol.* **33** 515–29
[51] Madaras M B, Spokane R B, Johnson J M and Wookward J R 1997 *Anal. Chem.* **69** 3674–8
[52] Higgins C F 2001 *Res. Microbiol.* **152** 205–10
[53] Nohno T, Saito T and Hong J-S 1986 *Mol. Gen. Genet.* **205** 260–9
[54] Weiner J H and Heppel L A 1971 *J. Biol. Chem.* **246** 6933–41

## Optical evidence of protein structural changes in porous silicon devices

The protein-ligand molecular interactions imply strong geometrical and structural rearrangements of the biological complex which are normally detected by high sensitivity optical techniques such as time-resolved fluorescence microscopy. In this section are reported the measurements, made by optical spectroscopic reflectometry in the visible-near infrared region, about the interaction between a sugars binding protein (TMBP), covalently bound on the surface of a porous silicon, and the glucose, at different concentrations and temperatures.

*I'm grateful to Dr. S. D'Auria from Institute for Protein Biochemistry, National Council of Research, Italy for supplying the TMBP protein and for helpful discussion about the experiments.*

## Introduction: proteins from extremophiles

The proteins purified from thermophilic organisms are characterized by high stability in harsh environment such as high temperature, high ionic strength, extreme pH values, even in presence of elevated concentration of detergents and chaotropic agents so that they can be successfully used as very effective bio-probes in sensors design[1].

In particular, it has been recently demonstrated that the D-trehalose/D-maltose-binding protein (TMBP), which is part of the sugars uptake system in the hyperthermophilic organism archaeon *T. litoralis*, is also able to bind glucose molecules. This result suggests the possibility of using TMBP as a stable probe within a biological recognition system for glucose monitoring [1]. TMBP is a monomeric 48 kDa macromolecule constituted by two-domains and containing twelve tryptophan residues. The presence of these fluorescent residues has been used to study the interaction between TMBP and glucose at different temperatures by means of time-resolved fluorescence spectroscopy by Herman et al. [1]: they found that the highest affinity between the protein and this ligand was at a temperature around 60 °C, with a dissociation constant ($K_d$) of about 40 μM. At room temperature TMBP still binds substrates while the activity of the TMBP based transport system becomes negligible [3,4], and this behaviour can be ascribed to an increased rigidity of TMBP structure at room temperature [5]. As other sugar-binding proteins, TMBP also consists of two globular lobes linked by a hinge region made of a few polypeptide chains. The deep cleft formed between the two lobes, which present similarly tertiary structure, contains the ligand-binding site [6].

In a recent published paper [7], we have found that, at room temperature, the reflectivity spectra of a PSi distributed Bragg reflector (DBR), properly functionalized with TMBP, undergo a red shift on exposure to glucose solutions. In particular, we observed a red shift of about 1.2 nm after the interaction with a 150 μM glucose solution. The estimated sensitivity of the monitoring method was 0.03 nm/μM.

On the other hand, some preliminary experiments conducted at 60 °C [8] have shown that the reflectivity spectra of different PSi-based structures, functionalized with TMBP, undergo blue-shifts as a consequence of the interaction with glucose.

Than these apparently conflicting results was explained by combining our investigation on two PSi devices, both TMBP functionalized: an optical microcavity (PSMC), characterized by optical spectroscopic reflectometry, and a thin PSi monolayer, as a model system for the ellipsometric characterization in order to correlate the observed blue shifts of the PSMC spectra to the typical conformational changes of TMBP at 60 °C.

## Materials and methods

D-Glucose and all the other chemicals used in this experiment were from Sigma. All commercial samples were of the best available quality. The TMBP was purified and supplied by dr. S. D'Auria of the Institute for Protein Biochemistry, National Council of Research, Napoli, Italy. Proteins were expressed, purified and quantified by his laboratory as described in reference 5, and references therein.

In this experiment were designed and fabricated two PSi-based structures: a monolayer, that is a porous layer with fixed porosity, and a microcavity, which is constituted by a low-porosity (high refractive index) layer between two Bragg reflectors, each one obtained by alternating low and high porosity layers for 7 times. Both the samples were produced by electrochemical etching of a very highly doped $n^{++}$-silicon wafers (Siltronix Inc., USA), <100> oriented, 0.001 Ω cm resistivity, 400 μm thick, in a HF-based solution. The silicon was etched using a 50 wt.% HF/ethanol solution with halogen lamp illumination and at room temperature. Before anodization the substrate was placed in HF solution to remove the native oxide. The monolayer, characterized by variable angle spectroscopic

ellipsometry (Horiba-Jobin-Yvon, mod. UV-VISEL) in the wavelength range between 400 and 1700 nm, was 503±1 nm thick with a porosity of 77.5±0.3 %. The porous silicon microcavity (PSMC) was electrochemically etched applying a current density of 400 mA/cm$^2$ for 0.3 s to obtain the low refractive index layers, with a porosity of 59±1 %, while one of 50 mA/cm$^2$ was applied for 0.5 s for the high index layers, with a porosity of 50±1 %. This optical structure has a characteristic resonance peak at 1017 nm, centered in a 105 nm wide stop band.

The covalent bind of the TMBP on the porous silicon surface is based on a three steps functionalization process constituted by a chemical passivation of the PSi surface after oxidation, as it is shown in Figure 1. The PSi optical structures have been thermally oxidized in $O_2$ atmosphere, at 900 °C for 15 min; then, we have treated the surfaces with a proper chemical linker, the aminopropyltriethoxysilane (APTES). Samples have been rinsed by dipping in a 5 % solution of APTES and a hydroalcoholic mixture of water and methanol (1:1) for 20 min at room temperature. The chips were then washed by deionized water, and methanol, and dried in $N_2$ stream. The silanized devices were then baked at 100°C for 10 min. To create a surface able to link the amino group of the proteins, we have immersed the chips in a 2.5% glutaraldehyde (GA) solution in 20 mM HEPES buffer (pH 7.4) for 30 min, and then rinsed it in deionized water and finally dried in $N_2$ stream. The glutaraldehyde reacts with the amino groups on the silanized surface and coats the internal surface of the pores.

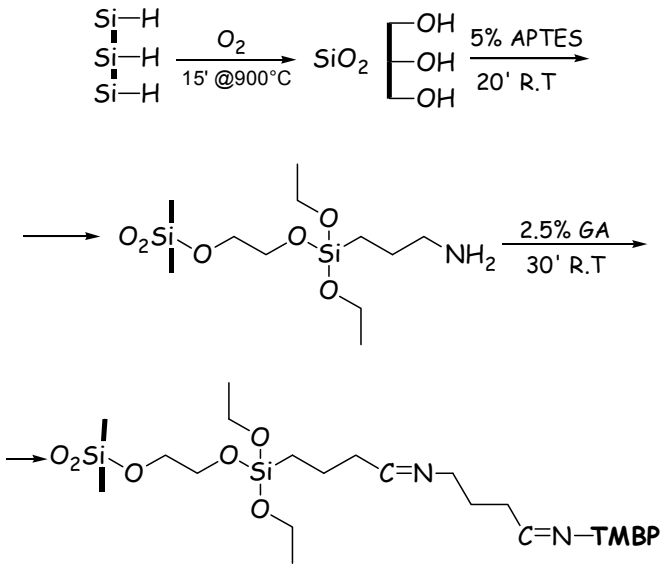


Figure 1. Porous silicon functionalization scheme: from the as-etched material up to the organic-inorganic chip.

The experimental set-up (Figure 2) used to measure the reflectivity spectra is constituted by a white light, as source, directed on the porous silicon chip through a Y fiber. The same fiber was used to guide the output signal to an optical spectrum analyzer (OSA, Ando, Japan). The spectrum was measured over the range 600-1400 nm with a resolution of 0.2 nm. A hot plate, driven by a temperature controller, has been used to perform measurements at 60±1 °C, verified by a thermocouple placed directly on the chip.

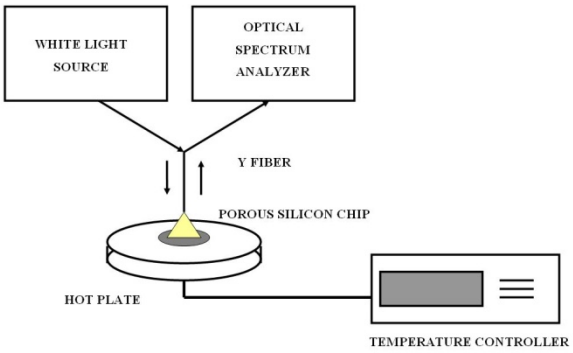


Figure 2. Experimental setup used to measure the optical reflectivity spectra of porous silicon microcavity.

The functionalized PSi samples work as active substrates for the TMBP protein: on each PSi optical structures were spotted 20 μl of a 173 μM TMBP solution in 2mM phosphate buffer solution (pH 7.3) and incubated the system at 4 °C over night. After incubation and three washing steps of five minutes each, used to remove the excess of biological matter non covalently linked to the PSi surface, the presence of the protein in the spongy structure was optically verified as a red shift of about 60 nm in the reflectivity spectrum in the case of PSMC.

## Experimental results and discussion

When recorded at the temperature of 25 °C, the PSMC characteristic resonance peak undergoes only very small red shifts, of the order of 1 nm, on exposure to glucose solutions with increasing concentrations, up to 200 μM, according to the low affinity of TMBP with glucose at room temperature [7]: at this temperature few proteins can re-arrange their conformational structure and efficiently bind the ligand. The results of this biomolecular interaction change dramatically if the same measurements are performed at 60 °C: in Figure 3 is reported the peak shift of the functionalized microcavity on exposure to a 200 μM glucose concentration. The optical resonance undergoes a 4.5 nm shift toward lower wavelengths.

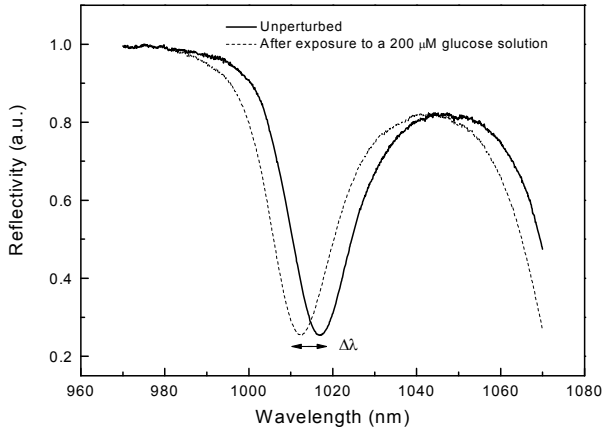


Figure 3. PSMC resonance blue shift on exposure to a glucose solution of 200 μM concentration.

The dose-response curve is shown in Figure 4: the curve is linear in the range of glucose concentrations between 0 and 200 μM, with an estimated sensitivity to solute

concentration variations of 0.022 (4) nm/μM. For higher glucose concentrations, the blue shift did not increased any more, which means that all the active proteins have bound their ligands.

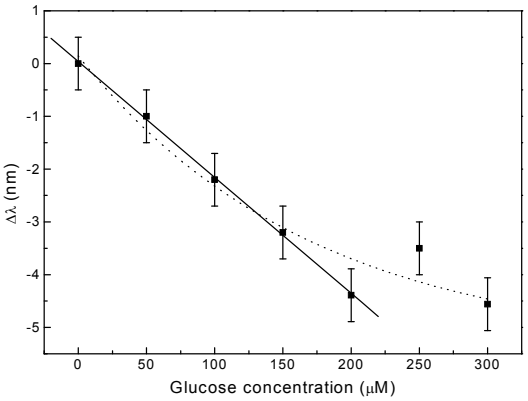


Figure 4: Dose-response curve for functionalized PSMC exposed to different concentrations of glucose.

The large blue-shift recorded corresponds to a decrease of the optical path that the light exploits when reflected by the porous structure. Since the optical path is defined as the thickness times the average refractive index, and there is not any variation of the multilayer thickness, the blue-shift can be attributed to a decrease in the value of the average refractive index. The chemical passivated surface of the PSi is highly stable respect to the biological chemical buffer solutions, so that there can not be any further oxidation nor any corrosion of the silicon matrix: the apparent increase of the porosity is due to the proteins volume reduction after the interaction with the glucose. Most of the key-lock recognition mechanisms, which are at the basis of the biological interactions such as antibody-antigen or protein-ligand, require large rearrangement of one bio-molecule to host the other. The binding of glucose to TMBP is strongly related to a movement of the protein lobes as well as to profound conformational changes in the hinge region. The lobes envelope on to the binding site and cause a net reduction of protein's volume, as confirmed by fluorescence measurements [1]. In order to confirm these results, a very sensitive optical technique was used, the variable angle spectroscopic ellipsometry (VASE), to quantify the porosity changes of a thin PSi layer after TMBP functionalization and on exposure to increasing concentration of glucose solutions. In Table 1 the porosities estimated by ellipsometry after each functionalization step of the monolayer, are reported.

| | Porosity (%) |
|---|---|
| As etched | 77.5 ± 0.3 |
| After oxidation | 49.1 ± 0.3 |
| After APTES treatment | 41.7 ± 0.5 |
| After GA treatment | 35.5 ± 0.4 |
| After TMBP incubation | 31.9 ± 0.5 |

Table 1: Porosity decrease of the PSi monolayer due to the functionalization steps.

Chemical and biological functionalization steps considerably reduce the average porosity of the PSi layer. Ellipsometric spectra have been also acquired after each addition of glucose solutions with increasing concentrations. In Figure 5 the changes in porosity of the PSi layer, $\Delta P$, as estimated from the ellipsometric data, are shown as function of glucose concentration. On exposure to ligand buffer solutions, the VASE characterization gives a direct measurement of the variation of each layer component. Using these experimental data, we have estimated, after the addition of 250 $\mu$M of glucose, an increase of more than the 3.5 % in the monolayer porosity.

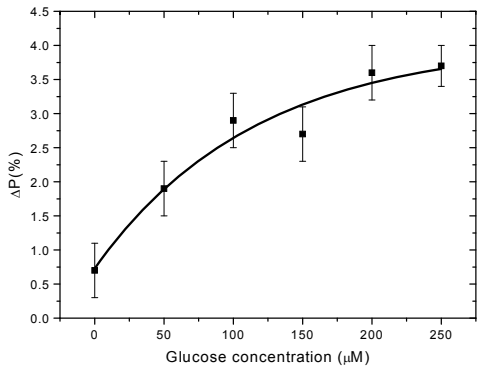


Figure 5: The porosity increase of a functionalized PSi monolayer as a function of glucose concentrations. On exposure to a concentration of 250 $\mu$M of glucose, an enhancement of more than 3.5 % in porosity is obtained.

On the other hand, it was also numerically calculate which is the effect of such a porosity increment on the reflectivity spectrum of the PSi microcavity. The reflectivity spectrum of a microcavity with the same porosities and thicknesses of the one realized was simulated. The organic phase of the system has been modeled by supposing a Gaussian distribution for both the TMBP molecules presence throughout the upper layers of the microcavity and also for the correspondent increment of porosity, $\Delta P$, due to the glucose interaction [9]. In particular, the $\Delta P$ distribution was peaked at the top of the structure (with a maximum value of 3.5 %) and was characterized by a HWHM of about 3 $\mu$m, which equals the half-width of the first Bragg reflector in the microcavity structure. The reflectivity spectra have been simulated by standard transfer matrix method [10] and results are reported in Figure 6.

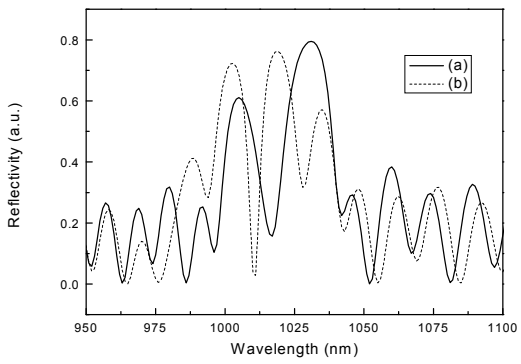

Figure 6: (a) Simulated reflectivity spectrum of the PSi microcavity used in the experiment. (b) Simulated reflectivity spectrum of the same structure after a non-homogeneous increase of porosity.

The result of such simulations is a blue shift of the resonant peak of 6.0±1.0 nm, which is consistent with the experimental one of 4.6±0.5 nm, observed after the addition of a glucose solution, 250 μM.
Even if highly specific, the protein-ligand interaction is in general reversible, so that proteins release completely the target molecules, especially when in buffer solutions. But when bound on the surface of a nanostructured material, proteins could be limited in their activity: after an overnight dialysis in deionized water, it was found a 2 nm red-shift of the resonant peak, which means that the ligand has been released only by some proteins. Anyway, when the measurements were repeated, the same blue-shift always about 5 nm with a 250 μM concentration of glucose was obtained, so that can be concluded that the effect was reproducible, at least for five replica made in the same experimental conditions, but was not perfectly reversible.

## References


1. P. Herman, I. Barvik, M. Staiano, A. Vitale, J. Vecer, M. Rossi and S. D'Auria, *Biochimica et Biophysica Acta* **2007,** *1774*, 540-544.
2. J. Diez, K. Diederichs, G. Greller, R. Horlacher, W. Boos, W. Welte, *J. Mol. Biol.* **2001**;*305*:905-915.
3. K. B. Xavier, L. O. Martins, R. Peist, M. Kossmann, W. Boos, H. Santos, *J. Bacteriol.* **1996**, *178*, 4773-4777.
4. R. Horlacher, K. B. Xavier, H. Santos, J. Di Ruggiero, M. Kossmann, W. Boos, *J. Bacteriol.* **1998**, *180*, 680-689.
5. P. Herman, M. Staiano, A. Marabutti, A. Variale, A. Scire, F. Tanfani, J. Vecer, M. Rossi, S. D'Auria, *Proteins* **2006**, *63***,** 754-767.
6. Y. J. Sun, J. Rose, B. C. Wang, C. D. Hsiao, *J. Mol. Biol.* **1998**, *278*, 219-222.
7. L. De Stefano, A. Vitale, I. Rea, M. Staiano, L. Rotiroti, T. Labella, I. Rendina, V. Aurilia, M. Rossi, S. D'Auria, *Extremophiles*, DOI 10.1007/s00792-006-0058-6.
8. L. De Stefano, L. Rotiroti, E. De Tommasi, A. Vitale, M. Rossi, I. Rendina and S. D'Auria, *Proceedings of the SPIE* **2007** *Volume 6585,* pp. 658517 .
9. L. De Stefano and S. D'Auria, *Journal of Physics Condensed Matter* **2007**, *19*, 395009 (7pp).
10. M. A. Muriel and A. Carballar, *IEEE P. Technol. Lett.* **9**, 955 (1997).

# Oligonucleotides direct synthesis on porous silicon chip

In this section is report the design, fabrication and characterization of a oligonucleotide (ON) biochip based on the PSi nanotechnology for direct DNA solid phase synthesis.

*In collaboration with Prof. G. Piccialli of University of Naples “Federico II”, Italy*

# Oligonucleotides direct synthesis on porous silicon chip

**Luca De Stefano[1], Edoardo De Tommasi[1], Ilaria Rea[1], Lucia Rotiroti[1], Luca Giangrande[1], Giorgia Oliviero[2], Nicola Borbone[2], Aldo Galeone[2] and Gennaro Piccialli[2]***

[1]Istituto per la Microelettronica e Microsistemi - Unità di Napoli, Consiglio Nazionale delle Ricerche, via P. Castellino 111, I-80131 Napoli, Italy and [2]Dipartimento di Chimica delle Sostanze Naturali, Università degli Studi di Napoli "Federico II", Via D. Montesano 49, I-80131 Napoli, Italy

## ABSTRACT

**A solid phase oligonucleotide (ON) synthesis on porous silicon (PSi) chip is presented. The prepared Si-OH surface were analyzed by FT-IR and the OH functions were quantified by reaction with 3'-phosphoramidite nucleotide building block. Short ONs were synthesized on the chip surface and the coupling yields evaluated.**

## INTRODUCTION

The interest in DNA-based diagnostic tests has recently increased since they can be used in a lot of important applications such as gene analysis, fast detection of biological warfare agents, and also in forensic cases. Numerous DNA detection systems, both optical and electrochemical, based on the hybridization between a DNA target and its complementary probe fixed on a solid support have been described.[1] DNA biochips, due to integration and miniaturization of all components, allow continuous, fast and sensitive detection of DNA interactions. The fabrication of a DNA biochip requires the immobilization of the DNA probe on the support surface,[1,2] or, as an alternative, the synthesis of the ON strand directly on the device surface.[3-5]

On the other hand, Porous silicon (PSi) structures are quite ideal support material for chemical and biological sensing, mainly due to their high specific area, up to 600 $m^2cm^{-3}$, low cost and compatibility with standard integrated circuit processes. PSi is fabricated by the electrochemical etching of a doped silicon wafer in a hydrofluoridic aqueous solution. Moreover, its surface can be properly functionalised to covalently link the DNA probe.

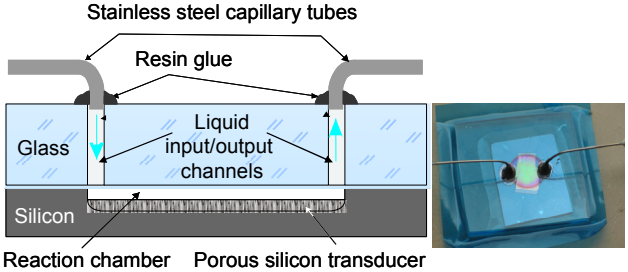


**Fig. 1.** Schematic and real view of the μ-chamber for DNA biochip applications.

In this work, we report the design, fabrication and characterization of a ON biochip based on the PSi nanotechnology for direct DNA solid phase synthesis.

## RESULTS AND DISCUSSION

***Porous silicon formation and chip assembly***. We have designed and fabricated a DNA biochip, just integrating PSi, as the transducer material, and a glass slide, which ensures sealing and the interconnections for fluids inlet and outlet. The silicon wafer used in this work is a $p^+$ type, <100> crystal orientation, with a resistivity of 8-12 mΩcm.[6] The glass is a Borofloat 33 type, 1 mm thick. The reaction microchamber has been realised by a two-step electrochemical etching. The first step is a high current density (800 mA/$cm^2$ for about 300 s) electrochemical etch in hydrofluoric acid and ethanol (HF/EtOH 1:1,v/v) solution which creates a μ-well (100 μm deep and a volume of 10 μL) in the bulk silicon. The second step is a consecutive electrochemical etch which is used to fabricate the PSi layer at the bottom of the μ-chamber. The process parameters for this last step were: current density of 400 mA/$cm^2$ and etching time of 3.2 s. After the mechanical drilling of the flow channels, the glass slide has been cleaned and activated for the anodic bonding process following standard cleaning procedures. The silicon chip has also been carefully rinsed in deionized water for several minutes. Silicon etched wafer and glass top prefabricated components were anodically bonded together with mutual alignment: a successful bonding, in terms of mechanical strength and bond quality, has been obtained at a temperature of 200 °C, voltage of 2.5 kV, with a process time of 1.5 minutes. The cross section of the chip structure and the general-view of the real device are shown in Figure 1.

***Functionalization of porous silicon layer and ON syntheses***. The successive treatment of porous silicon layer with a solution of conc. $H_2SO_4/H_2O_2$ (8:2, v/v, 15 min R.T.) assure the formation of Si-OH groups on the solid matrix. The chip was, then, rinsed in deionized water for several minutes and dried under reduced pressure. The FT-IR spectrum (Figure 2) of the chip surface showed the appearance of the characteristic broad bands around 1050

$cm^{-1}$ (Si-O-Si) and 1065, 880 $cm^{-1}$ attributable to Si-OH bonds. To determine the surface coverage of Si-OH groups, we reacted the chip **1** with tetrazole activated 5'-DMT-3'-phosporamidite-timidine nucleotide (**2** Scheme 1) which assure the presence of a very reactive phosphorous(III) and

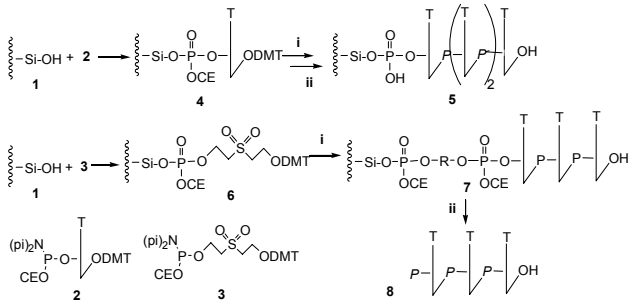

**Scheme 1**. Solid phase synthesis on PSi-OH chip **1**; P: phosphotriester function; R: $-(CH_2)_2SO_2(CH_2)_2$; P: phosphodiester function; CE: 2-cyanoethyl; i: standard ON chain elongation; ii; treatment with methylamine.

a 5'-dimethoxytrytil group (DMT).

The reaction cycle including the standard phosphorous oxidation and the capping step, afforded the PSi-3'-thymidine **4** which was quantified by UV/VIS spectroscopy monitoring 5'-dimethoxytrytil cation released by DCA treatment ($\varepsilon$ =71700, $\lambda$ = 498 nm). The Si-OH functionalization resulted to be in the range of 35-40 nmol/chip and no significative differences were observed varying the concentration of the nucleotide/activator solution (30-60 mg/mL) or prolonging the coupling reaction time (30-180-min). Alternatively, PSi chip **1** was reacted with the phosphoramidite **3** thus obtaining the PSi support **6** (30-40 nmol/chip). The linker **3** ensures a more long and flexible arm for the reaction of terminal alcoholic OH groups and allows the release of the synthesized ON chains by a mild basic treatment, as well. On the supports **4** and **6** three coupling cycles were performed with phosphoramidite **2** thus obtaining PSi supports **5** and **7** respectively. The DMT measurements after each cycle indicated a coupling efficiency of 87-90 % for support **4** and 92-95% for support **6**. These findings are in agreement with previous reported ON synthetic procedures on PSi chips which demonstrated the important role of the spacer linker attached on porous silicon surface.[3-5] The detachment of the synthesized short thymidine oligomer from support **7** was obtained by treatment with anhydrous methylamine (20 min at room temperature). The combined amine solution and washings (methanol and then water), dried under reduced pressure, were analyzed by ESI-MS spectroscopy. The mass data confirmed the presence of expected 3'-phosphate-$T_3$-5'-OH product (m/z 931.2 $MH^+$). The treatment of **5** with methylamine did not release significative amount of nucleotide material from the chip, also confirmed by DMT deprotection and measurement

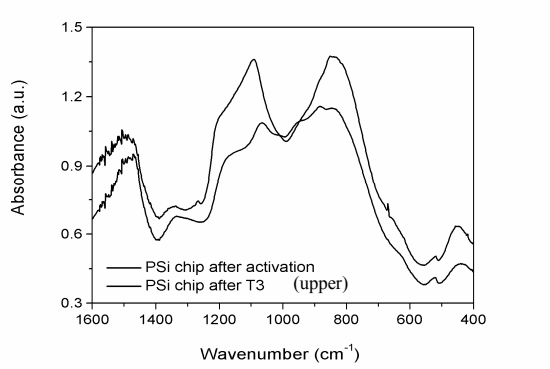


**Fig. 2**. FT-IR profiles of the PSi-surfaces **1** (bottom) and **5** (upper).

performed after the amine treatment. FT-IR spectrum (Figure 2) of the PSi-ON chip showed the appearance of the characteristic band around 1100 $cm^{-1}$ and 860 $cm^{-1}$ attributable, respectively, at P=O and 5'-$CH_2$-OH.

## CONCLUSION

In this preliminary experiments of ON synthesis we have tested the direct reactivity of the freshly prepared PSi OH functionalized chips with standard phosphoramidite building block and confirmed the compatibility of the PSi-3'-bonded thymidine with the chemical treatments required by standard ON solid phase synthesis. The synthesis of support **4** allowed as to estimate the amount of accessible OH groups on the silicon surface and to obtain a reproducible nucleotide functionalized chip. The data were also confirmed by the synthesis of the PSi-support **6**. We hypothesize that, after coupling yield optimization, the support types **4** and **6** could be exploited both to obtain deprotected ON bonded to a PSi chip and to achieve a standard ON solid phase synthesis on PSi matrix.

## REFERENCES


1. Sassolas, A., Leca-Bouvier, B.D., Blum, L.J. (2008) *Chem. Rev.*, 108, 109-139.
2. Di Francia, G., La Ferrara, V., Manzo, S., Chiavarini, S. (2005) *Biosensors and Bioelectronics*, 21, 661-665.
3. Pike, A.R., Lie, L.H., Eagling, R.A., Ryder, L.C., Patole, S.N., Connolly, B.A., Horrocks, B.R., Houlton, A. (2002) *Angew. Chem. Int. Ed.*, 41, 615-617.
4. Lie, L.H., Patole, S.N., Pike, A.R., Ryder, L.C., Connolly, B.A., Ward, A.D., Tuite, E.M., Houlton, A., Horrocks, B.R. (2004) Faraday Discuss., 125, 235-249.
5. Bessueille, F., Dugas, V., Vikulov, V., Cloarec, J.P., Souteyrand, E., Martin, J.R. (2005) *Biosensors and Bioelectronics,* 21, 908-916.
6. De Stefano, L., Arcari, P., Lamberti, A., Sanges, C., Rotiroti, L., Rea, I., Rendina, I. (2007) *Sensors*, 7, 214-221.



*Corresponding Author. E-mail: picciall@unina.it

# Porous silicon-based optical biosensors and biochips

This section is aimed at the demonstration that a PSi surface functionalized, allow the attachment of linkers through stable covalent Si–C bonds, and also demonstrated to be compatible to the high temperature anodic bonding processes used for the realization of silicon-glass biochips.

Available online at www.sciencedirect.com
ScienceDirect
Physica E 38 (2007) 188–192
PHYSICA E
www.elsevier.com/locate/physe

# Porous silicon-based optical biosensors and biochips

Ivo Rendina*, Ilaria Rea, Lucia Rotiroti, Luca De Stefano

*Institute for Microelectronics and Microsystems, National Council of Research, Via P. Castellino 111, 80131 Napoli, Italy*

Available online 31 December 2006

**Abstract**

Porous silicon multilayered microstructures have unique optical and morphological properties that can be exploited in chemical and biological sensing. The large specific surface of nanostructured porous silicon can be chemically modified to link different molecular probes (DNA strands, enzymes, proteins and so on), which recognize the target analytes, in order to enhance the selectivity and specificity of the sensor device. We designed fabricated and characterized several photonic porous silicon-based structures, which were used in sensing some specific molecular interactions. The next step is the integration of the porous silicon-based optical transducer in biochip devices: at this aim, we have tested an innovative anodic bonding process between porous silicon and glass, and its compatibility with the biological probes.
© 2007 Elsevier B.V. All rights reserved.

*PACS:* 87.80.−y; 07.07.Df; 42.79.Pw

*Keywords:* Optical biosensors; Porous silicon; Biochip

## 1. Introduction

Recently, lot of experimental work, concerning the worth noting properties of nanostructured porous silicon (PSi) in chemical and biological sensing has been reported, showing that, due to its morphological and physical properties, PSi is a very versatile sensing platform [1–5]. A key feature for a recognition transducer is a large surface area: PSi has a porous structure with a specific area of the order of 200–500 $m^2/cm^3$, so that it is very sensitive to the presence of biochemical species which penetrate inside the pores. Moreover, PSi is an available, low-cost material, completely compatible with VLSI and micromachining technologies, so that it could usefully be employed in the fabrication of MEMS, MOEMS and smart sensors.

The PSi optical sensing features are based on the changes of its photonic properties, such as photoluminescence or reflectance, on exposure to the gaseous or liquid substances. Unfortunately, these interactions are not specific, so that the PSi cannot be used as a selective optical transducer material. One way to overcome this limit is to chemically or physically modify the PSi hydrogenated surface in order to enhance the sensor selectivity through specific biochemical interactions. The reliability of the biosensor strongly depends on the functionalization process: how simple, homogenous and repeatable it can be. This fabrication step is also crucial for the stability of the sensor: it is well known that as-etched porous silicon has a very reactive Si–H terminated surface due to the Si dissolution process [6]. The substitution of the Si–H bonds with Si–C ones guarantees a much more stable surface from the thermodynamic point of view.

Testing and demonstrating the PSi capabilities as a useful functional material in the optical transduction of biochemical interactions is only the first action in the realization of an optical biochip based on this nanostructured material. In this case, all the fabrication processes should be compatible with the utilization of biological probes and the feasibility of such devices must be proven. This means that the standard integrated circuit microtechnologies should be modified and adapted to this new field of application. A very strong interdisciplinary is required to match and resolve all these problems.

*Corresponding author.
*E-mail address:* ivo.rendina@na.imm.cnr.it (I. Rendina).

1386-9477/$ - see front matter © 2007 Elsevier B.V. All rights reserved.
doi:10.1016/j.physe.2006.12.050

In this work, we review our recent experimental results in optical biosensing using PSi-based photonic devices and report our newest results about the design and fabrication of optical biochip by exploiting the PSi nanotechnology [7–12].

## 2. Materials and methods

Following the pioneering work of Mike Sailor's group [13], we started using the PSi monolayers, which optically act as Fabry–Perot interferometers, as basic transducer in biosensing experiments. This is a very convenient choice since PSi monolayers are very easy to fabricate and to characterize. These devices have also a high sensitivity to changes in refractive index, up to 70 ppm [14]. By exploiting the optical features of PSi Fabry–Perot interferometers, we studied several bio-molecular interactions: DNA single strands with their complementary strands, Glutamine binding protein (GlnBP) from *Escherichia coli* with Glutamine; GlnBP with Gliadine [8,11,12]. The high-quality optical response of PSi multilayers allows the fabrication of resonant optical devices and photonic crystals that are very attractive for sensing applications [15].

In biochemical sensors based on 1-D photonic bandgap (PBG) structures, usually there is both a reduced group velocity of light within the sample, which increases the interaction with the analyte and thus the sensitivity, and the presence of a resonant characteristic wavelength. In this case, sensors whose operation is based on the measurement of the shift of a very narrow resonance (for instance, a transmission or reflection peak having a full-width at half-maximum of few tens of microns) are characterized by increased sensitivity and resolution. We have used a PSi optical microcavity to study the molecular binding of GlnBP and glutamine with a higher sensitivity with respect to the interferometric characterization [10].

Another typical PBG structure used in optical sensing is the distributed Bragg mirror which is obtained by alternating high (A) refractive index layers (low porosity) and low (B) refractive index layers (high porosity). The thicknesses of each layer satisfy the following relationship: $n_A d_A + n_B d_B = m\lambda/2$, where $m$ is an integer and $\lambda$ is the Bragg resonant wavelength. The main optical feature of a Bragg mirror is the presence of a single, degenerate photonic band gap in a period of the reciprocal space. As a consequence, the reflectivity spectrum is characterized by a principal ($m = 1$) stop band, centred around $\lambda$, whose width depends on the refractive indexes contrast ($n_A/n_B$), while its height, depends on the number of the layers. The higher orders of the resonance ($m = 2,\ 3,\ 4,\ldots$) are characterized by a narrow width and a lower reflectivity [16].

We have designed, simulated and realized a low contrast, 20-layer-Bragg mirror, with the first-order ($m = 1$) resonant wavelength at 4800 nm. A highly doped $p^+$-silicon, $\langle 1\,0\,0 \rangle$ oriented, 0.01 Ω cm resistivity, 400 μm thick was used as substrate to realize the structures. The Bragg low-porosity layers (effective refractive index $n_L \cong 1.56$, thickness $d_L \cong 641$ nm) were produced by an etching current density of 125 mA/cm$^2$ for 2.58 s, while an etching current density of 150 mA/cm$^2$ for 3.62 s has been used for the high-porosity layers ($n_H \cong 1.50$, $d_H \cong 933$ nm).

For the biosensing experiments, a strong base post-etch treatment was used to increase the pore size and remove the superficial nano-residue due to the electrochemical etch process, so to improve the infiltration of biomolecular probes into the pores [17]. Unfortunately, this process removes most of the native Si–H bonds, required by the subsequent functionalization treatment, from the porous silicon surface: to restore these bonds, we rinsed the porous silicon device in a very diluted HF-based solution for 30 s.

The reflectivity spectra were measured over the range 800–1600 nm with a resolution of 0.2 nm by using an Y optical fibre connected to a tungsten lamp, as a light source, and to an optical spectrum analyzer.

We have estimated the refractive index sensitivity, i.e., the response of the sensor to the changes of the average refractive index, by measuring the peak shift of a higher order Bragg resonance on exposure to several organic volatile substances with different and increasing refractive indexes. Each measurement starts after that a small amount of volatile substance is added to reaction chamber and saturates with its vapours the atmosphere surrounding the sensor. The vapours penetrate into the nanometric pores, substituting the air. The average refractive index of the layers changes, so that the reflectivity spectrum of the device shifts towards higher wavelengths.

Procedures for the immobilization of biomolecules on porous silicon are usually based on a chemistry that involves the silanization of the oxidized PSi surface [18]. A promising recently proposed alternative is that exploiting the reaction of acids molecules with the hydrogen-terminated porous silicon surface in order to obtain a more stable organic layer covalently attached to the PSi

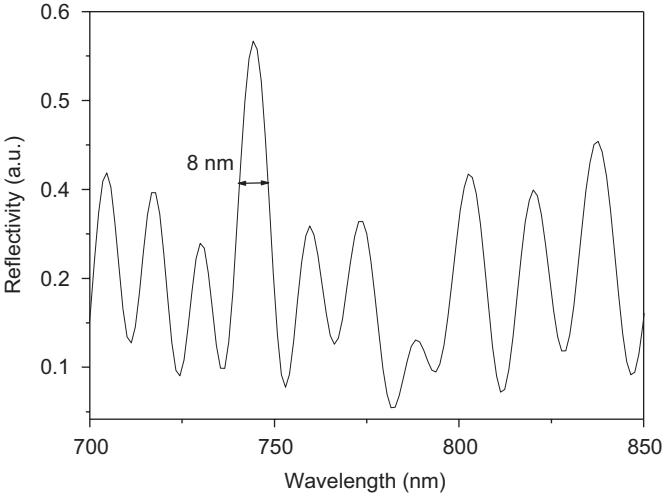


Fig. 1. Reflectivity spectra of a porous silicon Bragg mirror.

surface through Si–C bonds. We have exploited a photo-activated modification of PSi surface based on the UV exposure of an *N*-hydroxysuccinimide ester (UANHS) solution [19]. This kind of treatment is very fast since the time required for the complete surface passivation is of the order of few minutes. Moreover, after UV exposition the chip can be analysed by FT–IR microscopy to verify the state of the process. In view of a possible integration of the PSi-based biosensor into a lab-on-chip, we have verified the thermal stability of the Si–C bonds up to the temperature adopted in the packaging process of the chip. Once functionalized, the PSi optical transducer was bonded to a glass slide by an innovative anodic bonding process that takes into account the very peculiar characteristic of this material. Details of the process and of the microfluidic solutions adopted are elsewhere described [7].

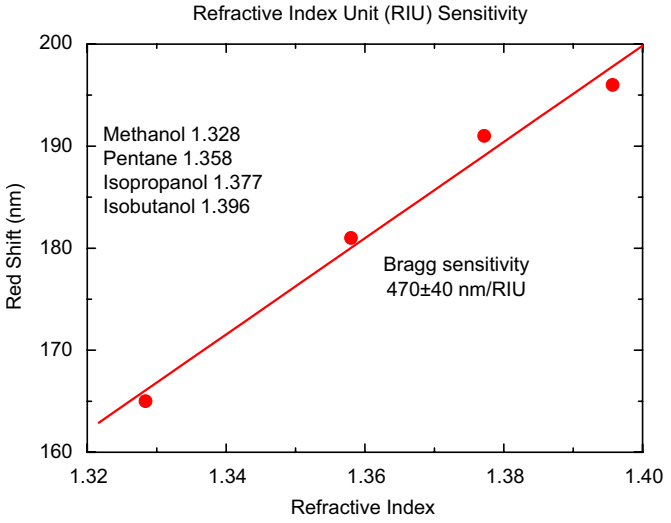


Fig. 2. Red shift of the Bragg peak at 750 nm versus the refractive index of vapor substances.

Even if our aim is the realization of a label-free optical biosensor based on the PSi nanotechnology, we have used a fluorescent protein to control the distribution of the biological matter on the chip surface and to preliminary test the chemical stability of the covalent link between the protein and the PSi surface.

## 3. Experimental results and discussion

Fig. 1 shows the reflectivity spectrum of the PSi Bragg mirror in the range 700–850 nm: we have found that despite the high order of the resonance ($m = 6$), the resonant peak at $\lambda = 750$ nm has a reflectivity which is the 60% of the first order and the width is less than 10 nm. Note that due to refractive index and thickness fabrication uncertainties the $m = 6$ Bragg wavelength is about 750 nm instead of 800 nm.

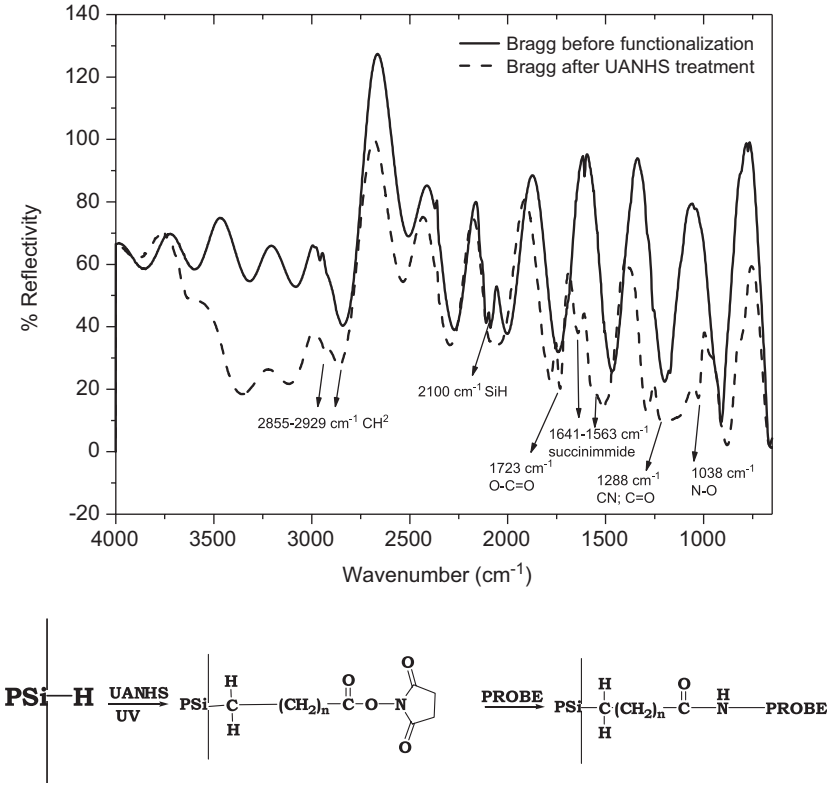


Fig. 3. FT–IR spectra of the realized porous silicon Bragg structure before and after the photoinduced functionalization process based on UV exposure, together with the reaction scheme.

In Fig. 2, the red shifts of the $m = 6$ Bragg resonance peak at 750 nm are reported as function of the refractive index of each volatile substance employed. A well linear response is observed and a sensitivity of 470 (40) nm/RIU can be estimated, where RIU is the acronym for refractive index unit. Since the resolution of our spectrometer is 0.05 nm, a limit of detection for the refractive index change of $1.06 \times 10^{-4}$ can be estimated for this kind of optical device.

The UV-induced surface passivation process results in covalent attachment of UANHS to the porous silicon surface, as clearly shown in the FT–IR spectrum reported in Fig. 3 together with the reaction scheme: all the characteristic absorption peaks due to the organic compounds are present in the sample after the functionalization process. The chip was also optically characterized: a red shift of about 54 nm in the reflectivity spectrum is observed.

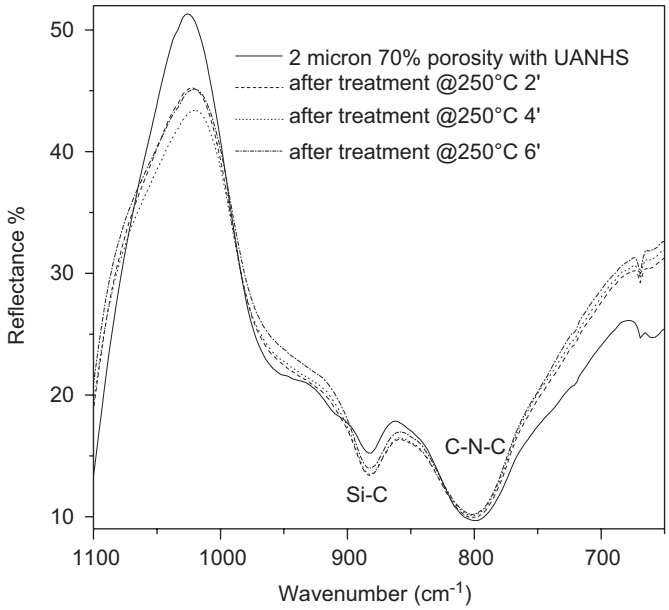


Fig. 4. FT–IR spectra of a PSi chip after a thermal treatment at different times.

Then the device was incubated over night with the biological probe. The selective recognition of the biomolecular target is optically verified by a further red shift (data will be published elsewhere).

The FT–IR spectrum of a PSi chip after functionalization at different temperatures is reported in Fig. 4: it is well evident that the link between the inorganic and organic phases is stable up to 250 °C. The Si–C and C–N–C bonds have high thermodynamic strength so that the passivated chip is still working after the anodic bonding process.

In Fig. 5, a real view of the hybrid porous silicon-glass chip (A) is reported, while in the insets (B) and (C) the fluorescent images observed by a Leica Z16 APO fluorescence macroscopy system after incubation of the labelled bioprobes bonded to the chip, are shown. By illuminating the chip spotted with labelled proteins (fluorescent glutamine binding protein, purified by *E. coli* [8]) by a 100 W high-pressure mercury source, we found that the fluorescence is very high and homogeneous on the whole surface (see Fig. 5(B)). In Fig. 5(C) a detail of a scratch on the chip surface can be seen, showing that the fluorescent probes also penetrate into the inner pores of the chip. After several flushing run with demineralized water, injected by a micro-syringe, we found that the fluorescence is still bright.

## 4. Conclusions

In this work, our recent experimental results in optical biosensing using PSi-based photonic devices are reviewed. Newest results about the fabrication and characterization of PSi sensors based on the exploitation of distributed Bragg reflectors operating at higher order harmonics are also presented. The PSi surface functionalization of such structures by UV stimulated processes, allowing the attachment of linkers through stable covalent Si–C bonds, is also demonstrated to be compatible to the high-temperature anodic bonding processes used for the realization of silicon-glass biochips.

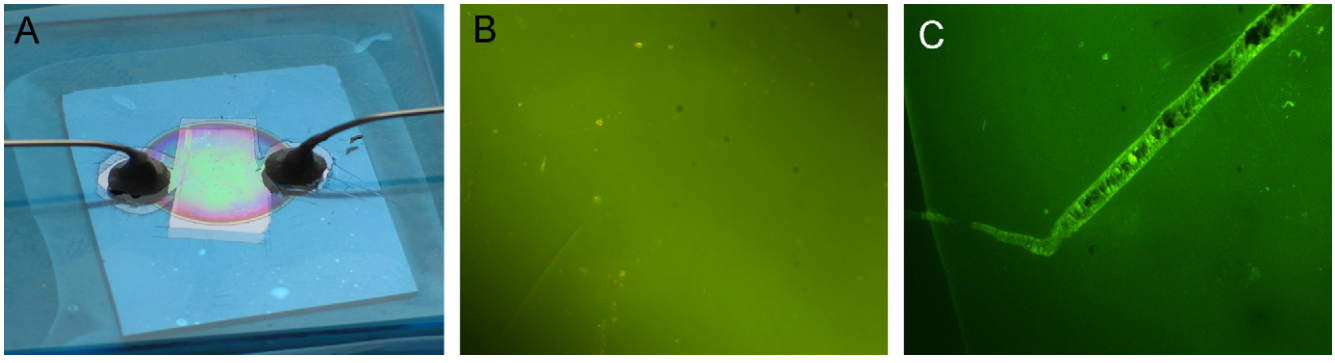


Fig. 5. Images of the basic element of a lab-on-chip based on a PSi optical transducer: (A) a real view of the porous hybrid silicon-glass chip; (B) fluorescent images of labelled proteins; (C) particular of a scratch on the chip surface.

## Acknowledgments

The authors are grateful to Prof. Mosè Rossi and Prof. Paolo Arcari for the helpful discussions. They also wish to thank Dr. Sabato D'Auria and Dr. Annalisa Lamberti for all the contributes given in preparing and making the experiments with the biological matter.

## References

[1] H. Ouyang, M. Christophersen, R. Viard, B.L. Miller, P.M. Fauchet, Adv. Funct. Mater. 15 (2005) 1851.
[2] S.M. Weiss, H. Ouyang, J. Zhang, P.M. Fauchet, Opt. Express 13 (2005) 1090.
[3] F.P. Mathew, E.C. Alocilja, Biosensors Bioelectron. 20 (2005) 1656.
[4] F. Besseueille, V. Dugas, V. Vikulov, J.P. Cloarec, E. Souteyrand, Biosensors Bioelectron. 21 (2005) 908.
[5] C. Pacholski, M. Sartor, M.J. Sailor, F. Cunin, G.M. Miskelly, J. Am. Chem. Soc. 127 (2005) 11636.
[6] L. Canham (Ed.), Properties of Porous Silicon, IEE Inspec, London, UK, 1997.
[7] L. De Stefano, K. Malecki, F.G. Della Corte, L. Moretti, L. Rotiroti, I. Rendina, Sensor Actuat B 114 (2006) 625.
[8] L. De Stefano, I. Rendina, L. Rotiroti, L. Moretti, V. Scognamiglio, M. Rossi, S. D'Auria, Biosensors Bioelectron. 21/8 (2006) 1664.
[9] L. De Stefano, I. Rea, I. Rendina, L. Rotiroti, M. Rossi, S. D'Auria, Phys. Stat. Sol. (a) 203 (2006) 886.
[10] S. D'Auria, S. Boarino, A. Vitale, A.M. Rossi, I. Rea, I. Rendina, L. Rotiroti, M. Staiano, M. de Champdorè, V. Aurilia, A. Parracino, M. Rossi, L. De Stefano, J. Phys.: Condens. Matter 18 (2006) S2019.
[11] L. De Stefano, M. Rossi, M. Staiano, G. Mamone, A. Parracino, L. Rotiroti, I. Rendina, M. Rossi, S. D'Auria, J. Proteome Res. 5 (5) (2006) 1241.
[12] L. De Stefano, L. Rotiroti, I. Rea, I. Rendina, L. Moretti, G. Di Francia, E. Massera, P. Arcari, A. Lamberti, C. Sangez, J. Opt. A 8 (2006) S540.
[13] V.S.-Y. Lin, K. Motesharei, K.-P.S. Dancil, M.J. Sailor, M.R. Ghadiri, Science 278 (1997) 840.
[14] M.A. Anderson, A. Tinsley-Brown, P. Allcock, E.A. Perkins, P. Snow, M. Hollings, R.G. Smith, C. Reeves, D.J. Squirrell, S. Nicklin, T.I. Cox, Phys. Stat. Sol. (A) 197 (2) (2003) 528.
[15] S. Chan, Y. Li, L.J. Rothberg, B.L. Miller, P.M. Fauchet, Mater. Sci. Eng. C 15 (2001) 277.
[16] L. Pavesi, RIV. Nuovo Cimento 20 (1997) 1.
[17] L.A. DeLouise, B.L. Miller, Mater. Res. Soc. Symp. Proc. 782 (2004) A5.3.1.
[18] B.R. Hart, S.E. Letant, S.R. Kane, M.Z. Hadi, S.J. Shields, J.G. Reynolds, Chem. Commun. (2003) 322.
[19] H.B. Yin, T. Brown, R. Gref, J.S. Wilkinson, T. Melvin, Microelectron. Eng. 73–74 (2004) 830.

# Chapter 3

*Hybrid systems based on Porous Silicon and biocompatible materials*

**Introduction: PSi hybrid systems**

Much attention has been attracted in the field of porous silicon (PSi) for its diverse applications in bio- and chemical sensing [1–3]. Unique properties for theses applications include the significantly increased surface interaction area, simplicity and repeatability of fabrication, and compatibility with the well-established silicon microfabrication technology. One reason of this clear success is the easy fabrication of sophisticated optical multilayers, such as the one-dimensional photonic crystals, by a simple, but not trivial, electrochemical etch process, computer controlled [4, 5]. The reflectivity spectrum of the PSi based photonic crystals can show single or multiple resonances [6], band-gap and other characteristic shapes, depending on the spatial arrangement of the porous layers [7], which are very useful in lot of applications from biochemical sensing to medical imaging.

But the major drawback preventing a wide diffusion of PSi devices is the instability of its native interface with a metastable $Si–H_x$ termination. The metastable hydrosilicon can undergo spontaneous oxidation in ambient atmosphere and results in the degradation of surface structures.

Moreover, it has been shown that porous silicon wafer can be dissolved under the physiological conditions which are very often used in biological experiments [8].

Therefore, surface passivation is crucial for the technological success of this material. Many organic molecules such as alkenes or alkynes had been covalently grafted onto the PSi surface by wet chemical approaches to passivate its surface [Chapter 2].

A very promising approach to overcome these difficulties is in fabricate hybrid systems based on the infiltration of polymers or biofilm resulting from the self-assembling of proteins in the nanometric pores of the PSi matrix. This is an alternative to the conventional chemical surface modification strategies.

Recently, beside hydrocarbon monomer monolayers, polymer films, are of special interest because they provide a strong shield to protect the surface nanostructure.

An example of hybrid PSi-polymer systems are the monodisperse microparticles containing a tunable nanostructure, these devices are desired for various high-throughput screening and targeted drug delivery applications [9,10]. The applicability of porous silicon-based particles and films has been demonstrated [11-21].

Moreover the field of tissue engineering entails the creation of a degradable three dimensional scaffold structure that has the appropriate physical, chemical, and mechanical properties to enable cell penetration and subsequent tissue formation for the purpose of disease or trauma repair at the desired site [22]. Bone engineering specifically attempts to replace or increase current graft approaches by using porous scaffolds that are designed to support the migration, proliferation, and differentiation of osteoprogenitor cells and aid in the organization of these cells in the proper dimensions. While these scaffolds may be made from a wide variety of both natural and synthetic materials, many of the existing porous biodegradable polymeric systems have been found to have limitations for use as orthopedic scaffolds [23].

Mesoporous Silicon, also referred to by its proprietary name BioSilicon™ , possesses several unique features highlighting its utility as a biomaterial. Previous studies by Bowditch et al have demonstrated its ability to be resorbed in soft tissue with a negligible inflammatory response in vivo [24]. When coupled with an established biopolymer such as polycaprolactone (PCL), it can be processed into a broad range of self-assembling structures useful to tissue engineering [25].

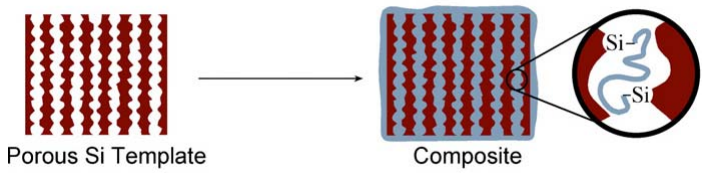


Schematic of a PSi device as etched and after polymer infiltration.

As was pointed out in the previous chapter, biomolecules can be linked via Si–C bonds or Si–O. Covalent attachment provides a convenient means to link a biomolecular capture probe to the inner pore walls of PSi for biosensor applications.
Hybrid materials, in which the functional material consists of an organic polymer or a biopolymer, forms an additional class of devices. Composites are attractive candidates for biological devices because they can display a combination of advantageous chemical and physical characteristics not exhibited by the individual constituents. Advances in polymer and materials chemistries have greatly expanded the design options for nanomaterial composites in the past few years, and synthesis of materials using nanostructured templates has emerged as a versatile technique to generate ordered nanostructures [26]. Templates consisting of micro or mesoporous membranes, zeolites, and crystalline colloidal arrays have been used, and many elaborate electronic, mechanical, or optical structures have resulted.
In this chapter the modification of PSi structures by infiltration of chemical and biological polymers is describes. In particular, it was used a biocompatible multi-block copolymer based on PCL and a high stable and resistant biofilm resulting from the self-assembling of the hydrophobins (HFBs) [27-29].
The polymer contains pendant functional groups regularly spaced along the chain. The reactive groups are available for the attachment of chemical substances and their distribution, can be tuned according to the molecular weight of both segments. In this way, the physical and chemical properties of the porous silicon surface were changed and modulated.
On the other hand HFBs are a family of small and cysteine-rich fungal proteins produced in the hyphal cell walls and that can be purified by the culture medium. The HFBs self-assemble into thin and amphiphilic membranes at hydrophilic-hydrophobic interfaces. In this way the wettability of a surface can be controlled and the hydrophobic behaviour can be converted in hydrophilic, and vice versa [30-32].
A general classification of HFBs is made on the basis of the biofilm resistance: the class I HFBs form high insoluble assemblies, which can be dissolved in strong acids, whereas class II biofilms can be dissolved in ethanol or in sodium dodecyl sulphate [27].
Solutions with HFB or PCL have been used at different concentration and the infiltration process has been monitored by variable angle spectroscopic ellipsometry (VASE) measurements.

## References

1. V.S. Lin, K. Motesharei, K.S. Dancil, M.J. Sailor, M.R. Ghadiri, Science 278 (1997) 840.
2. J. Gao, T. Gao, M.J. Sailor, Appl. Phys. Lett. 77 (2000) 901.
3. S. Le´tant, M.J. Sailor, Adv. Mater. 12 (2000) 355.
4. F. Müller, A. Birner, U. Gösele, V. Lehmann, S. Ottow, H. Föll, Journal of Porous Materials 2000, 7, 201.
5. H. F. Arrand, T.M. Benson, A. Loni, R. Arens-Fischer, M. Kruger, M. Thonissen, H. Luth, S. Kershaw, IEEE Phot. Techn. Lett. 1998, 10, 1467.
6. V. Mulloni, L. Pavesi, Appl. Phys. Lett. 2000, 76, 2523.
7. L. Moretti, L. De Stefano, I. Rea, I. Rendina, Appl. Phys. Lett. 2007, 90, 191112.

8. S.H.C. Anderson, H. Elliot, D.J. Wallis, L.T. Canham, J.J. Powell, Phys. Stat. Sol. (a) 2003, 197, 331.
9. R. Duncan, Natl. Rev. Drug Discov. 126, 1470 (2003).
10. New Types of Polymer Particles, AnalytiX: Advances in Analytical Chemistry, No. 5 (Sigma-Aldrich/Fluka Chemicals, 2001).
11. J. R. Link and M. J. Sailor, Proc. Natl. Acad. Sci. USA 100, 607 (2003).
12. V. S.-Y. Lin, K. Motesharei, K. S. Dancil, M. J. Sailor, and M. R. Ghadiri, Science 278, 840 (1997).
13. K.-P. S. Dancil, D. P. Greiner, and M. J. Sailor, J. Am. Chem. Soc. 121, 7925 (1999).
14. P. A. Snow, E. K. Squire, P. S. J. Russell, and L. T. Canham, J. Appl. Phys. 86, 1781 (1999).
15. S. Chan, P. M. Fauchet, Y. Li, L. J. Rothberg, and B. L. Miller, phys. stat. sol. (a) 182, 541 (2000).
16. S. Chan, S. R. Horner, B. L. Miller, and P. M. Fauchet, J. Am. Chem. Soc. 123, 797 (2001).
17. T. A. Schmedake, F. Cunin, J. R. Link, and M. J. Sailor, Adv. Mater. 14, 1270 (2002).
18. F. Cunin, T. A. Schmedake, J. R. Link, Y. Y. Li, J. Koh, S. N. Bhatia, and M. J. Sailor, Nature Mater. 1, 39 (2002).
19. S. O. Meade, M. S. Yoon, K. H. Ahn, and M. J. Sailor, Adv. Mater. 16, 1811 (2004).
20. L. T. Canham, Adv. Mater. 7, 1033 (1995).
21. L. T. Chanham, M. P. Stewart, J. M. Buriak, C. L. Reeves, M. Anderson, E. K. Squire, P. Allcock, and P. A. Snow, phys. stat. sol. (a) 182, 521 (2000).
22. Karp, J.M.; Dalton, P.D.; Shoichet, M.S., Mater. Res. Bull. 2003, 28,301.
23. Hutmacher, D.W.. Biomaterials, 2000, 21, 2529.
24. Bowditch, A.; Waters, K.; Gale, H.; Rice, P.; Scott, E.; Canham, L.T.;Reeves, C.; Loni, A.; Cox, T. Mater. Res. Soc. Symp. Proc.,1999, 536,149.
25. Coffer, J.; Whitehead, M.A.; Nagesha, D.; Mukherjee, P.; Akkaraju,G.;Totolici, M.;Saffie, R.; Canham, L.. Phys. Stat. Sol (a), 2005, 202,1451.
26. K.S. Soppimath, T.M. Aminabhavi, A.R. Kulkarni, W.E. Rudzinski, Biodegradable polymeric nanoparticles as drug delivery devices, J. Control Release 70 (2001) 1–20.
27. H. J. Hektor, K. Scholtmeijer, Current Opinion in Biotechnology 2005, 16, 434.
28. H.A.B. Wosten, M. L. de Vocht, Biochimica and Biophysica Acta 2000, 1469, 79.
29. G.R. Szilvay, A. Paananen, K. Laurikainen, E. Vuorimaa, H. Lemmetyinen, J. Peltonen, M.B. Linder, Biochemistry 2007, 46, 2345.
30. J. T. Han, S. Kim, A. Karim, Langmuir 2007, 23, 2608.
31. R. Wang, Y. Yang, M. Qin, L. Wang, L. Yu, B. Shao, M. Qiao, C. Wang, X. Feng, Chem. Mater. 2007, 19, 3227.
32. R. Wang, Y. Yang, M. Qin, L. Wang, L. Yu, B. Shao, M. Qiao, C. Wang, X. Feng, Langmuir 2007, 23, 4465.

## Porous silicon-polymer composite matrix for an innovative class of optical biosensors

This section is aimed at the characterization of PSi surface modification, based on the infiltration of Poly(ε-caprolactone) (PCL) macro-monomers in the nanometric pores of its matrix.

*In collaboration with Prof. R. Palumbo of University of Naples “Federico II”, Italy*

# A NANOSTRUCTURED HYBRID DEVICE BASED ON POLYMERS INFILTRATED POROUS SILICON LAYERS FOR BIOTECHNOLOGICAL APPLICATIONS

**L. Rotiroti[1,2*], I. Rendina[1], E. De Tommasi[1], M. Canciello[3], G. Maglio[3], R. Palumbo[3], and L. De Stefano[1]**
[1] *IMM-CNR - Sezione di Napoli, Via P. Castellino 111, 80131 Napoli, Italy – lucia.rotiroti@na.imm.cnr.it*
[2] *Dept. of Organic Chemistry and Biochemistry, "Federico II" University of Naples, Monte S. Angelo, Naples, Italy*
[3] *Dept. Of Chemistry, "Federico II" University of Naples, Monte S. Angelo, 80126 Naples, Italy*

Abstract - Hydrophobic aliphatic polyesters, such as poly(ε-caprolattone) (PCL), polylactide (PLA) and their copolymers, have been intensively investigated in applications such as medical devices used in the regeneration of damaged tissues and also in the pharmaceutical field for the drugs controlled release systems.
Porous silicon (PSi) is really an amazing platform material due to its physical and structural features: the PSi sponge-like morphology shows a high surface area which strongly interacts with the surrounding environment. As a consequence, some physical parameters, such as the dielectric constant, the conductivity and the photoluminescence of PSi samples strongly change. Due to the sensing mechanism, these kinds of devices are not able to identify the components of a complex mixture. In order to enhance the sensor selectivity through specific interactions, some chemical or physical strategies are employed to modify the PSi surface. As an alternative to the conventional chemical surface modification strategies, we have infiltrated biocompatible polymers, containing pendant functional groups regularly spaced along the chain, which can be used as passivation coatings of PSi. The reactive groups are available for the attachment of chemical substances and their distribution, as well as the hydrophilic/hydrophobic ratio, can be modulated according to the molecular weight of both segments. In this way, we can change and tune the physical and chemical properties of the porous silicon surface.

## Introduction

Amphiphilic di-, tri- and multiblock poly(ether–ester)s, based on PCL and PEO, have been recently investigated in tissue engineering experiments and for the development of pharmaceutical controlled release systems, due to their peculiar characteristics: these polymers support the growth of cells into tissue-like structures, degrade into natural metabolites, and can form micro- or nanoparticles [1, 2]. On the other hand, lot of experimental work, concerning the worth noting properties of porous silicon (PSi) in chemical and biological sensing, has been reported, showing that, due to its morphological and physical properties, PSi is a very versatile sensing platform [3-5]. PSi is produced from crystalline silicon by electrochemical etching in a water solution of hydrofluoridric acid and ethanol. This process gives a characteristic sponge-like structure to the PSi with an elevated value of specific area (up to 500 $m^2/cm^3$). The silicon skeleton is constituted by nanocrystals with variable dimensions, from few nanometres up to microns, depending on the process conditions and the doping level of the silicon wafer. The nano nature of the bulk material is evident especially by some physical phenomena such as photoluminescence under blue light illumination or the capillary condensation of volatile substances in its nanometric pores. Moreover, PSi is an available, low cost material, completely compatible with VLSI and micromachining technologies, so that it could usefully be employed in the fabrication of MEMS, MOEMS and smart sensors.
The PSi optical sensing features are based on the changes of its photonic properties, such as photoluminescence or reflectance, on exposure to the gaseous or liquid substances. Unfortunately, these interactions are not specific, so that the PSi cannot be used as a selective optical transducer material. One way to overcome this limit is to chemically or physically modify the PSi hydrogenated surface in order to enhance the sensor selectivity through specific biochemical interactions. The reliability of the biosensor strongly depends on the functionalization process: how simple, homogenous and repeatable it can be. This fabrication step is also crucial for the stability of the sensor: it is well known that the porous silicon "as-etched" has a very reactive Si-H terminated surface due to the Si dissolution process [6]. This chemical instability is one of the major drawbacks of the PSi based device: the hydrogen terminated PSi surface is slowly oxidized at room temperature by the atmospheric water content, resulting in a blue shift of the optical spectrum since the oxide has a refractive index lower than the silicon [6]. Moreover, it has been shown that porous silicon wafer can be dissolved under the physiological conditions which are very often used in biological experiments [7].
We have tested the use of PCL co-polymers to control the surface properties of PSi structures, in order to improve their chemical stability and give a proper functionalization to the PSi based sensors.

In this work, we have studied the infiltration by spin coating of the PCL in porous silicon monolayers and multilayers: the process has been monitored by variable angle spectroscopic ellipsometry (VASE) measurements and spectroscopic reflectometry.

## Experimental

*Poly(ε-caprolattone) synthesis*

Poly(ε-caprolactone) (PCL) macro-monomers (Mn = 3.7 kDa) which contain one Z-protected $-NH_2$ group were synthesized by ring-opening polymerization of ε-caprolactone (εCL) in the presence of $Sn(oct)_2$ using as initiator a diamine (Lys-Nε-Z-HMD).
Deprotection, accomplished without chain degradation, yielded $-NH_2$ groups available for further reactions. The molecular structure of macro-monomers was investigated by $^1$H-NMR and SEC. In figure 1 the reaction scheme is reported.

Figure **1** - Reaction pathway for the polymer deprotection

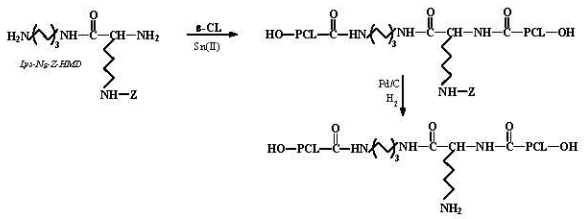


*Porous silicon chip preparation and PCL infiltration*

Proof of PSi in optical biosensing has been experimentally demonstrated in a variety of sensors photonic devices including rugate filters, Bragg filters, single layer films, protein and DNA microarray due to the large internal surface area which, depending upon depth, can easily be over 1000 times that of a planar surface of equal diameter thus enabling the immobilization of large amounts of selective receptors [8-10]. However, for the device to function effectively, the porous morphology should enable homogeneous diffusion everywhere in the matrix. In the case of porous silicon, the porosity, determined by pores size and distribution, is tunable over a rather wide range by properly setting the fabrication parameters, i.e. current density, etching time, etching solution and wafer type.
In our experiments we have used PSi monolayers, which optically act as Fabry-Perot interferometers, and PSi Bragg multilayers obtained alternating high and low porosity layer, both fabricated by electrochemical etching of $p^+$-type (100) crystalline silicon (resistivity 3-5 mΩ cm) in HF/EtOH (30:70) solution. In these conditions, PSi is a mesoporous material, having pores size between 5 and 50 nanometres. Monolayer thickness was about 4 μm and the porosity about 65 % (values estimated by fitting the optical reflectivity data); Bragg multilayers were constituted by ten couples of 64 % and 72 % porosities and 135 nm and 161 nm thicknesses, respectively.
In Figure 2 a cross section and a top view image of a PSi monolayer are reported, where is evident the sponge like feature of this material.

**Figure 2 – A)** SEM cross section of a monolayer **B)** SEM plan view of a PSi surface

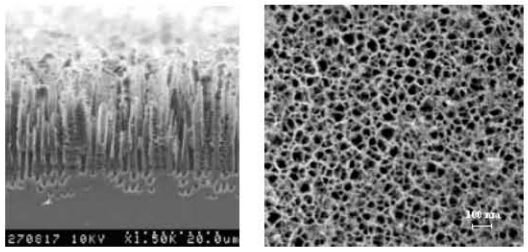

The Bragg mirror is instead a multilayer device made of alternating layers of high ($n_H$) and low ($n_L$) refractive index, whose thicknesses satisfy the Bragg condition: $n_H d_H + n_L d_L = \lambda_B/2$. From the optical point of view this is a resonant device, i.e. its optical spectrum is characterised by a specific wavelenght $\lambda_B$ which is the center of the high reflectivity stop band as it can be see in Figure 3 where a scheme and a reflectivity spectrum of this structure are reported.

**Figure 3 –** PSi Bragg reflector **A)** schematic of the device; **B)** the reflectivity spectrum.

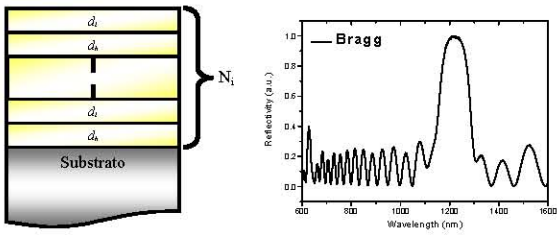


In this communication only monolayer results will be presented. The optical set-up required for spectroscopic reflectometry was very simple: a tungsten lamp (400 nm < λ < 1800 nm) inquired the monolayer, through an optical fibre and a collimator. The reflected light was collected by an objective, coupled into a multimode fibre, and then directed in an optical spectrum analyzer (Ando, AQ6315A).
The polymer solutions were prepared by solving the polymer, at different concentration, in $CH_2Cl_2$. A solution volume of 100 μl was directly spotted on the PSi surface and spun at 2000 rpm for 5 seconds.

## Results and Discussion

In Figure 4 the red shifts induced in the fringes of the monolayer reflectivity spectrum after the spin coating with PCL solutions are reported as a function of the solutions concentrations. The VASE characterisation of a 560 nm PSi monolayer (starting porosity of about

79%) after PCL infiltration revelead a reduction of the porosity down to 75.2 % and a vertical dishomogeneity in the polymer distribution: due to the hydrophobic interaction, the PCL penetrates in the whole stack, but cumulates at the bottom where the hydrogen concentration is higher, and the hydrostatic pressure stops the air penetration. When spun on planar crystalline silicon with a concentration of 0.35 mg/ml, the PCL film measures about 4 nm compatible with the size dimension of the mesoporous material, ranging from 5 to 30 nm.

**Figure 4** – Red shifts induced in the fringes of the monolayer reflectivity spectrum versus different concentrations of PCL.

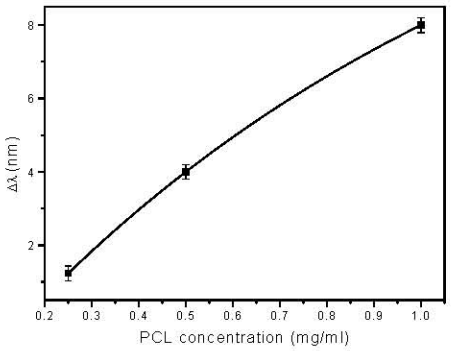


In order to test the new properties of the polymer-coated PSi monolayer, we have exposed it to a 0.1 M aqueous solution of sodium hydroxide. We have compared the dissolution time evolution with a non-coated monolayer: initially both undergo a blue-shift, due to the removal by NaOH dissolution of some unprotected silicon nanocrystals, but while after 75 s the uncoated sample is almost completely dissolved, the PCL coated still shows the optical modulation. In Figure 5 we have reported the optical spectra of both samples for direct comparison.

**Figure 5** - Comparison between a coated (solid line) and an uncoated (dotted line) PSi monolayer before ***(a)*** and after 75seconds in 0.1 M NaOH solution ***(b)***.

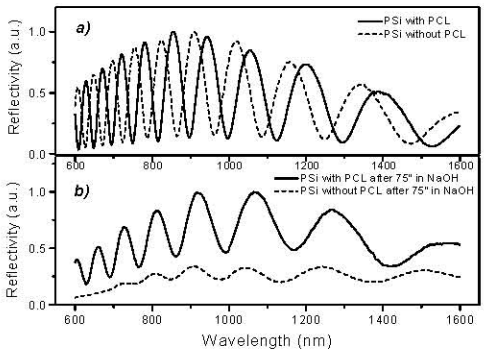


The polymer layer is also able to modify the wettability of the PSi surface: after electrochemical etching process, the PSi is highly hydrophobic resulting in a contact angle value of 131°, while after PCL infiltration the same surface shows a hydrophobic behaviour and the water contact angle is reduce to 60.5°.
The ability to switch between to different wettability regime could be a key feature in designing bioactive interfaces for miniaturization of biosensors.

## Conclusions

PSi modification, based on the infiltration of polymers in the nanometric pores of its matrix, has been presented. We have infiltrated biocompatible multi-block copolymers based on PCL and poly(oxyethylene), containing pendant functional groups regularly spaced along the chain, in PSi monolayers and tested this device against the basic environments. We demonstrated that PCL coatings change the wettability of the PSi structures, moreover protect PSi structures from exposure to NaOH solutions. Next experiments will be focused on the exploitation of the PCL chains amino-groups for the attachment of biological probes to PSi surface.

## References


1. H. M. Aliabadi, A. Mahmud, A. D. Sharifabadi, A. Lavasanifar, J. Control. Release 2005, 104, 301.
2. M. Canciello, G. Maglio, G. Nese, R. Palumbo, *Macromol. Biosci.* **2007,** 7, 491-499.
3. S.M. Weiss, H. Ouyang, J. Zhang, and P.M. Fauchet, Opt. Express **13**, 1090, 2005.
4. L. De Stefano, I. Rendina, L. Moretti, L. Rotiroti**,** Sensor and Actuators B 111-112, 522-825, 2005.
5. L. De Stefano, I. Rea, I. Rendina, L. Rotiroti, M. Rossi, and S. D'Auria, Phys Stat Sol (A) , 203 (2006) 886-891.
6. L. Canham in Properties of Porous Silicon, Vol. 18 (Ed: L. Canham), INSPEC, 1997, p. 154.
7. S.H.C. Anderson, H. Elliot, D.J. Wallis, L.T. Canham, J.J. Powell, Phys. Stat. Sol. (a) 2003, 197,331.
8. L. De Stefano, P. Arcari, A. Lamberti, C. Sanchez, L. Rotiroti, I. Rea, I. Rendina, Sensors, 7 (2007) 214-221.
9. L. De Stefano, M. Rossi, M. Staiano, G. Mamone, A. Parracino, L. Rotiroti, I. Rendina, M. Rossi, and S. D'Auria, Journal of Proteome Research 5,5, 1241-1245, 2006
10. Yin H.B., Brown T., Gref R., Wilkinson J.S., Melvin T. (2004), Microelectronic Engineering 73-74, 830-836.

# A polymer modified PSi optical device for biochemical sensing

## Introduction

Due to their widespread utilisation, there are all over the world tens of thousand of hydrocarbons contaminated sites, where the pollution is caused by leaking of storage tanks, by chemical wastes dumps and also by extraction and transport operations. In addition, there is the real problem of vapours leaks from distributed gas pipelines in metropolitan areas. Therefore, an accurate characterization and long-term monitoring is required to reduce and control health risk and public safety. Four general groups of chemical sensors can be categorized on the base of physics and operating mechanisms: chromatography and spectrometry, electrochemical sensors, mass sensors and optical sensors [1]. Although a number of these devices are commercially available, there is a strong need of low-cost, robust and on field sensors of chemical species, especially for long, real-time monitoring [1].

In particular, PSi optical sensor based on reflectivity measurements in Bragg grating mirrors [2] or on photoluminescence experiments in optical microcavities operating in the visible wavelength region [3, 4] have been already reported.

A typical photonic band gap (PBG) structure used in optical sensing is the distributed Bragg mirror which is obtained by alternating high (A) refractive index layers (low-porosity) and low (B) refractive index layers (high-porosity). The thicknesses of each layer satisfy the following relationship: $n_A d_A + n_B d_B = m\ \lambda/2$, where m is an integer and $\lambda$ is the Bragg resonant wavelength.

When the PSi Bragg mirror is exposed to vapors, or dip in liquid hydrocarbons, a repeatable and completely reversible change in the reflectivity spectrum is observed. In fact, the substitution of air in the pores by the organic molecules causes an increasing of the average refractive index of the microcavity, shifting towards longer wavelengths its characteristic peaks.

- *PSi functionalization by polymer infiltration*

Covalent attachment provides a convenient means to link a biomolecular capture probe to the inner pore walls of PSi for biosensor applications. As was pointed out in the previous section, biomolecules can be linked via Si–C bonds or Si–O.

Advances in polymer [5] and materials chemistries have greatly expanded the design options for nanomaterial composites in the past few years, and synthesis of materials using nanostructured templates has emerged as a versatile technique to generate ordered nanostructures. Templates consisting of micro or mesoporous membranes, zeolites, and crystalline colloidal arrays have been used, and many elaborate electronic, mechanical, or optical structures have resulted.

## Materials and methods

Bragg multilayers were constituted by 15 couples of 58 % and 69 % porosities and 72 nm and 117 nm thicknesses, respectively.

A highly doped p+-silicon, <100> oriented, 0.01 Ω cm resistivity, 400 μm thick was used as substrate to realize the structures. The Bragg low-porosity layers (effective refractive index $n_L \cong 1.903$) have been produced by an etching current density of 100 mA/cm$^2$ for 2.2 s, while an etching current density of 200 mA/cm$^2$ for 2.3 s has been used for the high-porosity layers ($n_H \cong 1.632$).

The electrochemical dissolution process leaves nanodimensional residues into the channels which partially fill the pores in the layers and prevent a homogeneous diffusion of biological solutions. To remove the nanostructures and improve pore infiltration of polymer, a KOH post-etch process elsewhere described [6] was used. It was verified that the alkaline treatment does not degrade the optical response of our devices. In order to leave an hydrophobic surface the Si-H bonds were replaced on the surface, by immersing the samples in a very diluted HF solution for few seconds.

The polymer solutions were prepared by solving the polymer in dichloromethane ($CH_2Cl_2$). A solution volume of 100 μl was directly spotted on the PSi surface, spun at 2000 rpm for 5 seconds, and baked at 100°C for 5 minutes.
In Figure 1 the red shift induced in the Bragg reflectivity spectrum by the presence of PCL is reported.

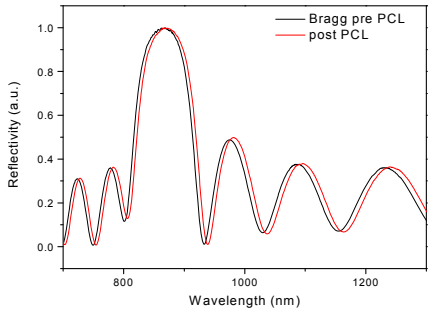


Figure 1: PSi reflectivity spectra before and after PCL infiltration.

- *PSi/PCL hybrid system: alkaline stability*

In order to test the new properties of the PSi-polymer composite device, two twins chips, one polymer infiltrated and the other bare, were exposed to a 0.1 M aqueous solution of sodium hydroxide. The dissolution time evolution of both the samples were compared: initially both undergo a shift through minor wavelength, due to the removal by NaOH dissolution of some unprotected silicon nanocrystals, but while after 80 s the uncoated sample is almost completely dissolved, while the PCL coated PSi Bragg still resist for 15 minutes. In Figure 2 are reported the optical spectra of both samples for direct comparison.

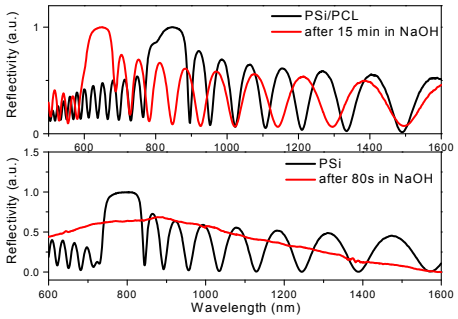


Figure 2: Comparison between a coated (A) and an uncoated (B) PSi Bragg mirrors before (black) and after immersion in 0.1 M NaOH solution (red).

Even if blue-shifted the optical spectrum (A) yet shows a reflectivity stop band.

- *PSi/PCL hybrid system: chemical sensing*

After the basic etch process the hybrid organic-inorganic device is still working as chemical optical transducer: it was tested its ability in sensing the vapours of different volatile substances. In Figure 3-A, are reported the characteristic red-shift due to the capillary condensation of the vapours inside the nanometric pores of the PSi Bragg. The shift is completely reversible and the polymer coated device can be used with different substances (Isopropanol, ethanol and methanol) giving high reproducible results.

| Organic compound | Refractive index |
|---|---|
| Isopropanol | 1.375 |
| Ethanol | 1.361 |
| Methanol | 1.329 |

It was also calculated the sensitivity of this optical transducer to the refractive index changes by exposing it to substances having different refractive index. Assuming that the three solvents equally penetrates the nanostructured spongy multilayer, was estimated a sensitivity of 585 (3) nm expressed in refractive index units [7].

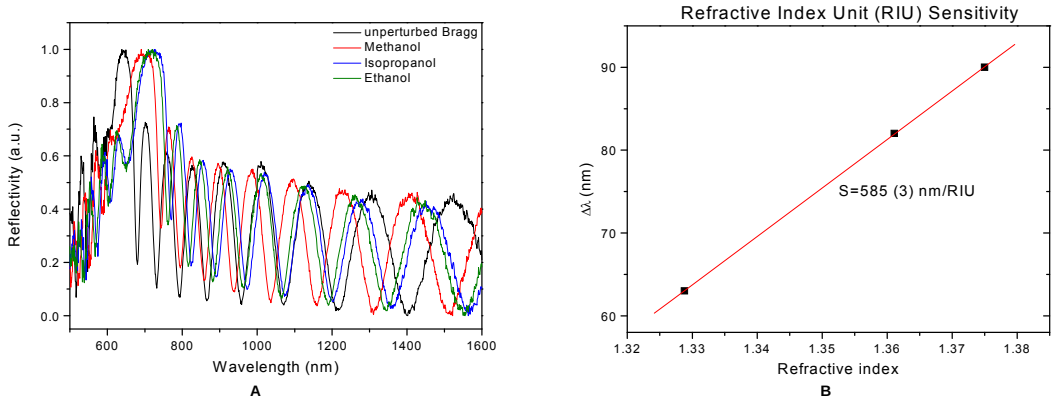


Figure 3: The PSi polymer modified Bragg still works as optical transducer for vapour and liquid detection. A: the characteristic red shift of the optical spectrum on exposure to methanol, isopropanol and ethanol. B: determination of the sensitivity to refractive index changes of the optical transducer.

It was demonstrated that the passivation of some optical devices based on the porous silicon technology when infiltrated by polymer not only protects the nanocrystalline material from basic dissolution in NaOH, but also leaves unaltered the sensing ability of such optical transducers adding the chemical stability which can be a key feature in biomolecular experiments.
It was moreover experimentally studied a feasible optical sensor for hydrocarbons detecting in the gaseous state. The optical experimental setup adopted and the structure of the sensing element do not prevent from the scaling down of each component in a compact sensor system with minimum effort. In fact, the white source can be replaced by small, wide bandwidth LEDs and the OSA bench version by an integrated fiber optic spectrometer, already available on the market. Moreover, the use of a resonant device allows “on/off” digital reading of the sensor element by a single-wavelength source. A net red-shift of the transmittance peak in the reflectivity spectrum has been repeatable observed when the sensor is exposed to the hydrocarbons species. The shift values, due to capillary condensation of the liquid into the pores, are characteristic of each species and depend on their physical and chemical properties. The sensing process is completely reversible.

- *PSi/PCL hybrid system:biochemical sensing*

The hybrid interface of silicon and PCL should act as an active substrate for covalently binding of different bioprobes, so that the quality and the characteristic of this polymer layer are key features for the entire device. This represents an alternative to the conventional chemical surface modification strategies. The reactive groups, introduced by infiltration of biocompatible polymer into PSi matrix, are available for the attachment of chemical substances and biological probes, in order to verify this feature a methanol

solution of 5(6)-Carboxyfluorescein *N*-hydroxysuccinimide ester (FITC) 300 μM was used as ligand. A schematic of immobilization chemistry is reported in figure 4.

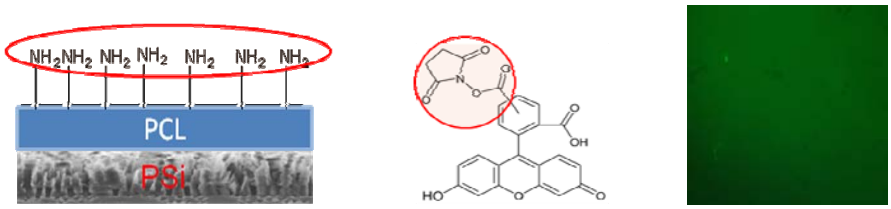


A B C

Figure 4: The PSi polymer modified device. A: the characteristic reactive groups on the PSi surface after spin coating. B: 5(6)-Carboxyfluorescein *N*-hydroxysuccinimide ester (FITC) molecular formula. C: Fluorescence image after incubation.

The immobilization was carried in methanol solution at room temperature over night. After incubation, the sample was rinsed three times in methanol. By illuminating the fluorescent FITC samples, a bright fluorescence signal was recorded, and it was quite homogeneous on the whole surface. It was also qualitatively tested the strength of the binding between the PCL and the FITC, by washing the chip in a dialysis membrane overnight in methanol. Since the fluorescent intensities before and after the dialysis do not differ, can be concluded that the PCL-FITC system is very stable.

## References


1. C. K. Ho, M. T. Itamura, M. Kelley and R. G. Hughes, Sandia Report SAND2001-0643, Sandia National Laboratories, (2001) 1-27.
2. P. A. Snow, E. K. Squire, P. St. J. Russel, and L. T. Canham, J. Appl. Phys. 86, (1999) 1781-1784.
3. V. Mulloni and L. Pavesi, Appl. Phys. Lett. 76, (2000) 2523-2525.
4. M. Ben-Chorin, A. Kux, and I. Schechter, Appl. Phys. Lett. 64, (1994) 481-483.
5. P. A. Snow, E. K. Squire, P. St. J. Russel, and L. T. Canham, J. Appl. Phys. 86, (1999) 1781-1784.
6. L. A. De Louise and B. L. Miller (2004), Mat. Res. Soc. Symp. Proc. Vol. 782, A5.3.1- A5.3.7.
7. L. De Stefano, I. Rendina, L. Moretti, A.M. Rossi, Materials Science and Engineering B 2003, 100/3, 271.

## Bio/NON Bio Interfaces for a new class of proteins Microarrays

This section is aimed at the characterization of PSi surface biological passivation, based on the infiltration by the fungal proteins called hydrophobins. The self-assembled biofilm changes the wettability of the PSi structures and protects the PSi structures from alcaline agent. Moreover these is a new active substrate as a functional one for proteins microarrays development.

*In collaboration with Prof.ssa P. Giardina of University of Naples “Federico II”, Italy*

ARTICLE TYPE www.rsc.org/xxxxxx | XXXXXXXX

# Bioactive Modification of Silicon Surface using Self-assembled Hydrophobins from *Pleurotus ostreatus*.

**L. De Stefano*[a], I. Rea [a,b], E. De Tommasi[a], I. Rendina[a], L. Rotiroti[a,c], M. Giocondo[d], S. Longobardi[e], A. Armenante[e], and P. Giardina [e] .**

***Received (in XXX, XXX) Xth XXXXXXXXX 200X, Accepted Xth XXXXXXXXX 200X***
***First published on the web Xth XXXXXXXXX 200X***
**DOI: 10.1039/b000000x**

A crystalline silicon surface can be made biocompatible and chemically stable by a self-assembled biofilm of proteins, the hydrophobins (HFBs) purified from the fungus Pleurotus ostreatus. The protein modified silicon surface shows an improvement in wettability and is suitable for proteins immobilization. Two different proteins were successfully immobilized on the HFBs coated chips: the bovine serum albumin and an enzyme, a laccase, which retains its catalytic activity even when bound on the chip. Variable angle spectroscopic ellipsometry (VASE), water contact angle (WCA), and fluorescence measurements demonstrated that the proposed approach in silicon surface bioactivation is a feasible strategy for the fabrication of a new class of hybrid biodevices.

## Introduction

Biological molecules are more and more used in a large class of research and commercial applications such as biosensors, DNA and protein microarrays, cell culturing, immunological assays, and so on. The fabrication of a new generation of hybrid biodevices, where a biological counterpart is integrated in a micro or a nano-electronic platform, is strictly related to the bio-compatibilization treatments of the surfaces involved. [1] The design ad the realization of bio/non-bio interfaces with specific properties of chemical stability, wettability, and biomolecules immobilization are key features in the miniaturization of devices needed in the development of genomic and proteomic research.[2] In particular, protein immobilization is a hot topic in biotechnology since commercial solutions such as the DNA array are not still available. Proteins are, due to their composition, a class of very heterogeneous macromolecules with variable properties. For these reasons, it is extremely complex to find a common surface suitable for different proteins with a broad range in molecular weight and physical–chemical properties such as charge and hydrophobicity. A further aspect is the orientation of spotted compounds, that becomes of crucial relevance for some applications, like quantitative analysis, enzymatic reactions, interaction studies. Besides tethering the proteins to the surface by adhesion or non-oriented covalent attachment, recent developments for the directed immobilization of proteins are emerging. These efforts are addressing challenges such as loss of enzymatic activity due to unfavourable orientation of the immobilized enzyme.[3] Despite the development of many different surfaces in the last five years, notably only few systematic investigations have been conducted and yet, no universal surface ideal for all applications could be identified[4-8]. Among others, silicon is a very interesting platform due to its wide use in all the micro and nanotechnologies developed for the integrated circuits industry. Lot of studies about the chemical functionalization of silicon in order to make it compatible with the organic chemistry have been published in the last ten year.[9] A completely different approach is to use a biological substrate to passivate the silicon surface: recently, a nanostructured self-assembled biofilm of amphiphilic proteins, the hydrophobins, was deposited by solution deposition on crystalline silicon and proved to be efficient as masking material in the KOH wet etch of the crystalline silicon.[10] HFBs are a group of very surface active proteins.[11] They are small (around 10 kDa) proteins that originate from filamentous fungi, where they coat the spores and aerial structures, and they mediate the attachment of fungal structures to hydrophobic surfaces and affect the cell wall composition.[12-13] HFBs self-assemble at the air/water interface and lower the surface tension of water. Furthermore, they shown self-assembling properties also at interfaces between oil and water, and between water and a hydrophobic solid.[14] The primary structure of HFBs is characterized by a conserved pattern of eight cysteine residues, forming four intramolecular disulfide bridges.[15] HFBs are further divided into classes I and II based on their hydropathy patterns, although the amino acid sequence similarity both within and between the classes is small. Class I HB assemblies are remarkable due to their insolubility. They are insoluble even in hot solutions of sodium dodecyl sulfate (SDS) and can only be dissolved in some strong acids, such as trifluoroacetic acid.[11]

Some very recent applications of class II hydrophobins in protein immobilization have been reported, nevertheless only one example of enzyme immobilization on a Class I hydrophobin (SC3) layer formed on a glassy carbon electrode has been investigated.[12] Inspired by these very promising results, we have studied the immobilization of a fluorescent protein and a laccase enzyme on a Class I hydrophobin layer when self-assembled on silicon surface.

## Matherials and methods

*Protein purification.* The HFB and the laccase POXC were isolated from the culture broth of P. ostreatus (type: Florida ATCC no. MYA-2306). For HFBs production, mycelia were grown at 28 °C in static cultures in 2 L flasks containing 500 mL of potato dextrose (24 g/l) broth with 0.5% yeast extract. After 10 days of fungal growth, the HFBs aggregates were obtained by air bubbling of the culture broth by using a Waring blender. Foam was then collected by centrifugation at 4000 g. The precipitate was freeze dried, treated with trifluoroacetic acid (TFA 100%) for 2h, and sonicated for 30 min. The sample was dried again in a stream of air and then dissolved in 60% ethanol. The precipitate formed was separated by centrifugation at 4000g. the purity of the HFB was ascertained by SDS-PAGE, by using a silver staining method. Mycelium growth and laccase purification were carried out following the procedures described by Palmieri et al..[16]

*Hydrophobin self-assembly on silicon chip.* Silicon samples, single side polished, <100> oriented (chip size: 1cm×1cm), after standard cleaning procedure,[18] have been washed in hydrofluoridic acid solution for three minutes to remove the native oxide thin layer (1-2 nm) due to silicon oxidation. Then samples have been incubated in HFBs solutions (0.1 mg/mL in 80% ethanol) for 1 h, dried for 10 min on the hot plate (80°C), and then washed by the solvent solution (80% ethanol in water).

*Laccase immobilization method.* The laccase immobilization procedure on HFB modified silicon surface was carried at 4 °C for 1 hour, followed by a over night rinsing in 50 mM phosphate buffer, pH 7. After 16 hours, the silicon biochip was washed in the same buffer at 25°C till to no laccase activity was found in the washing buffer. Then each chip was dust-protected and kept at constant humidity conditions when not in use.

*BSA immobilization method.* Bovine serum albumin (BSA) was labelled by rhodamine, following the Molecular Probes© procedure MP06161, and solubilised in water at three different concentration (3, 6, 12 μM). To assess the protein binding on the chip surface, we have spotted on the chips covered by the HFBs biofilm 50 μl of water solution containing the labeled protein. The immobilization was carried in water solution at 4°C over night. After incubation, the samples were rinsed three times in deionized water at room temperature.

Enzyme assay Laccase activity was assayed at 25°C using 2,6-dimethoxyphenol (DMP) 10mM in McIlvaine citrate–phosphate buffer, pH 5. Oxidation of DMP was followed by the absorption increment at 477 nm ($\varepsilon_{477}$=14.8×10$^3$ M$^{-1}$ cm$^{-1}$) using Beckman DU 7500 spectrophotometer (Beckman Instruments). Enzyme activity was expressed in International Units (IU). Immobilized enzyme was assayed by silicon dip in 10 ml of McIlvaine citrate–phosphate buffer, pH 5. The absorption increment at 477 nm was followed withdrawing 200 μl of reaction mixture each 30s for 10 min. The total immobilised activity per unit of silicon (chip) were calculated as U/chip = $\Delta A\ min^{-1}/\varepsilon \times 10^4$.

*Optical Techniques.* Ellipsometric characterization of the hydrophobin biofilm deposited on the silicon substrate has been performed by a variable-angle spectroscopic ellipsometry model (UVISEL, Horiba-Jobin-Yvon). Ellipsometric parameters Δ and Φ have been measured at an angle of incidence of 65° over the range of 360-1600 nm with a resolution of 5 nm. Fluorescence images were recorded by a Leica Z16 APO fluorescence macroscopy system. Contact angle measurements have been performed by using a KSV Instruments LTD CAM 200 Optical Contact Angle Meter: each contact angle has been calculated as the average between the values obtained from three drops having the same volume (about 3 μL), spotted on different points of the chip.You can also put lists into the text.

## Results and Discussion

The immobilization of proteins and enzymes on the silicon modified surface is schematized in Figure 1.

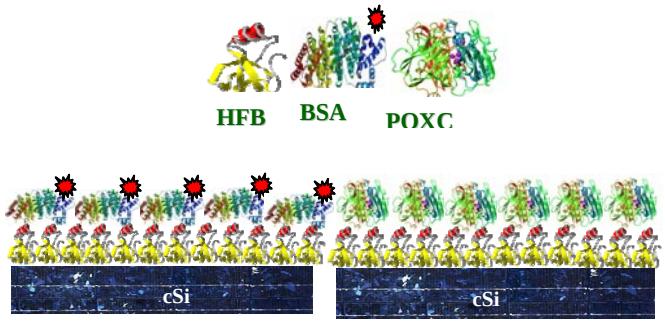


**Figure 1**. Schematic of immobilization of enzyme (POXC) and protein (rhodamine fluorescent BSA) on a crystalline silicon wafer biologically modified by a self-assembled biofilm of hydrophobin.

The hybrid interface of silicon and HFB should act as an active substrate for non-covalently binding of different bioprobes, so that the quality and the characteristic of this proteins layer are key features for the entire device. The coating of a solid surface by chemical solution deposition is not a finely controlled process, even if the covering substance has self-assembling properties, as it is the case of HFBs. The result is that the HFB biofilms self-assembled on the silicon surface by deposition of equal concentration solutions could have thicknesses ranging between 10 and 30 nanometers. This behaviour could be ascribed to different local aggregation of HFB in the solution covering the silicon chip, due to the strong hydrophobic interactions among the proteins. In fact, during HFB deposition, solvent evaporation can determine local increases of protein concentration, thus favouring multimers and aggregate formation that can deposit on the layer. In this step there is no way to control the clustering and stacking of the proteins which are constituting the self-assembled biofilm. The association of hydrophobins in solution and their self assembly have both been attributed to the amphiphilic structure of the HFB monomer.[19-20] Before using the HFB biofilm as a nanostructured template for protein binding, we have tested its stability and some features by optical methods such as VASE, spectrofometry, and WCA.


This journal is © The Royal Society of Chemistry [year]

The HFB biofilm self-assembled on the hydrophobic silicon shows a strong adhesion to the surface: the protein layers always exhibit great stability to alkaline solutions even at high temperature. After 10 minutes washing in sodium hydroxide and SDS at 100 °C, a residual biofilm, which has on average a thickness of about 3.1±0.7 nm, is still present. The biofilm characterization has been performed by VASE on 12 samples realized in the same experimental conditions; the optical model for experimental data fitting has been developed in our previous work.[10] We believe that this is the thickness of a monolayer of HFBs when self-assembled on hydrophobic silicon: this value is also consistent with a typical molecular size and comparable to atomic force microscopy measurements.[21] According to the above described model, the washing step of the chip is strong enough to remove the aggregates deposited on the HFB monolayer that directly interacts with the hydrophobic silicon surface. This behaviour points out the stronger interactions between the silicon surface and the HFB monolayer with respect to those between the HFB aggregates and the HFB monolayer.

In a recent article, we have already demonstrated that the nanometric HFB biofilm uniformly covers the silicon surface: [10] on exposure to the potassium hydroxide (KOH), which anisotropically dissolves the silicon, a silicon wafer coated by HFB is completely shielded by the etching agent, at least for several minutes. The protection against KOH can be prolonged at any time by increasing the thickness of the HFB biofilm self-assembled on the silicon surface. This is possible since successive depositions of proteins form a biofilm having thickness proportional to the number of depositions, as it is shown in Figure 2: we have reported the thicknesses of the HFB films after each one of three consecutive depositions and plotted them as function of the deposition cycle.

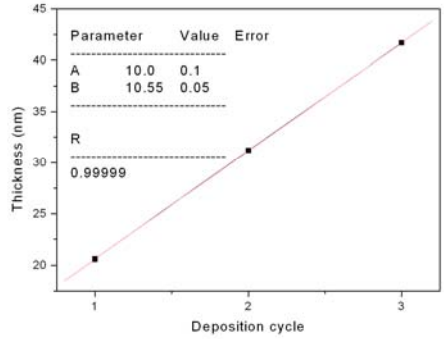


**Figure 2**. Growth of a thick HFB biofilm by repeated cycles of deposition on a hydrophobic silicon substrate

Moreover, the presence of the biofilms does not alter the optical behaviour of the silicon surface as it is shown in Figure 3, where the transmission curves of two different biofilms on silicon are reported. In both cases the self-assembled layer is transparent in a very large interval of wavelengths: the transmittance is still the 80 % at 290 nm.

The improvement in the silicon wettability is also a key features in biodevices realization: the silicon surface, after standard cleaning process and washing in HF, is hydrophobic, this occurrence can constitute a severe limit in the fabrication of microchannels for microfluidics applications. Since HFBs self-assemble in stable biofilm on a variety of different surfaces, such as mica, Teflon, and polystyrene[6-7] due to the amphiphilic interaction with hydrophobic or hydrophilic surfaces, we can modify the silicon behaviour with respect to the water interaction by covering its surface by HFBs.

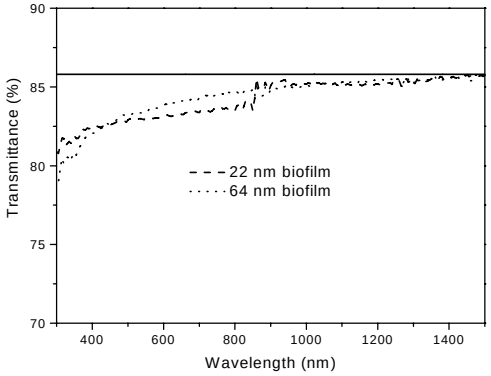


**Figure 3**. Figure caption. Transmission curves of two different samples of HFB self-assembled biofilm on silicon.

The changing in silicon wettability has been monitored by water contact angle measurements. In Figure 4 A and B are reported the WCA results in case of the bare silicon surface and after the deposition of the HFB biofilm. The dramatic increase in wettability of the silicon surface is well evident: in the first case, the WCA results in 90°±1°, so that the surface can be classified as hydrophobic, while after the HFB deposition the WCA falls down to 25°±2° so that the surface is clearly hydrophilic. The HFB modified silicon surface is highly stable and the WCA value does not change after months, even if stored at room temperature without particular saving condition.

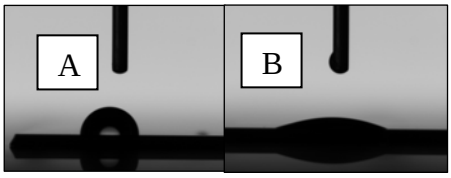


**Figure 4**. Changing the wettability of c-Si: the hydrophobin nanolayer turns the hydrophobic surface of c-Si into a hydrophilic one. A: a water drop on the c-Si after washing in hydrofluoridic acid forms a contact angle of 90°±1°. B: a water drop after the hydrophobin deposition forms a contact angle of 25°±2°.

The HFB modified silicon surface has been tested by BSA immobilization: solutions containing the rhodamine labelled protein, at different concentration, between 3 and 12 μM, have been spotted on the HFB film. The labelled bioprobes have been spotted also on some surface which have not been treated with the hydrophobins, as a negative control on the possible

aspecific binding between the silicon and the probe. All the samples have been washed in deionized water to remove the excess of biological matter and observed by the fluorescence macroscopy system.

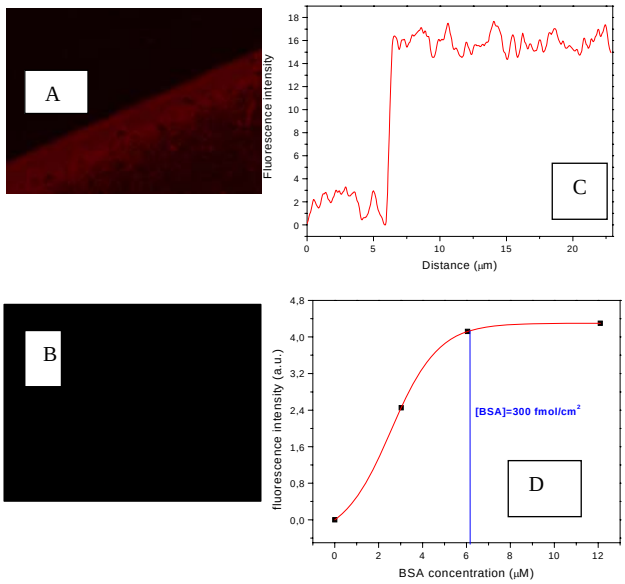


**Figure 5**. A: Fluorescence image of labelled BSA spotted on a silicon chip covered by HFBs. B: Negative control sample: BSA spotted directly on silicon. C: Intensity profile of fluorescencent BSA on HFB biofilm inside and outside the drop. D: The dose-response curve of fluorescence intensity as function of the BSA concentration.

By illuminating the fluorescent BSA samples, we found that the fluorescence is brighter than the negative control as it can be seen in Figure 5A and 5B. The fluorescence signal is also quite homogeneous on the whole surface, as confirmed by the intensity profile on a treated surface reported in Figure 5C. We have qualitatively tested the strength of the affinity bond between the HFB and the BSA, by washing the chip in a dialysis membrane overnight in deionized water. Since the fluorescent intensities before and after the dialysis do not differ, we can conclude that the HFB-BSA system is very stable. We have also realized a dose-response curve of fluorescence intensity as function of BSA concentration, shown in Figure 5D, and we have estimated a saturation concentration equal to 3.12 μM corresponding to 300 fmol/cm$^2$.

Protein immobilization on the HFB film has been also verified and analyzed using an enzyme, POXC laccase, produced by the same fungus *P. ostreatus*[16], easily available in our laboratory and whose activity assay is simple and sensitive. The enzymatic assay on the immobilized enzyme has been performed dipping the chip into the buffer containing the substrate and following its absorbance during several minutes. We chose to use a pH 5 buffer and DMP as a substrate, a good settlement between stability and activity of the enzyme. A volume of 30 μl of the enzyme solution (about 700 U/ml) have been deposited on the chips (10mm x 10mm) and, after several washing, an activity of 0.1÷0.2 U has been determined on each chip (Figure 6), with an immobilization yield of 0.5÷1%.

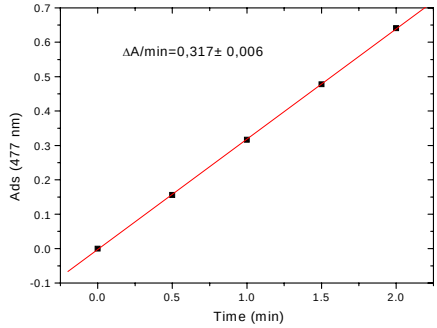


**Figure 6**. Enzymatic activity determination of POXC laccase immobilized on a chip.

This value is comparable to that one (7%) obtained in the optimized conditions for laccase immobilization on EUPERGIT C 250L©.[22] Taking into account the specific activity of the free enzyme (430 Umg$^{-1}$) and its molecular mass (59 kDa), 0.5μg of laccase corresponding to about 8 pmol (5 x 10$^{12}$ molecules) have been immobilized on each chip. A reasonable evaluation of the surface occupied by a single protein molecule can be based on crystal structures of laccases[23-24] and homology among these proteins. This surface should be 28 x 10$^{-12}$ mm$^2$, considering the protein as a sphere with radius of 3 x 10$^{-6}$ mm. On this basis the maximal number of laccase molecule on each chip should be 3 x 10$^{12}$. These data can indicate that the number of active immobilized laccase molecules on each chip is of the same order of magnitude than the expected maximum. Laccase assays have been repeated on the same chip after 24 and 48 hours in the same conditions. Figure 7 shows that about one half of the activity was lost after one day, but no variation of the residual activity was observed after the second day.

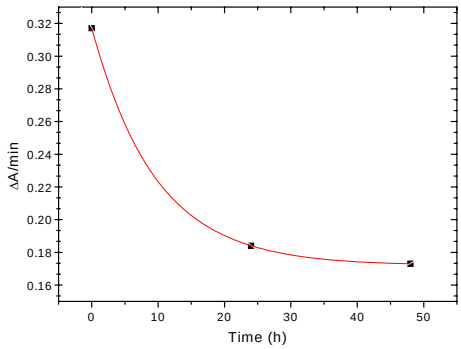


**Figure 7.** Time resolved profile of laccase activity of the immobilized enzyme.


This journal is © The Royal Society of Chemistry [year]

## Conclusions

We have demonstrated the bio-modification of the silicon surface by using the self-assembling features of the HFB, an amphiphilic protein purified by the fungus *P. ostreatus*. The nanometric biofilm of proteins, casted on the silicon surface by solution deposition, is very stable from the chemical point of view, since it is still present after strong denaturing washing in NaOH and SDS at 100 °C. The biofilm turns the hydrophobic silicon surface into a hydrophilic one, which can be very useful in microfluidic integrated application. Moreover, the biofilm can arrange both in a monolayer or in a multilayer stack of proteins depending on deposition conditions. The HFB monolayer acts as a bioactive substrate to bind other proteins, such as BSA and laccase. These results can be the starting point in the fabrication of a new generation of hybrid devices for proteomic applications.

ACKNOWLEDGMENT. The authors gratefully acknowledge dr. N. Malagnino of ST. Microelectronics in Portici (NA), Italy, for water contact angle measurements, Prof. P. Arcari (Dept. of Biochemistry and Medical Biotechnologies, University of Naples "Federico II") for fluorescent BSA, dr. F. Autore for the purification of POXC laccase and G. Armenante for technical support.

## Notes and references

[a] *Unit of Naples-Institute for Microelectronics and Microsystems, National Council of Research, Via P. Castellino 111, 80131, Naples, Italy Fax: +390816132598; Tel: +390816132375; E-mail: luca.destefano@na.imm.cnr.it*
[b] *Dept. of Physical Sciences, University of Naples "Federico II", Via Cintia 4, 80126, Naples, Italy.*
[c] *Dept. of Organic Chemistry and Biochemistry, University of Naples "Federico II", Via Cintia 4, 80126, Naples, Italy.*
[d] *LYCRIL – INFM-CNR, Via P. Bucci, Cubo 33/B, 87036 Arcavacata di Rende, Cosenza, Italy.*

1. 1 Yam, C. M.; Mayeux, A.; Milenkovic, A.; Cai, C. Z. *Langmuir* **2002**, *18*, 10274-10278.
2. W. Xing and J. Cheng , Eds., *Frontiers in Biochip Technology*, **2006,** Springer.
3. Cha T, Guo A, Zhu XY. *Proteomics* **2005**, *5*, 416-419.
4. Angenendt P, Glokler J, Murphy D, Lehrach H, Cahill DJ. *Anal. Biochem.* **2002**, *309*, 253-260.
5. Angenendt P, Glokler J, Sobek J, Lehrach H, Cahill DJ. *J. Chromatogr.* A **2003**, *1009*, 97-104.
6. Qin, M.; Wang, L. K.; Feng, X. Z.; Yang, Y. L.; Wang, R.; Wang, C.; Yu, L.; Shao, B.; Qiao, M.Q. *Langmuir* **2007**, *23*, 4465-4471.
7. Wang, R.; Yang, Y. L.; Qin, M.; Wang, L. K.; .Yu, L; Shao, B.; Qiao, M. Q.; Wang, C.; Feng, X.Z. *Chem. Mater.* **2007**, *19*, 3227-3231.
8. Gutmann O, Kuehlewein R, Reinbold S, Niekrawietz R, Steinert CP, de Heij B, Zengerle R, Daub M. *Lab Chip* **2005**, *5*, 675-681.
9. Buriak, J. M. *Advanced Materials*, **1999**, *11*, 265-268.
10. L. De Stefano, I. Rea, P. Giardina, A. Armenante, M. Giocondo, I. Rendina. *Langmuir* **2007**, 23, 7920,.
11. Hektor H.J. and Scholtmeijer K. *Current Opinion in Biotechnology* **2005**, *16*, 434-439.
12. Sunde M., Kwan A.H.Y., Templeton M.D., Beever R.E., Mackay JP. *Micron* **2007** doi:10.1016/j.micron.2007.08.003.
13. Linder MB, Szilvay GR, Nakari-Setälä T, Penttilä ME. *FEMS Microbiol Rev.* **2005**, *29(5)*, 877-96.
14. Lumsdon SO, Green J, Stieglitz B. *Colloids Surf B Biointerfaces* **2005**, *44(4)*, 172-8.
15. Kershaw M. J., Thornton C.R., Gavin E. Wakley and Talbot N. *Molecular Microbiology* **2005**, *56(1)*, 117-125.
16. Palmieri G., Giardina P., Marzullo L., Desiderio B., Nitti G. and Sannia G. *Appl. Microbiol. Biotechnol.*, **1993**, *39*, 632-636
17. Corvis Y, Walcarius A, Rink R, Mrabet NT, Rogalska E. *Anal Chem.* **2005**, *77(6)*, 1622-30.
18. Kern W 1993, Ed., *Handbook of Semiconductor Cleaning Technology*, Noyes Publishing: Park Ridge, NJ, Ch 1.
19. Kisko K, Szilvay GR, Vainio U, Linder MB, Serimaa R. *Biophys J.* **2008**, *94(1)*, 198-206.
20. Kwan AH, Winefield RD, Sunde M, Matthews JM, Haverkamp RG, Templeton MD, Mackay JP. *Proc Nat Acad Sci USA* **2006**, *103(10)*, 3621-6.
21. Yu L, Zhang B, Szilvay GR, Sun R, Jänis J, Wang Z, Feng S, Xu H, Linder MB, Qiao M. *Microbiology*, **2008**, 1541677-85.
22. Russo M.E., Giardina P., Marzocchella A., Salatino P., Sannia G. *Enz. Microbiol. Biotechnol*., **2008**, *42*, 521–530
23. Piontek K, Antorini M, Choinowski T. *J Biol Chem.* **2002**; *77*, 37663-9.
24. Ferraroni M, Myasoedova NM, Schmatchenko V, Leontievsky AA, Golovleva LA, Scozzafava A, Briganti F. *BMC Struct Biol.* **2007**, *7*, 60.

# Chapter 4
…towards the Lab-on-Chip

## Introduction to Lab-on-chip technologies

A heart attack is a typical situation for which a fast diagnostic is of paramount importance. In addition to an electrocardiogram, a blood test is often necessary, that is conventionally done in a laboratory. With the portable system marked by the Biosite company, this diagnostic can be made in only 10 min, directly with the patience [1]. The drop of blood is simply deposited in a reservoir in the system that then performs the entire test: minute quantities of blood are displaced and injected into several tiny chambers in which different reactions take place.

This example clearly illustrates the principle of a Lab-on-Chip: integrating all the functions of a human-scale test laboratory including transferring samples, drawing off a precise volume of a chemical product, mixing with reagents, heating, titration, etc, on a system of a few square centimeters.

A LOC includes many functions depending on the application such as pumps, valves, sensors, electronics, etc. Therefore, it can be considered as a complex microsystem including mechanical, electronic, fluid functions, etc.. It also needs a network of microchannels.

Since the 'planar' technology was introduced into microelectronics at the end of the 1950s, micromanufacturing techniques have never stopped improving, continuously extending the limits of miniaturization. Silicon was initially chosen for its semi-conducting properties and the excellent quality of its oxide, and was also used to develop mechanical functions including resonant beams, micro-motors, etc [2-4].

The concept of microsystems such as (MEMS—Micro-Electro-Mechanical Systems) emerged during the 1980s at the University of Berkeley as the integration of the different functions of a complete system on a single chip [5]. The first example of a microsystem marketed by Analog Devices in 1993 was the ADXL50 accelerometer that consisted of a capacitive sensor accompanied by its associated electronics monolithically integrated onto a 10 $mm^2$ substrate [6]. MEMS technology takes advantages from microelectronic production tools that allow for the manufacturing of thousands of miniaturized objects in parallel and thus reduces drastically fabrication costs.

Several examples of microsystems are now used in daily life: accelerometers that are present in modern cars (airbag trigger system) [7,8], and also in Nike shoes (integrated pedometer), Sony Playstation games consoles (measurement of the inclination of the joystick) and GPS systems [9,10], inkjet print heads [11-14], arrays of micromirrors in video projectors [15,16]. Many sectors are now concerned such as optical and radio frequency telecommunications (switches, variable capacitances and inductances) [17-19].

Finally, the interest in microsystems in the chemistry and biomedical fields has never ceased increasing, particularly since the development of the miniaturized total chemical analysis system ($\mu$TAS) concept by A Manz at the beginning of the 1990s and then since the development of LOC [20].

Over the last 10 years, this popularity has been a driving force for the development of new types of microsystems combining electrical and mechanical functions with microfluidic functions (microwells, microchannels, valves, pumps). It also encouraged the introduction of new processes and materials in microtechnologies. The glass technology widely used at first, combining wet etching and thermal bonding, is limited by difficulties in terms of integration and aspect ratio, while etching of silicon is much more developed.

## Silicon and glass technologies

- *Bulk micromachining*

Bulk micromachining refers to the situation in which patterns are defined in the substrate itself. The example of wet etching of glass is shown in figure 1.

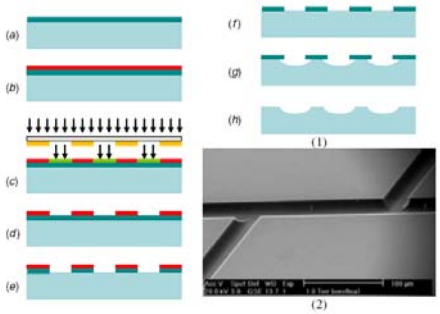

Figure 1: (1) An example of bulk micromachining: wet etching of glass; (2) microchannels etched by wet etching in glass [IMT Neuchˆatel] [21] (© 2003 IEEE).

It clearly illustrates the generic approach to bulk machining. After the substrate has been cleaned, the material that will be used for protection during the etching step is deposited (*a*). A photoresist is coated using a spin coater (*b*). This resist is exposed to ultraviolet radiation through a mask with transparent and opaque areas (*c*). The resist is then developed (*d*) and exposed areas are eliminated (positive resist, as illustrated in figure 1) or remain (negative resist), depending on its polarity. The protective material is etched (*e*) and the resist is removed from the substrate (*f* ). The next step is the glass etching step (*g*). Finally, the mask material is removed from the substrate (*h*).

- *Wet etching*

The etching step is fundamental in bulk micromachining [22, 23]. Etching as presented in figure 2 is isotropic, i.e. the etching rate is the same in all directions. Typical examples are wet etching of silicon in a mixture of hydrofluoric acid, nitric acid and ethanol [24], or wet etching of glass in hydrofluoric acid [25, 26]. Isotropic wet etching has several disadvantages, including difficulty in controlling the profile due to the strong influence of stirring and isotropy that severely limits the possible resolution and depth, as illustrated in figure 2.

Figure 2: Under-etching phenomenon during isotropic wet etching

Anisotropic wet etching of silicon [27-30] in solutions such as potassium hydroxide (KOH) or tetramethyl ammonium hydroxide (TMAH) [31-33] can be used to create patterns defined by crystallographic planes of silicon as illustrated in figure 3. This process, together with etching-stop techniques (geometric, electrochemical, implantation of boron) [34-36] makes it easy for manufacturing very thin membranes or suspended structures. However, some simple shapes such as a circular hole cannot be made, the etching profile limits the integration density and the chemicals used are relatively aggressive.

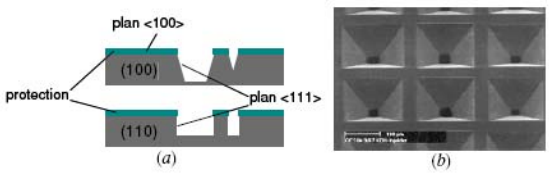


Figure 3: (*a*) Different anisotropic wet etching profiles in single-crystalline silicon; (*b*) examples of microwells made by anisotropic wet etching [GESIM] [37], © 1999, with permission from Elsevier.

- *Glass etching*

The technology for the microfabrication of glass is gaining importance because more and more glass substrates are currently being used to fabricate MEMS devices. Glass has many advantages as a material for MEMS applications, such as good mechanical properties, good optical properties, high electrical insulation, and it can be easily bonded to silicon substrates at temperatures lower than for fusion bonding.

Glass is particularly useful for fabrication of microfluidic devices used for bioanalysis due to its high chemical resistance. Microfluidic dispensing and controlling devices, such as micro pumps, micro pressure/flow sensors, monolithic membrane valve/diaphragm pumps, have been developed with integrated glass components. DNA related microfluidic devices, such as micro flow cells for DNA single molecule handling, micro injectors for DNA mass spectrometry, and micro polymerase chain reaction (PCR) devices for DNA amplification, have also been presented [38]. Being transparent under a wide wavelength range (~300–2000 nm for Pyrex), glass is a prime candidate for incorporation into micro bioanalytical devices where optical detection of the bioanalytes is used, for example, micro capillary electrophoresis (μCE) devices [39].

Extensive investigation of glass microfabrication technologies is paving the way for increasing utilization of glass substrates in MEMS. These technologies include wet chemical etching using various concentrations of hydrofluoric acid (HF) [40, 41], dry etch techniques like deep reactive ion etching (DRIE) using SF6 plasma [42], laser micromachining [43] and ultrasonic drilling [44]. Laser drilling and ultrasonic drilling are suitable for fabricating the small numbers of through holes in the glass.

Wet glass etching with various concentrations of HF is the most widely used method because the etching rate is fast and a large quantity of glass wafers can be processed simultaneously. Masks for glass etching in HF are normally photoresist [40] and Cr/Au photoresist combinations [45]. However, the formation of pinholes through defects within the metal mask is a notorious problem. This becomes especially severe when deep etching is required. A second problem found for HF etching is rapid undercutting of the Cr mask, which leads to a more rapid lateral etching of the glass than vertical etching. This leads to a poor aspect ratio generally smaller than one for etched cavities. Although the application of metal masks, for deep etching with HF, has the problem of pinholes and large lateral undercutting as mentioned above, the approach is simple and compatible with standard microfabrication facilities.

- *Assembly*

An assembly step between two machined substrates is usually necessary to seal structures. Several types of bonding techniques have been developed for different applications. Wafer bonding is a cost-effective method for zero-level MEMS packaging and has increasingly become a key technology for materials integration in various areas of MEMS, microelectronics and optoelectronics. Different wafer bonding approaches are currently used in the MEMS industry: fusion, adhesive, eutectic, anodic, solder bonding [46, 47].

These bonding techniques are summarized in figure 4. One of the main concerns is the thermal stress, mainly in the case of heterogeneous assembly, i.e. assembly of materials with different thermal expansion coefficients. The required level of cleanness may also be an obstacle in a process such as thermal bonding. Adhesive bonding is a low-temperature process and does not require complex cleaning procedures but introduces a supplementary material into the structure which may be undesirable in microfluidics in which the control of surface properties is critical. It is often estimated that assembly is frequently the most expensive step in microsystem processes.

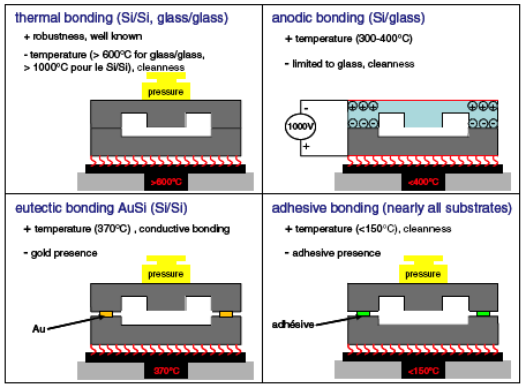


Figure 4: Different types of bonding between substrates

As fusion bonding processes require a high temperature annealing which is not always suitable for the devices with aluminum or copper integrated circuits; adhesive bonding is non-hermetic, more and more interests are focused on low temperature bonding (maximum process temperature below 300°), which can not only reduce process cost and time, but also minimize bonding-induced stress and warpage after cooling. Moreover, the wafers with large difference in coefficient of thermal expansion can also be bonded. The hybrid integration approach appears better adapted to a lab-on-chip integration. The challenge is then to couple the different elements, for example a sensor made using the silicon technology and a microfluidic network replicated in a thermoplastic, with good alignment and without introducing additional dead volumes, and obviously at the lowest cost.

Anodic bonding is one of the most used wafer level packaging procedures. In anodic bonding, the substrates are heated to a typical temperature above 400° and a typical voltage above 600V is applied to the wafer pair to be bonded, electrostatic force and the migration of ions lead to an irreversible chemical bond at the boundary layer between the individual wafers. Conventionally, this is done in the furnace or on the hotplate, which require long ramp times, consume large amounts of power, and have significant manufacturing footprints. Currently, many efforts are focusing on improving anodic bonding quality [48, 49].

However, the bond quality is reduced with decrease in the bonding temperature, low bonding strength will result in the bubbles or cavities at the interface, only few literature reports the success in low temperature anodic bonding with high bond strength and bubble-free interface [49].

The concept of $\mu$TAS, later extended to the lab-on-a-chip concept, was introduced in 1990 to mitigate the deficiencies of chemical sensors, particularly in terms of selectivity and life time [20]. Integration onto a chip can also very strongly reduce the consumption of chemicals that may be rare, expensive and/or polluting. Similarly, it reduces the production of waste. Automation of procedures illustrated by the DNA analysis station marketed by the Caliper Company, increases analysis rates and reduces the risk of error due to the human factor [50].

Furthermore, these products enjoy the advantages of prices for mass production processes. Miniaturization also provides a means of making these systems portable.

Cost and size reductions are not the only advantages; performance gain is also important. For example, an immunoassay was carried out in less than 25s while more than 10 min are necessary under classical conditions [51]. Therefore miniaturization of volumes provides a means of reducing the time for the operation.

Many lab-on-chip applications have been developed in genomics, under the emphasis of the human genome project and sequencing needs [52]. Moreover genetic analyses became increasingly routine operations, efforts have been made and are still being made on analysis of proteins. Its traditional approach includes extraction from cells, separation by electrophoresis on gel, digestion and analysis by a mass spectrometer. These operations are slow and time consuming. A system was made to perform the digestion, separation and analysis steps [53]. The operation that normally takes hours is done in a few minutes.

## References


1. Biosite, Inc http://www.biosite.com/
2. Nathanson H C, Newell W E, Wickstrom R A and Davis J R 1967 The resonant gate transistor *IEEE Trans. Electron Devices* **14** 117
3. Jolly R D and Muller R S 1980 Miniature cantilever beams fabricated by anisotropic etching of silicon *J. Electrochem.Soc.* **127** 2750
4. Tai Y C and Muller R S 1989 IC-processed electrostatic synchronous micromotors *Sensors Actuators* **20** 49
5. Chen P L, Muller R S and Andrews A P 1984 Integrated silicon PI-FET accelerometer with proof mass *Sensors Actuators* **5** 119
6. Chau K H L, Lewis S R, Zhao Y, Howe R T, Bart S F and Marcheselli R G 1996 An integrated force-balanced capacitive accelerometer for low-g applications *Sensors Actuators* A **54** 472
7. Zimmerman L, Ebershol J P, Lehung F, Berry J P, Bailleu F, Rey P, Diem B, Renart S and Caillat P 1995 Airbag application—a microsystem including a silicon capacitive accelerometer, cmos switched-capacitor electronics and true self-test capability *Sensors Actuators* A **46** 190–5
8. Kim K H, Ko J S, Cho Y H, Lee K, Kwak B M and Park K 1995 A skew-symmetric cantilever accelerometer for automotive airbag applications *Sensors Actuators* A **50** 121–6
9. Hanse J G 2004 Honeywell MEMS inertial technology & product status *Proc. IEEE Position Location and Navigation Symp. (Monterey, CA)* pp 43–48
10. Fujino Y, Kitagawa K, Furukawa T and Ishii H 2005 Development of vehicle intelligent monitoring system (VIMS) smart structures and materials 2005: sensors and smart structures technologies for civil, mechanical, and aerospace *Proc. SPIE* **5765** 148–57
11. Allen R R, Meyer J D and Knight W R 1985 Thermodynamics and hydrodynamics of thermal ink jets *Hewlett-Packard J.* (May) 21–7
12. O'Horo M, O'Neill J, Peters E and Vanderbroek S 1996 Micro electro mechanical system technology for commercial thermal inkjet document output products *Proc. Eurosensors X (Leuven, Belgium)* pp 431–5
13. Lee J-D, Yoon J-B, Kim J-K, Chung H-J, Lee C-S, Lee H-D, Lee H-J, Kim C-K and Han C-H 1999 A thermal inkjet printhead with monolithically fabricated nozzle plate and self-aligned ink feed hole *J. Microelectromech. Syst.* **8** 229–35
14. Krause P, Obermeier E and Whel W 1996 A micromachined single chip inkjet printhead *Sensors Actuators* A **21–23** 198–202
15. Van Kessel P F, Hornbeck L J, Meier R E and Douglas Hornbeck M R 1998 *Proc. IEEE* **86** 1687–704
16. Yoder L 1996 Texas Instruments-DLPTM product literature
17. Rebeiz G M 2006 RF MEMS for wireless-bands tunable networks *Topical Meeting on Silicon Monolithic Integrated Circuits in RF Systems, Dig. of Papers* pp 23–23
18. Dubuc D *et al* 2004 3D MEMS circuits integration for RF and millimeter wave communications *Proc. 2004 Int. Semiconductor Conf.* vols 1 and 2 pp 119–28
19. Tentzeris M and Laskar J 2003 RF system-on-package (SOP) development for compact low cost wireless front-end systems *Adv. Electron. Packag.* **2** 19–24
20. Manz A, Graber N and Widmer H M 1990 Miniaturized total chemical analysis systems: a novel concept for chemical sensing *Sensors Actuators* B **1** 244
21. Verpoorte E and De Rooij N F 2003 Microfluidics meets MEMS *Proc. IEEE* **91** 930
22. Petersen K E 1998 Silicon as a mechanical material *Proc.IEEE* **70** 420–57
23. Kendall D L and Shoultz R A 1997 Wet chemical etching of silicon and $SiO_2$, and ten challenges for micromachiners *Handbook of Microlithography, Micromachining, and Microfabrication* vol 2 ed P Rai-Choudury (Bellingham,WA: SPIE Optical Engineering Press)
24. Gardeniers J G E, Tjerkstra R W and Van den Berg A 2000 Fabrication and application of silicon-based microchannels *Microreaction Technologies: Industrial Prospects* pp 36–44
25. Iliescu C and Tay F 2001 Wet etching of glass *CAS 2005: Int.Semiconductor Conf.* vols 1 and 2 pp 35–44
26. Ilie M, Foglietti V and Cianci E 2002 Deep wet etching of borosilicate glass for microfluidic devices *Sensors Microsyst., Proc. 6th Italian Conf.* pp 55–9
27. Seidel H, Csepregi L, Heuberger A and Baumgartel H 1990 Anisotropic etching of crystalline silicon in alkaline solutions *J. Electrochem. Soc.* **137** 3612
28. Kendall D L 1975 On etching very narrow grooves in silicon *Appl. Phys. Lett.* **26** 195–8
29. Kendall D L 1990 A new theory for anisotropic etching of Si and some underdeveloped chemical micromachining concepts *J. Vac. Sci. Technol.* A **8** 3598

30. Camon H and Moktadir Z 1997 Simulation of silicon etching with HOH *Microelectron. J.* **28** 142–5
31. Tabata O, Asahi R, Funabashi H, Shimaoka K and Sugiyama S 1992 Anisotropic etching of silicon in TMAH solutions *Sensors Actuators* A **34** 51–7
32. Sato K, Shikida M, Yamashiro T, Asaumi K, Iriye Y and Yamamoto M 2000 Anisotropic etching rates of single-crystal silicon for TMAH water solution as a function of crystalline orientation *Sensors Actuators* A **73** 131–7
33. Biswas K, Bas S, Maurya D K, Kal S and Lahiri S K 2006 Bulk micromachining of silicon in TMAH-based etchants for aluminium passivation and smooth surface *Microelectron. J.* **37** 321–7
34. French P J, Nagao M and Esashi M 1996 Electrochemical etch-stop in TMAH without externally applied bias *Sensors Actuators* A **56** 279–80
35. Wallman L, Bengtsson J, Danielsen N and Laurell T 2002 Electrochemical etch-stop technique for silicon membranes with p- and n-type regions and its application to neural sieve electrodes *J. Micromech. Microeng.* **12** 265–70
36. Gianchandani Y B and Najafi K 1992 A bulk silicon dissolved wafer process for microelectromechanical devices IEEE J. Microelectromech. Syst. 1 77–85
37. Richter K, Orfert M, Howitz S and Thierbach S 1999 Deep plasma silicon etch for microfluidic applications Surf. Coat. Technol. 461 116–9.
38. Yokokawa R, Yumi Y, Takeuchi S, Kon T, Fujita H (2006) Nanotechnology 17:289–294
39. Berthold, A and Laugere, F and Schellevis, H and de Boer, CR and Laros, M and Guijt, RM and Sarro, PM and Vellekoop, MJ (2002) Electrophoresis, 23 (20). pp. 3511-3519.
40. C. Lin, G. Lee, Y. Lin, G. Chang, A fast prototyping process for fabrication of microfluidic systems on soda-lime glass, J. Micromech. Microeng. 11 (2001) 726–732
41. T. Corman, P. Enoksson, G. Stemme, Deep wet etching of borosilicate glass using an anodically bonded silicon substrate as mask, J.Micromech. Microeng. 8 (1998) 84–87.
42. X. Li, T. Abe, M. Esashi, Deep reactive ion etching of Pyrex glass using SF6 plasma, Sens. Actuatators A 87 (2001) 139–145.
43. T. Abe, X. Li, M. Esashi, Endpoint detectable plating through femtosecond laser drilled glass wafers for electrical interconnctions, Sens. Actuatators A 108 (2003) 234–238.
44. J.A. Plaza, M.J. Lopez, A. Moreno, M. Duch, C. Cane, Definition of high aspect ratio glass columns, Sens. Actuatators A 105 (2003) 305–310.
45. I. Schneega_, R. Brautigam, J.M. Kohler, Miniaturized flow-through PCR with different template types in a silicon thermocycler, Lab Chip 1 (2001) 42–49.
46. Martin A. Schmidt 1998 Proceedings of the IEEE 86 1575
47. Wen H. Ko 1995 Materials chemistry and physics 42 169
48. T. Rogers and J. Kowal 1995 Sensors Actuators A 46–47 113
49. J.S. Go, Y.H. Cho 1995 Sens. Actuators A 73 52
50. J. Wei, H. Xie, M. L. Nai, C. K. Wong and L. C. Lee 2003 J. Micromech. Microeng. 13 217
51. Caliper Life Sciences http://www.caliperls.com/
52. Hatch A, Kamholz A E, Hawkins K R, Munson M S, Schilling E A, Weigl B H and Yager P 2001 A rapid diffusion immunoassay in a T-sensor Nature Biotechnol. 19 46.
53. Khandurina J and Guttman A 2002 Bioanalysis in microfluidic devices J. Chromatogr. A 943 159.

# Microsystems Based on Porous Silicon-Glass Anodic Bonding technologies

This section is aimed to the demonstration of the compatibility of porous silicon and anodic bonding technologies for the realization of sensing micro-components in lab-on-chip applications. In particular, it was developed and tested an innovative anodic bonding process: voltage, time and temperature have been properly matched in order not to affect the properties of the transducing material, which can be strongly modified by thermal treatments through oxidation.

*Sensors* **2006**, *6*, 680-687

**sensors**

**ISSN 1424-8220**
© 2006 by MDPI
http://www.mdpi.org/sensors

*Full Research Paper*

# A Microsystem Based on Porous Silicon-Glass Anodic Bonding for Gas and Liquid Optical Sensing

**Luca De Stefano [1,*], Krzysztof Malecki [1], Francesco G. Della Corte [2], Luigi Moretti [2], Ilaria Rea [1], Lucia Rotiroti [1] and Ivo Rendina [1]**

[1] Institute for Microelectronics and Microsystems, National Council of Research, Via P. Castellino 111, 80131 Naples, Italy (E-mail for Ilaria Rea: ilaria.rea@na.imm.cnr.it)
[2] DIMET "Mediterranea" University of Reggio Calabria, Località Feo di Vito, 89060 Reggio Calabria, Italy

* Author to whom correspondence should be addressed. E-mail: luca.destefano@na.imm.cnr.it

*Received: 15 March 2006 / Accepted: 22 June 2006 / Published: 23 June 2006*

---

**Abstract:** We have recently presented an integrated silicon-glass opto-chemical sensor for lab-on-chip applications, based on porous silicon and anodic bonding technologies. In this work, we have optically characterized the sensor response on exposure to vapors of several organic compounds by means of reflectivity measurements. The interaction between the porous silicon, which acts as transducer layer, and the organic vapors fluxed into the glass sealed microchamber, is preserved by the fabrication process, resulting in optical path increase, due to the capillary condensation of the vapors into the pores. Using the Bruggemann theory, we have calculated the filled pores volume for each substance. The sensor dynamic has been described by time-resolved measurements: due to the analysis chamber miniaturization, the response time is only of 2 s. All these results have been compared with data acquired on the same PSi structure before the anodic bonding process.

**Keywords:** Porous Silicon, Anodic Bonding, Microchamber, Lab-on-Chip.

---

## Introduction

The physical and structural properties of porous silicon (PSi), first of all its high surface area matrix, have led many scientific researchers to investigate this material, using it as a transducer in sensing systems. In particular, high sensitivity results have been obtained by monitoring changes in optical properties, such as photoluminescence [1], reflectivity [2-3] and ellipsometry [4]. Both monolayers, which act as Fabry-Perot interferometers, and multilayer devices, like Bragg filters and

optical microcavities, can be easily fabricated and exploited in optical sensing experiments. The integration of sensitive elements into complex microsystems, i.e. lab on chip or micro-total-analysis systems, is of straightforward interest, especially for the miniaturisation of each component. This step is never a trivial one: the fabrication process often requires high temperatures and mechanical stresses which can damage or even destroy the bio- or chemo- sensitive transducer structures.

The anodic bonding (AB) is a standard IC fabrication technique which is widely used in microfluidic due to a wide spectrum of advantages among which the hermetic sealing [5-6]. Due to the good bonding quality, glass transparency, technological cleanness and high passivity to most of chemicals and biological substances, AB is also commonly exploited in the fabrication of lab-on-chip devices. The compatibility of this primary integration technique with highly demanding sensing micro-components plays a basic role in view of the realization of lab-on-chip devices. We have recently reported on the optimisation of the standard silicon-glass AB parameters, searching for low temperature, low voltage and short time, taking into account the electrode type and thickness of glass wafers [7].

In the present work, the above mentioned results have been exploited and combined with new bonding findings, to ensure AB compatibility with the features of porous silicon (PSi) transducer. We have studied the static and dynamic sensor response on exposure to vapours of several organic compounds. The results have been compared with those obtained for the same PSi layer before the integration process.

## Theory

Even if we have already realised μ-chambers with porous silicon multilayer optical structures, such as Bragg filters and optical microcavities which are more performing in terms of sensitivity and resolution, in this first optical characterisation, we have followed the approach of Sailor et al. [2] choosing the simple case of a single layer of porous silicon as our transducer device. Figure 1 shows a typical reflectivity spectrum from a PSi layer under white light illumination.

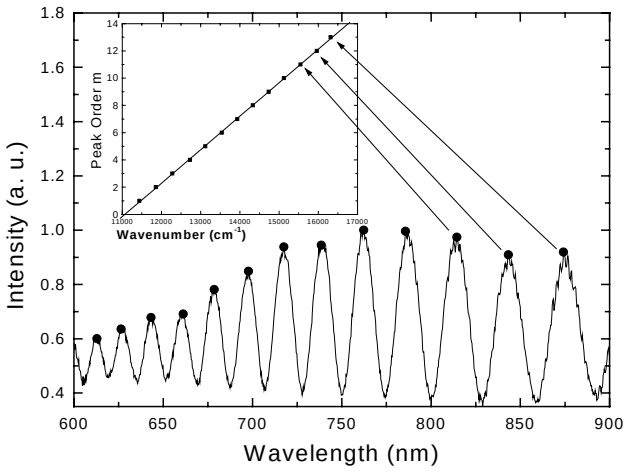


**Figure 1**. Reflectivity spectrum of PSi layer. In the inset the m-order peak are plotted as function of the wavenumber.

From the optical point of view, this structure is an optical Fabry-Perot interferometer, so that the maxima in the reflectivity spectrum appear at wavelengths $\lambda_m$ which satisfy:

$$m = 2nd / \lambda_m \tag{1}$$

where *m* is an integer, *d* is the film thickness and *n* is the average refractive index of the layer [8-9]. If we assume that the refractive index is independent on the wavelength over the considered range, the maxima are equally spaced in the wavenumber $(1/\lambda_m)$. When the maximum order *m* is plotted as a function of the wavenumber, each point lies on a straight line which slope is the optical path, as it is shown in the inset of Fig. 1. When the PSi layer is exposed to vapors, or dip in the liquid phase of the same substance, the substitution of air in the pores by its molecules causes a fringes shift in wavelength, which corresponds to a change in the optical path *nd*. Since the thickness *d* is fixed by the physical dimension of the PSi matrix, the variation is clearly due to changes in the average refractive index. In the case of vapors and gases, the filling liquid phase is due to the capillary condensation phenomenon, which is regulated from the Kelvin equation:

$$K_B T_{\rho_l} \ln(p_{sat} / p) = 2\gamma_{\mathrm{lg}} \cos\theta / R \tag{2}$$

where $\rho_l$ is the density of the liquid phase, $\gamma_{lg}$ is the liquid-gas surface tension coefficient at room temperature *T*, *R* is the radius of the pores, $p/p_{sat}$ is the relative vapor pressure into the pores, and $\theta$ is the contact angle [10].

A quantitative model taking into account the optical path increase can be realized by applying the Bruggemann effective medium approximation theory. The relation between the volume fraction of each medium and its dielectric constant can be written as:

$$(1-p)\left(\frac{\varepsilon_{Si}-\varepsilon_p}{\varepsilon_{Si}+2\varepsilon_p}\right)+(p-V)\left(\frac{\varepsilon_{air}-\varepsilon_p}{\varepsilon_{air}+2\varepsilon_p}\right)+V\left(\frac{\varepsilon_{ch}-\varepsilon_p}{\varepsilon_{ch}+2\varepsilon_p}\right)=0 \tag{3}$$

where *p*, *V*, $\varepsilon_{si}$, $\varepsilon_{air}$, $\varepsilon_{ch}$ and $\varepsilon_p$ are the layer porosity, the layer liquid fraction (LLF), the dielectric constants of silicon, air, chemical substance and porous silicon, respectively [11].

## Experimental Section

We have designed and fabricated a sensor device which can be considered the basic element of a lab-on-chip, just integrating PSi, as the transducer material, and a glass slide, which ensures sealing and the interconnections for fluids inlet and outlet. The silicon wafer used in this work is a p+ type, <100> crystal orientation, with a resistivity of 8-12 mΩcm. The glass is a Borofloat 33 type, 1 mm thick. The reaction microchamber has been realized by a two-step electrochemical etching. The first step is a high current density (800 mA/cm$^2$ for about 300 s) electrochemical etch in hydrofluoric acid and ethanol (HF:EtOH/50:50) solution which creates a μ-well (100 μm deep) in the bulk silicon. The second step is a consecutive electrochemical etch which is used to fabricate the PSi layer at the bottom of the μ-chamber. The process parameters for this last step were: current density of 400 mA/cm$^2$ and etching time of 3.2 s. More details on μ-chamber fabrication can be found elsewhere [12]. The thickness and porosity of the PSi layer was measured by variable angle spectroscopic ellipsometry using a Horiba-Jobin-Yvon UVISEL ellipsometer. After the mechanical drilling of the flow channels, the glass slide has been cleaned and activated for the AB process following standard RCA and $H_2O_2$ procedures. Because of the highly reactive PSi nature, the standard cleaning procedures had to be

changed with a soft cleaning procedure based on trichloroethylene, acetone and ethanol. The silicon chip has also been carefully rinsed in deionized water for several minutes. Silicon etched wafer and glass top prefabricated components have been anodically bonded together with mutual alignment: a successful bonding, in terms of mechanical strength and bond quality, has been obtained at a temperature of 200$^{o}$C, voltage of 2.5 kV, with a process time of 1.5 minutes. The cross section of the chip structure and the general-view of the real device are shown in Figure 2. The reflectivity spectra in the VIS-IR wavelength region have been recorded with a very simple experimental set-up: a white source illuminates, through an optical fiber and a collimator, the porous silicon at nearly normal incidence. The reflected light is collected by an objective and coupled into a multimode fiber. The signal is directed in an optical spectrum analyzer (Ando, Mod. AQ-6315B) and measured with a 0.2 nm resolution. We have also performed time-resolved measurement in order to characterize the sensor dynamic: using the laser beam from an IR source, we have measured, as a function of time, the signal of a receiving photodetector before, during and after the exposure to acetone.

**Results and Discussion**

From the ellipsometric measurements we have estimated the thickness and the porosity of the porous silicon sensitive layer, resulting in about 9.1 μm and 79 %, respectively.

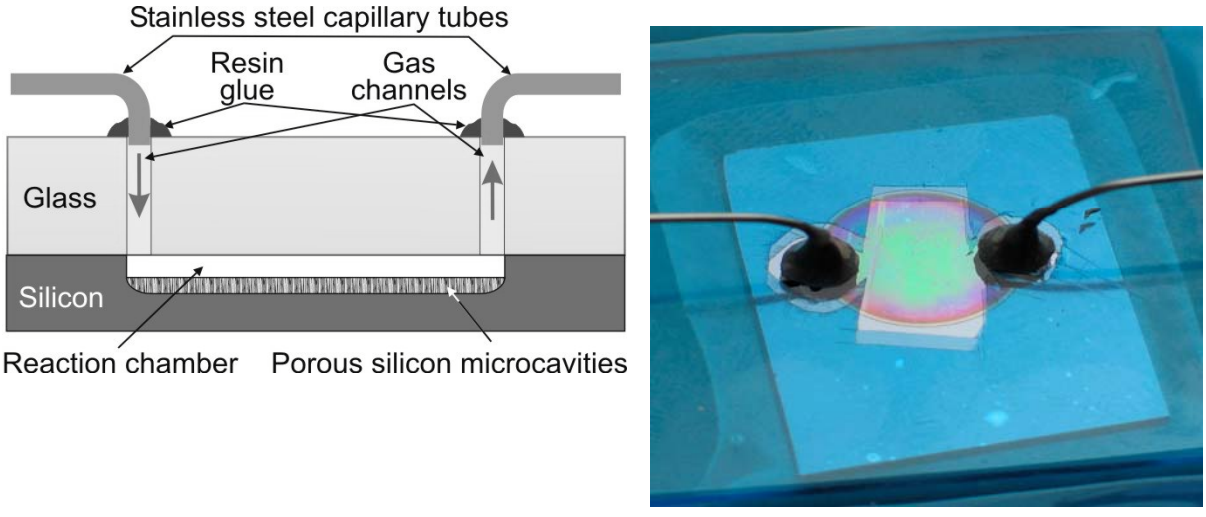


**Figure 2**. Schematic and real view of the μ-chamber for lab-on-chip applications.

Using the Bruggemann relation in Eq. (2), the refractive index is calculated as 1.34. As it can be noted in the reflectivity spectra reported in Figure 3, on exposure to several volatile substances in non-saturated atmosphere, due to the phenomenon of capillary condensation, the average refractive index of the layer increases, and, as a consequence the optical thickness of the porous silicon layer also increases.

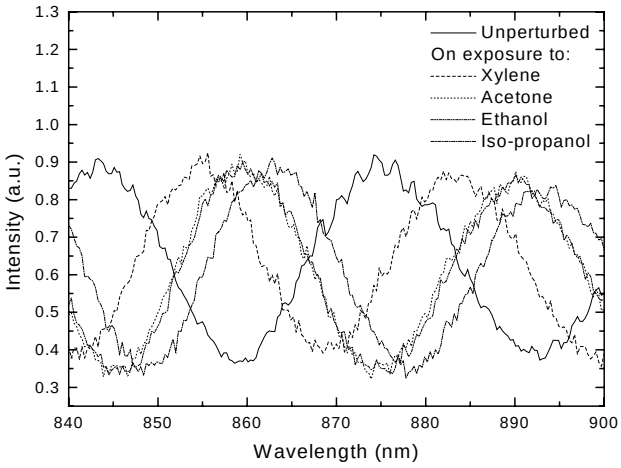


**Figure 3**. Reflectivity spectra of the unperturbed sensor and on exposure to vapours of organic compounds.

In Figure 4 the maxima of order m as function of wavenumber are shown; the slopes of the lines give the optical thickness of the layer for each substance. In the wavelength range considered, the assumption of a refractive index independent on the wavelength is satisfied since the PSi refractive index changes less then 2 % in this interval. Using the Eq. (3), the LLF, which is the filled volume by the condensed liquid, has been calculated for each substance obtaining the values reported in Table 1. The LLF values are about 30 % lower than ones obtained in the case of the PSi transducer before of the AB process [13]. These differences can be ascribed to a slight oxidation of the porous silicon layer due to the AB temperature process.

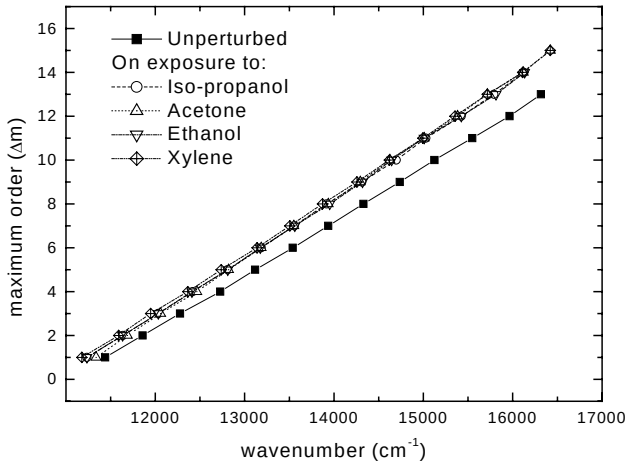


**Figure 4.** Maximum m-order as function of wavenumber ($1/\lambda_m$). The slopes of the straight lines are the optical thicknesses of the unperturbed layer and on exposure to the vapours.

The silicon oxide can fill or obstruct the very small pores of the sponge-like structure, preventing the liquid to condense into them. Moreover, due to the air present during the AB process, there

probably exists an extra pressure into the μ-chamber because some air has been entrapped in the PSi matrix. As a consequence, according to the Kelvin equation (2), the capillary condensation of the liquid phase decreases.

**Table 1**. Chemical organics substances used in sensing experiments and some relevant physical-chemical properties [a].

| **Chemical compounds** | ***n*** | **$\rho$ (g/$cm^3$)** | **STC (mN/m)** | **VP (kPa)** | **BP (°C)** | **Δ<*nd*> (nm)** | **LLF** |
|---|---|---|---|---|---|---|---|
| Iso-propanol | 1.377 | 0.785 | 20.93 | 6.8 | 82.4 | 1000 | 0.22 |
| Ethanol | 1.360 | 0.785 | 22.8 | 5.8 | 78 | 950 | 0.23 |
| Xylene | 1.501 | 1.454 | 38.8 | 0.046 | 214 | 1400 | 0.22 |
| Acetone | 1.359 | 0.791 | 23.46 | 30.8 | 56 | 998 | 0.23 |

[a] *n* is the liquid refractive index; $\rho$ is the density (@ 25 °C); STC is the surface tension coefficient (@ 25 °C); VP is the vapor pressure; BP is the boiling point; Δ<*nd*> is the average optical path increase and LLF the layer liquid fraction.

The result of time-resolved measurement is compared in Figure 5 to the data acquired on the same PSi layer before the AB integration process: it is well evident that, due to chamber miniaturization, the identification time ($\tau_{id}$=2 s) is significantly shorter.

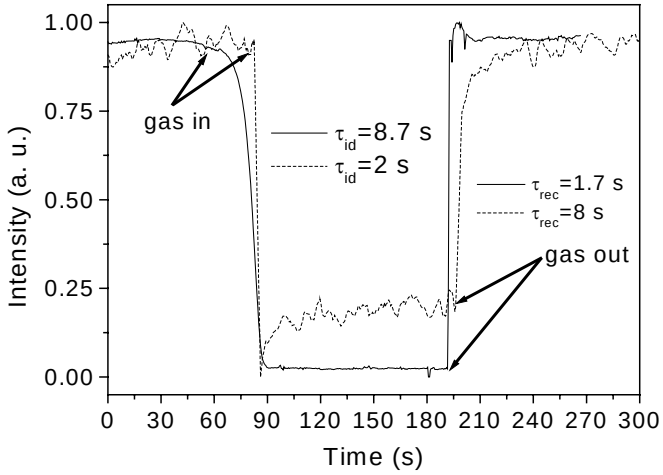


**Figure 5.** Time-resolved measurements of porous silicon layer during the monitoring of acetone in 0.4 l test chamber (solid line) and in the integrated 14 μl μ-chamber (dashed line).

The values of response time depends not only on the physical phenomena involved (i.e., equilibrium between adsorption and desorption in the PSi layer) but also on the geometry of the test

chamber and on the measurement procedure, i.e. static or continuous flow mode. In static condition, the identification time is mainly determined by the diffusion of the gas into the chamber volume: in fact, when vapor is in contact with the porous silicon surface, the capillary condensation takes place instantaneously [14-15]. For the same reason, the recovery time is longer ($\tau_{rec}$=8 s): as soon as Nitrogen is introduced into the μ-chamber, the conditions for capillary condensation are not still valid so that the liquid phase disappears, depending on atmosphere rate exchange. As it is shown in this graphic, the sensor response is completely reversible.

## Conclusions

In this work, we have optically characterized an original hybrid silicon-glass sensor system, based on PSi and AB technologies, which can be thought as the reaction chamber of a more complex lab-on-chip. Reflectivity spectrum of the device has been studied on exposure to vapors of organic volatile solvents. An increase of the optical path, due to capillary condensation of the vapor into the pores, has been observed. Using the Bruggemann effective medium approximation we have calculated the liquid volume fraction adsorbed into the layer for each substance, obtaining values between 0.22 and 0.23. We have characterized the sensor dynamic by time-resolved measurement during exposure to acetone. The data assure fast analysis time and the complete reversibility of the sensing mechanism. The comparison with data obtained from the same PSi transducer before the AB, shows that the integration process did not degrade the sensor features.

## Acknowledgements

This work has been supported by Marie Currie Fellowship of the European Community programme “Technologies for micro-opto-mechanical systems” under contract number CO-IMM-NA-01-2002.

## References

1. Mulloni, V.; Pavesi, L. Porous silicon microcavities as optical chemical sensors. *Appl. Phys. Lett.* **2000**, *76*, 2523-2525.
2. Gao, J.; Gao, T.; Sailor, M.J. Porous-silicon vapor sensor based on laser interferometry. *Appl. Phys. Lett.* **2000,** *77*, 901-903.
3. Benson, T. M.; Arrand, H. F.; Sewell, P.; Niemeyer, D.; Loni, A.; Bozeat, R. J.; Kruger, M.; Arens-Fischer, R.; Thoenissen, M.; Luth, H. Progress towards achieving integrated circuit functionality using porous silicon optoelectronic components. *Mat. Sci. Eng. B* **1999,** *69-70*, 92-95.
4. Wongmanerod, C.; Zangooie, S.; Arwin, H. Determination of pore size distribution and surface area of thin porous silicon layers by spectroscopic ellipsometry. *Applied Surface Science* **2001,** *172*, 117-125.
5. Puers, B.; Peeters, E.; Van Den Bossche, A.; Sansen, W. A capacitive pressure sensor with low impedance output and active suppression of parasitic effects. *Sens. Actuat. A* **1990,** *21-23*, 108-114.

6. Obermeier, E. *Proc.* Semiconductor Wafer Bonding, *Science, Technology and Applications. Electrochem. Soc*, **1995**, 212-220.
**7.** Malecki, K.; Della Corte, F.G.; Silicon-glass anodic bonding at low temperature. *Proc. of Micromachining and Microfabrication Process Technology X, SPIE Vol. 5715* **2005**, 180-189.
8.Lin, V. S.-Y.; Motesharei, K.; Dancil, K.-P. S.; Sailor, M. J.; Ghadiri, M. R. A porous silicon-based optical interferometric biosensor. *Science* **1997,** *278*, 840-843.
**9.** Anderson, M. A.; Tinsley-Brown, A.; Allcock, P.; Perkins, E. A.; Snow, P.; Hollings, M.; Smith, R. G.; Reeves, C.; Squirrell, D. J.; Nicklin, S.; Cox; T. I. Sensitivity of the optical properties of porous silicon layers to the refractive index of liquid in the pores. *Phys. Stat. Sol. A* **2003**, *197*, 528-533.
**10.** Neimark, V.; Ravikovitch, P. I. Capillary condensation in MMS and pore structure characterization. *Microporous Mesoporous Mater.* **2001,** *44-45*, 697-707.
**11.** Spanier, J. E.; Herman, I. P. Use of hybrid phenomenological and statistical effective-medium theories of dielectric functions to model the infrared reflectance of porous SiC films. *Phys. Rev. B* **2000**, *61*, 10437-10450.
12. De Stefano, L.; Malecki, K.; Moretti, L.; Rendina, I. Anodically bonded silicon-glass optical chip for biochemical sensing applications. *Proc. SPIE Int. Soc. Opt. Eng.* **2005**, 5718-7, 38-47.
13. De Stefano, L.; Rendina, I.; Moretti, L.; Rossi, A.M.; Tundo, S. Smart optical sensors for chemical substances based on porous silicon technology. *Applied Optics* **2004,** *43/1*, 167-172.
14. Allcock, P.; Snow, P.A. Time-resolved sensing of organic vapors in low modulating porous silicon dielectric mirrors. *J. Appl. Phys.* **2001**, *90*, 50525057.
15. De Stefano, L.; Moretti, L.; Rendina, I.; Rossi, A. M. Time-resolved sensing of chemical species in porous silicon optical microcavity. *Sensor and Actuators B* **2004,** *100*, 168-172.

© 2006 by MDPI (http://www.mdpi.org). Reproduction is permitted for noncommercial purposes.

# Laser oxidation micropatterning of a porous silicon based biosensor for multianalytes microarrays

The aim of this section is to present the fabrication and characterization of oxidized micropatterned biosensors based on PSi, obtained by direct laser writing and their chemical functionalization for biological applications. The laser local oxidation technique is a good alternative to the traditional photolithographic process, in fact the standard masking of PSi by means of photoresist presents remarkable difficulties since the developer, being alkaline, causes the dissolution of the PSi.

# LASER OXIDATION MICROPATTERNING OF A POROUS SILICON BASED BIOSENSOR FOR MULTIANALYTES MICROARRAYS

L. DE STEFANO[1], L. ROTIROTI[1,3], I. REA[1,2], E. DE TOMMASI[1], M. A. NIGRO[4], F. G. DELLA CORTE[4], AND I. RENDINA[1]

[1]*IMM-CNR - Sezione di Napoli, Via P. Castellino 111, 80131 Napoli, Italy*
[2]*Dept. of Physics, "Federico II" University of Naples, Monte S. Angelo, 80126 Naples, Italy*
[3] *Dept. of Organic Chemistry and Biochemistry, "Federico II" University of Naples, Monte S. Angelo, 80126 Naples, Italy*
[4]*"Mediterranea" University of Reggio Calabria Department of Computer Science, Mathematics, Electronics and Transports, Località Vito di Feo, Reggio Calabria, Italy*

## Abstract

In this communication, we present the fabrication and characterization of oxidized porous silicon (PSi) micropatterns, obtained by direct laser writing, and chemically functionalized for biological applications. The laser local oxidation technique is a good alternative to the traditional photolithographic process since this approach allows the development of micropatterned biosensors. In fact, from a technological point of view, the standard masking of PSi by means of photoresist presents remarkable difficulties because of the low resistance to the electrochemical process. The micropatterned PSi oxidized surfaces can be properly functionalized by a specific chemical linker. The modified surface is able to link the carboxylic or aminic groups of biological probes. The binding between the functionalized surface and the biological matter has been tested by directly spotting on the PSi local oxide a fluorescent labelled antibody. The device has been characterized by FT-IR measurements and fluorescence macroscopy.

**Keywords**

Porous silicon, laser writing, biosensors, microarrays.

## INTRODUCTION

Porous silicon based optical biosensors offer several advantages in label-free detection and identification of organic molecules due to the well known properties of this material [1, 2]. PSi has a spongy structure with a large specific surface of the order of 100–500 $m^2$ $cm^{-3}$ [3], so that a very effective interaction with several adsorbates is assured. When a biological solution penetrates into the PSi pores, it substitutes the air, so that the average dielectric properties of the heterogeneous silicon-air-liquid system change inducing a red-shift in the reflectivity spectrum of the device. The effect depends on the refractive index value of the solution but also on how it penetrates into the pores. Due to this sensing mechanism, PSi optical devices cannot identify the

single components of a complex mixture. In order to enhance the sensor selectivity, several biological probes, which exploit very specific interactions only with selected biochemical molecules, can be linked to the PSi surface: most common examples are DNA strands, proteins, enzymes, antibodies and so on. In this work, the fabrication and characterization of oxidized porous silicon micropatterns obtained by direct laser writing [5] and their chemical functionalization for biological applications are reported. In particular we have employed a murine monoclonal antibody (IgG) UN1 previously selected for the specific reactivity with human thymocytes as compared to peripheral blood cells [4]. The antigen recognized by UN1 is a 100–120 kDa transmembrane glycoprotein showing biochemical features of cell membrane-associated mucin-like glycoproteins, a class of macromolecules that are involved in cell-to-cell interactions and cancer progression [6].

## EXPERIMENTAL AND RESULTS

The device was a PSi monolayer, 1 μm thick and with a porosity of 70%, produced by electrochemical etch in a HF-based solution, starting from a highly doped p+-silicon, <100> oriented, 0.04 Ω cm resistivity, 400 μm thick. The silicon was etched using a 30 wt. % HF/ethanol solution in dark and at room temperature. After the etching the samples were rinsed in ethanol and dried under a stream of $N_2$.

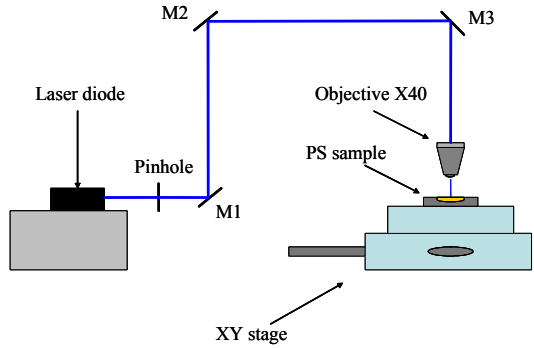


**Fig. 1**: Scheme of the setup used to write the channel waveguides.

The localized oxidation is obtained by exposing the sample to the beam of a laser diode (μLS Micro Laser Sistem) at 408 nm with an output power of

48mW, using a setup composed of a microscope objective and a motorized xy micrometric stage as shown in Figure 1. The beam dimension is about 1.4/0.32 mm. We have directly written on the sample some oxide strips, 10 μm wide, with a laser fluence of 38 mJ/mm$^2$.

Starting from our previous experience on chemical modification of the oxidised porous silicon, we have used an organosilane compound such as the aminopropyltriethoxysilane (APTES) and a functional crosslinker such as Glutaraldehyde (GA) which reacts with the amino groups on the silanized surface and coats the micropatterned PSi oxidized surfaces. [7]. The obtained modified surface works as an active substrate for the chemistry of the following attachment of other biological probes, such as DNA single strand, proteins, enzymes, and antibodies.

The functionalization process takes place directly on the chip surface, simply covering it with the chemical solutions. In Fig. 2 is reported the scheme of the functionalisation process. The PSi device has been rinsed by immersion in a 5% solution of APTES and an hydroalcoholic mixture of water and methanol (1:1), for 20 min at room temperature. After the reaction time, we have washed the sample with demi-water and methanol and dried in $N_2$ stream. The silanized surface was then baked at 100°C for 10 min.

The APTES modified surface is able to link the carboxylic group of a biological probe such as IgG or other antibodies. A further step of functionalization is required to bind the amino group always present in biological matter through the aldehydic group of opportune chemical linker. To this aim, we have treated the chip in a 2.5% glutaraldehyde solution for 30 min. The glutaraldehyde reacts with the amino groups on the silanized surface and coats the internal surface of the pores with another thin layer of molecules.

Infrared spectra were collected by using a Fourier transform spectrometer equipped with a microscope (Nicolet Continuμm XL, Thermo Scientific) and are reported in Fig. 3, where it is well evident that, after the functionalization processes, the Si-OH peaks are completely substituted by the organic linkers characteristics ones.

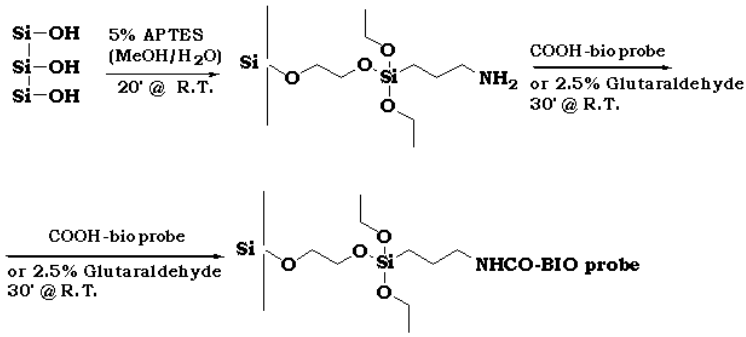


**Fig. 2:** functionalization steps of PSi surface by means of APTES and Glutaraldehyde and subsequent binding of the biological probe.

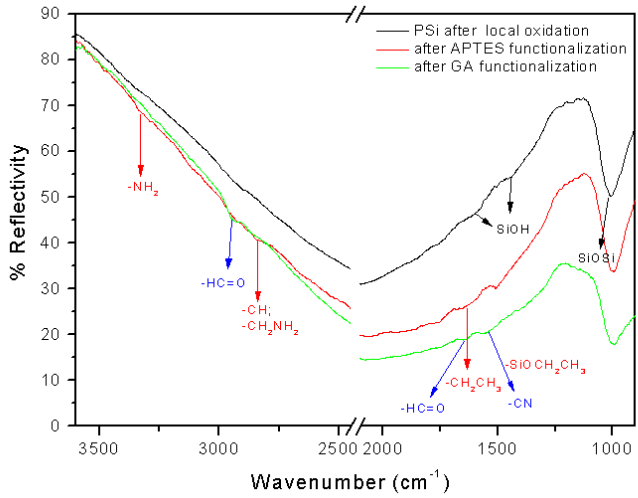


**Fig. 3:** FT-IR spectra of the micropatterned PSi oxidized surfaces before and after the chemical surface modification treatments.

The binding between the surface and the biological matter has been tested by using fluorescent labelled bioprobes directly spotted on the PSi chemical modified structures. We have spotted on the porous silicon chip a solution containing the rhodamine labelled IgG antibody, 6.8 μM, and incubated overnight at room temperature. The device has been observed by a Leica Z16

APO fluorescence macroscopy system. By 100W high-pressure mercury source we found that the fluorescence is very high and homogeneous on the region locally oxidized by the laser as shown in Fig. 4.

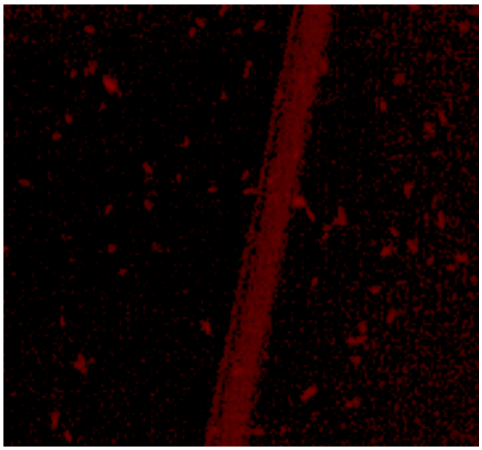

**Fig. 4:** Post-dialysis fluorescence image of the chip after rhodamine labeled IgG binding

## CONCLUSIONS

In this work, we have exploited the possibility to locally functionalize the PSi surface.
A micropattern has been directly written on the porous silicon layer by a laser oxidation process. The pattern, constituted by strips 2 μm wide, has been functionalized by specific chemical linkers such as APTES and glutaraldehyde; then we have spotted on the PSi sample a fluorescent labelled antibody. The interaction between the modified surface and the biological matter has been verified by fluorescence macroscopy; a high fluorescence signal has been observed only in the oxidized region.

## REFERENCES

[1] H. Ouyang, C.C. Striemer, P.M. Fauchet, APL 88, 163108, 2006.
[2] C. Pacholski, M. Sartor, M.J. Sailor, F. Cunin, G.M. Miskelly, J. Am. Chem. Soc. 127, 11636-11645, 2005.

[3] R. Herino, G. Bomchil, K. Barla, C. Bertrand, J.L. Ginoux, J. Electrochem. Soc. 134-8, 1994, 1987.
[4] Hilkens J., M.J. Ligtenberg, H.L. Vos, S.G. Litinov, Cell membrane-associated mucins and their adhesion-modulating property, Trends Biochem. Sci. 1992, 17, 359.
[5] A. M. Rossi, S. Borini, L. Boarino, and G. Amato, Phys. Stat. Sol. (a) **197**, No. 1, 284–287 (2003).
[6] Cecco L., H.M. Bond, P. Bonelli, et al., Tissue Antigens 1998, 51, 23.
[7] De Stefano L., A. Vitale, I. Rea, M. Staiano, L. Rotiroti, T. Labella, I. Rendina, V. Aurilia, M. Rossi, S. D'Auria, Extremophiles (2007), DOI 10.1007/s00792-006-0058-6.

**PUBLICATIONS**:

J1. Luca De Stefano, F. G. Della Corte, K. Malecki, Ivo Rendina, **Lucia Rotiroti**, Luigi Moretti, Andrea M. Rossi, "*Integrated silicon-glass opto-chemical sensors for lab-on-chip application",* Sensor and Actuators B,114, 625-630, (2006).

J2. L. De Stefano, I. Rendina, **L. Rotiroti**, L. Moretti, V. Scognamiglio, M. Rossi, S. D'Auria, "*Porous silicon-based optical microsensor for the detection of L-Glutamine*", Biosensors and Bioelectronics 21/8, 1664-1667, 2006.

J3. L. Moretti, I. Rea, **L. Rotiroti**, I. Rendina, G. Abbate, A. Marino, L. De Stefano **"***Photonic band gaps analysis of Thue-Morse multilayers made of porous silicon*" Optics Express, 14 (2006) 6264-6272.

J4. L. De Stefano, I. Rea, I. Rendina, **L. Rotiroti**, M. Rossi, and S. D'Auria, "*Resonant cavity enhanced optical microsensor for molecular interactions based on porous silicon*", Phys Stat Sol (A) , 203 (2006) 886-891.

J5. S. D'Auria, S. Borino, A. Vitale, A.M. Rossi, I. Rea, I. Rendina, **L. Rotiroti**, M. Staiano, M. de Champdorè, V. Aurilia, A. Parracino, M. Rossi, L. De Stefano, "*Nanostructured silicon-based biosensors for the selective identification of analytes of social interest*", Journal of Physics: Condensed Matter, **18** S2019-S2028, (2006).

J6. L. De Stefano, **L. Rotiroti**, I. Rea, I. Rendina, L. Moretti, G. Di Francia, E. Massera, A. Lamberti, P. Arcari, C. Sangez, *"Porous silicon-based optical biochips"* Journal of Optics A: Pure and Applied Optics, S540-S544, 8 (2006).

J7. L. De Stefano, K.Malecki, F. G. Della Corte , L. Moretti , I. Rea , **L. Rotiroti,** I. Rendina "*A Microsystem Based on Porous Silicon-Glass Anodic Bonding for Gas and Liquid Optical Sensing*" Sensors, 6 (2006) 680-687.

J8. L. De Stefano, M. Rossi, M. Staiano, G. Mamone, A. Parracino, **L. Rotiroti**, I. Rendina, M. Rossi, and S. D'Auria, *"Glutamine-binding protein from Escherichia coli specifically binds a wheat gliadin peptide allowing the design of a new porous silicon-based optical biosensor"*, Journal of Proteome Research 5,5, 1241-1245, 2006

J9. L. De Stefano, **L. Rotiroti,** I. Rea, F. Della Corte, D. Alfieri, L. Moretti, I. Rendina, "An integrated pressure-driven microsystem based on porous silicon for optical monitoring of gaseous and liquid substances"; Phys. Stat. Sol. (a) 204, No. 5, 1459-1463 (2007).

J10. L. De Stefano, **L. Rotiroti**, I. Rea, I. Rendina, L. Moretti, "*Quantitative determinations in hydro-alcoholic binary mixtures by porous silicon optical microsensors*", Phys. Stat. Sol. (c), **4**, No. 6, 1941– 1945 (2007).

J11. L. De Stefano, I. Rea, L. Moretti, **L. Rotiroti**, I. Rendina, "*Optical properties of porous silicon Thue-Morse structures*", Phys. Stat. Sol. (c) **4**, No. 6, 1966-1970 (2007).

J12. I. Rendina, I. Rea, L. Rotiroti, L. De Stefano, "*Porous Silicon Based Optical Biosensors and Biochips",* Physica E*, 38* (2007) 188-192 **invited paper**.

J13. L. De Stefano, I. Rea, **L. Rotiroti**, I. Rendina, L. Fragomeni, F.G. Della Corte*, "An integrated hybrid optical device for sensing applications",* Phys. Stat. Sol. (c), **4**, No. 6, 1946–1950 (2007)

J14. L. De Stefano, **L. Rotiroti,** I. Rea, I. Rendina, M. Rossi, S. D'Auria, *"Assessment of a porous silicon transducer for the development of optical biochips",* Rivista di Materiali Nanocompositi e Nanotecnologie **3**, 39-41, 2006

J15. L. De Stefano, I. Rea, **L. Rotiroti,** M. Iodice, I. Rendina, *"Optical microsystems based on a nanomaterial technology",* J. Phys.: Condens. Matter **19** 395008, doi:10.1088/0953-8984/19/39/395008, (2007).

J16. L. De Stefano, **L. Rotiroti**, I. Rendina, A.M. Rossi, M. Rossi, S. D'Auria, "*Biochips at work: porous silicon microbiosensor for proteomic diagnostic*", *Phys.: Condens. Matter* **19** 395007, doi:10.1088/0953-8984/19/39/395007 (2007).

J17. L. De Stefano, P. Arcari, A. Lamberti, C. Sanchez, **L. Rotiroti**, I. Rea, I. Rendina, *"DNA optical detection based on porous silicon technology: from biosensors to biochips"* Sensors*,* 7 (2007) 214-221.

J18. L. De Stefano, A. Lamberti, **L. Rotiroti**, M. De Stefano, "*Interfacing the nanostructured biosilica microshells of the marine diatom Coscinodiscus wailesii with biological matter*", Acta Biomaterialia Volume 4, Issue 1, January 2008, Pages 126-130.

J19. Ivo Rendina, Edoardo De Tommasi, Ilaria Rea, **Lucia Rotiroti**, and Luca De Stefano, "*Porous silicon optical transducers offer versatile platforms for biosensors*" SPIE NEWSROOM DOI: 10.1117/2.1200801.0982 **invited paper**

J20. L. De Stefano, A. Vitale, I. Rea, M. Staiano, **L. Rotiroti**, T. Labella, I. Rendina, V. Aurilia, M. Rossi, S. D'Auria, *"Enzymes and proteins from extremophiles as hyperstable probes in nanotechnology: the use of D-trehalose/D-maltose-binding protein from the hyperthermophilic archaeon Thermococcus litoralis for sugars monitoring",* Extremophiles*,* 12, 1, 69-73 (2008).

J21. L. De Stefano, E. De Tommasi, I. Rea, **L. Rotiroti**, L. Giangrande, G. Oliviero, N. Borbone, A. Galeone and G. Piccialli, "Oligonucleotides direct synthesis on porous silicon chip", Nucleic Acids Symposium Series No. 52 721–722

J22. L. De Stefano, **L. Rotiroti,** M. De Stefano, A. Lamberti, S. Lettieri, A. Setaro, P. Maddalena, "Marine Diatoms as Optical Biosensors" has been accepted for publication in Biosensors and Bioelectronics, 2008.

J23. E. De Tommasi, L. De Stefano, I. Rea, V. Di Sarno, **L. Rotiroti**, P. Arcari, A. Lamberti, C. Sanges, and I. Rendina, "Porous Silicon Based Resonant Mirrors for Biochemical Sensing", Sensors 2008, Volume *8* (10), Page 6549-6556.

**PROCEEDINGS**:

P1. L. De Stefano, **L. Rotiroti**, I. Rea, L. Moretti, I. Rendina, "Quantitative determinations in liquid and gaseous binary misture by porous silicon optical microsensors", Advances in Sensors and Interfaces, Proc. of IWASI 2005, Eds. D. De Venuto and B. Courtois, 178-180, (2005).

P2. L. De Stefano, I. Rendina, **L. Rotiroti**, L. Moretti, V. Scognamiglio, M. Rossi, S. D'Auria, "Protein-ligand interaction detection by a porous silicon optical sensor", Proceedings of the 10$^{th}$ Italian Conference Sensors and Microsystems 2005, World Scientific, 89.

P3. Luca De Stefano, F. G. Della Corte, K. Malecki, Ivo Rendina, Lucia Rotiroti, Luigi Moretti, Andrea M. Rossi, "A microchamber for lab-on-chip applications based on silicon-glass anodic bonding", Proceedings of the 10$^{th}$ Italian Conference Sensors and Microsystems 2005, World Scientific, 450, 2005.

P4. L. De Stefano, K. Malecki, F. Della Corte, L. Moretti, I. Rea, **L. Rotiroti**, I. Rendina, "Silicon/glass integrated optical sensor based on porous silicon for gas and liquid inspection" Proceedings EUROSENSORS XIX, Settembre 11-14, 2005, Barcellona, Spagna.

P5. **L. Rotiroti**, L. De Stefano, I. Rea, L. Moretti, G. Di Francia, V. La Ferrara, A. Lamberti, P. Arcari, C. Sanges, I. Rendina; "Porous silicon based optical biochips" Book of Abstract, European Optical Society Topical Meeting on Optical Microsystems, Settembre 15-18, 2005, Capri, Italia.

P6. L. De Stefano, I. Rea, **L. Rotiroti**, I. Rendina, A. Lamberti, P. Arcari, C. Sanges, A. M. Rossi, "Resonant cavity enhanced optical microsensor for molecular interaction based on porous silicon"; Book of Abstract, The 11th National Conference on Sensor and Microsystems, p. 139-140, Febbraio 8-10, 2006, Lecce, Italia.

P7. L. De Stefano, **L. Rotiroti**, I. Rea, I. Rendina, L. Moretti, "Optical quantitative determination of the alcohol fraction in binary mixtures"; Book of Abstract, The 11th National Conference on Sensor and Microsystems, p. 141-142, Febbraio 8-10, 2006, Lecce, Italia.

P8. L. De Stefano, I. Rea, **L. Rotiroti**, I. Rendina, L. Fragomeni, F. G. Della Corte, "A hybrid integrated optical microsystem for sensing application"; Book of Abstract, The 11th National Conference on Sensor and Microsystems, p. 245-246, Febbraio 8-10, 2006, Lecce, Italia.

P9. L. De Stefano, I. Rea, **L. Rotiroti**, K. Malecki, L. Moretti, F. G. Della Corte, I. Rendina, Sensors and Microsystems, 227-231 (2006).

P10. L. De Stefano, I. Rea, **L. Rotiroti**, L. Moretti, I. Rendina, "Optical properties of porous silicon Thue-Morse structures"; Extended Abstracts of 5th International Conference on Porous Semiconductuctors-Science and Technology, p. 73-74, Marzo 12-17, 2006, Sitges-Barcellona, Spagna.

P11. L. De Stefano, **L. Rotiroti**, I. Rea, F. Della Corte, D. Alfieri, L. Moretti, I. Rendina, "An integrated pressure-driven microsystem based on porous silicon for optical monitoring of gaseous and liquid substances"; Extended Abstracts of 5th International Conference on Porous Semiconductuctors-Science and Technology, p. 126-127, Marzo 12-17, 2006, Sitges-Barcellona, Spagna.

P12. L. De Stefano, **L. Rotiroti**, I. Rea, L. Moretti, I. Rendina, “Quantitative determinations in hydro-alcoholic binary mixtures by porous silicon optical microsensors”; Extended Abstracts of 5th International Conference on Porous Semiconductuctors-Science and Technology, p. 248-249, Marzo 12-17, 2006, Sitges-Barcellona, Spagna.

P13. L. De Stefano, I. Rea, **L. Rotiroti**, L. Fragomeni, F. Della Corte, I. Rendina, ”An integrated hybrid optical device for sensing applications”; Extended Abstracts of 5th International Conference on Porous Semiconductuctors-Science and Technology, p. 250-251, Marzo 12-17, 2006, Sitges-Barcellona, Spagna.

P14. L. De Stefano, P. Maddalena, L. Moretti, I. Rea, I. Rendina, “Porous biosilica from marine diatoms: a new brand porous material for photonic applications”; Extended Abstracts of 5th International Conference on Porous Semiconductuctors-Science and Technology, p. 252-253, Marzo 12-17, 2006, Sitges-Barcellona, Spagna.

P15. L. De Stefano, I. Rea, **L. Rotiroti**, L. Moretti, I. Rendina “Resonant photonic devices based on porous silicon: a perfect tool for optical sensing”; Proceedings of XX EUROSENSORS Conference, p. 294-295, Settembre 17-20, 2006, Göteborg, Svezia.

P16. L. De Stefano, **L. Rotiroti**, I. Rea, E. De Tommasi, M. A. Nigro, F. G. Della Corte, and I. Rendina, Laser oxidation micropatterning of a porous silicon based biosensor for multianalytes microarray, Proceedings of the 12$^{th}$ Italian Conference Sensors and Microsystems 2007, World Scientific, 382-387.

P17. L, De Stefano, **L. Rotiroti**, I. Rea, E. De Tommasi, A. Vitale, M. Rossi, I. Rendina and S. D’Auria, "Design and realization of highly stable porous silicon optical biosensor based on proteins from extremophiles" Proc. of SPIE (2007) Vol. 6585 658517-1

P18. L. De Stefano, I. Rendina, I. Rea, **L. Rotiroti**, E. De Tommasi, and G. Barillaro, " An optical microsystem based on silicon-air Bragg mirror for the continuous monitoring of liquid substances" Proc. of SPIE (2007) Vol. 6585 65850N-1

P19. Ivo Rendina, Edoardo De Tommasi, Ilaria Rea, Lucia Rotiroti, and Luca De Stefano, “Porous silicon optical transducers offer versatile platforms for biosensors” DOI: 10.1117/2.1200801.0982

P20. L. De Stefano, I. Rendina, I. Rea, L. Moretti, **L. Rotiroti**, “Aperiodic photonic bandgap devices based on nanostructured porous silicon”, Proceedings of SPIE, Volume 6593, Photonic Materials, Devices, and Applications II, Ali Serpengüzel, Gonçal Badenes, Giancarlo C. Righini, Editors, 65931A (Jun. 5, 2007).

P21. I. Rendina, I. Rea, **L. Rotiroti**, E. De Tommasi, L. De Stefano, “Integrated optical biosensors and biochips based on porous silicon technology”, Proceedings of SPIE -- Volume 6898, Silicon Photonics III, Joel A. Kubby, Graham T. Reed, Editors, 68981D (Feb. 13, 2008)

P22. **Lucia Rotiroti,** Paolo Arcari, Annalisa Lamberti, Carmen Sanges, Edoardo De Tommasi, Ilaria Rea, Ivo Rendina, and Luca De Stefano, “Optical detection of PNA/DNA hybridization in resonant porous silicon-based devices” Proc. SPIE 6991, 699120 (2008).

P23. **L. Rotiroti**, E. De Tommasi, I. Rendina, M. Canciello, G. Maglio, R. Palumbo, and L. De Stefano,” BIOACTIVE POLIMERS MODIFIED POROUS SILICON NANOSTRUCTURES”, 6th International Conference on Porous Semiconductuctors-Science and Technology, p. 348-349, Marzo 10-14, 2008, Mallorca, Spagna.

P24. **L. Rotiroti**, I. Rendina, E. De Tommasi, M. Canciello, G. Maglio, R. Palumbo, and L. De Stefano, A Nanostructured Hybrid Device Based On Polymers Infiltrated Porous Silicon Layers For Biotechnological Applications, Proceedings of the Polymer Processing Society 24th Annual Meeting ~ PPS-24 ~ June 15-19, 2008 Salerno (Italy).

P25. **L. Rotiroti**, I. Rendina, E. De Tommasi, M. Canciello, G. Maglio, R. Palumbo, and L. De Stefano, A Hybrid Optical Biosensor Based on Polymer Infiltrated Porous Silicon Device, IEEE SENSORS 2008, Lecce (Italy).

**NATIONAL AND INTERNATIONAL CONGRESS**

C1. L. De Stefano, I. Rendina, **L. Rotiroti**, L. Moretti, V. Scognamiglio, M. Rossi, S. D’Auria, “Protein-ligand interaction detection by a porous silicon optical sensor”, **Oral**, AISEM 2005, Firenze, 15-17 Febbraio, 2005.

C2. Luca De Stefano, F. G. Della Corte, K. Malecki, Ivo Rendina, Lucia Rotiroti, Luigi Moretti, Andrea M. Rossi, “A microchamber for lab-on-chip applications based on silicon-glass anodic bonding”, **Poster**, AISEM 2005, Firenze, 15-17 Febbraio, 2005.

C3. L. De Stefano, **L. Rotiroti**, I. Rea, L. Moretti, I. Rendina, “Quantitative determinations in liquid and gaseous binary mixtures by porous silicon optical microsensors”, **Oral**, IWASI 2005, Bari, 19-20 April, 2005.

C4. L. De Stefano, **L. Rotiroti**, I. Rea, L. Moretti, I. Rendina, “Microsensori ottici per applicazioni biochimiche basati sulla nanotecnologia del silicio poroso”, **Oral**, GE2005, Giardini Naxos (CT), 29 giugno – 2 luglio, 2005.

C5. M. A. Ferrara, L. Sirleto, **L. Rotiroti**, L. Moretti, E. Santamato, I. Rendina “EMISSIONE RAMAN IN SILICIO POROSO A 1.5 μm”, **Oral**, GE2005, Giardini Naxos (CT), 29 giugno – 2 luglio, 2005.

C6. L. De Stefano, K. Malecki, F. G. Della Corte, L. Moretti, I. Rea, **L. Rotiroti**, I. Rendina, **Oral**, “Silicon/glass integrated optical sensor based on porous silicon for gas and liquid inspection”, Eurosensors XIX, Barcelona, Spain, 9-14 September, 2005.

C7. **L. Rotiroti**, L. De Stefano, I. Rea, L. Moretti, G. Di Francia, V. La Ferrara, A. Lamberti, P. Arcari, C. Sanges, I. Rendina, “Porous silicon based optical biochips”; **Oral**, European Optical Society Topical Meeting on Optical Microsystems, Settembre 15-18, 2005, Capri, Italia.

C8. M. A. Ferrara, L. Sirleto, G. Messina, M.G. Donato, **L. Rotiroti** and I. Rendina, “STRAIN MEASUREMENTS IN POROUS SILICON BY RAMAN SCATTERING”, AISEM 2006, Lecce, 8-10 Febbraio, 2006.

C9. M. A. Ferrara, L. Sirleto, L. Moretti, **L. Rotiroti**, B. Jalali and I. Rendina, “RAMAN EMISSION IN POROUS SILICON: PROSPECT FOR AN AMPLIFIER”, SPIE Silicon Photonics.

C10. L. De Stefano, I. Rea, **L. Rotiroti**, I. Rendina, A. Lamberti, P. Arcari, C. Sanges, A. M. Rossi, “Resonant cavity enhanced optical microsensor for molecular interaction based on porous silicon”; The 11th National Conference on Sensor and Microsystems, Febbraio 8-10, 2006, Lecce, Italia.

C11. L. De Stefano, **L. Rotiroti**, I. Rea, I. Rendina, L. Moretti, “Optical quantitative determination of the alcohol fraction in binary mixtures”; The 11th National Conference on Sensor and Microsystems, Febbraio 8-10, 2006, Lecce, Italia.

C12. L. De Stefano, I. Rea, **L. Rotiroti**, I. Rendina, L. Fragomeni, F. G. Della Corte, “A hybrid integrated optical microsystem for sensing application”; The 11th National Conference on Sensor and Microsystems, Febbraio 8-10, 2006, Lecce, Italia.

C13. I. Rea, D. Alfieri, K. Malecki, I. Rendina, **L. Rotiroti**, L. De Stefano, L. Moretti, F.G. Della Corte, “Fast optical detection of chemical substances in integrated silicon-glass chip”; The 11th National Conference on Sensor and Microsystems, Febbraio 8-10, 2006, Lecce, Italia.

C14. L. De Stefano, I. Rea, **L. Rotiroti**, L. Moretti, I. Rendina, “Optical properties of porous silicon Thue-Morse structures”; of 5th International Conference on Porous Semiconductuctors-Science and Technology, Marzo 12-17, 2006, Sitges-Barcellona, Spagna.

C15. L. De Stefano, **L. Rotiroti**, I. Rea, F. Della Corte, D. Alfieri, L. Moretti, I. Rendina, “An integrated pressure-driven microsystem based on porous silicon for optical monitoring of gaseous and liquid substances”; 5th International Conference on Porous Semiconductuctors-Science and Technology, Marzo 12-17, 2006, Sitges-Barcellona, Spagna.

C16. L. De Stefano, **L. Rotiroti**, I. Rea, L. Moretti, I. Rendina, “Quantitative determinations in hydro-alcoholic binary mixtures by porous silicon optical microsensors”; 5th International Conference on Porous Semiconductuctors-Science and Technology, Marzo 12-17, 2006, Sitges-Barcellona, Spagna.

C17. L. De Stefano, I. Rea, **L. Rotiroti**, L. Fragomeni, F. Della Corte, I. Rendina, “An integrated hybrid optical device for sensing applications”; 5th International Conference on Porous Semiconductuctors-Science and Technology, Marzo 12-17, 2006, Sitges-Barcellona, Spagna.

C18. L. De Stefano, I. Rea, **L. Rotiroti**, I. Rendina, “Porous silicon biosensors and biochips”, **Invited**, EMRS 2006, May 29-June 2, Nice, France, 2006.

C19. M. Angeloni, L. Moretti, V. Mocella, L. De Stefano, **L. Rotiroti**, I. Rea, S. Bernstorff, “In situ investigation of capillary condensation phenomena in porous silicon nanostructured by means of GISAX and SAXS measurements”, **Poster**, EMRS 2006, May 29-June 2, Nice, France, 2006.

C20. L. De Stefano, I. Rea, **L. Rotiroti**, L. Moretti, F. G. Della Corte, I. Rendina, “Integrated optical microsensors based on porous silicon technology for liquid and gas detection”, **Poster**, EMRS 2006, May 29-June 2, Nice, France, 2006.

C21. M. A. Ferrara, L. Sirleto, M. Angeloni, **L. Rotiroti**, B. Jalalii, I. Rendina, “Raman emission in porous silicon: prospects fora n amplifier”, **Poster**, EMRS 2006, May 29-June 2, Nice, France, 2006.

C22. C. Sanges, A. Lamberti, **L. Rotiroti**, L. De Stefano, I. Rendina, P. Arcari, “Biochip ottici in Silicio Poroso”, **Poster**, XII GIORNATE SCIENTIFICHE - Facoltà di Medicina e Chirurgia, Agraria, Medicina veterinaria, Farmacia, Scienze MM.FF.NN., Scienze Biotecnologiche, 15-16 June, Napoli, Italy, 2006.

C23. I. Rea, **L. Rotiroti**, I. Rendina. L. Moretti, L. De Stefano; “Proprietà ottiche di multistrati thue-morse realizzati con la tecnologia del silicio poroso” Riunione Annuale del Gruppo Elettronica (GE 2006), Giugno 21-23, Ischia (NA), Italia.

C24. **L. Rotiroti**, I. Rea, D. Alfieri, L. Moretti I. Rendina, F. Della Corte, L. De Stefano; “Microsensori ottici integrati basati sulla tecnologia del silicio poroso per il riconoscimento di sostanze liquide e gassose” Riunione Annuale del Gruppo Elettronica (GE 2006), Giugno 21-23, Ischia (NA), Italia.

C25. L. De Stefano, **L. Rotiroti**, I. Rea, S. D’Auria, A. Vitale, M. Rossi, I. Rendina, “A biosensor for selective identification of analites of social interest based on porous silicon technology”, IMCS11, July 16-19, Brescia, Italy, 2006.

C26. L. De Stefano, I. Rea, **L. Rotiroti**, L. Moretti, I. Rendina “Resonant photonic devices based on porous silicon: a perfect tool for optical sensing”; XX EUROSENSORS, Settembre 17-20, 2006, Göteborg, Svezia.

C27. I. Rea, L. De Stefano, **L. Rotiroti**, M. Iodice, I. Rendina; “Optical microsystems based on a nanomaterial technology” **Oral**, Nanoscience & Nanotechnology 2006, Novembre 6-9, 2006, Monte Porzio Catone (Rome), Italy.

C28. I. Rea, L. De Stefano, **L. Rotiroti**, E. De Tommasi, A. Nigro, F.G. Della Corte, I. Rendina, “Laser oxidation micropatterning of a porous silicon based biosensor for multianalytes microarrays”, **Poster**, AISEM 2007, Febbraio 12-14 2007, Napoli, Italy.

C29. L. De Stefano, **L. Rotiroti**, I. Rea, L. Moretti, I. Rendina, “High-sensitivity optical sensors based on aperiodic multilayer structures”, **Poster**, AISEM 2007, Febbraio 12-14 2007, Napoli, Italy.

C30. L. De Stefano, **L. Rotiroti**, I. Rea, E. De Tommasi, A, Vitale, M. Rossi. I. Rendina and S. D’Auria “Design and realization of highly stable porous silicon optical biosensor based on proteins from extremophiles” – **Oral presentation.** SPIE Europe, Optics and Optoelectronics, 2007, Prague, Czech Republic.

C31. L. D Stefano, I. Rendina, I. Rea, **L. Rotiroti**, E. De Tommasi and G. Barillaro “An optical microsystem based on vertical silicon-air Bragg mirror for liquid substances monitoring” – **Oral presentation.** SPIE Europe, Optics and Optoelectronics, 2007, Prague, Czech Republic.

C32. **L. Rotiroti**, E. De Tommasi, I. Rea, A. Lamberti, C. Sanges, I. Rendina, P. Arcari and L. De Stefano “Optical detection of PNA-DNA hybridization in resonant porous silicon based devices” – **Poster presentation**. Europtrode 2008, Dublin, Ireland.

C33. E. De Tommasi, I. Rea. V. Di Sarno, **L. Rotiroti**, I. Rendina and L. De Stefano “Porous Silicon Resonant Mirrors Biosensors” – **Poster presentation**. Porous Semiconductors Science & Technology, 2008, Mallorca, Spain.

C34. E. De Tommasi, I. Rea. V. Di Sarno, **L. Rotiroti**, I. Rendina and L. De Stefano “Porous Silicon Resonant Mirrors for Optical Biosensing” – **Oral presentation**. 13th National Conference AISEM, 2008, Rome.

C35. **L. Rotiroti**, E. De Tommasi, I. Rendina, M. Canciello, G. Maglio, R. Palumbo, and L. De Stefano," BIOACTIVE POLIMERS MODIFIED POROUS SILICON NANOSTRUCTURES", 6th International Conference on Porous Semiconductuctors-Science and Technology, **Poster presentation**., Marzo 10-14, 2008, Mallorca, Spagna.

C36. **L. Rotiroti,** P. Arcari, A. Lamberti, C. Sanges, E. De Tommasi, I. Rea, I. Rendina and L. De Stefano "Optical detection of PNA-DNA hybridization in resonant porous silicon based devices" – **Poster presentation**. SPIE Photonics Europe, 2008, Strasbourg, France.

C37. L. De Stefano, E. De Tommasi, I. Rea, **L. Rotiroti,** I. Rendina "Porous Silicon resonant devices as optical transducers for nanostructured hybrid biosensors", **Invited**, New Frontiers in Micro and Nano Photonics, 23-26 Aprile 2008, Firenze, Italia.

C38. **L. Rotiroti**, I. Rendina, E. De Tommasi, M. Canciello, G. Maglio, R. Palumbo, and L. De Stefano, "A nanostructured hybrid device based on polymers infiltrated porous silicon layers for biotechnological applications", **oral presentation,** PPS-24 Meeting The Polymer Processing Society 24th Annual Meeting June 15-19, 2008, Salerno, ITALY.

C39. E. De Tommasi, I. Rea, V. Di Sarno, **L. Rotiroti**, I. Rendina and L. De Stefano "Porous silicon resonant mirrors in the high sensitive monitoring of biological interactions" – **Oral presentation.** First Mediterranean Photonics Conference of the European Optical Society, 2008, Ischia (Naples), Italy.

C40. **L. Rotiroti,** I. Rendina, E. De Tommasi, M. Canciello, G. Maglio, R. Palumbo, and L. De Stefano, A Hybrid Optical Biosensor Based on Polymer Infiltrated Porous Silicon Device, – **Oral presentation**, IEEE SENSORS 2008, Lecce (Italy).

**PATENTS**

Patent n. RM 2005 A 0002280 " An integrated device for the optical determination of the alcoholic content, in particular for wines and liquors, main procedures of fabrication, and main procedures of measurements"

**SCHOOLS AND WORKSHOPS**:

1. **11 giugno 2008** SPETTROSCOPY SEMPLIFIED – THERMO FISCHER SCIENTIFIC, *Hotel Selene*, Pomezia
2. **6 febbraio 2008** LA BUONA PRATICA DI PESATA - GWP®, METTLER TOLEDO, *Holiday Inn*, Napoli.
3. **17 luglio 2007** MICROSCOPIA A SONDA NELLA SCIENZA DEI MATERIALI, seminario indetto da 2M STRUMENTI "Veeco", Portici (Napoli).
4. **26 febbraio-2 marzo 2007** ADVANCED COURSE in design, synthesis, analysis and evaluation of bioactive molecules, Napoli.
5. **5-6 Luglio 2006** *Ciclo di seminari sulla Luce di Sincrotrone*, Napoli.
6. **26-27 giugno 2006** corso "ENZIMI DA IPERTERMOFILI E NANOTECNOLOGIE: ASPETTI APPLICATIVI", Napoli.
7. **19-21 Giugno 2006** *scuola di dottorato del Gruppo Elettronica (GE 2006)*, Benevento (BN), Italia.
8. **15-17 maggio 2006** corso teorico/pratico "FUNZIONALIZZAZIONE DI SUPERFICI VIA PLASMA PER APPLICAZIONI BIOTECNOLOGICHE", Napoli.
9. **12 marzo 2006** Short Course "5$^{th}$ International Conference on Porous Semiconductuctors-Science and Technology", Sitges-Barcellona, Spagna.

Appendix

INSTITUTE OF PHYSICS PUBLISHING JOURNAL OF OPTICS A: PURE AND APPLIED OPTICS

J. Opt. A: Pure Appl. Opt. **8** (2006) S540–S544 doi:10.1088/1464-4258/8/7/S37

# Porous silicon-based optical biochips

**Luca De Stefano[1], Lucia Rotiroti[1], Ilaria Rea[1], Luigi Moretti[2], Girolamo Di Francia[3], Ettore Massera[3], Annalisa Lamberti[4], Paolo Arcari[4], Carmen Sanges[4] and Ivo Rendina[1]**

[1] Institute for Microelectronics and Microsystems, CNR—Department of Naples, Via P Castellino 111, 80131 Naples, Italy
[2] DIMET, University 'Mediterranea' of Reggio Calabria, Località Feo di Vito, 89060 Reggio Calabria, Italy
[3] ENEA—Centro Ricerche Portici, 80055 Portici (NA), Italy
[4] DBBM—Università di Napoli 'Federico II', Via S Pansini 5, 80131 Napoli, Italy

Received 28 December 2005, accepted for publication 17 March 2006
Published 12 June 2006
Online at stacks.iop.org/JOptA/8/S540

**Abstract**

In this paper, we present our work on an optical biosensor for the detection of the interaction between a DNA single strand and its complementary oligonucleotide, based on the porous silicon (PSi) microtechnology. The crucial point in this sensing device is how to make a stable and repeatable link between the DNA probe and the PSi surface. We have experimentally compared some functionalization processes which modify the PSi surface in order to covalently fix the DNA probe on it: a pure chemical passivation procedure, a photochemical functionalization process, and a chemical modification during the electrochemical etching of the PSi. We have quantitatively measured the efficiency of the chemical bond between the DNA and the porous silicon surface using Fourier transform infrared spectroscopy (FT-IR) and light induced photoluminescence emission. From the results and for its intrinsic simplicity, photochemical passivation seems to be the most promising method.

The interaction between a label-free 50 $\mu$M DNA probe with complementary and non-complementary oligonucleotides sequences has been also successfully monitored by means of optical reflectivity measurements.

**Keywords:** porous silicon, optical biosensor, surface functionalization, DNA analysis

(Some figures in this article are in colour only in the electronic version)

## 1. Introduction

In the past two decades, the biological and medical fields have seen great advances in the development of biosensors and biochips for characterizing and quantifying biomolecules.

A biosensor can be generally defined as a device that consists of a biological recognition system, often called a bioreceptor, and a transducer. The interaction of the bioreceptor with the analyte is designed to produce an effect measured by the transducer, which converts the information into a measurable effect, such as an electrical signal.

Using bioreceptors from biological organisms or receptors that have been patterned after biological systems, scientists have developed new methods of biochemical analysis that exploit the high selectivity of the biological recognition systems [1].

Porous silicon (PSi) is an almost ideal material as a transducer due to its porous structure, with hydrogen terminated surface, having a specific area of the order of 200–500 $m^2\ cm^{-3}$, so that a very effective interaction with several adsorbates is assured. Moreover, PSi is an available and low cost material, completely compatible with standard integrated circuit processes. Therefore, it could usefully be employed in the so-called smart sensors [2]. Recently, much experimental work, exploiting the noteworthy properties of PSi in chemical and biological sensing, has been reported [3–6].

PSi optical sensing devices are based on changes of its physical properties, such as photoluminescence or reflectance, on exposure to the surrounding environment. Unfortunately, this interaction is not specific, so a PSi sensor cannot discriminate the components of a complex mixture. Some researchers have chemically or physically modified the Si–H

 © 2006 IOP Publishing Ltd Printed in the UK 

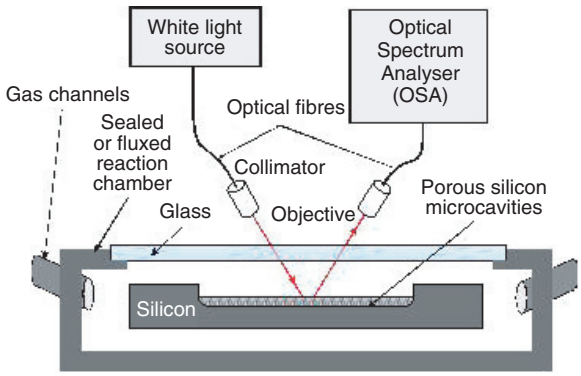


**Figure 1.** The experimental optical set-up.

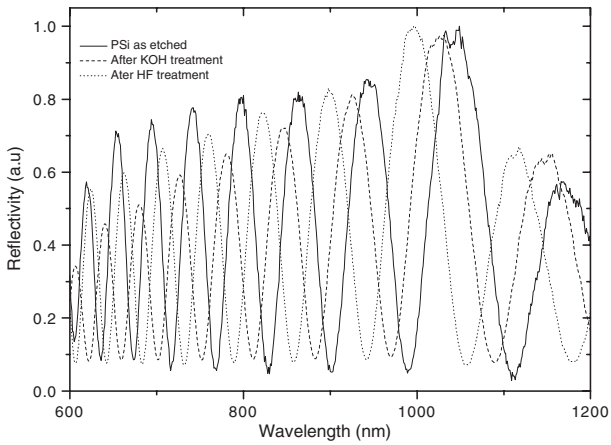


**Figure 2.** Reflectivity optical spectra of the porous silicon layer after KOH and HF treatments.

surface sites in order to enhance the sensor selectivity through specific interactions. The common approach is to create a covalent bond between the PSi surface and the biomolecules which specifically recognize the target analytes [7, 8].

The reliability of a biosensor strongly depends on the functionalization process: how fast, simple, homogenous and repeatable it is. This step is also very important for the stability of the sensor: it is well known that 'as-etched' PSi has a Si–H terminated surface due to the Si dissolution process which is very reactive [9]. The substitution of the Si–H bonds with Si–C ones guarantees a much more stable surface from the thermodynamic point of view.

In this work, we report some PSi surface modification strategies in order to realize an optical biosensor: the target is the fabrication of sensitive label-free biosensors, which are highly requested for applications in high throughput drug monitoring and disease diagnostics; unlabelled analytes require in fact easier and faster analytical procedures.

## 2. Materials and methods

Porous silicon is a very attractive material due to the possibility of fabricating high quality optical structures, either as single layers, like Fabry–Perot interferometers, or multilayers, such as Bragg or rugate filters [12]. In this study we used as a sensor a Fabry–Perot single layer. The PSi layer was obtained by electrochemical etch in a HF-based solution at room temperature. A highly doped $p^+$-silicon substrate, $\langle 100 \rangle$ oriented, 0.01 $\Omega$ cm resistivity, 400 $\mu$m thick was used. Before anodization, the substrate was placed in HF solution to remove the native oxide.

The dielectric and physical properties of the PSi layer were investigated by spectroscopic ellipsometry and scanning electron microscopy. Both the analysis methods showed the presence of a top layer on the PSi structure of about 50 nm thickness, characterized by a very low porosity. The top layer is due to a hydrogen contamination which passivates boron and changes the local resistivity. The presence of the top layer reduces pore infiltration. To remove the contamination we pre-treated the crystalline silicon substrate before the electrochemical etching by heating the wafer at 300 °C in $N_2$ atmosphere for 30 min [10]. The ellipsometric measurements on the pre-treated PSi layer show that the top layer was eliminated.

Due to the nanostructured nature of PSi, it is necessary to improve the pore infiltration of biomolecular probes: with this aim, we optimized our device by employing a strong base post-etch process. We immersed the device in an aqueous ethanol solution, containing millimolar concentration of KOH, for 15 min. This treatment produces an increase of about 15–20% in the porosity without affecting the optical quality of the device [11].

We used a very simple experimental set-up (see figure 1) to characterize the PSi device from an optical point of view: a tungsten lamp (400 nm $< \lambda <$ 1800 nm) probed, through an optical fibre and a collimator, the sensor closed in a glass vial which can be fluxed by liquids or gases. The reflected beam is collected by an objective, coupled into a multimode fiber, and then directed in an optical spectrum analyser (Ando, AQ6315A). The reflectivity spectra were measured with a resolution of 0.2 nm. In figure 2 the optical reflectivity spectra of the PSi layer as-etched and after KOH and HF treatments are reported.

Even though there are a lot of scientific works about silicon and PSi biochips for DNA analysis, reports on the attachments of biomolecular compounds to these substrates are not very common. We have spent much experimental effort to select the most reliable functionalization method. FT-IR spectroscopy (Thermo-Nicolet Nexus) was used to compare three different passivation procedures of the PSi surface: a pure chemical process based on Grignard reagents; a photoinduced chemical modification based on undecenoic organic acid; and a passivation method simultaneous to the etching process. In each case the carboxyl-terminated monolayer covering the PSi surface acts as a substrate for the chemistry of the subsequent attachment of the DNA sequences. Once a chemical procedure was chosen to modify the PSi surface, we also quantitatively measured the efficiency of the photochemical binding between the DNA and the PSi surface using a fluorescent DNA probe (GGACTTGCCCGAATCTACGTGTCCC, Primm) labelled with a proper chromophore group (Fluorescein CY3.5: the absorption peak is at 581 nm and the emission is at 596 nm). We compared the photoluminescence (PL) emission, induced by a halogen lamp, from several PSi monolayers, some having a chemically modified surface and others not.

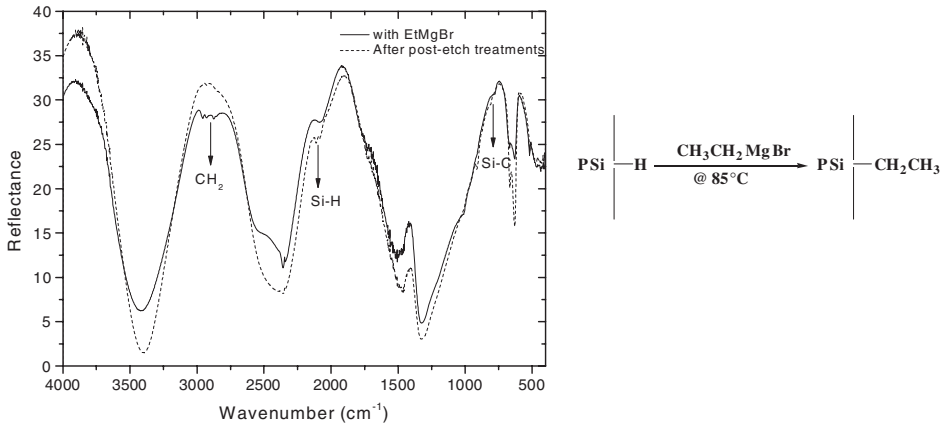


**Figure 3.** FT-IR spectra of the PSi monolayer before and after the pure chemical functionalization process based on EtMgBr, together with the reaction scheme.

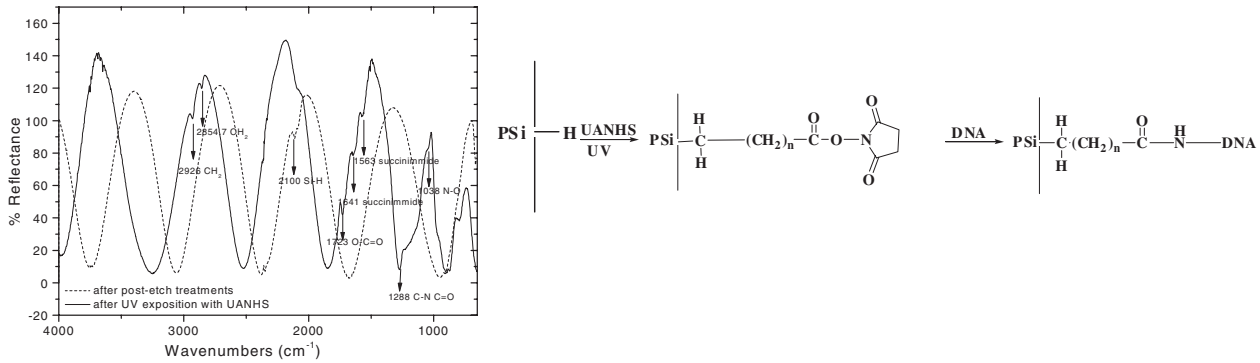


**Figure 4.** FT-IR spectra of the PSi monolayer before and after the photoinduced functionalization process based on UV exposure, together with the reaction scheme.

### *2.1. Chemical functionalization by Grignard reactives*

The chemical functionalization is based on ethyl magnesium bromide ($CH_3CH_2MgBr$) as a nucleophilic agent which substitutes the Si–H bonds with the Si–C. The reaction was performed at 85 °C in an inert atmosphere (argon) to avoid the deactivation of the reactive, for 8 h. The chip was then washed with a 1% solution of $CF_3COOH$ in diethyl ether, and then with deionized water and pure diethyl ether. The modified surface chip was characterized by infrared spectroscopy to verify the efficiency of the method. The FT-IR spectrum and the reaction scheme are reported in figure 3.

### *2.2. Photochemical functionalization*

The photo-activated chemical modification of the PSi surface was based on the UV exposure of a solution of alkenes which bring some carboxylic acid groups. The PSi chip was pre-cleaned in an ultrasonic acetone bath for 10 min then washed in deionized water. After being dried in a $N_2$ stream, it was immediately covered with 10% *N*-hydroxysuccinimide ester (UANHS) solution in $CH_2Cl_2$. The UANHS was synthesized in house as described in [7]. This treatment results in covalent attachment of UANHS to the PSi surface, clearly shown in the FT-IR spectrum, reported in figure 4 together with the reaction scheme. The chip was then washed in dichloromethane in an ultrasonic bath for 10 min and rinsed in acetone to remove any adsorbed alkene from the surface.

### *2.3. Functionalization during the etch process*

We also tried to chemically modify the surface of the PSi by directly using a functionalizing agent during the etching process. We introduced some organic acids (eptinoic and pentenoic acid with concentrations from 0.4 M to 3 M) in an electrochemical cell in the presence of a dilute HF solution (HF:EtOH=1:2). In this case a current density of 60 mA $cm^{-2}$ was applied to etch an area of 0.07 $cm^2$. The FT-IR spectrum is reported in figure 5.

## 3. Experimental results

We studied the infrared spectrum in each case of functionalization method in order to determine the best reaction conditions and the maximum yield in the Si–H/Si–C substitution. The post-etch KOH treatment, which we used to increase the porosity and to improve the pore infiltration, removes most of Si–H bonds on the fresh PSi surface and also induces its oxidation. To assure the formation of the Si–C bonds, we had first to restore the Si–H bonds by rinsing the PSi in a very dilute HF-based solution for 30 s. FT-IR spectroscopy confirmed the presence of Si–H bonds on the PSi surface after all pretreatments.

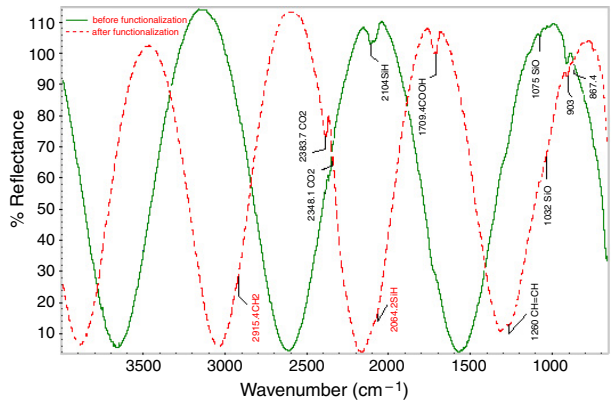


**Figure 5.** FT-IR spectra of the PSi monolayer before (solid line) and after (dashed line) functionalization during the etching process.

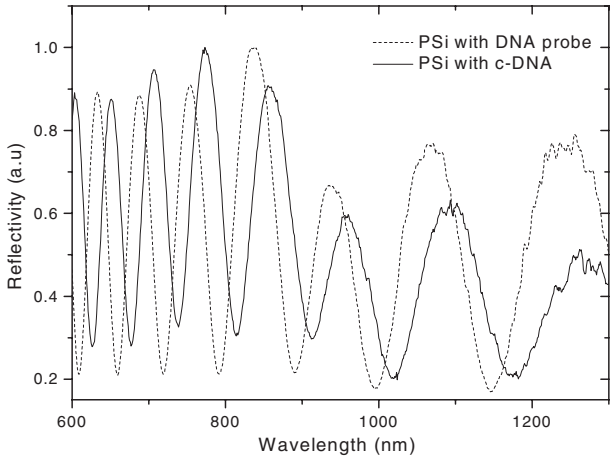


**Figure 6.** Reflectivity optical spectra of the PSi device after DNA probe immobilization and after cDNA hybridization.

For each method we studied, we report the infrared spectrum (figures 3–5). In all of them, the characteristic peaks of the Si–C bonds can be observed, even if with different intensities. In the case of the pure chemical functionalization method, the FT-IR spectrum (figure 3) shows an incomplete substitution of the Si–H bonds, since their characteristic peaks (at 2100 $cm^{-1}$) are still present.

In figure 4 we can also easily distinguish all the characteristic peaks of the reactive (UANHS) immobilized on the PSi surface. The infrared analysis of the chip prepared by direct functionalization during the etch process, shows a –COOH peak, whose intensity increases on increasing the acid concentration, as reported in figure 5.

Among the three procedures experimented, we believe that the photoinduced method is the best one for several reasons: the relaxed reaction conditions (atmospheric pressure and room temperature); the shorter reaction time; and the best reaction yield (from FT-IR measurements). This last result is somewhat expected because the reactive considered has a so-called 'outgoing group' which promotes its substitution with the amine group of the DNA probe.

In view of these considerations, on each chip with a photochemical modified surface we incubated, overnight, a luminescent DNA probe. After washing, we measured the photoluminescence emission with a microscope equipped with a CCD. As a reference sample, we used the signal coming from chips not washed after labelled DNA incubation.

The PL measurements showed that the photochemical modification of the PSi surface is very efficient: we registered $52 \pm 8$ counts from treated chips, $5 \pm 1$ counts from the unfunctionalized chips, and $63 \pm 6$ counts from the reference samples. The count values are the arithmetic mean over three different chip samples and the errors are the standard deviations. A total yield of about 83% can be thus estimated.

The optical monitoring of DNA–cDNA hybridization is a two-step procedure: first, we registered the optical spectrum of the PSi layer after the UANHS and probe immobilization on the chip surface and, then, after the hybridization with the cDNA. Each step of the chip preparation increases the optical path in the reflectivity spectrum recorded, due to the substitution of the air into the pores by organic and biological compounds, so that several red-shifts can be observed after the functionalization (10 nm), and after the covalent binding of the DNA single strand (probe) with the linker on the porous silicon layer (31 nm). The interaction with the cDNA is also detected as a shift in wavelength of the optical path (33 nm). In figure 6 the reflectivity spectra of only these last two steps are reported for the sake of clarity. A control measurement was made using an *n*cDNA sequence: a very small shift (less than 2 nm) was recorded in the reflectivity spectrum with respect to the one obtained after probe linking.

## 4. Conclusion

In conclusion, we have presented our experimental results of the study of several procedures of porous silicon surface functionalization that are a fundamental step in realizing an optical porous silicon microsensor for DNA–cDNA interaction detection. The pore infiltration by the DNA single-strand solution was improved by introducing two more steps during the realization process: a pre-etch cleaning of the crystal substrate to remove hydrogen contamination; and an alkaline post-etching process that increases the device porosity. Among several surface functionalization methods used to immobilize in the PSi matrix a DNA probe which selectively recognizes its complementary sequence, we chose a photoinduced one because of the simplicity of the reaction conditions and the well performing results. We also demonstrated that an optical Fabry–Perot interferometer based on a PSi layer can be effectively used as a transducer of the DNA–cDNA hybridization interaction.

## Acknowledgments

This work was realised in the frame of the CRdC-NTAP and in the frame of the MIUR FIRB Project 2003 Costituzione di un laboratorio dedicato all'analisi delle interazioni ligando-recettore mediante biochip di silicio.

## References

[1] Sadana A 2002 *Engineering Biosensors* (San Diego, CA: Academic)

[2] De Stefano L, Moretti L, Rendina I, Rossi A M and Tundo S 2004 Smart optical sensors for chemical substances based on porous silicon technology *Appl. Opt.* **43** 167–72
[3] Dancil K-P S, Greiner D P and Sailor M J 1999 A porous silicon optical biosensor: detection of reversible binding of IgG to a protein A-modified surface *J. Am. Chem. Soc.* **121** 7925–30
[4] De Stefano L, Moretti L, Rossi A M, Rocchia M, Lamberti A, Longo O, Arcari P and Rendina I 2004 Optical sensors for vapors, liquids, and biological molecules based on porous silicon technology *IEEE Trans. Nanotech.* **3** 49–54
[5] Dattelbaum J D and Lakowicz J R 2001 Optical determination of glutamine using a genetically engineered protein *Anal. Biochem.* **291** 89–95
[6] Bradford M M 1976 A rapid and sensitive method for the quantitation of microgram quantities of protein utilizing the principle of protein-dye binding' *Anal. Biochem.* **72** 248–54
[7] Yin H B, Brown T, Gref R, Wilkinson J S and Melvin T 2004 Chemical modification and micropatterning of Si(100) with oligonucleotides *Microelectron. Eng.* **73/74** 830–6
[8] Hart B R, Letant S E, Kane S R, Hadi M Z, Shields S J and Reynolds J G 2003 New method for attachment of biomolecules to porous silicon *Chem. Commun.* 322–3
[9] Canham L (ed) 1997 *Properties of Porous Silicon* (London: IEE INSPEC)
[10] Chamard V, Dolino G and Muller F 1998 Origin of a parasitic surface film on p+ type porous silicon *J. Appl. Phys.* **84** 6659–66
[11] DeLouise L A and Miller B L 2004 Optimization of mesoporous silicon microcavities for proteomic sensing *Mater. Res. Soc. Symp. Proc.* **782** A5.3.1–A5.3.7
[12] Theiss W 1997 Optical properties of porous silicon *Surf. Sci. Rep.* **29** 91–192

IOP PUBLISHING JOURNAL OF PHYSICS: CONDENSED MATTER

J. Phys.: Condens. Matter **19** (2007) 395008 (7pp) doi:10.1088/0953-8984/19/39/395008

# Optical microsystems based on a nanomaterial technology

**L De Stefano[1], L Rotiroti[1,2], I Rea[1,3], M Iodice[1] and I Rendina[1]**

[1] National Council of Research-Institute for Microelectronic and Microsystems-Department of Naples, Via P Castellino 111, 80131 Naples, Italy
[2] Department of Organic Chemistry and Biochemistry, 'Federico II' University of Naples, Via Cinthia, 4-80126 Naples, Italy
[3] Department of Physics, 'Federico II' University of Naples, Via Cinthia, 4-80126 Naples, Italy

E-mail: luca.destefano@na.imm.cnr.it

Received 13 February 2007
Published 30 August 2007
Online at stacks.iop.org/JPhysCM/19/395008

**Abstract**

In this work, we present an optical sensor for quantitative determination of the alcohol content in hydro-alcohol mixtures, realized by using porous silicon (PSi) nanotechnology. The device is an oxidized PSi micro-cavity (PSMC) constituted by a Fabry–Perot layer between two distributed Bragg reflectors. Due to the capillary condensation, a red shift of the PSMC reflectivity spectrum is observed on exposure to vapour mixtures. The phenomenon is completely reversible. Moreover, to reduce the analysis time, we have designed the integration of the sensor in a thermally controlled lab-on-chip, by merging PSi and anodic bonding technologies. Numerical calculations have been performed to study the thermal behaviour of the integrated device.

(Some figures in this article are in colour only in the electronic version)

## 1. Introduction

The fast and intensive development of the lab-on-chip (LOC) for sensing applications is due to several factors that are essential for routine analytical determinations, such as very limited sample consumption and short analysis time, which can be obtained by measuring a transient signal in a flow-through detector. Due to their intrinsic features, in particular contactless monitoring capability, optical sensors are very attractive for many application fields.

In recent years, many devices based on porous silicon (PSi) technology have been realized for several sensing applications [1, 2]. PSi, fabricated by electrochemical etching of a silicon (Si) wafer in HF-based solution, is an ideal material for an optical transducer, due to its sponge-like nanostructure (specific surfaces up to 500 $m^2$ $cm^{-3}$) [3], that assures an effective interaction with several chemicals and biological molecules. On exposure to chemical substances, several physical parameters, such as refractive index, photoluminescence, and electrical conductivity,

 © 2007 IOP Publishing Ltd Printed in the UK 

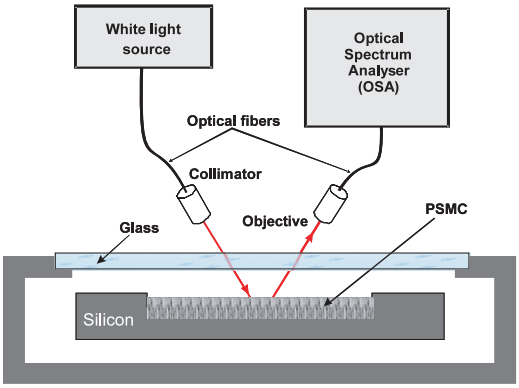


**Figure 1.** Experimental optical set-up used for the sensing experiments.

change drastically. It is also possible to realize in a single process multilayered structures that exhibit a high selective optical response, which is very attractive for sensing [4].

Silicon–glass anodic bonding (AB) is one of the most promising techniques in the micromachining field; it easily allows the encapsulation and sealing on silicon chips of three-dimensional microfluidic structures, such as channels, chambers, cavities and other complex gas and liquid routes. Additionally, glass transparency at optical wavelengths enables simple, but highly accurate, alignment of pre-patterned or structured glass and silicon wafers.

We have recently demonstrated the compatibility of PSi and AB technologies for the realization of sensing microcomponents for LOC applications [5, 6]. The integration was not easy or straightforward: the microfabrication techniques are typically optimized for the microelectronic industry and are not well appropriated or compatible with the non-standard materials such as the ones used in biological or chemical sensing.

We present here a simple optical sensor for the analysis of hydro-alcohol mixtures, based on PSi nanotechnology. Faster time analysis can be obtained by integrating the silicon–glass sensor for LOC applications by merging the PSi and AB technologies.

## 2. Materials and methods

For this study, we fabricated a $\lambda/2$ Fabry–Perot optical microcavity sandwiched between two Bragg reflectors of seven periods each, realized by alternating layers with high and low refractive indices. The porous silicon microcavity (PSMC) was obtained by electrochemical etch in a HF-based solution (50 wt% HF:ethanol = 1:1) in dark light and at room temperature. A current density of 400 mA cm$^{-2}$ for 0.8 s was applied to a highly doped p$^{+}$-type standard silicon wafer, $\langle 100 \rangle$ oriented, with 10 m$\Omega$ cm resistivity, 400 $\mu$m thick, producing the high-refractive index layer (with a porosity of 75%), while a current density of 80 mA cm$^{-2}$ was applied for 1.9 s in the case of the low-index layer (with a porosity of 67%). The $\lambda/2$ layer is a low-refractive-index one. This structure has a characteristic resonance peak at 1110 nm in the middle of a 280 nm wide stop band. To ensure the infiltration of aqueous solution, the device, which (as etched) is hydrophobic due to the presence of SiH bonds on its surface, was made hydrophilic by thermal oxidation at 1000 °C for 30 min. The optical set-up required for our sensing experiments was very simple (see figure 1). The PSMC was placed in a test chamber equipped with a glass window. A white light source interrogated the sensor through an optical fibre and a collimator. The reflected beam was collected by an objective, coupled into

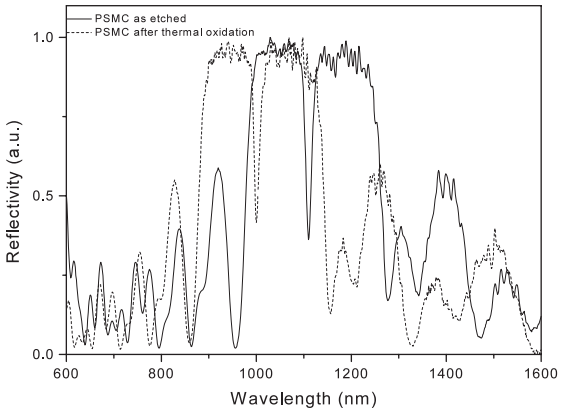


**Figure 2.** Optical spectra of the PSMC as etched and after thermal oxidation.

a multimode fibre, and then directed in an optical spectrum analyser (Ando model AQ6315A). The reflectivity spectra were measured over the range 600–1600 nm with a resolution of 0.2 nm. We studied the resonance peak shift on exposure to an ethanol/deionized water (DI) binary mixture at different concentrations, placing a drop of solution in the test chamber. Due to the capillary condensation of the solution vapours into the pores of the PSMC, a change in its reflectivity spectrum was observed: the partial substitution of air by liquid in each layer determines an increase of the average refractive index of the microcavity and, consequentially, a red shift of the spectrum. Measurements are stored when equilibrium conditions are reached, i.e. when the signal does not change any more in time. The phenomenon is completely reversible and reproducible.

## 3. Experimental results and discussion

In figure 2, the reflectivity spectra of the PSMC as etched and after thermal oxidation are reported. The oxidation process causes a blue shift in the spectrum of 110 nm due to the lower value of the $SiO_2$ refractive index ($n_{SiO_2} \approx 1.45$) with respect to the Si refractive index ($n_{Si} \approx 3.6$). We have not observed degradation in cavity quality ($Q = \lambda/\Delta\lambda \approx 70$ in both cases).

A very simple method, commonly used in analytical chemistry, in quantitative determinations of binary mixtures is the external standard method: calibration curves can be obtained by measuring the parameter under monitoring, such as an optical intensity, while the content of one component varies between 0 and 100%. In our case, the curve has been obtained by plotting the peak shift measured as a function of the volume percentage of ethanol in the binary mixture, as shown in figure 3. The errors on the experimental points are the standard deviations on five measurements, using the same chip and the same hydro-alcohol solution. After the calibration, unknown concentrations of the same mixture can be quantitative determined with a single measurement of the peak shift: the volume concentrations of both components can be picked out from the curve obtained by interpolating the experimental calibration data. In order to limit the wide error bars and the time necessary for the PSMC to reach equilibrium with the mixture (by limiting the volume), integration in a single chip of the device is proposed.

The compatibility of the porous silicon technology with the standard integrated circuit fabrication processes allows the design of complex microsystems in which the porous silicon

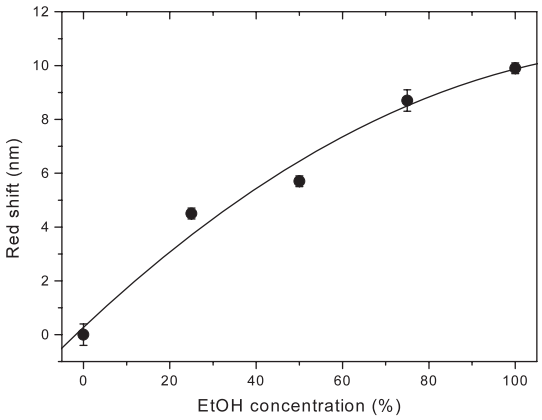


**Figure 3.** The calibration curve in case of an ethanol/DI binary mixture.

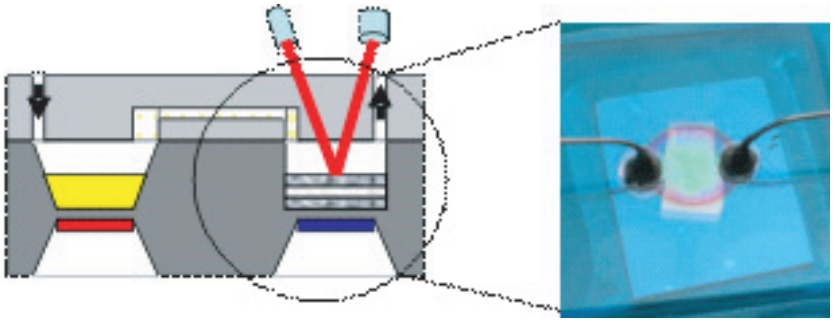

**Figure 4.** Sketch of the alcohol microsensor.

optical device is the transduction element. In figure 4, we report a rough and somehow intuitive sketch of the alcohol microsensor. The PSMC can be integrated in an LOC consisting of two $\mu$-chambers thermally controlled by integrated heaters, and sealed by a cover glass after the anodic bonding process. The mixture is injected in the left $\mu$-chamber by means of an appropriate microsyringe and here the integrated heater induces the hydro-alcohol mixture evaporation. The vapours produced diffuse and reach the second $\mu$-chamber, cooled by another integrated element, where the PSMC is and the capillary condensation happens.

## 4. Numerical calculations

Before proceeding towards the real fabrication steps of the whole device depicted in figure 4, it is mandatory to simulate its thermal behaviour since this is one of the key features in the measurement process. The precision and the accuracy in the quantitative determination of the mixture concentration strongly depend on the thermodynamic parameters such as the equilibrium time, i.e. the time required to have the same evaporation and condensation into the PSMC, and the temperature distribution in each layer used to realize the LOC. In order to simulate the thermal response of the device, a finite element model has been implemented with the commercial FEM code ANSYS Multiphysics 9.0 [7]. We have restricted the analysis to a two-dimensional (2D) model corresponding to the device middle cross section sketched (not to scale) in figure 4. Ignoring the minimal border effects at the device ends, a temperature

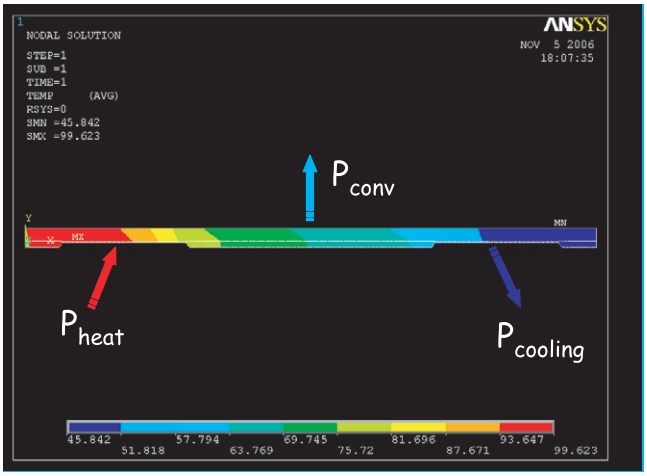


**Figure 5.** Temperature distribution in the device when the tank $\mu$-chamber is heated with a power density of 1.0 W cm$^{-2}$.

**Table 1.** Physical parameters for lab-on-chip materials used in thermal simulations.

| Material | Thermal conductivity (W m$^{-1}$ K$^{-1}$) | Density (kg m$^{-3}$) | Specific heat (J kg$^{-1}$ K$^{-1}$) |
|---|---|---|---|
| Silicon | 156 | 2640 | 917 |
| Glass | 1.05 | 2500 | 840 |
| Water | 0.58 | 1000 | 4186 |
| Air | 0.025 | 1.225 | 1005 |

gradient in fact exists only in this plane. This hypothesis can be justified by the observation that, for the proposed geometry, the aspect ratio between its width (46 mm) and thickness (1.5 mm) is about 1/30. Of course, a full 3D model could be more accurate, though it is very time consuming during the FEM analysis. The structure has been meshed with 2242 *isoparametric* linear elements of the type *plane 55*, with a mesh refinement in the active regions of the device. In table 1 we have reported the main physical parameters of the materials used for ANSYS thermal simulations.

The results of the numerical simulations depend on the boundary conditions fixed: we have supposed a natural convective heat exchange on the upper face of the glass slide which is in contact with air at 20 °C. We have assumed an exchange coefficient of 27 W m$^{-2}$ K$^{-1}$ [8]. Lateral and lower surfaces have been considered adiabatic; this model could be a good approximation of a device mounted on a plastic case. The lower surface of the left $\mu$-chamber, which is our tank for the liquid substance, is kept hot at constant temperature by a heater element. The right $\mu$-chamber is cooled by a Peltier $\mu$-cell with a maximum heat flux equal to 0.4 W cm$^{-2}$ (i.e. micro modules from TE Technology Inc., USA). In figure 5 we report the 2D steady-state thermal distribution, when the tank chamber is heated with a power density of 1.0 W cm$^{-2}$, corresponding to a maximum temperature on the hot side of about 100 °C. From this calculation it is clear that the PSMC region reaches a temperature of about 50 °C, which is a little bit higher of the evaporation temperature of ethanol; in this case the alcohol cannot condense inside the pores of the PSMC.

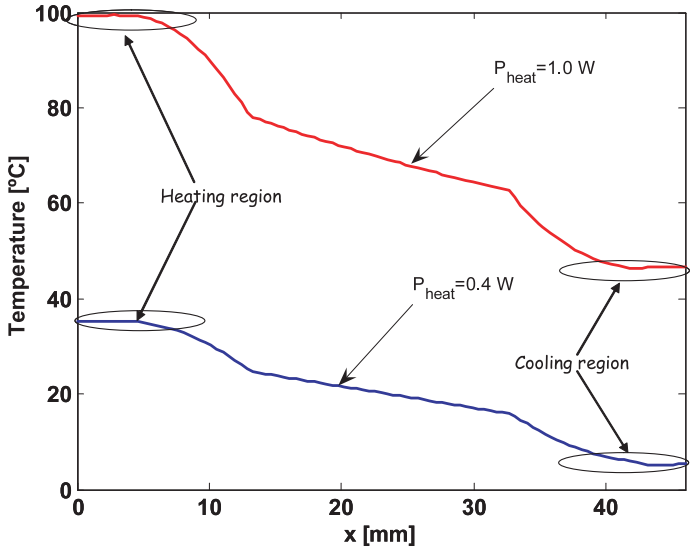


**Figure 6.** Temperature distribution versus the lateral dimension of the device for two different heating power densities.

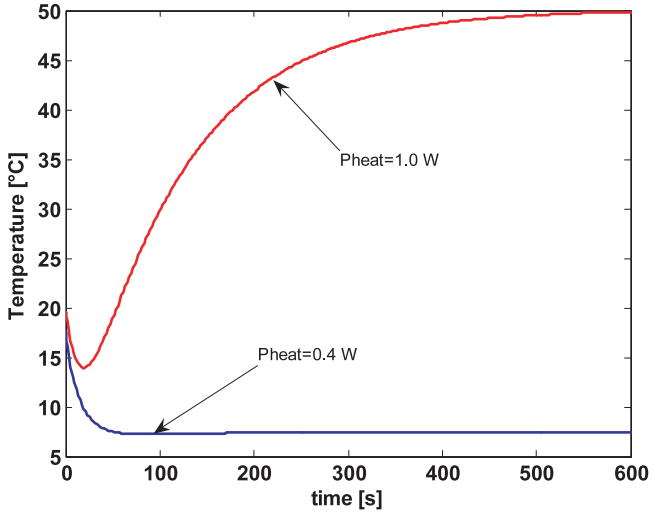


**Figure 7.** Temperature dynamic in the condensation chamber for two different heating power densities.

We have repeated the simulation considering a lower heating power density, 0.4 W cm$^{-2}$, corresponding to heating the tank $\mu$-chamber to 35 °C. In this case, the PSMC is cooled, thanks to the Peltier module, at about 5 °C: the analysis chamber temperature decreases quite linearly with the heat source temperature, as expected. These results are shown schematically in figure 6, where the 1D lateral temperature distribution, calculated at the silicon–glass interface, is reported versus the lateral dimension of the device for the two different heating power densities. We have also calculated the PSMC average temperature as a function of time for the two different heating power densities. The transient solver *Antype4* was used to perform

the analysis, using the *multi load-step method* provided in the code. From the plot in figure 7, it is well evident that, in the case of a heating power of 0.4 W $cm^{-2}$, the porous silicon–vapour system is at thermal equilibrium after about 50 s. In contrast, if we apply a heating power of 1.0 W $cm^{-2}$, a much longer time is necessary.

## 5. Conclusions

We have presented a simple and well performing optical sensor for ethanol/DI binary mixture analysis, based on PSMC. Due to capillary condensation, the reflectivity spectrum of the device shifts towards higher wavelengths on exposure to vapours. The shift is characteristic of the concentration of each component of the mixture. The sensing process is completely reversible. In order to limit the time needed for the PSMC to reach equilibrium with the mixture, we have proposed the integration of the device in a single chip that is thermally controlled. The thermal behaviour of the designed LOC has been studied by proper FEM numerical calculations.

## References

[1] Dancil K-P S, Greiner D P and Sailor M J 1999 *J. Am. Chem. Soc.* **121** 7925–30
[2] De Stefano L, Moretti L, Rossi A M, Rocchia M, Lamberti A, Longo O, Arcari P and Rendina I 2004 *IEEE Trans. Nanotech.* **3** 49–54
[3] Herino R, Bomchil G, Barla K, Bertrand C and Ginoux J L 1987 *J. Electrochem. Soc.* **134** 1994–2000
[4] Theiss W 1997 *Surf. Sci. Rep.* **29** 95–192
[5] Malecki K and Della Corte F G 2005 *Proc. Micromachining and Microfabrication Process Technology X*; *SPIE* **5715** 180–9
[6] De Stefano L, Malecki K, Della Corte F G, Moretti L, Rea I, Rotiroti L and Rendina I 2006 *Sensors* **6** 680–7
[7] Ansys 9.0 user manual see http://www.ansys.com
[8] Sturm J C, Wilson W and Iodice M 1998 *IEEE J. Sel. Top. Quantum Electron.* **4** 75–82

Extremophiles
DOI 10.1007/s00792-006-0058-6

ORIGINAL PAPER

# Enzymes and proteins from extremophiles as hyperstable probes in nanotechnology: the use of D-trehalose/D-maltose-binding protein from the hyperthermophilic archaeon *Thermococcus litoralis* for sugars monitoring

**Luca De Stefano · Annalisa Vitale · Ilaria Rea · Maria Staiano · Lucia Rotiroti · Tullio Labella · Ivo Rendina · Vincenzo Aurilia · Mose' Rossi · Sabato D'Auria**

Received: 30 October 2006 / Accepted: 29 November 2006
© Springer 2007

**Abstract** The D-trehalose/D-maltose-binding protein (TMBP), a monomeric protein of 48 kDa, is one component of the trehalose and maltose (Mal) uptake system. In the hyperthermophilic archaeon *Thermococcus litoralis*, this is mediated by a protein-dependent ATP-binding cassette system transporter. The gene coding for a thermostable TMBP from the archaeon *T. litoralis* has been cloned, and the recombinant protein has been expressed in *E. coli*. The recombinant TMBP has been purified to homogeneity and characterized. It exhibits the same functional and structural properties as the native one. In fact, it is highly thermostable and binds sugars, such as maltose, trehalose and glucose, with high affinity. In this work, we have immobilized TMBP on a porous silicon wafer. The immobilization of TMBP to the chip was monitored by reflectivity and Fourier Transformed Infrared spectroscopy. Furthermore, we have tested the optical response of the protein-Chip complex to glucose binding. The obtained data suggest the use of this protein for the design of advanced optical non-consuming analyte biosensors for glucose detection.

**Keywords** Trehalose/maltose-binding protein · Biosensors · Porous silicon · Glucose · Diabetes · Archaeon

Communicated by D. A. Cowan.

The authors wish to dedicate this work to Prof. Ignacy Gryczynski, University of North Texas, TX, USA, for his outstanding contribution to the development of new sensing methodologies.

L. De Stefano · I. Rea · L. Rotiroti · I. Rendina
Istituto di Microelettrica e Microsistemi, CNR, Napoli, Italy

A. Vitale · M. Staiano · T. Labella · V. Aurilia · M. Rossi · S. D'Auria (✉)
Istituto di Biochimica delle Proteine, CNR,
Via Pietro Castellino 111, 80131 Napoli, Italy
e-mail: s.dauria@ibp.cnr.it

## Introduction

The general interest in biomolecules, isolated from thermophilic organisms was originally due to the biotechnological advantages offered by the utilization of these highly stable molecules in industrial processes (Brock 1985). In fact, enzymes and proteins isolated from thermophilic microorganisms exhibit a high stability in conditions usually used to denature proteins: high temperature, ionic strength, extreme pH-values, elevated concentration of detergents and chaotropic agents (Jaenicke 1994). In addition to the potential industrial applications, it is important to highlight that proteins and enzymes that are stable and active over 100°C represent good models to shed light on the molecular adaptation of life at high temperature (D'Auria et al. 1998).

The D-trehalose/D-maltose-binding protein (TMBP) is one component of the trehalose (Tre) and maltose (Mal) uptake system, which, in the hyperthermophilic archaeon *Thermococcus litoralis*, is mediated by a protein-dependent ATP-binding cassette (ABC) system transporter (Xavier 1996). TMBP from *T. litoralis* is a monomeric 48 kDa two-domain macromolecule containing 12 tryptophan residues (Diez et al. 2001). TMBP shares common structural motifs

with a number of other sugar-binding proteins. This class of biomolecules is composed of proteins, whose structure consists of two globular domains connected by a hinge region made of two or three short peptide segments. The two domains are formed by non-contiguous polypeptide stretches and exhibit similar tertiary structure. The ligand-binding site is located in the deep cleft between the two domains and the binding is accompanied by a movement of the two lobes as well as by conformational changes in the hinge region (Sun et al. 1998).

The gene coding for the thermostable TMBP from the archaeon *T. litoralis* has been cloned, and the recombinant protein has been expressed in *E. coli* (Horlacher et al. 1998). The recombinant TMBP has been purified to homogeneity and characterized. It exhibits the same functional and structural properties as the native one (Horlacher et al. 1998).

In a recent work (Herman et al. 2006), we have investigated the binding of several sugars to TMBP by time-resolved fluorescence spectroscopy, and molecular dynamics methods. We found that TMBP is also able to bind glucose molecules. Since human blood does not contain Tre and Mal, it is not outrageous to envisage the use of the TMBP as a probe for the design of a minimally invasive biochip for glucose detection.

In this work, we have extended our investigation on the utilization of TMBP for sensing glucose by immobilizing the protein on a porous silicon chip. The TMBP-based chip has been characterized and tested as regards the response to glucose. The obtained results are discussed.

## Materials and methods

D-Glucose and all the other chemicals used in the present study were from Sigma. All commercial samples were of the best available quality.

### Purification of TMBP and protein concentration determination

An mount of 20 g wet weight of the *E. coli* cell pellet containing the expressed TMBP were resuspended in 50 mM Tris–HCl, pH 7.5, 500 mM NaCl (100 ml), ruptured by a French pressure cell at 16,000 psi, and centrifuged for 15 min at 19,000 *g*. The supernatant was heated to 90°C for 20 min and centrifuged for 15 min at 19,000 *g*. The supernatant was collected and dialyzed for 12 h against 10 mM Tris–HCl, pH 7.5 at 4°C. The solution was loaded onto a DEAE column previously equilibrated in 10 mM Tris–HCl, pH 7.5. After washing the column with 10 mM Tris–HCl, pH 7.5, TMBP was eluted by a NaCl gradient (0.0–1.0 M NaCl). Centricon 30 concentrator (Amicon, MA, USA) was used to concentrate and to dialyze TMBP against 10 mM Tris–HCl, pH 7.5. The purified protein was passed through a Blue A affinity column (Amersham, NJ, USA) in order to obtain DNA-free TMBP. The purity of TMBP was verified by SDS-PAGE and absorption spectra.

The protein concentration was determined by the method of Bradford (Bradford 1976) with bovine serum albumin as standard on a double beam Cary 1E spectrophotometer (Varian, Mulgrade, Victoria, Australia).

### Chip preparation and spectroscopic characterization

In this study, we used as sensor an apodized Bragg reflector obtained by alternating high (*A*) refractive index layers (low-porosity) and low (*B*) refractive index layers (high-porosity) whose thicknesses satisfy the following relationship: $n_A d_A + n_B d_B = m\ \lambda/2$, where $m$ is an integer and $\lambda$ is the Bragg resonant wavelength. The distributed Bragg reflector (DBR) was produced by electrochemical etch of a highly doped $p^+$-silicon, ⟨100⟩oriented, 0.04 Ω cm resistivity, 400 μm thick, in a HF-based solution. The silicon was etched using a 30 wt.%HF/ethanol solution in dark and at room temperature. Before anodization the substrate was placed in HF solution to remove the native oxide. A current density of 148 mA/cm$^2$ for 2.31 s was applied to obtain the low refractive index layer (effective refractive index $n_L \cong 1.505$, thickness $d_L \cong 598$ nm) with a porosity of 72%, while one of 110 mA/cm$^2$ was applied for 2.34 s for the high index layer ($n_H \cong 1.585$, thickness $d_H \cong 568$ nm) with a porosity of 69%. This structure is characterized by a first order ($m = 1$) resonance at 3,600 nm. In Fig.1, the experimental

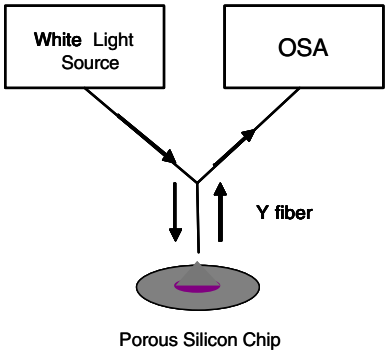


**Fig. 1** Experimental setup used to measure the optical reflectivity spectrum of porous silicon chip

setup, used to measure the reflectivity spectrum, is reported. We have used as source a white light directed on the porous silicon chip through a Y-fiber. The same fiber was used to guide the output signal to the optical spectrum analyzer. The spectrum was measured over the range 800–1,600 nm with a resolution of 0.2 nm. The porous silicon surface after electrochemical etching is hydrogenated and for this reason, very reactive and thermodynamically instable; in order to realize a sensor more stable and able to link the biological probes it is necessary to substitute the Si–H bonds with the Si–C or Si–O–C ones.

To promote a covalent link between the porous silicon and the TMBP, we have exploited a three-step functionalization process, based on the chemical passivation of the PSi surface after oxidation. We have first thermally treated the PSi DBR, in $O_2$ atmosphere, at 1,000°C for 30 min, to remove all the Si–H bonds and create an oxide layer on the pores' surface to assure the covalent attachment with a proper chemical linker, the minopropyltriethoxysilane (APTES). To this aim, we have rinsed by immersion the DBR in a 5% solution of APTES and a hydroalcoholic mixture of water and methanol (1:1), for 20 min at room temperature. After the reaction time, we have washed the chip with DI-water and methanol and dried in $N_2$ stream. The silanized device was then baked at 100°C for 10 min. The next step consists in creating a surface able to link the carboxylic group of the proteins: we have thus immersed the DBR in a 2.5% glutaraldehyde solution in 20 mM HEPES buffer (pH 7.4) for 30 min, and then rinsed it in DI-water and finally dried in $N_2$ stream. The glutaraldehyde reacts with the amino groups on the silanized surface and coats the internal surface of the pores with another thin layer of molecules.

We have monitored all the reaction steps by Fourier Transformed Infrared (FT-IR) Spectroscopy and the consequent modification of the optical response of the PSi device by reflectivity spectroscopy.

The modified surface obtained works as an active substrate for the chemistry of the following attachment of the protein: we have spotted on the PSi chip 20 μl of 7.5 μM sodium bicarbonate buffer (pH 7.35) containing a rhodamine labeled TMBP and incubated the system at –4°C overnight. Even if our aim is the realization of a label-free optical biosensor based on the PSi nanotechnology, we have used a fluorescent protein to control the distribution of the biological matter on the chip surface and to test the chemical stability of the covalent link between the TMBP and the PSi surface.

After this assessment phase, we have also optically detected the ligand-binding interaction by following the wavelength shift of the reflectivity spectrum. The experimental measurement of the TMBP–glucose binding is a two step procedure: first, we have registered the optical spectrum of the porous silicon layer after the TMBP immobilization on the DBR surface and after the Glucose solution has been spotted on it.

## Results

In Fig. 2, we have reported the optical spectra of our device as etched and after each step of the chemical

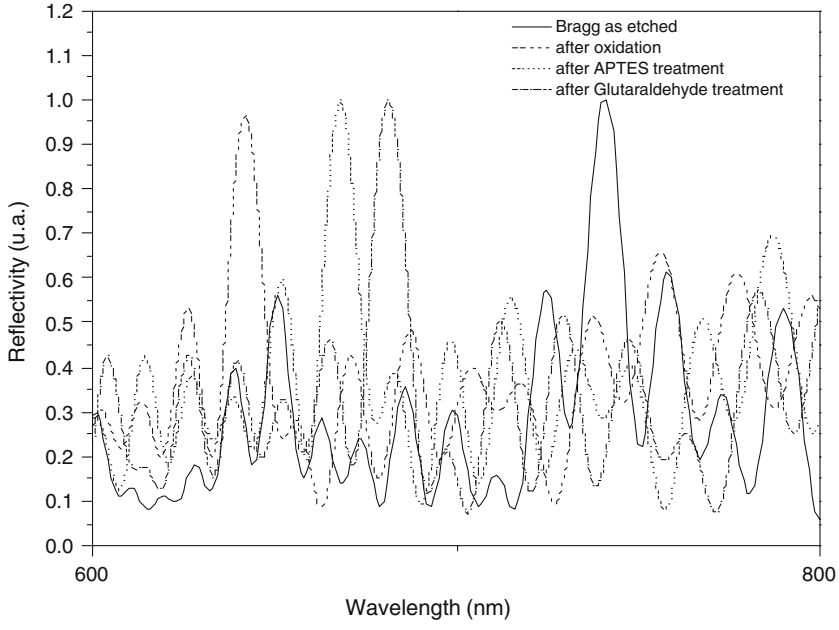


**Fig. 2** Optical reflectivity spectrum of the Bragg reflector as-etched (*continues curve*), after oxidation (*dashed curve*), after APTES treatment (*dot curve*) and after glutaraldehyde treatment (*dot-dashed curve*)

treatment in the range 600–800 nm, where the $m = 5$ Bragg resonance peak at about 720 nm is present. The oxidation process causes a blue shift of the reflectivity spectrum of 99.5 nm due to the lower value of the $SiO_2$ refractive index ($n_{oxi} \cong 1.5$)with respect to the Si refractive index ($n_{Si} \cong 3.2$). On the contrary, the silanisation steps by APTES and glutaraldehyde produce red shifts of the reflectivity spectrum of 28 and 17 nm, respectively, corresponding to an increasing of the average refractive index of the layers due to a filling of the pores by the organic layers.

Since the protein distributes uniformly on the pores surface, the TMBP attachment causes a new detectable red shift of only 9 nm in the reflectivity spectrum.

The FT-IR spectra of the oxide PSi sample and after the silanization process are reported in Fig. 3: the main characteristic peaks of silicon dioxide (at 1,124 $cm^{-1}$), of the APTES amino groups (at 3,300 and 3,352 $cm^{-1}$) and of gluteraldehyde cyano group (at 1,404 $cm^{-1}$) are easily recognized.

In Fig. 4a, is shown the DBR observed by a Leica Z16 APO fluorescence macroscopy system after incubation. By illuminating the chip spotted with the labeled protein by a 100 W high-pressure mercury source, we found that the fluorescence is very high and homogeneous on the whole surface. We have also qualitatively tested the strength of covalent bond between the protein and the porous silicon surface by washing the device in a dialysis membrane overnight in DI-water. Since the fluorescent intensities differ of only few counts, we can conclude that the PSi-TMBP double layer is very stable.

We have also measured the signal response to the glucose concentration after the interaction with the protein in a range between 10 and 150 μM. The maximum shift of the Bragg wavelength is 1.2 nm. Figure 5 shows the dose–response curve to glucose additions. The estimated sensitivity of the TMBP-Chip is 0.03 nm/μM. Interestingly, the concentration of glucose that induces a optical response of the protein is very close to the amount of the sugar present in the human interstitial fluids. This result suggests the use of this protein in designing of a non-consuming and minimally invasive biosensor for the

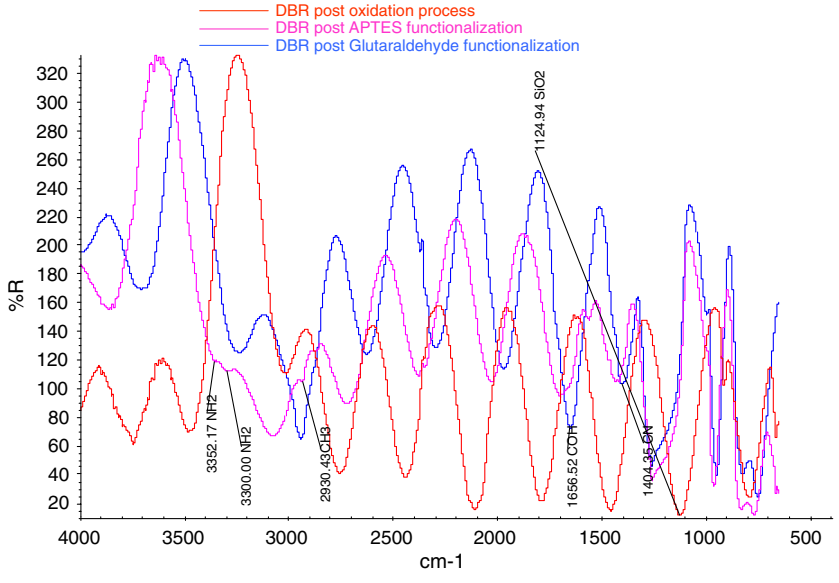


**Fig. 3** FT-IR spectra of the Bragg reflector after oxidation and APTES/ glutaraldehyde treatment

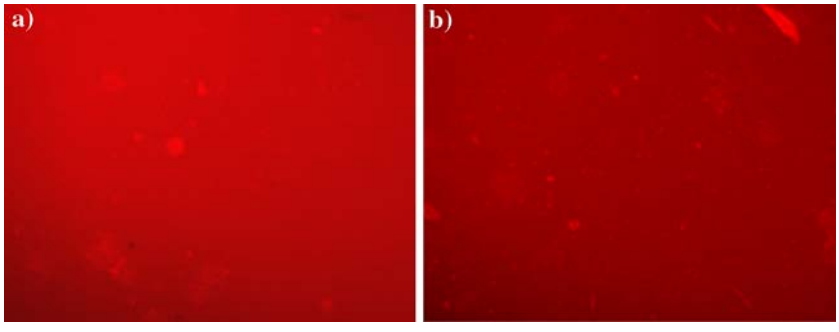


**Fig. 4** **a** Porous silicon chip after incubation with the labeled-TMBP. **b** Porous silicon chip after washings in demi-water

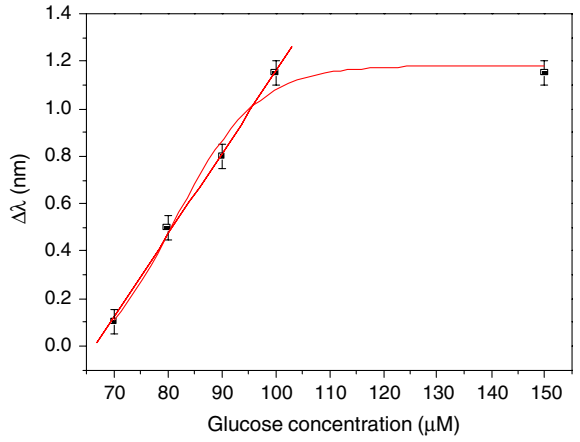


**Fig. 5** Dose–response curve for PSi DBR optical sensor exposed to several concentration of glucose

continuous detection of the level of glucose in diabetic patients.

In conclusion, we have reported an effective methodology for the covalent immobilization of proteins from extremophiles on a nanostructured material, such as porous silicon wafer, that can be utilized as general platform for the development of very stable protein-based arrays for analyses of high social interest.

**Acknowledgments** The authors thank Dr. Fabienne Chevance, University of Utah, Salt Lake City, USA, and Prof. Winfried Boos, University of Konstanz, Germany, for supplying a partially purified protein sample. This work is in the frame of the project ''Diagnostica Avanzata ed Alimentazione'' CNR Commessa of the Agro-Food Department (SD). This work was also supported by the ASI project MoMa No. 1/014/06/0 (SD) and by a grant from the Ministero degli Affari Esteri, Direzione Generale per la Promozione e la Cooperazione Culturale (SD).

## References

Bradford MM (1976) A rapid and sensitive method for the quantitation of microgram quantities of protein utilizing the principle of protein-dye binding. Anal Biochem 72:248–254

Brock TD (1985) Life at high temperatures. Science 239:132–138

D'Auria S, Moracci M, Febbraio F, Tanfani F, Nucci R, Rossi M (1998) Structure-function studies on *β*-glycosidase from *Sulfolobus solfataricus*. Molecular bases of thermostability. Biochemie 80:949–957

Diez J, Diederichs K, Greller G, Horlacher R, Boos W, Welte W (2001) The crystal structure of a liganded trehalose/maltose-binding protein from the hyperthermophilic archaeon *Thermococcus litoralis* at 1.85 A. J Mol Biol 305:905–915

Herman P, Staiano M, Marabotti A, Varriale A, Scirè A, Tanfani F, Vecer J, Rossi M, D'Auria S (2006) D-Trehalose/D-maltose-binding protein from the hyperthermophilic archaeon *Thermococcus litoralis*: The binding of trehalose and maltose results in different protein conformational states. Proteins Struct Func Bioinform 63:754–767

Horlacher R, Xavier KB, Santos H, DiRuggiero J, Kossmann M, Boos W (1998) Archaeal binding protein-dependent ABC transporter: molecular and biochemical analysis of the trehalose/maltose transport system of the hyperthermophilic archaeon *Thermococcus litoralis*. J Bacteriol 180:680–689

Jaenicke R (1994) Studies on hyperstable proteins: crystallins from the eye-lens and enzymes from thermophilic bacteria. In: Doniach S (ed) Statistical mechanics, protein structure, and protein substrate interactions. Plenum, New York, pp 49–62

Sun YJ, Rose J, Wang BC, Hsiao CD (1998) The structure of glutamine-binding protein complexed with glutamine at 1.94 angstrom resolution: comparisons with other amino acid binding proteins. J Mol Biol 278:219–222

Xavier KB, Martins LO, Peist R, Kossmann M, Boos W, Santos H (1996) High-affinity maltose/trehalose transport system in the hyperthermophilic archaeon *Thermococcus litoralis*. J Bacteriol 178:4773–4777

*Sensors* **2008**, *8*, 1-x manuscripts; DOI: 10.3390/sensors

**sensors**

**ISSN 1424-8220**
www.mdpi.com/journal/sensors

*Article*

# Porous Silicon Based Resonant Mirrors for Biochemical Sensing

**Edoardo De Tommasi [1,*], Luca De Stefano [1], Ilaria Rea [1, 2], Valentina Di Sarno [1, 2], Lucia Rotiroti[1, 3], Paolo Arcari [4], Annalisa Lamberti [4], Carmen Sanges [4] and Ivo Rendina [1]**

[1] Institute for Microelectronics and Microsystems – Unit of Naples – National Council of Research, Via P. Castellino 111, 80131 Napoli, Italy.
[2] Department of Physical Sciences, University of Naples "Federico II", Via Cinthia, 80126 Naples, Italy
[3] Department of Organic Chemistry and Biochemistry, University of Naples "Federico II", Via Cinthia, 80128 Napoli, Italy
[4] Department of Biochemistry and Medical Biotechnologies, University of Naples "Federico II", Via S. Pansini 5, 80131 Napoli, Italy.

* Author to whom correspondence should be addressed: edetommasi@na.imm.cnr.it

*Received: 14 Oct 2008; in revised form: 6 Oct 2008 / Accepted: 21 Oct 2008 / Published:*

---

**Abstract:** We report on our preliminary results in the realization and characterization of a porous silicon (PSi) resonant mirror (RM) for optical biosensing. We have numerically and experimentally studied the coupling between the electromagnetic field, totally reflected at the base of a high refractive index prism, and the optical modes of a PSi waveguide. This configuration is very sensitive to changes in the refractive index and/or in thickness of the sensor surface. Due to the high specific area of the PSi waveguide, very low DNA concentrations can be detected confirming that the RM could be a very sensitive and label-free optical biosensor.

**Keywords:** DNA Optical Biosensors, Porous Silicon, Resonant Mirrors.

---

## 1. Introduction

Optical label-free biosensors are ideal candidates for high throughput screening in the prevention of bio-threat agents or social illnesses: all the different configurations proposed in the literature, such as optical microcantilever [1], interferometric devices [2, 3], and also the recent photonic crystals geometries [4], show very high sensitivities in the recognition of specific molecules. The detection of

analytes present in complex mixtures in ultra-low concentration, such as viruses in human blood, is possible due to two key factors: the utilization of bioprobres, properly linked on the sensor surface, and an optimized design to maximize the interaction between the biological matter and the electromagnetic field.

Resonant Mirrors (RMs) are optical sensors which exploit the evanescent fields features to probe changes in refractive index and thickness taking place on their surface after exposure to gaseous or liquid substances. From the optical point of view, RMs are refractometric sensing devices similar to grating coupler sensors: they are characterized by the high sensitivity typical of waveguiding devices, and, on the other hand, by the simple scheme of Surface Plasmon Resonance (SPR) sensors [5]. In RMs, in fact, incident light gives rise to an evanescent wave at the interface between a prism and an optical waveguide; the coupling of light into the waveguide occurs only at those specific incident angles for which the propagation constant of the evanescent wave matches that of a waveguide mode. This matching produces a dip in the angular spectrum of the reflected light, so that each change in the refractive index and-or in thickness at the sensor surface produces a corresponding shift in the position of the dip [5, 6].

In this work, we report on the realization of a porous silicon (PSi) based RM prototype on chip, whose modal properties and characteristic angular resonances have been both numerically computed and experimentally measured.

PSi is by far one of the most intriguing material in optical sensing: the refractive index is widely tuneable, namely between the silicon refractive index and that of the air, and its specific surface is very large, up to 500 $m^2 cm^{-3}$. Due to these characteristics, lot of optical structures, such as rugate filters [7] and microcavities [8] have been proposed in literature for biosensing. Recently, a PSi waveguide biosensor have been theoretically and experimentally demonstrated [9]. We have studied and reported in this paper the feasibility of such biosensor for DNA-DNA hybridization experiment.

**Figure 1**. Experimental setup. DL: diode laser emitting s-polarized radiation at 785 nm; L: lens with focal length f=7.5 cm; RM: resonant mirror; RS: rotation stage; PM: power meter on an independent rotation stage.

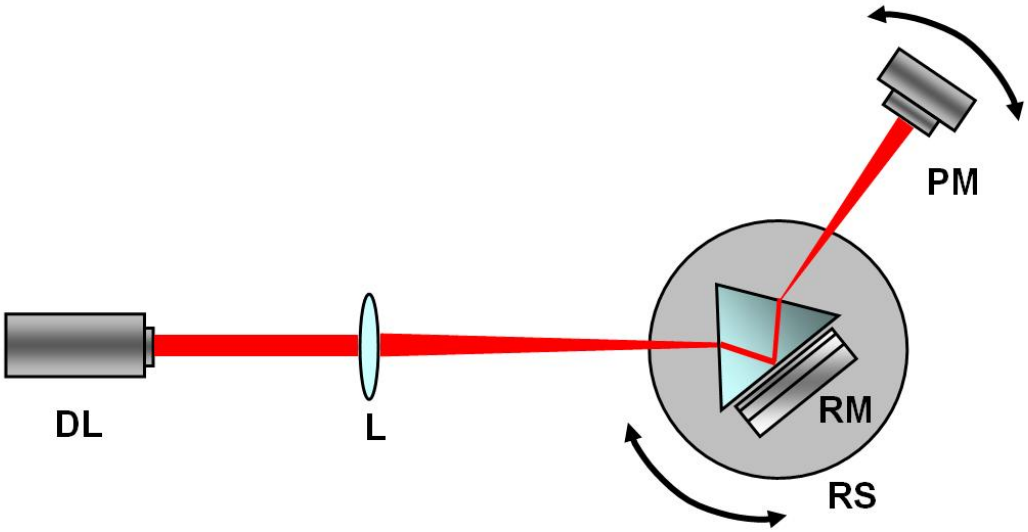

## 2. Experimental

A highly doped p+-silicon, <100> oriented, 0.01 Ω·cm resistivity, 400 μm thick was used as substrate in the waveguide fabrication. The structure was obtained by electrochemical etching of crystalline silicon in a HF-based solution (50 wt. % HF:ethanol = 3:7) at room temperature. A current density of 10 mA/cm$^2$ was applied for 18.9 s to produce the core layer of thickness 2.5 μm and porosity 65 %, while a current density of 109 mA/cm$^2$ was applied for 13.6 s in the case of the cladding layer with thickness 2.5 μm and porosity 78 %. These porosities correspond to a core and cladding refractive indexes of 1.749 and 1.384, respectively, calculated by the Bruggeman model [10] at a wavelength of 785 nm. The device was then fully oxidized in pure $O_2$ by a two step thermal treatment (400 °C for 30 min and 900 °C for 15 min).

In Figure 1 a wide view of our experimental set-up is shown. RM is mounted on a rotation stage (Melles Griot, model 07 TRS 501); the light source is a diode laser emitting s-polarized radiation at λ=785 nm (CrystaLaser, model RCL-080-785-5); the laser beam exiting the prism is collected by a photometer (Newport, model 1830-C). The waveguide has been brought in close contact with one side of an SF6 prism (n=1.784), still allowing the presence of a sub-micrometric air layer acting as a coupling zone between the prism and the waveguide.

The covalent bond of the DNA single strand (5'-GGACTTGCCCGAATCTACGTGTCC-3') on the PSi surface is based on a three steps functionalization process constituted by a chemical passivation of the surfaces, as it is shown in Figure 2 (all the chemicals used in the present study were from Sigma). We have treated the surfaces with a proper chemical linker, the aminopropyltriethoxysilane (APTES). Samples have been rinsed by dipping in a 5 % solution of APTES and a hydroalcoholic mixture of water and methanol (1:1) for 20 min at room temperature. After the reaction time, we have washed the chips by deionized water and methanol, and dried in $N_2$ stream. The silanized devices were then baked at 100 °C for 10 min. To create a surface able to link the amino group of the biological probes, we have thus immersed the chips in a 2.5% glutaraldehyde (GA) solution in 20 mM HEPES buffer (pH 7.4) for 30 min, and then rinsed it in deionized water and finally dried in $N_2$ stream. The GA reacts with the amino groups on the silanized surface and coats the internal surface of the pores with another thin layer of molecules. All these reaction steps have been monitored by means of FT-IR spectroscopy to verify the presence of the characteristic peaks of the organic linkers. The main characteristic peaks of Si-O-Si (1040 cm$^{-1}$) and Si-OH bonds (3740 and 1646 cm$^{-1}$) are present, after oxidation, on the PSi. After the silanization process, the APTES characteristic peaks of the ethylic (at 1626, 1529 and 1379 cm$^{-1}$), amino (at 1060 cm$^{-1}$) and also the –CH (at 2908 and 2851 cm$^{-1}$) groups are well evident. Finally, after the GA treatment, the characteristic imine group (at 1627 cm-1) due to the reaction with APTES is easily recognized.

The PSi surface was covered overnight at room temperature with a 50 μM DNA probe solution (30 μL). For each measurement, complementary (5'-GGACACGTAGATTCGGGCAAGTCC-3') and non-complementary (5'-CACTGTACGTGCGAATTAGGTGAA-3') DNA (10 μL) were spotted on the chip and incubated for two hours. Before optical measurements, all samples have been extensively rinsed in deionized water to remove the excess of biological matter.

**Figure 2**. Schematic of the functionalization process, from the oxidized PSi chip to the covalent attachment of the DNA single strands.

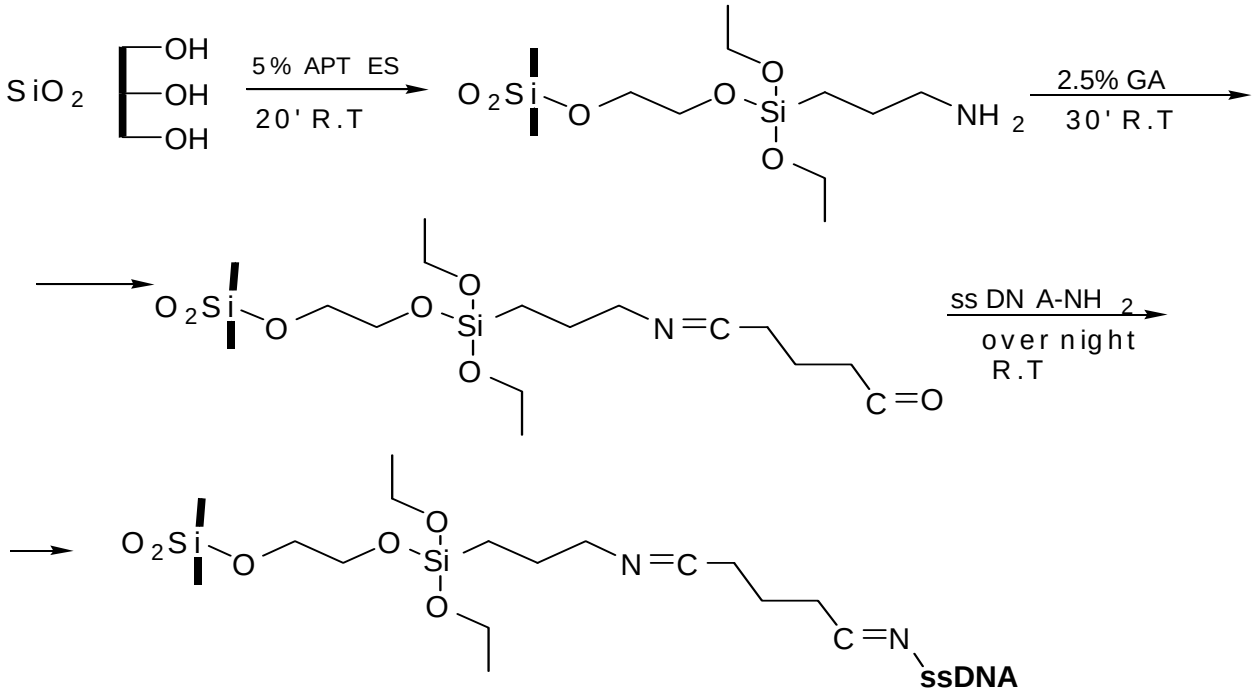


## 3. Results and Discussion

The PSi waveguide, once oxidized in order to reduce the scattering losses [11] and to allow the bond with biological linkers, has been characterized by means of "m lines" technique, which determines the modal behavior of the waveguide at different wavelengths and estimates the refractive indices $n_c$ and $n_b$ for the core an the buffer layers [12]. In Figure 3, is reported a standard m-lines spectrum due to the excitation of four adjacent modes in transverse electric (TE) polarization of the electromagnetic field at 785 nm: by measuring the coupling angles position is possible to quantify the core and cladding thicknesses and refractive indexes. We have obtained the refractive indexes of core and buffer and the thickness of the core equal to $n_c = 1.370 \pm 0.001$, $n_b = 1.18 \pm 0.01$, and $d_c = 2.71 \pm 0.01\mu m$ respectively. It is important to notice the strong reduction of the refractive indexes after the thermal oxidation process, mainly due to the substitution of silicon with silicon dioxide.

The close contact between the prism and the waveguide still allows the presence of a sub-micrometric air layer where the evanescent fields coming from the prism and the waveguide can overlap, thus transferring the light energy from the prism to the waveguide. The thickness of this air layer strongly affects the efficiency of the coupling of the incoming light into the waveguide. In Figure 4, some simulations of RM spectra corresponding to different air thicknesses are shown: the lower the thickness, the stronger the coupling of the evanescent wave with the waveguide. The dips present in the total reflection zone (i.e. for incident angle $\theta_i > 34°$ ), correspond to the characteristic modes propagating in the waveguide. The number of these modes can be obtained from the well known relation $M = \frac{2d}{\lambda}\sqrt{n_c^2 - n_b^2} \approx 5$, where $d$ stands for the thickness of the waveguiding layer.

**Figure 3.** Resonant peaks of the waveguide, corresponding to four guided modes in TE polarization at 785 nm, after functionalization with APTES and GA.

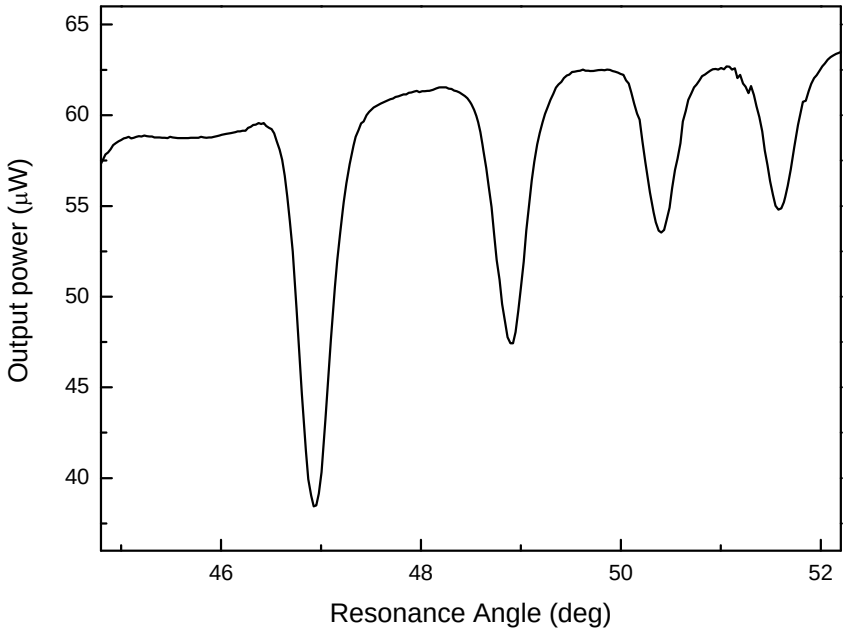


**Figure 4.** Numerical simulations of RM spectra as a function of the air gap thickness

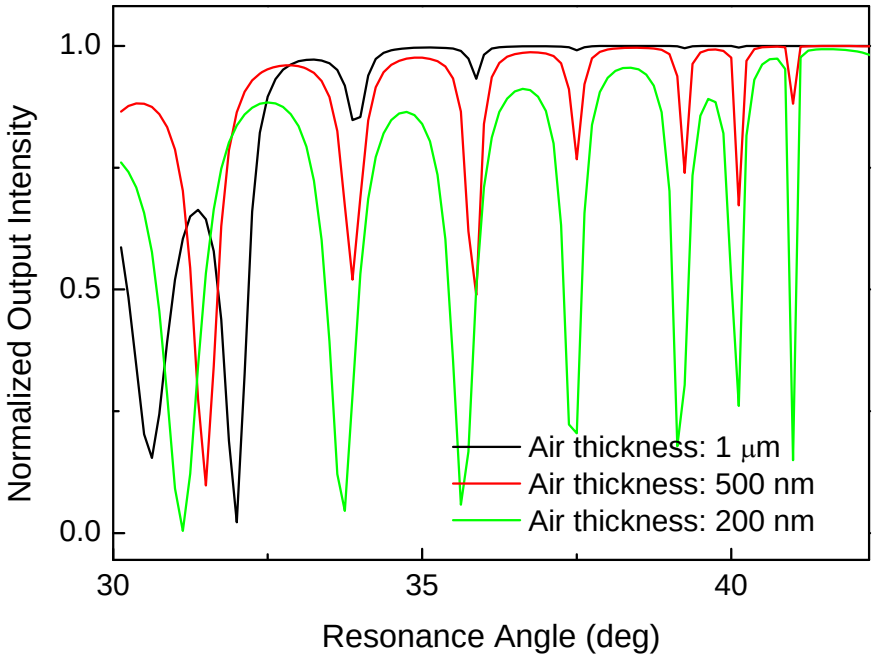


.

In Figure 5, the results of angular measurements after incubation with probe DNA and after two steps of the DNA hybridization process at two different concentrations are reported: the resonance shifts confirm the effectiveness of the DNA binding.

**Figure 5.** PSi RM resonances after functionalization with probe DNA and after two DNA hybridization steps: the coupling angle shifts demonstrate the molecular interaction between the probe DNA and its complementary target at different concentration.

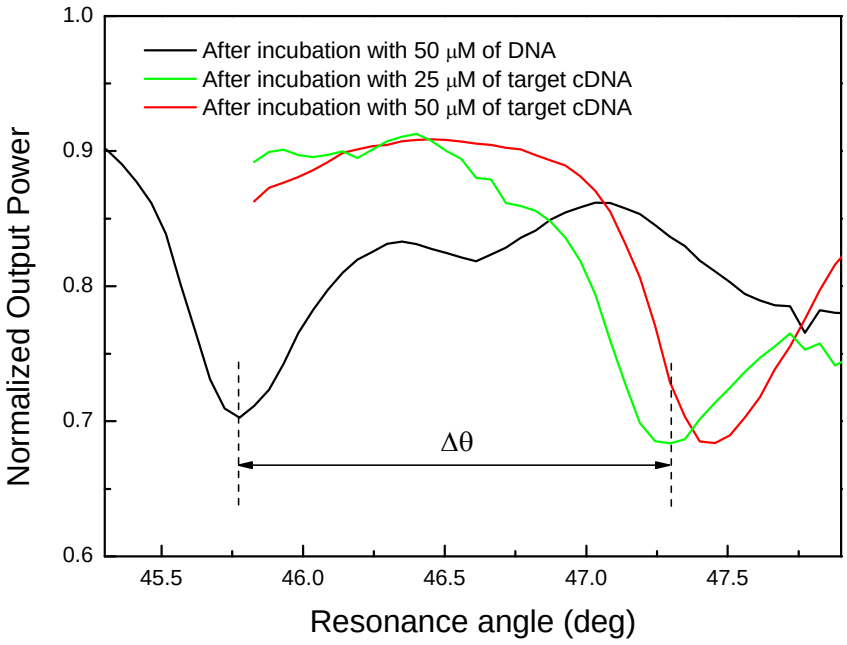


The coupling angle shifts as a function of the concentration of the complementary DNA, as it can be seen in Figure 6. The high efficiency of hybridization is confirmed by the fact that, after exposure to 50 μM of complementary DNA, the sensor response curve reaches a plateau, corresponding to a saturation of almost all of the active sites. The experimental points can be well fitted ($R^2$=0.99, $\chi^2$<1) by a molecular growth exponential curve: from this fit a sensitivity of 0.13±0.02 deg/μM can be estimated. Since the angular resolution of the experimental setup is 0.01 deg, we can estimate, for our measuring system, a technical limit of 77±12 nM. This value, that has been estimated from experimental data, is of the same order of magnitude of that reported in ref. [13], where a detection limit of 50 nM is predicted on the basis of numerical simulations and under the assumption of an optimal 50% probe coverage of the PSi surface. On exposure to the non complementary DNA sequence the angular resonance does not undergo any detectable shift, i.e. no shifts more than 0.01 deg can be observed. The width of the resonances (e.g. FWHM of about 0.37 deg for the first resonance) can be considerably reduced, thus increasing the sensitivity of the sensor, by reducing the waveguide losses, mainly due to the roughness of the structure. A dramatic reduction of these losses can be achieved, for example, by performing the etching process at low temperatures [14] and/or by making use of a mono-modal waveguide.

**Figure 6.** Resonance shifts of the waveguide mode coupling angle as a function of the DNA concentration.

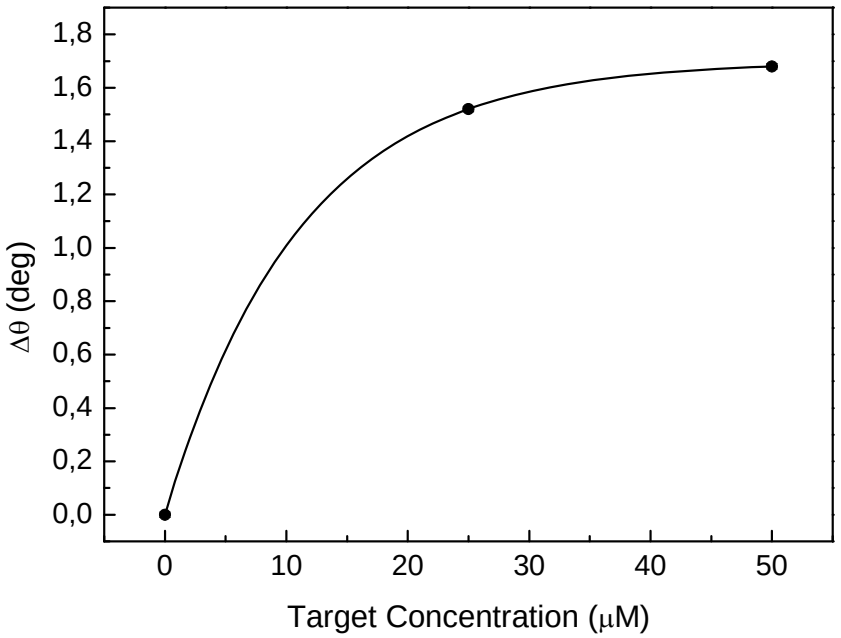


## 4. Conclusions

We have experimentally confirmed the ability of a PSi RM to detect a DNA-DNA hybridization process with very high sensitivity. The use of PSi technology in the fabrication of the waveguide, which is the heart of a RM sensor, allows the presence of a high specific-surface available for interaction with great amounts of analytes. We have demonstrated that our measuring system is characterized by a technical limit of about 80 nM of DNA, in good agreement with previously published theoretical calculations [13]. Next efforts will be aimed at the fabrication of a free-standing waveguide (no crystalline silicon substrate), which, in conjunction with a flow delivery system, could allow to reduce considerably the time of incubation of the DNA probe and targets over the functionalized surface.

## Acknowledgements

This work is partially supported by the FIRB Italian project RBLA033WJX_005.

## References and Notes

1. Lechuga, L.M.; Tamayo, J.; Álvarez, M.; Carrascosa, L.G.; Yufera, A.; Doldán, R.; Peralías, E.; Rueda, A.; Plaza, A.J.; Zinoviev, K.; Domínguez, C.; Zaballos, A.; Moreno, M.; Martínez-A, C.; Wenn, D.; Harris, N.; Bringer, C.; Bardinal, V.; Camps, T.; Vergenègre, C.; Fontaine, C.; Díaz, V.; Bernad, A. A highly sensitive microsystem based on nanomechanical biosensors for genomics applications. *Sensor. Actuat. B-Chem.* **2006**, *118*, 2-10.

2. Pacholski C.; Sartor M.; Sailor M. J.; Cunin F.; Miskelly G. M. Biosensing using porous silicon double-layer interferometers: Reflective interferometric fourier transform spectroscopy. *J. Am. Chem. Soc.* **2005**, *127*, 11636-11645.
3. De Stefano, L.; Rotiroti, L.; Rea, I.; Rendina, I.; Moretti, L.; Di Francia, G.; Massera, E.; Lamberti, A.; Arcari, P.; Sangez, C. Porous silicon-based optical biochips. *J. Opt. A-Pure Appl. Op.* **2006,** *8*, S540-S544.
4. Lee, M.R.; Fauchet, P.M. Two-dimensional silicon photonic crystal based biosensing platform for protein detection. *Opt. Express* **2007,** *15***,** 4530-4535.
5. Cush, R.; Cronin, J.M.; Stewart, W.J.; Maule, C.H.; Molloy, J.; Goddard, N.J. The resonant mirror: a novel optical biosensor for direct sensing of biomolecular interactions. I: Principle of operation and associated instrumentation. *Biosens Bioelectron*. **1993,** *8*, 347-353.
6. Baldini, F.; Chester, A.N.; Homola, J.; Martellucci, S. *Optical Chemical Sensors*. Springer: Dordrecht, The Netherlands, 2006.
7. Chapron, J.; Alekseev, S.A.; Lysenko, V.; Zaitsev, V.N.; Barbier, D. Analysis of interaction between chemical agents and porous Si nanostructures using optical sensing properties of infra-red Rugate filters. *Sensor. Actuat. B-Chem.* **2007**, *120*, 706-711.
8. Ouyang, H.; Chrtistophersen, M.; Viard, R.; Miller, B.L.; Fauchet, P.M. Macroporous silicon microcavities for macromolecule detection. *Adv. Funct. Mater.* **2005,** *15*, 1851-1859**.**
9. Saarinen, J.J.; Weiss, S.M.; Fauchet, P.M.; Sipe, J.E. Optical sensor based on resonant porous silicon structures. *Opt. Express* **2005,** *13*, 3754-3764.
10. Khardani, M.; Bouaïcha, M.; Bessaïs, B. Bruggeman effective medium approach for modelling optical properties of porous silicon: comparison with experiment. *Phys. Stat. Sol.* **2007**, *4*, 1986-1990.
11. Pirasteh, P.; Charrier, J.; Dumeige, Y.; Haesaert, S.; Joubert P. Optical loss of porous silicon and oxidized porous silicon planar waveguides. *J. Appl. Phys.* **2007,** *101*, 083110.
12. Ulrich, R.; Torge, R. Measurement of thin film parameters with a prism coupler. *Appl. Optics* **1973**, *12*, 2901-2908.
13. Rong, G.; Najmaie, A.; Sipe, J. E.; Weiss, S. M. Nanoscale porous silicon waveguide for label-free DNA sensing. *Biosens. Bioelectron.* **2008,** *23*, 1572-1576.
14. Descrovi, E.; Frascella, F.; Sciacca, B.; Geobaldo, F.; Dominici, L.; Michelotti, F. Coupling of surface waves in highly defined one-dimensional porous silicon photonic crystals for gas sensing applications. *Appl. Phys. Lett.* **2007**, *91*, 241109.

© 2008 by the authors; licensee Molecular Diversity Preservation International, Basel, Switzerland. This article is an open-access article distributed under the terms and conditions of the Creative Commons Attribution license (http://creativecommons.org/licenses/by/3.0/).